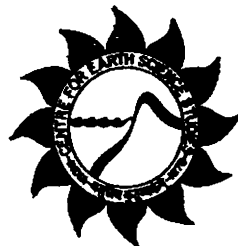# MASS TRANSPORT IN THE EQUATORIAL INDIAN OCEAN

THESIS SUBMITTED TO THE
COCHIN UNIVERSITY OF SCIENCE AND TECHNOLOGY
FOR THE DEGREE OF

DOCTOR OF PHILOSOPHY
IN
PHYSICAL OCEANOGRAPHY
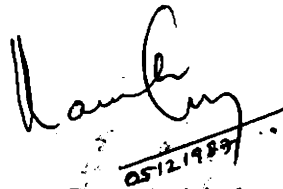
UNDER THE FACULTY OF MARINE SCIENCES

By
CHANDANAVEETIL MARTHANKANDY HARISH

CENTRE FOR EARTH SCIENCE STUDIES
COCHIN - 682 018

DECEMBER 1987

DECLARATION

I do hereby declare that this thesis. entitled 'Mass transport in the Indian Ocean', contains results of research carried out by me under the guidance of Dr. G.S.Sharma, and this has not previously formed the basis of the award of any degree, diploma, associateship, fellowship or other similar title/s of recognition.
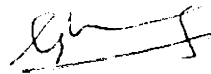
C.M.Harish
Centre for Earth Science Studies
Ernakulam
Regional Centre, M.S.D.
December, 1987.
Cochin - 682 018.

C E R T I F I C A T E

This is to certify that this Thesis is an authentic record of research work carried out by Sri. Chandanaveetil Marthankandy Harish, M.Sc. under my supervision and guidance in the Centre for Earth Science Studies for the Ph.D. Degree of the Cochin University of Science and Technology and no part of it has previously formed the basis for the award of any other degree in any University.

Dr. G.S. SHARMA
(Supervising Teacher)

ACKNOWLEDGEMENT

CONTENTS

PREFACE

The recent awareness that the tropical oceans play a
major role in controlling the climatic fluctuations around
the globe led to a more concerted effort by both
meteorologists and oceanographers in understanding the
relation between the oceans and the atmosphere. The currents
in the tropical oceans generally are zonal except for the
eastern and western boundary currents near the coasts. These
currents play a vital role in redistributing heat and salt.
Since the heat storage available in the oceans is the most
important single parameter in the energy exchange processes
with the atmosphere, a basic understanding of the thermal
regime of the tropical oceans is necessary. Tropical oceans
are the stores of oceanic heat energy. The seasonal and
annual variability in the upper few hundred meters
determines the climatic fluctuations of the tropical
regions, Salinity is another most important parameter in the
oceans which influences the density of the waters and is
responsible for the generation of some currents. Ever since
Helland-Hansen (1916) found a definite relation between
temperature and salinity, the T-S diagrams have been
extensively used for characterising definite water bodies in
the oceans, which from their sources of formation, spread
and distribute both heat and salt. The density of sea water

(i)

(alternately the thermosteric anomaly) derived from temperature and salinity is important in determining the currents, and therefore, an understanding of the mass structure of the tropical oceans is necessary. All the above three parameters have been used in identifying the various water bodies with distinct characteristics and currents which are responsible for the zonal transports in the Equatorial Indian Ocean.

Indian Ocean is peculiar in the sense that it is subjected to seasonal reversal of currents north of 10° S. Considering the limitations of the availability of oceanographic data in the Indian Ocean, especially south of the equator, an effort has been made to estimate the zonal transports for the two monsoons and the transition periods in the tropical belt. The method of Montgomery and Stroup (1962) has been used for estimating the zonal transports and the net transport has been discussed in relation to the presence/absence of the various currents in the tropical oceans like the North and South Equatorial Currents, Equatorial Countercurrent, Equatorial Undercurrent, Tropical Countercurrent, Equatorial Jet and intrusion and advection of various water masses into the region. The study is limited to the upper 1000 m only.

In Chapter I, introduction to the various studies conducted in the Indian Ocean and elsewhere on the zonal

transport together with the data and method of analysis has been presented.

Chapter II deals with the thermal structure in the vertical along the various transequatorial sections. An understanding of this will give some conclusions on the presence/absence of the currents. The discussion, is limited mainly to two seasons, with emphasis on western, central and eastern regions of the Indian Ocean.

Vertical salinity distribution along the transequatorial sections is presented in Chapter III. The water masses found in this region have been presented. Some conclusions on the presence of the Equatorial Undercurrent, which is characterised by a salinity core have been drawn.

Chapter IV deals with the vertical mass distribution along the transequatorial sections. The distribution of thermosteric anomaly has been used in inferring any strong current systems in the region of study.

The zonal transports in the Indian Ocean have been presented in Chapter V. The whole area of study has been divided into 5° latitude belts from 5^oN to 20^oS .The total eastward and westward transports between 53°-106^oE across different sections are worked out and presented on T-S diagrams in terms of km^3/hr. Comparison is made between the

transports for different latitudinal belts for the sa
season wherever possible. These transports are discussed
relation to the existing dominant currents in the region.

The important conclusions drawn from the above stu
are_ summarised in Chapter VI. The limitations of the da
and some of the suggestions for future studies are mention
in this chapter.

ABBREVIATIONS

Fig.	:	Figure
^{o}C	:	Degree centigrade
cm/s	:	Centimeter per second
cm/year	:	Centimeter per year
m^3/s	:	Meter cubed per second
km^3/hr	:	Kilometer cubed per hour
m	:	Meter
km	:	Kilometer
%	:	Percentage
%.	:	Parts per mille
cl/t	:	Centilitre per ton
db	:	Decibar

LIST OF FIGURES

(x)

LIST OF TABLES

CHAPTER I

SECTION I

1.1 INTRODUCTION

Ocean currents play a pivotal role in the 'creation and elimination of heterogeneity in the hydrosphere'. The tropics, which derives maximum energy from the sun, has a profound influence on the general atmospheric and oceanic circulations, which in turn govern the weather and climate over the whole globe. The equatorial current system constitute a major mechanism towards transport of heat and mass and is aptly considered as the 'backbone' of the general ocean circulation. At shorter time scales, the growing evidence of correlation between sea surface temperature (SST) anomalies in the tropics and the anomalies in the global atmospheric circulation, highlights the need for a better understanding of the different physical processes involved. It is equally important from a biological point of view, since the current speeds and turbulence levels in the equatorial region are substantially above the oceanic average which leads to exeptionally high primary productivity, comparable to that of the coastal waters.

The equatorial regions of the ocean are unique in several aspects due to the vanishing of local vertical

component of the earth's rotation vector. Away from the coasts, the flow in the upper layers is mainly zonal, as a consequence of this, the major transport is either to the west (by the westward flowing North and South Equatorial Currents) or to the east by the Equatorial Countercurrent and the Equatorial Undercurrent. The transport by the major currents is quasi-permanent on an annual time scale, although recent theoretical studies (Moore and Philander, 1977) and observational evidences (Wunsch and Gill, 1976 and Weisberg et al., 1979) have highlighted the short term variability mainly arising from a wide variety of low frequency equatorially trapped waves. However, computed mass transport, for large oceanic areas helps in validating the numerous, relatively simple ocean circulation models put forth in understanding the gross circulation features which in turn will be used in refining the crude models, be it diagnostic or prognostic.

In contrast to the Pacific and the Atlantic Oceans, the seasonally varying atmospheric circulation over the North Indian Ocean induces a unique set of seasonal variability in the Indian Ocean, north of 10° S. This necessitates a thorough investigation of the time varying total mass transport which would help in estimating the response of the oceans to atmospheric forcing. The main objective of this study is to evaluate the zonal mass transport in the

2

Equatorial Indian Ocean using the oceanographic data mainly collected during and after the International Indian Ocean Expedition(IIOE), though a more integrated picture can only be evolved out of a more systematic and wider data base, which is very much lacking for the Indian Ocean as a whole and particularly for the region south of the equator.

1.1.1 LITERATURE REVIEW

More than 50% of the navigable waters of the world oceans belong to the tropical oceans, and the earliest information on the average surface circulation is based exclusively on observations collected by navigators (Schott, 1898,1942; Schumacher, 1940,1943; British Admiralty, 1949; K.N.M.I., 1952; U.S. Hydrographic Office, 1944; and others). The outstanding feature of the surface circulation in all the oceans is that, away from the coasts, the currents are more or less zonal. The fascinating equatorial currents are a subject of study by several investigators and a brief review of the earlier studies in the Pacific, Atlantic and Indian Oceans is presented.

1.1.1.1 THE PACIFIC OCEAN

The surface circulation in the Pacific is mainly driven by the trade wind system with the Intertropical Convergence Zone (ITCZ) separating the northeast and southeast trades. The North Equatorial Current (NEC), generally, found between

20° N and 10° N, attains maximum width and speed in February. Mean velocities are of the order of 25 m/s with an average westward flux of 45×10^6 m^3/s (Masuzawa, 1964). At 150° W, the net westward transport between 8° N and 12° N is 7×10^6 m^3/s which is far less than that of the entire NEC (Montgomery and Stroup, 1962). The South Equatorial Current(SEC), situated between 3° to 4° N and 20° S, attains maximum intensity in August with mean velocities of about 50 to 60 cm/s and has a mean transport of 50×10^6 m^3/s. In the Western Pacific, the NEC divides into two, the northward flowing branch having a mean transport of 25×10^6 m^3/s, while the other branch feeds the North Equatorial Countercurrent (NECC), found generally between 3-4° N and 10° N. The NECC in the Pacific is more consistent and powerful than that in the Atlantic. The characteristic pressure field associated with the NECC is clearly demonstrated by Sverdrup (1932), Defant (1935,1941), Montgomery and Palmen (1940) and Thorade (1941). In February-March, it is most shrunken, when its north-south extent is about two degrees, with a transport of 15×10^6 m^3/s, while in August it draws water from the northern branch of the SEC at its maximum intensity, with speeds of the order, 65 cm/s and a transport of about 25×10^6 m^3/s.

As early as 1952, Cromwell et al. (1954) showed the existence of the Equatorial Undercurrent (EUC). Further

studies on the EUC were carried out by King et al. (1957), Knauss (1960,1961,1962), Arthur (1960), Charney (1960) and Stommel (1960). Quantitative evidence of approximate geostrophic balance within the undercurrent to latitudes as low as half a degree from the equator was presented by Montgomery and Stroup (1962), and the estimated flux at 150^oW was found to be 34×10^6 m^3/s. The EUC generally found between 2^oN and 2^oS and at depths ranging from 30 m to 300 m showed wide variability with longitude and season. In the Western Pacific, the transport was maximum in July (55×10^6 m^3/s) and minimum in April (15×10^6 m^3/s)(Hisard et al.,1969). The transport at 140^oW, 115° 30'W and 93° 30'W were found to be 22, 19 and $8 \times (10^6$ m^3/s) respectively (Knauss, 1966; Taft and Jones, 1973). The eastward transport decreases downstream, with a decrease in the width of the undercurrent. In the Eastern Pacific, Christensen (1971) estimated the transport both at 92^oW and 89^oW (west and east of Galapagos islands) to be about 3×10^6 m^3/s, while Knauss's (1966) value at 87^oW was 4×10^6 m^3/s. Seasonal variation in speed at the core was also observed by Sakai (1972), Wyrtki et al. (1977) and Firing et al. (1981). A southward extension of the EUC from the equator is also noticed (Wooster and Gilmartin, 1961; Wyrtki, 1963, 1967; Rinkel et al., 1966; Hisard, 1973; Hisard and Morliere, 1973 and Zuta et al., 1978).

5

Between 155°E and 180°E, Ried (1959) reported a count-ercurrent around 10°S to 12°S. The South Equatorial Count-ercurrent (SECC) is quite narrow and weak. Charts prepared by Air Ministry (1939) showed an easterly flow at 10°S from November through April starting from the Solomon Isles. It is stronger in the west and becomes weaker in the east.

1.1.1.2 CURRENTS IN THE ATLANTIC

The NEC is generally found between 25°N and 10°N and is broader during northern winter, when the westerly flow can be detected upto 5°N. The current has a mean speed of about 35 cm/s and a mean transport of 16x10^{6} m^{3}/s. The SEC of the Atlantic is stronger than the NEC and more persistent and flows between 20°S and 3°N. It attains maximum speed during July-August. The thickness of the current increases from east to west, so also the speed from 30 cm/s in the east to about 130 cm/s in the west. The mean transport was estimated to be 23x10^{6} m^{3}/s (Tcherniya, 1980).

Early studies on the EUC of the Atlantic were carried out by Buchanan (1886), Puls (1895), Neumann (1960), Voigt (1961) and Metcalf, Voorhis and Stalcup (1962). Neumann and Williams (1965) estimated a mean transport of 30x10^{6} m^{3}/s for the current with a width of about 200 to 300 km at depths between 100 to 300 m. The EUC exhibits seasonal variability and generally SEC is found to overlie the EUC. The EUC

carries high salinity water with a maximum at the core of the undercurrent (Montgomery, 1962; Cornus and Mienke, 1979). The transport of the EUC is minimum during northern winter and is of the order of 20×10^6 m^3/s. The eastward flux is about 40×10^6 m^3/s around 10^oW during northern hemisphere summer and is only about 19×10^6 m^3/s at 5^oW (Khanaichenko, 1974). Recent estimates by Katz et al. (1981) gives an average of 21×10^6 m^3/s with a maximum of 44×10^6 m^3/s.

The presence of Sub-thermocline Countercurrent on either side of the main EUC was noted by Reid (1964a), Cochrane (1965, 1968a,b), Khanaichenko and Khlystov (1966), Mazieka (1968), Khanaichenko (1970) and Hisard et al. (1976). Khanaichenko (1974) estimated the mean eastward flux of the Sub-thermocline Countercurrent to be 36×10^6 m^3/s and 20×10^6 m^3/s for the northern and southern branches respectively, while estimates of Mazieka (1968) and Dubravin (1970) varied between 5 and 20×10^6 m^3/s for the southern branch. Cochrane et al. (1979), however, puts it at 20×10^6 m^3/s for the northern branch and 15×10^6 m^3/s for the southern branch, while estimates for the Pacific are only 8×10^6 m^3/s for the northern branch and 4×10^6 m^3/s for the southern branch (Tsuchiya 1975).

1.1.1.3 THE INDIAN OCEAN

Seasonal variability associated with the reversing wind regime is the hallmark of the surface circulation particularly north of 10° S. As a result, the equatorial circulation shows some semblance with that of the Pacific and the Atlantic only during the northern hemisphere winter.

Though there is pronounced seasonal variation, the SEC is the most permanent feature in the Equatorial Indian Ocean. Instead of passing slightly northward of the equator, as in the Atlantic, its northern limit is found to be 8° S to 10° S. The flow is more complex in the western region owing to the presence of Malagasy and Mozambique Channel. The SEC originates in between Australia and Java and flows roughly between 8° S and 20° S, attaining maximum velocity (> 50 cm/s) during southern hemisphere winter. The minimum estimated transport of 40×10^6 m^3/s occurs during northern winter with a maximum of 54×10^6 m^3/s during July-August (Tcherniya, 1980).

During the southwest monsoon the current structure in the North Indian Ocean differs from that of the Pacific and Atlantic. The difference is characteristically depicted in the distribution of temperature, salinity and thermosteric anomaly (Sharma, 1976b). During northern hemisphere winter, the NEC with a general eastward flow, is found between 10° N and 2° to 3° S; originating near Sumatra. It is confined to

the south of Sri Lanka, then spreads to the northwest and even more to the southwest. At 65° E, contrary to the conventional concept that the NEC is absent during the southwest monsoon season, Sharma (1976b) reports the existence of the NEC even after the onset of the southwest monsoon. The ECC is generally found between 3° S and 10° S, and is mainly nourished by the NEC and also receives water from the SEC.

During the southwest monsoon, the NEC is replaced by the Southwest Monsoon Current which merges with the ECC (Sverdrup et al., 1942; Defant, 1961; Varadachari and Sharma, 1967 and Sharma, 1971). The narrow and weak SECC at 13° S embedded in the broad SEC and the Tropical Countercurrent (TCC) round the year between 22° and 26° S were also observed (Sharma, 1976; and Sharma et al., 1978).

The EUC appears only during the northeast monsoon, originating around 50° E and gradually spreading towards east, and could be detected upto 98° E (Sharma, 1968). It has a mean transport of 26×10^{6} m^{3}/s (Khanaichenko, 1974).

Montgomery and Palmen (1940) and Neumann (1947) have estimated the east-west slope of the naviface which has been attributed to the driving force of the EUC. A similar slope down to the east was reported for the Pacific (Austin, 1958). But during the southwest monsoon, the navifacial

slope is from east down to the west in the Indian Ocean (Taft and Knauss, 1967) which explains the absence of EUC during the southwest monsoon.

Recent studies indicate that the equatorial currents, particularly, in the Western Indian Ocean exhibit appreciable seasonal variability (Fieux and Levy, 1983). The SEC, located between 6°S and 9°S, was steadier and stronger during the southwest monsoon when the southeast trades are also relatively stronger. During the northeast monsoon, the SEC retreats towards south. At the equator, the Equatorial Jet appears east of around 50°E during the transition periods between the two monsoons (Wyrtki, 1973b; Luyten et al., 1980; Cresswell et al., 1981). The Equatorial Jet is caused by the accumulation of mass above the thermocline in the Western Indian Ocean, a redistribution of which occurs, possibly related to the curl of the wind stress in the area (Cox, 1979). Studies by Knox (1976) near Gan Island also support the idea. Various observations reveal that equatorial waves occur over a very large domain from 2 to 3 days to a year (Weisberg et al., 1979; Eriksen, 1981 and Luyten and Roemmich, 1982).

From measurements made by drifting buoys, Reverdin et al. (1983) observed that, on the average the flow at the equator is directed towards east, and the Equatorial Jet is concentrated in the vicinity of the equator with maximum

monthly drift of the order of 100 cm/s. Studies by Philander (1979), Cane (1979), Philander and Pacanowski (1980), Gonella et al. (1981) and Luyten and Roemmich (1982) contributed to the knowledge of the appearance, growth and the gradual disappearance of the Jet from the east to the west.

From the survey of the earlier studies conducted, it is evident that the flow is mainly zonal in character and shows marked seasonal variability. A comprehensive picture on the zonal transport of the well established equatorial currents is lacking, let alone the seasonal variability. With the identification of relatively recent countercurrents and the biannual existence of the Equatorial Jet in the Indian Ocean, the need to estimate the zonal transport is all the more important. The aim of the study, is therefore, to estimate the geostrophic zonal flux, from the available hydrographic data, for the northeast and southwest monsoons and the two intermonsoon periods and discuss the variability in transport with respect to space and time. This would help in understanding the variability of the ocean circulation in relation to the seasonal forcing of the meteorological regime and serve in arriving at more realistic inputs for ocean circulation model studies. The zonal transport in the tropical oceans greatly influence the global climatic changes also.

1.1.2 DESCRIPTION OF THE AREA

On a Mercator Projection, the area of study looks more or less rectangular with the long axis running west to east, bounded by about 5°N and 20°S, 40°E in the west and 115 E in the east. Since the Indian Ocean is completely closed on its northern boundary by the Asian land mass, with the Indian Peninsula jutting southward as much as 5°N, the North Indian Ocean has a peculiar meteorological regime of the monsoons which impose a hydrological regime peculiar over the region north of 10°S. During northern hemisphere winter (December to February), the northeast monsoon prevails when moderate amounts of cool, dry continental air flow from the northeast over the Bay of Bengal, Indian Subcontinent and the Arabian Sea absorbing heat and water vapour. During the northern summer (June to August) strong southwest winds blow over the Arabian Sea, and is found to be in continuity with the southeast trades which flow from 20°S across the equator.

This seasonal variability in the meteorological regime is manifested in the seasonal variation of the sea surface temperatures within the area of study. The southern half of the area under study is mainly characterised by a tropical type (Panfilova, 1972) with a distinct annual trend in SST having a total amplitude of 4° to 6°C with a peak during March-April and a minimum during July-August. The northwestern part of the area exhibits semi-annual

12

variability with a peak during April-May and a secondary in October-November, a primary minimum in January-February and a secondary in August with a semi-annual amplitude of 2° to $4^{\circ}C$. Between $8^{\circ}S$ and $10^{\circ}S$ in the west and $10^{\circ}N$ to $10^{\circ}S$ in the east is a zone of relatively weak seasonal variability.

1.1.3 THEORETICAL STUDIES

Theoretical studies on the net transport of mass with little stress on the vertical current structure started with the classical work of Sverdrup (1947). The Sverdrup Transport Concept allowed investigators to make complex studies upon an idealised ocean under an ideal or realistic wind field to achieve important results in terms of total transport. This was followed by contributions on the westward intensification by Stommel (1948), on equatorial circulation by Reid (1948) and by Munk's (1950) treatment of the large scale wind driven circulation. Fofonoff (1960) computed the monthly Ekman and total transports for the North Pacific Ocean from the monthly mean sea level atmospheric pressure. The integrated geostrophic mass transport across the latitude circles was then estimated from the difference between the meridional component of the total transport and the meridional component of the Ekman Transport.

Earliest theoretical attempts were made to explain the NEC system. Montgomery and Palman (1940) suggested that the easterly wind stress in the equatorial zone is balanced by the vertically integrated zonal pressure gradient. Sverdrup (1947) suggested that the NEC was not only a consequence of the zonal wind stress, but also related to the curl of the wind stress. Transport computations from the monthly mean stress field (Wyrtki and Meyers, 1975) were compared with the geostrophic transport computations from Love (1972), for two degree bands of latitude from 2° N to 12° N. The observed geostrophic transport patterns showed good qualitative agreement with the theoretical pattern.

The discovery of the EUC activated a great deal of equatorial modelling. All the early models considered baroclinic effects in a crude way (Yoshida, 1959; Stommel, 1960; and Charney, 1960). Stommel's(1960) model is the first successful extension of classical Ekman Theory to the equator.

SECTION II

DATA AND METHODOLOGY

1.2 CHOICE OF DATA

The material used for this study comprises of data collected on board the various research vessels during the International Indian Ocean Expedition (IIOE), conducted during 1960-1965. This was supplimented by data collected subsequently by different research vessels. Since the reference pressure surface chosen for the computation of mass transport was 1000 db (Duing, 1970), only those hydrographic station data that extend upto 1000 m or more were used for the analysis.

To avoid temporal ambiguity, as far as possible, meridional sections made up of stations covered by single cruises were used. Meridional sections were chosen so as to cover the Western, Central and Eastern Indian Ocean, also taking into consideration that the data covers the two monsoon periods and the intermonsoon months, to assess the seasonal variability of the zonal transport. The details of the data used are presented in Table 1, while their geographical positions with different notations of the collecting vessels are shown in Fig. 1.
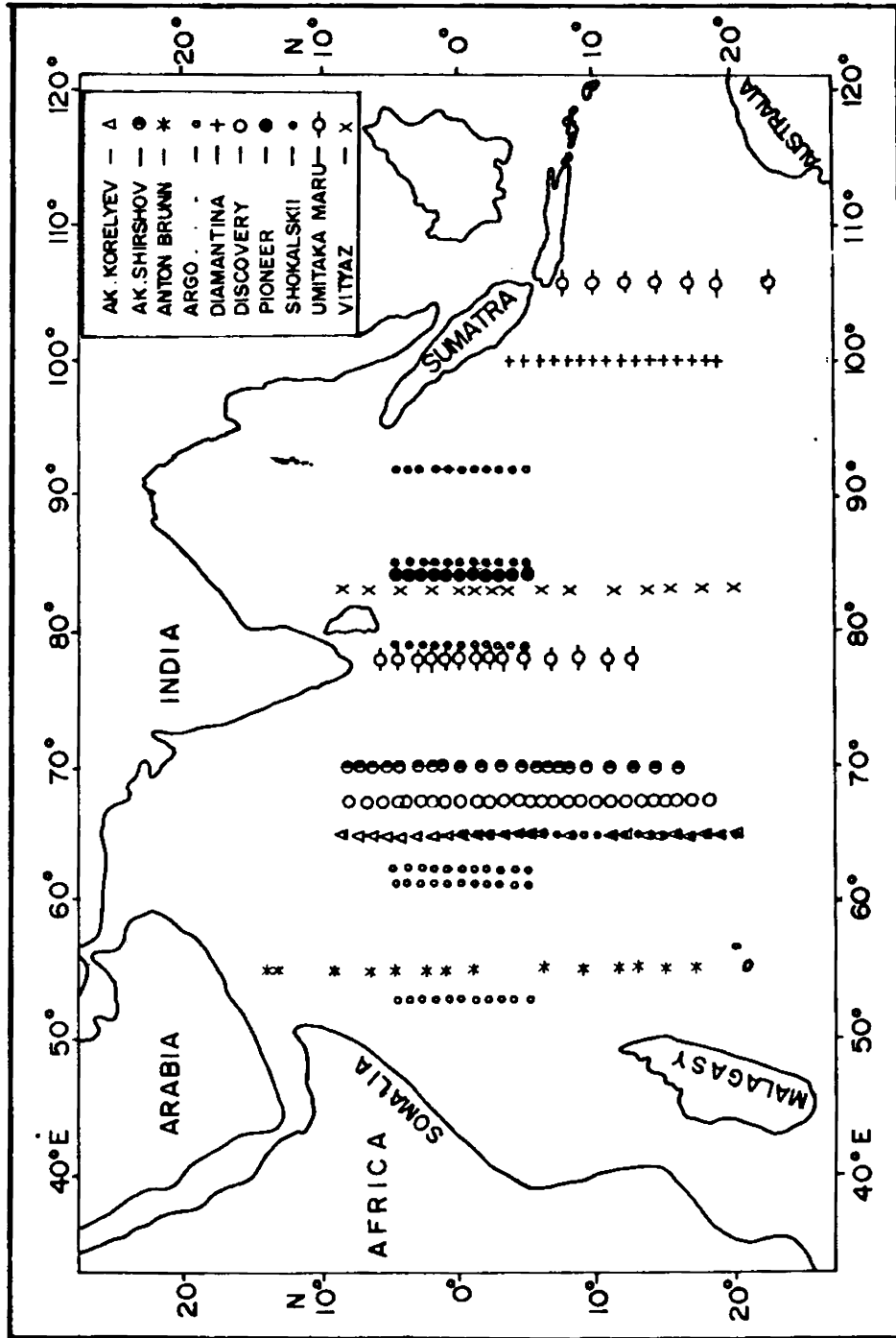
Fig. I — STATION LOCATIONS OF DIFFERENT HYDROGRAPHIC SECTIONS

TABLE I. Details of transequatorial hydrographic sections.

Ser. No.	Ship's Name	Period	Latitudinal extent	Longitude
1	Anton Brunn	Feb. 1964	14°N - 17°S	55°E
2	Akademik Korelyev	Mar. 1973	9°N - 21°S	65°E
3	Shokalski	Dec. 1976	0° - 20°S	65°E
4	Discovery	Apr/May1962	8°30'N - 19°S	67°30'E
5	Akademik Shirshov	Oct/Nov.'70	8°N - 16°S	70°E
6	Umitaka Maru	Dec. 1962	6°N - 11°S	78°E
7	Vityaz	Jan. 1961	9°N - 20°S	83°E
8	Pioneer	May 1964	5°N - 5°S	84°E
9	Diamantina	July 1962	4°S - 19°S	100°E
10	Umitaka Maru	Dec. 1962	7°S - 25°S	106°E
11	Argo (LUSIAD)	Aug. 1962	5°N - 5°S	53°E
12	,,	May 1963	5°N - 4°S	53°E
13	,,	Mar. 1963	5°N - 5°S	61°E
14	,,	Aug. 1962	5°N - 5°S	62°20'E
15	,,	Aug/Sep.'62	5°N - 5°S	79°E
16	,,	Feb. 1963	5°N - 5°S	84°E
17	,,	Apr. 1963	5°N - 5°S	92°E

1.2.1 METHODOLOGY

Several methods have been evolved to determine the gross circulation pattern, qualitatively and quantitatively from the water properties of the ocean. With the lack of extensive current measurements for large oceanic areas, the temperature as well as the salinity fields have provided very interesting information on the current field (Sarkisyan and Keonjiyan, 1975). Using hydrostatic equation, the field of pressure is obtained from the density field. Currents are in turn computed from the field of pressure (Sandstrom and Helland-Hansen, 1903). The currents, thus, obtained are the relative currents with respect to some reference pressure surface where the horizontal motion is assumed to be absent (Defant, 1941).

1.2.1.1 ISENTROPIC ANALYSIS

In a hydrodynamic system, flow tends to take place along surfaces of equal entropy. Isentropic analysis in the oceans was introduced by Montgomery (1937, 1938) and Parr (1938), in analogy to a similar method applied in meteorology, where the distribution of meteorological elements are depicted on isentropic surfaces. Isentropic surfaces are difficult to define in the oceans (Montgomery, 1937), and are best approximated by isosteric surfaces or surfaces of equal specific volume anomaly; and in the upper

layers by surfaces of equal thermosteric anomaly (Montgomery
and Wooster, 1954). This method has been successfully
employed for the computation of geostrophic currents by
Reid (1965), Tsuchiya (1968), Reid and Lynn (1971),
Sharma (1976b), Sharma et al. (1978), Cochrane
et al. (1979), Muraleedharan (1984) and Sharma and Basil
Mathew (1985).

The validity of the geostrophic approximation need to
be examined. A review of the calculation of ocean currents
in the vicinity of the equator was made by Arthur (1960).
Both observational evidence and theoretical studies have
indicated the validity of geostrophic balance within half a
degree from the equator. Early measurements (Knauss, 1960;
Montgomery and Stroup, 1962) pointed out that the meridional
structure of the undercurrent core was consistent with
geostrophy. However, Knauss (1966) presented meridional
density sections which did not indicate geostrophic balance.
Further observations (Taft and Jones, 1973; Taft et al.,
1974) found qualitative evidence of a geostrophic component
to the EUC, although temporal variability was considered too
large to permit quantitative comparisons. Recent theoretical
models assume geostrophic balance in the meridional momentum
equation (Moore and Philander, 1977; McCreary, 1981). This
balance also holds good for the low frequency variability,
if this variability can be described by linear equatorially

17

trapped waves (Moore and Philander, 1977). Measurements by Eriksen (1981) and Ripa and Hayes (1981) suggest that the temporal variability at the equator may be dominated by internal Kelvin Modes. At low frequencies, these modes are geostrophic. Eriksen (1982) had reasonable success in computing profiles of deep currents near the equator using geostrophy.

Following Montgomery and Stroup (1962) the geostrophic computation of zonal flow was carried out at chosen isanosteric surfaces, by computing the function of acceleration potential (Montgomery and Spilhaus, 1941). The acceleration potential is given by,

$$
(\phi_a + p \delta_T) = p_0 \delta_{T_0} + \int_{\delta_{T_0}}^{\delta_T} p \, d \delta_T
$$

where

$$
\phi_a = \int_p^{p_0} \delta \, dp
$$

p_o is the reference pressure and δ_{T_0} the thermosteric anomaly at the reference pressure. Two other methods of graphical computation from a vertical section of specific volume anomaly has been discussed by Montgomery and Wooster (1954). The method employed here is advantageous in that, acceleration potential is simpler to compute than ϕ_a alone and it directly leads to geostrophic currents at

18

chosen isanosteric surfaces. The reference pressure is taken as 1000 db and the numerical integration for the computation of acceleration potential was carried out at whole degrees of latitudes at δ_T = 60, 80, 100, 120, 140, 160, 180, 200, 300, 400, 460, 480, 500, 520, ... cl/t, wherever these chosen or standard isanosteres exist and at the sea surface. The depth scale in metres is used as the pressure scale in decibars. Since,

$$\frac{1}{\rho}\left(\frac{dp}{dy}\right)_\phi = \left(\frac{d\phi}{dy}\right)_p = \left[\frac{d(\phi_a + p\,\delta_r)}{dy}\right]_{\delta_r}$$

(where ϕ is the geopotential), the zonal component of geostrophic velocity is calculated from

$$- f\, u_x = \left[\frac{d(\phi_a + p\,\delta_r)}{dy}\right]_{\delta_T}$$

The method of representation of zonal flux is followed as given in Montgomery and Stroup (1962) and Muraleedharan (1984).

The zonal flux, through each vertical meridional quadrangle formed by two successive whole degrees of latitude and two successive standard isanosteres is then computed. For each such quadrangle, the average of the two

19

differences in acceleration potential is multiplied by the average difference in depth and divided by the Coriolis Parameter at the mean latitude to obtain the mass flux. Although SI units are normally preferable, in the present computation the unit of mass transport chosen is km^3/hr following Tait (1955), Timofeev (1956), Montgomery and Stroup (1962) and Masuzawa (1964) for an easy comparison with the earlier results ($3.6km^3/hr = 10^{-6} m^3/s$).

An additional advantage of the method is that the computed flux can be displayed on a T-S diagram. Thus the flows could be discussed in relation to their temperature, salinity characteristics, quantifying the water types that are transported by the currents (Montgomery and Stroup, 1962; Masuzawa, 1964, and Muraleedharan, 1984). The computed flux for each degree of latitude pair and between a pair of standard isanosteric surfaces is divided into characteristic classes of thermosteric anomaly and salinity. The fluxes are then summed up separately for the different current domains. Modes in the different fluxes can be determined by taking into consideration the fewest classes that together make up 50% and 75% of the flux, etc.

1.2.2 LIMITATIONS

For the computation of the vertical distribution of vertically integrated geostrophic flux between two

successive stations, the reference surface chosen was 1000db, following similar studies carried out in all the three major oceans. However, the assumption that the reference surface is uniform over the whole meridional extent may be untenable and may cause slight errors in the computation of mass transport.

A more serious error may occur because of the smallness of the Coriolis Parameter in the vicinity of the equator. Though there is ample theoretical and observational evidence on the validity of geostrophic balance, the method was found to overestimate the transports near the equator. In order to limit this error the computations of fluxes between the stations located on either side of the equator are avoided.

CHAPTER II

TRANSEQUATORIAL TEMPERATURE DISTRIBUTION

Oceanographers have heavily relied on temperature, salinity characteristics in order to delineate the current regime in the absence of direct current measurements over large oceanic areas. This chapter deals with the distribution of temperature, while salinity and thermosteric anomaly are presented and discussed in the following chapters. Temperature sections impart a rudimentary picture of the current structure in the oceans, for example, the Equatorial Undercurrent in the Pacific and Atlantic has been closely associated with certain characteristic features of the distribution of water properties, interpreted both as features dependant on the undercurrent for their maintenance and as an evidence of motion in the vertical and horizontal planes. The establishment of such close correspondence between the hydrographic structure and the undercurrent can serve as a means for detecting the presence of the current, in the absence of the direct current measurements. The same logic can be applied in the case of the Equatorial Jet, where a pinching of the thermocline and spreading on either side of the equator is observed in the temperature distribution. The ridging or troughing of the

isotherms/isanosteres can be useful in that it can demarcate the boundaries between the eastward and westward flows.

The eastwest navifacial slope along the equator is generally attributed to the driving force of the Equatorial Undercurrent. Sea surface temperatures in the Pacific and Atlantic show the temperature increasing from east to west (Schott, 1942 and Muromtsev, 1958). Associated with the westward increase of temperature at the sea surface in both oceans is an upward slope towards the east of the isotherms in the thermocline (Austin, 1958 and Fuglister, 1960). Meridional temperature distributions show minimum sea surface temperatures in the vicinity of the equator (Austin and Rinkel, 1958; Muromtsev, 1958; Schott, 1942; Metcalf et al., 1962 and Reid, 1964a). The equatorial temperature minimum is more common in the Pacific than in the Atlantic.

Using the data collected during the International Indian Ocean Expedition (IIOE) and supplimented with some recent as well as archived data, the surface layer and the permanent thermocline were analysed on a seasonal basis (Colborn, 1975). The results show that the sea surface temperatures are higher in the east than in the west. Based on LUSIAD sections Taft and Knauss (1967) reported that the thermal structure along the equator of the Indian Ocean appears to differ from the other equatorial oceans in the following respects: (1) sea suface temperature generally

increases from west to east across the ocean (2) isotherms in the upper portion of the thermocline slope down to the east in the central and eastern part of the ocean and (3) a reversal with depth in the sign of the longitudinal slope of the isotherms in the thermocline occurs during the months March and April.

The upper 1000 m of the oceans comprises of (1) a shallow layer containing the summer thermocline and the mixed layer, and (2) the main oceanic thermocline which serves to separate the warm water sphere from the cold water sphere.

The seasonal variation in the parameters controlling the heat content of the surface layer produces a dynamic response and subsequent shifts in the vertical of the isotherms, which leads to variations in the circulation. Together with the advection of water masses of different temperatures, any of these three may become dominant at any particular time and location.

The 20 degree isotherm generally found in the mid-thermocline region in the tropical oceans can be used to infer the depth of the thermocline (Wyrtki, 1971 and Quadfasel, 1982). To infer the spreading of the isotherms, the depth difference between 16 degree and 26 degree isotherms have been used here following Sharma (1976).

24

2.1   Temperature   distribution   along   55°E   during

February,   is shown in Fig.2.1. The sea surface temperature
is minimum around 14°N (24°C) and gradually increases to
28.2°C near the equator. The thickness of the mixed layer is
minimum (21 m) at 11°S suggesting an eastward flow north of
11°S and westward flow south of it. Troughing of
thermocline is seen near 5°N possibly associated with the
clockwise gyre off Somalia (Bruce, 1979). The mixed layer
thickness varies between 30 and 40 m south of 1°N, while it
is > 55 m north of 2°N. Spreading of the thermocline near
1°N, possibly associated with the Equatorial Undercurrent
showing a northward shift during premonsoon, is consistent
with the observations of Leetma and Stommel(1980).

In the thermocline, maximum temperature gradient is
observed at 5°N where the thickness of the thermocline is
59 m, increasing to 148 m at 9°N. From 2°S to 10°S the
thickness is more or less constant (90 m), gradually
increasing in thickness to 180 m at 17°S. Doming of the
isotherms in the thermocline is observed near the equator,
while south of 9°S the thermocline slopes down to the south.
Spreading of the thermocline is observed between 5°N and 3°S
with thickness of 111 m at 1°N.

2.2   Along 65°E during March (Fig. 2.2), the sea surface
temperature varies from 28.2°C around 9°N to about 27.4°C at
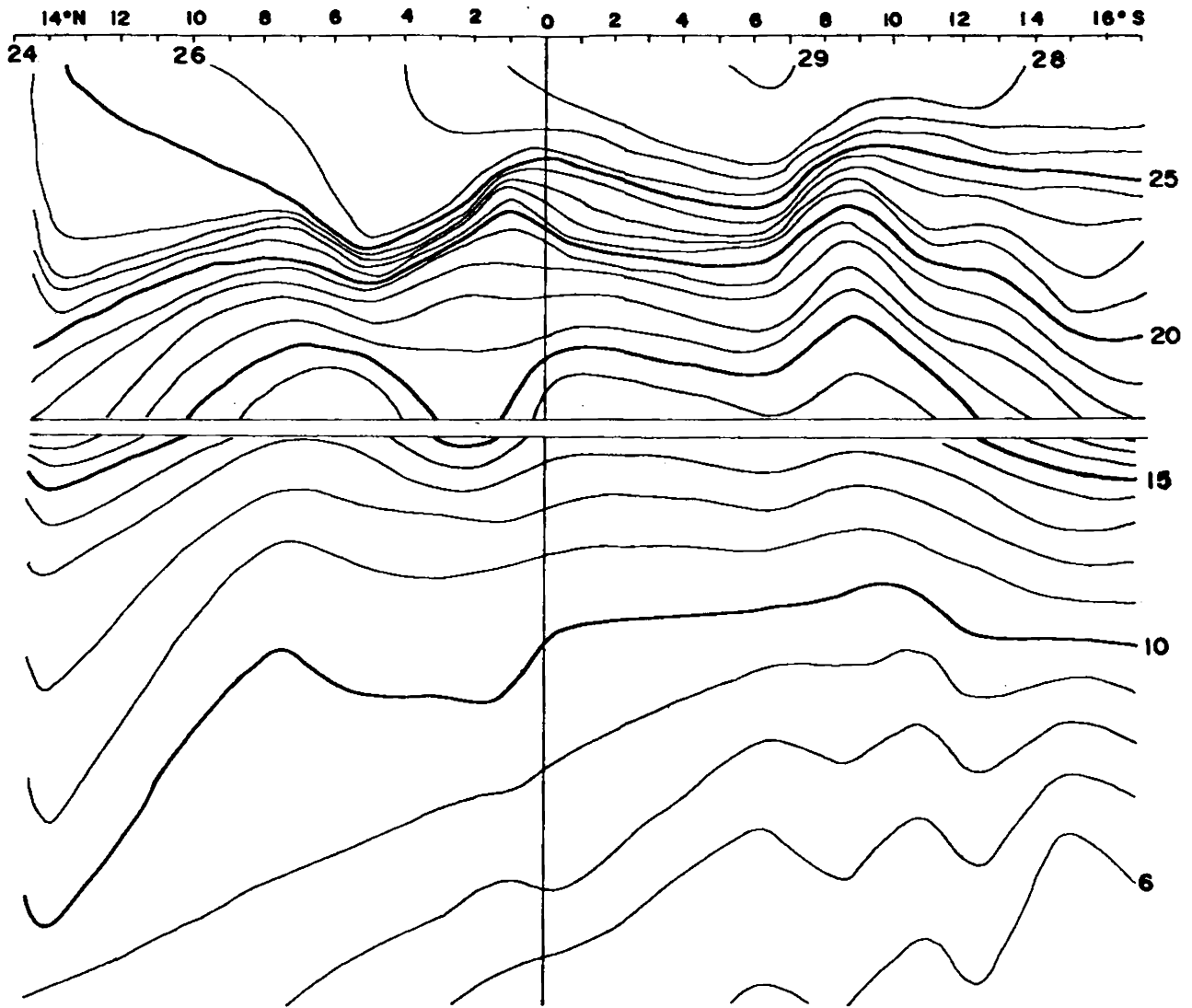
Fig. 2.1 _ Vertical section of temperature along 55°E during February 1964
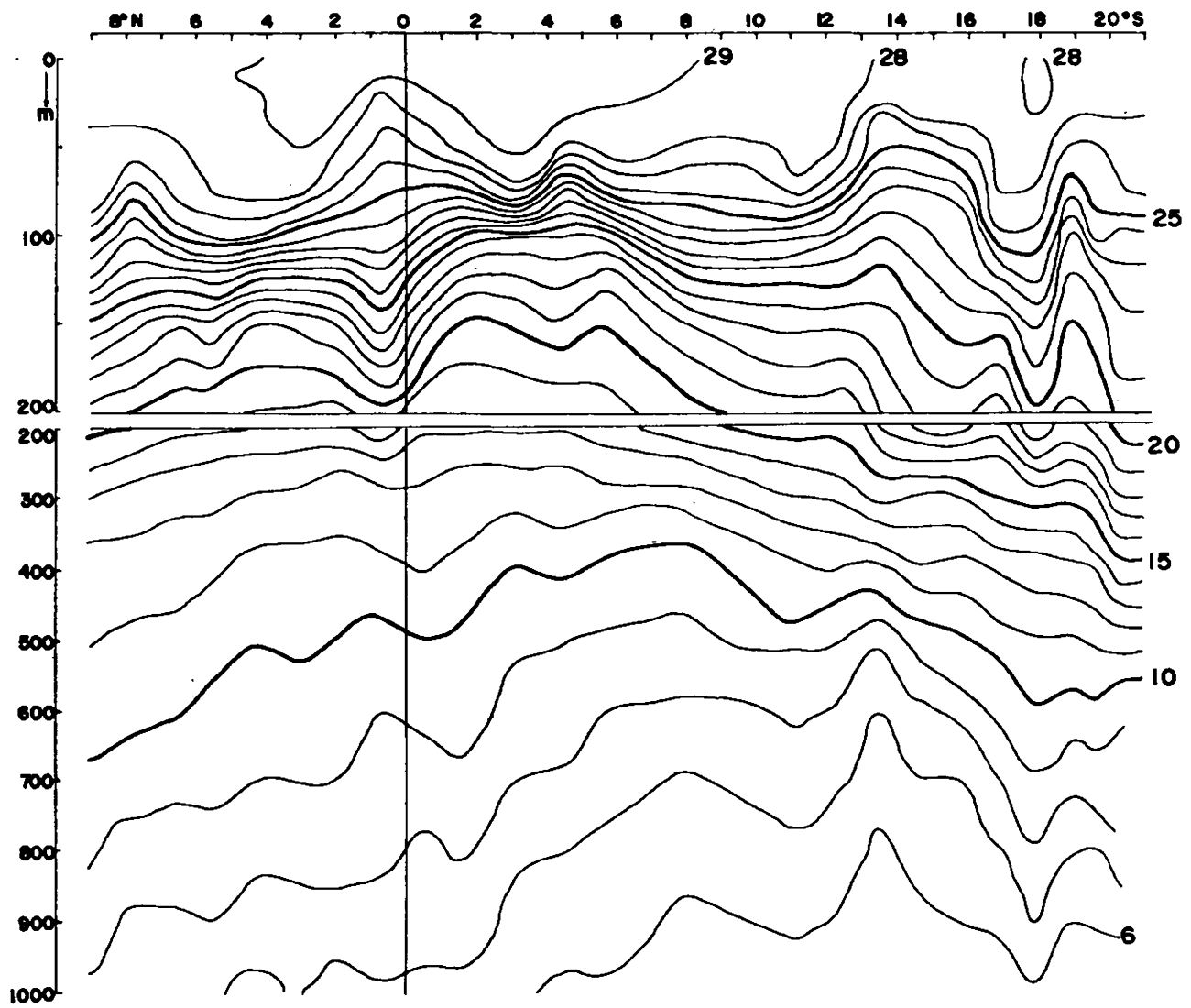
Fig. 2.2 – Vertical section of temperature along 65°E during March, 1973

20°S, with temperature greater than 29°C observed between 4°N and 8°S. The sea surface temperature maximum occurs between 1° and 2°S. South of 13°S, surface temperatures decrease monotonically upto 20°S, but for a thin and narrow warm layer around 18°S (28°C), slightly north of which the maximum thickness in the surface mixed layer is observed along this section. The depth of the mixed layer varies considerably and is about 80 m deep for short stretches. The mixed layer is considerably shallow in the vicinity of the equator (17 m at 1°N).

Marked spreading of the thermocline is evident between 0° and 1°N (128 m) indicating an eastward flow in the thermocline region associated with the Equatorial Undercurrent. The isotherms in the upper half of the thermocline exhibit strong gradient between 3° and 4°S, and on either side the thermocline slopes down. Maximum temperature gradient in the thermocline is observed at 4°N. The thermocline thickness is more than 200m south of 13°S which shows pinching around 17°S. The ridging of isotherms near 13°S appear to be associated with the eastward flowing South Equatorial Countercurrent.

2.3   This section is also along 65°E covered during December. The sea surface temperature along this section increases from 28.5°C at the equator to 28.9°C at 4°S, attaining a maximum at 8°S. A steady decrease in the sea
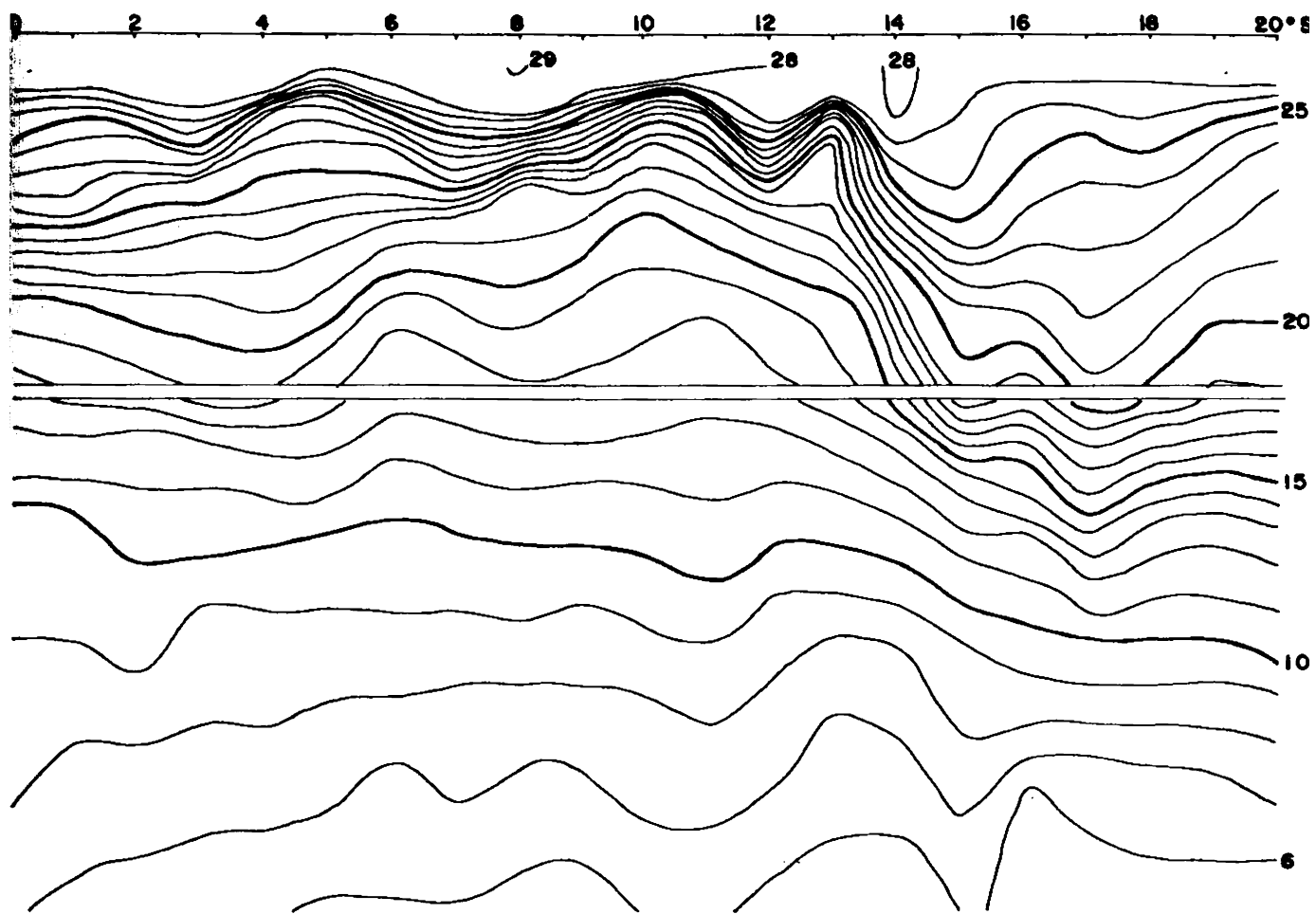
Fig. 2.3 — Vertical section of temperature along 65°E during December, 1976

surface temperature is noticed with a minimum at 16°S, but for a lens of warm water of temperature (>28°C) around 14°S which extends to a depth of about 30m. Further south of 16°S, a slight increase in temperature is noticed.

The most striking feature along this section is that the mixed layer is very thin and the thermocline almost surfaces around 5°S, indicating opposing flows on either side of it. Thickness of the mixed layer is maximum at 14°S where the lens of relatively warm water is present.

The temperature gradient in the thermocline is weak upto 5°S with maximum spreading occurring at 4°S. South of 5°S pinching is observed with maximum temperature gradient occurring at 10°S (60 m). The thermocline gets gradually weaker with maximum thickness occurring at 17°S (321 m). Troughing is observed at 12°S and doming at 13°S south of which the thermocline slopes steeply down south indicating a broad westward flow. North of 13°N, the thermocline slants down slightly to the north.

2.4   In May, along 67°30'E (Fig.2.4), the sea surface temperature is more than 29°C all along the transect from 8°30'N to 11°30'S. It decreases from 29.1°C at 13°S to 27.5°C at 18°30'S. The thickness of the mixed layer is more than 33 m all along this section and is deeper than 50 m between 2°N and the equator . The mixed layer thickness is maximum

27
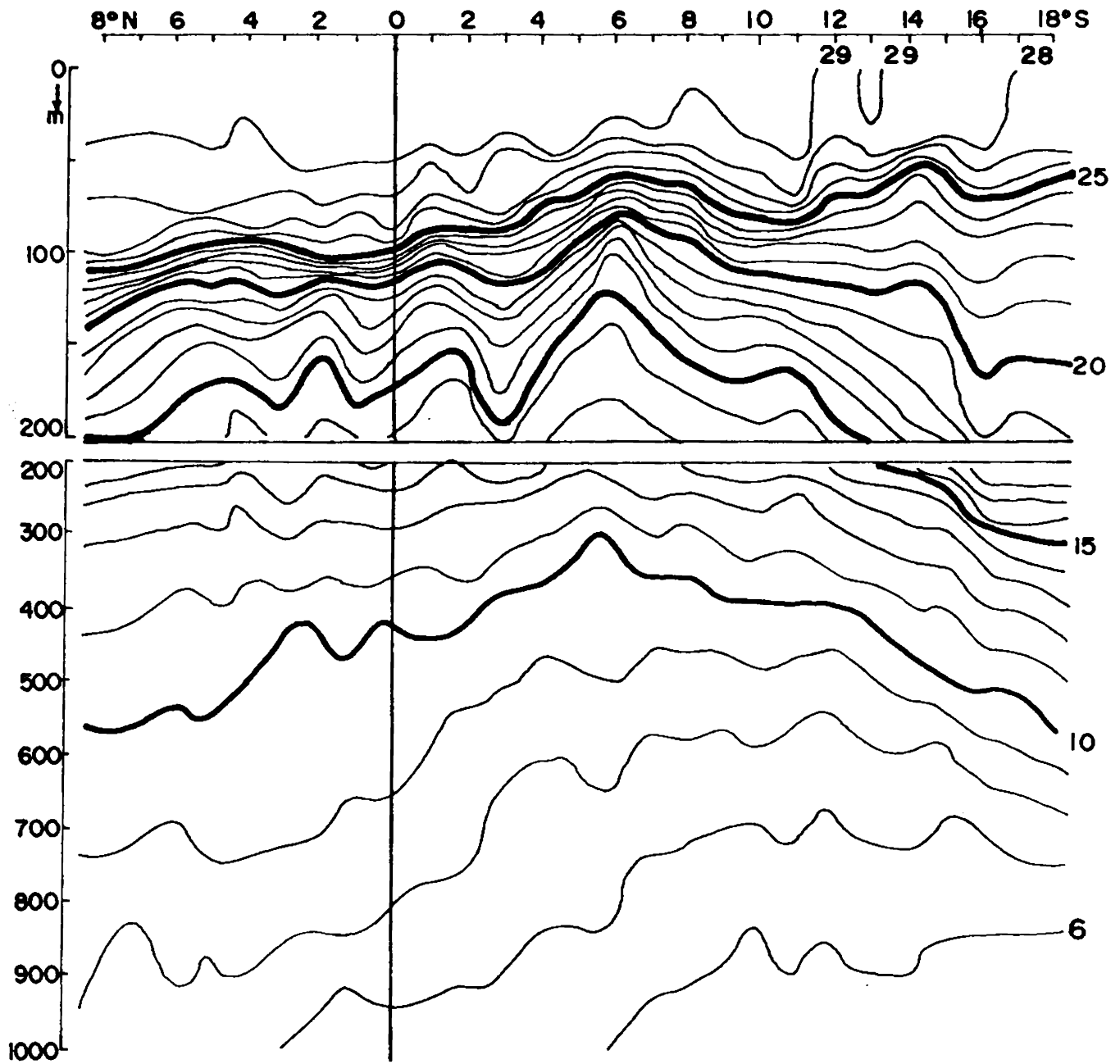
Fig. 2.4 — Vertical section of temperature along 67°30'E during Apr_May,1964

around 5° N (65 m) and a secondary peak is observed between 10° and 11° S.

The thermocline slopes down towards north and south from 6° N where the thickness of the thermocline is minimum. Conspicuous troughing of the isotherms is noticed at 3° S in the lower thermocline, indicating strong currents on either side of 3° S in the upper 200 m. Doming is observed at 6° S suggesting eastward flow between 3° and 6° S. Thickness of the thermocline varies from 46 m at 6° S to 223 m at 18° S. In the deeper layers (below 200 m), the isotherms slope down on either side of 6° S indicating westward flow south of 6° S.

2.5 The temperature distribution along 70° E during November, is shown in Fig. 2.5. The sea surface temperature is maximum around 5° S (28.9° C) and varies between 24.7° C at 16° S to 28.5° C at 8° 30'N. The mixed layer thickness increases from 8° N to the equator and south of 1° S it again shoals suggesting eastward flow (Equatorial Jet) in the vicinity of the equator. Pinching of the isotherms is observed around 1° S while maximum spreading is seen at 3° S.

2.6 During December, the surface temperature in the northern hemisphere along 78° E (Fig. 2.6) is higher ($>28^{\circ}$ C) than in the southern hemisphere. However a warm thin surface layer exists between 5° and 10° S. The thickness of the mixed layer is 70 m at the equator which is more or less uniform
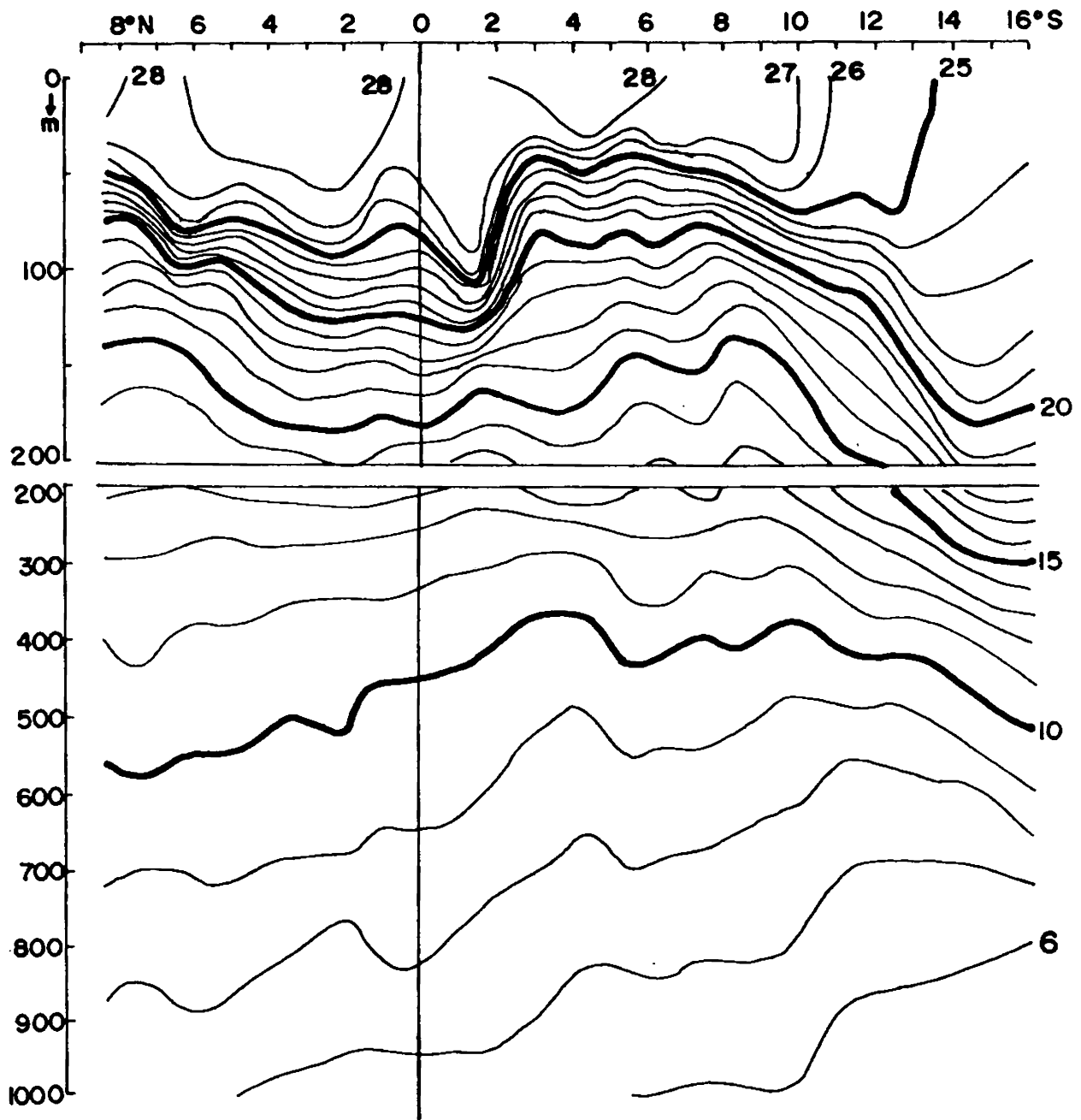
Fig. 2.5 _ Vertical section of temperature along 70°E during Oct_Nov., 1970
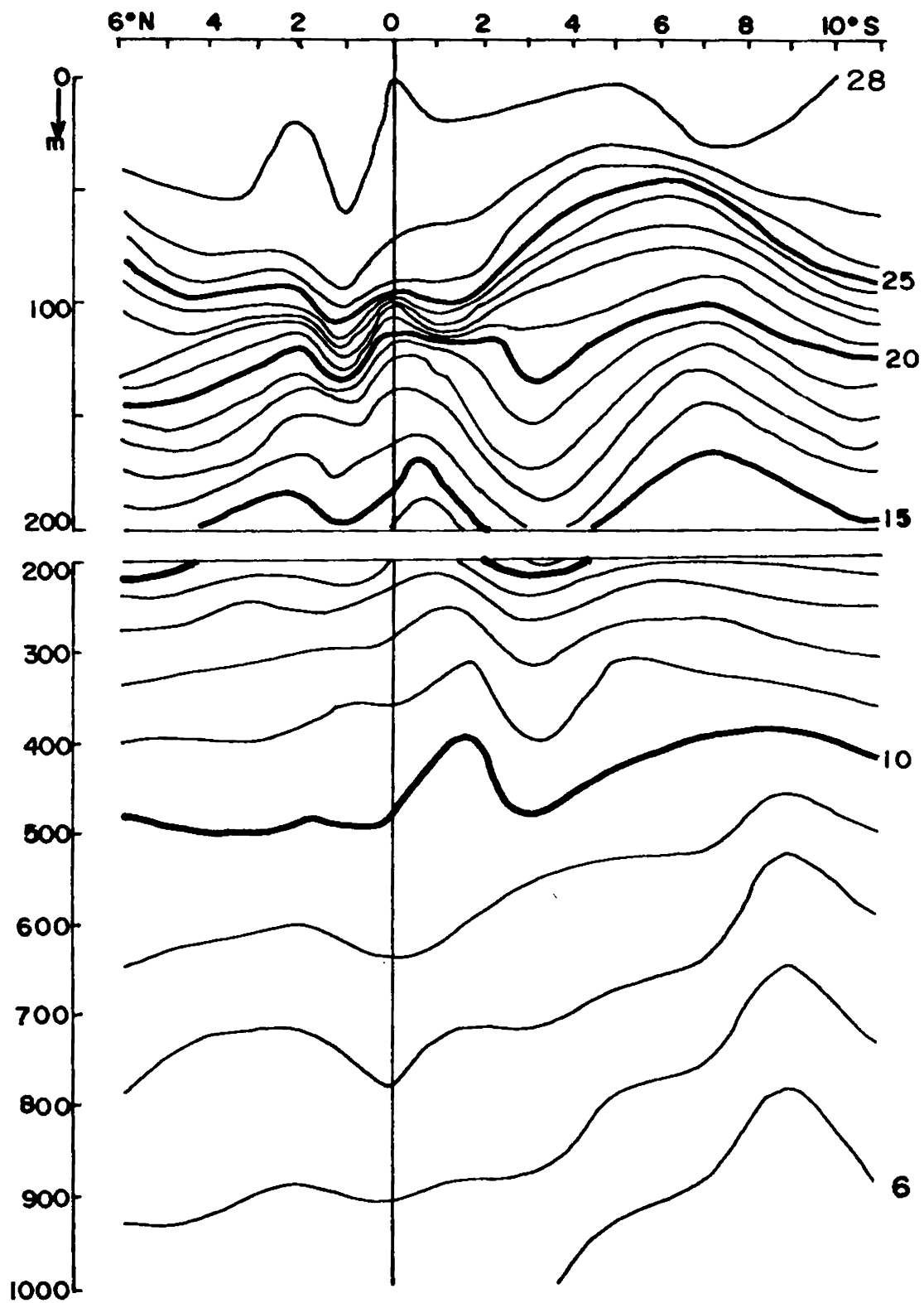
Fig. 2.6 — Vertical section of temperature along 78 °E during December, 1962

in the north latitudes except for a sharp minimum at 2° N (20 m). The mixed layer is shallow between 4° and 9° S.

The maximum temperature gradient in the thermocline is found around 13° S and a slight pinching is observed in the vicinity of the equator, while maximum spreading is seen around 4° S. Troughing of the isotherms in the lower thermocline occurs around 3° S while doming of the isotherms in the upper thermocline occurs between 5° and 7° S revealing westward flow south of 7° S and eastward flow north of it especially in the surface layers.

2.7   Temperature distribution along 83° E during December-January is shown in Fig.2.7. The temperature at the surface varies from 27.6^o C around 9° N to 25.8^o C at 20° S. It is warmer than 28° C between 4° N and 3° S and between 9° and 11° S. The thickness of the mixed layer is more than in the southern hemisphere with a shoaling between 6° and 8° S and also near 15° S, which are indicative of current boundaries. South of 16° S, isotherms slope down towards south especially below 125 m indicating westward flow.

2.8   The sea surface temperature distribution along 84° E during May (Fig. 2.8),increases from 28.5^o C at 5° N to 29.1^o C at the equator, then decreases less rapidly to 28.9^o C at 5° S. The sea surface temperature between 3° and 4° S is 28.7^o C. The thickness of the mixed layer is more than twice
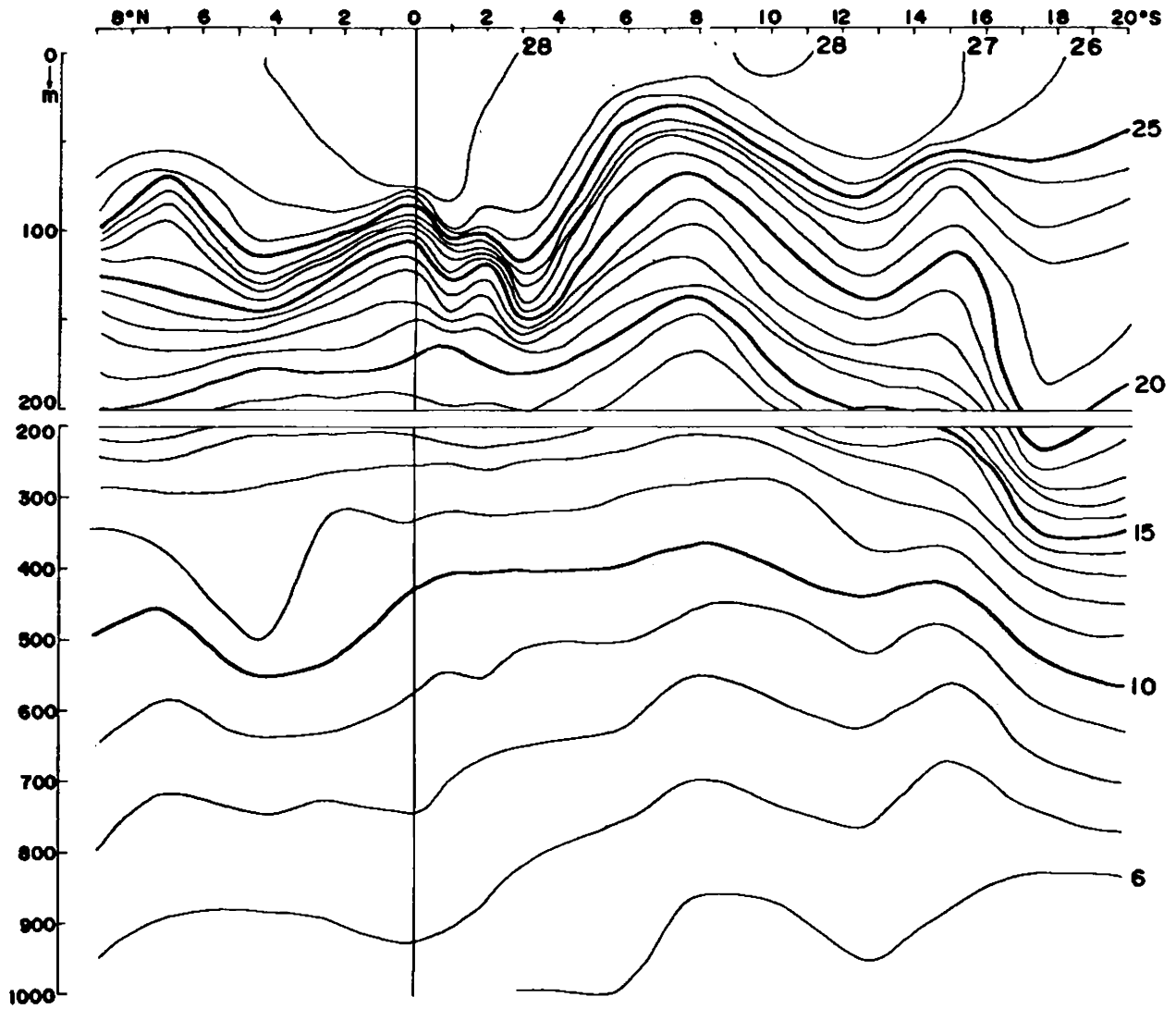
Fig. 2.7 _Vertical section of temperature along 83°E during January 1961
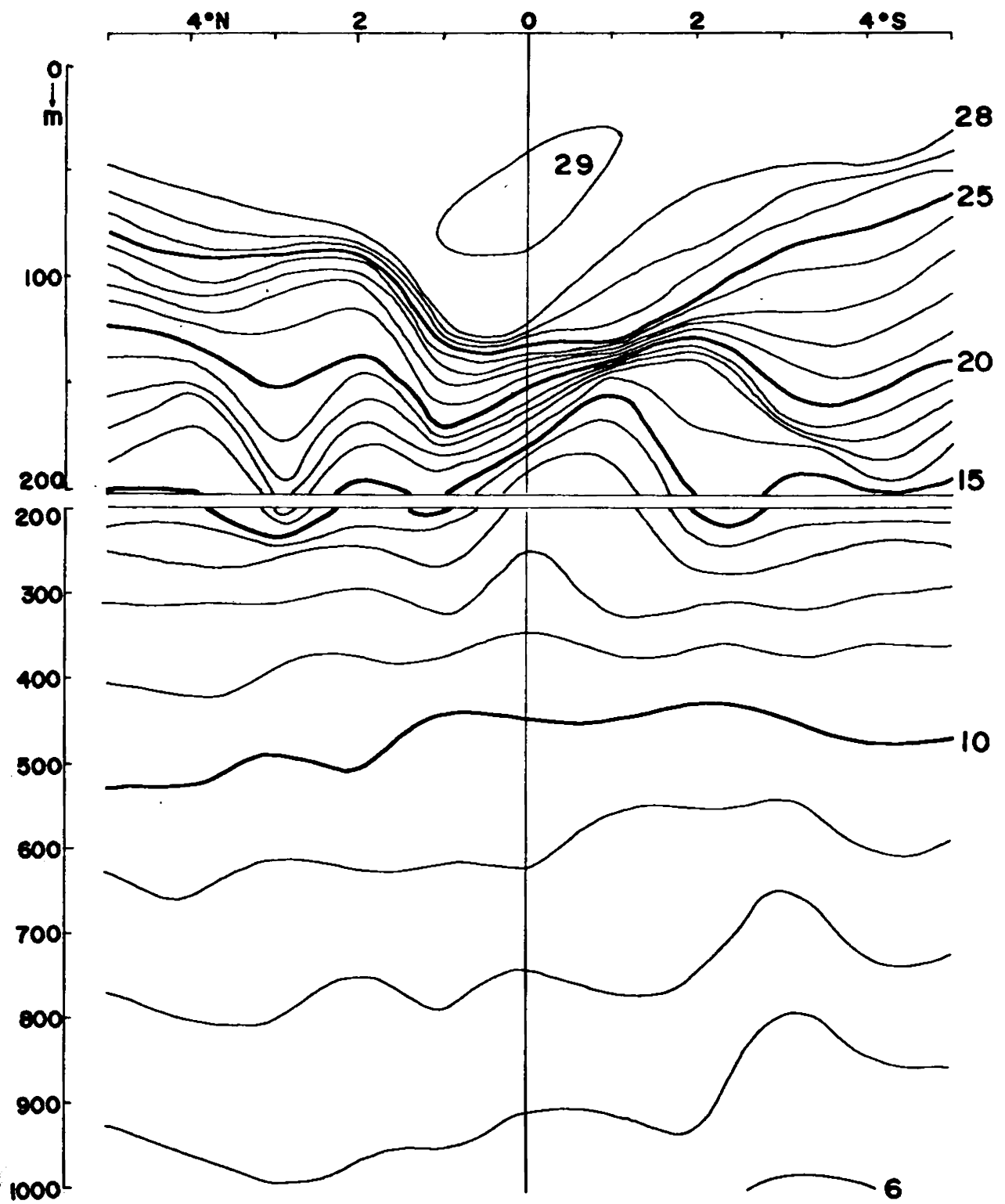
Fig. 2.8 — Vertical section of temperature along 84° E during May 1964

at the equator than at 5°N (54 m) and decreases gradually to
31 m at 5°S. The maximum temperature gradient in the
thermocline is observed at 1°S where its thickness is 25 m.
Spreading of the thermocline is observed north and south of
this latitude with a maximum thickness at 3°N (129 m).
Troughing of the isotherms in the thermocline is seen at 3°N
and around 2°S. The 9° isotherm does not show much variation
with latitude.

The most conspicuous feature in this section is the
presence of a deep mixed layer ($\sim$100 m) and a very sharp
thermocline at the equator with spreading on either side.
This indicates very strong eastward flow near the equator in
the surface layers. In the lower thermocline, the
configuration of the isotherms are just opposite to that in
the upper layers suggesting westward flow immediately below
the surface eastward flow.

2.9   Fig. 2.9 shows the temperature distribution along
100°E during July. The sea surface temperature decreases
from 29.1°C at 4°S to 25°C around 19°S. The rate of
temperature decrease is 0.45°C/degree latitude upto 7°S,
south of which the rate of decrease is 0.23°C/degree
latitude. Slight increase in the sea surface temperature is
noted around 13° and 14°S. The maximum temperature gradient
in the thermocline is observed at 4°S, with the thermocline

30
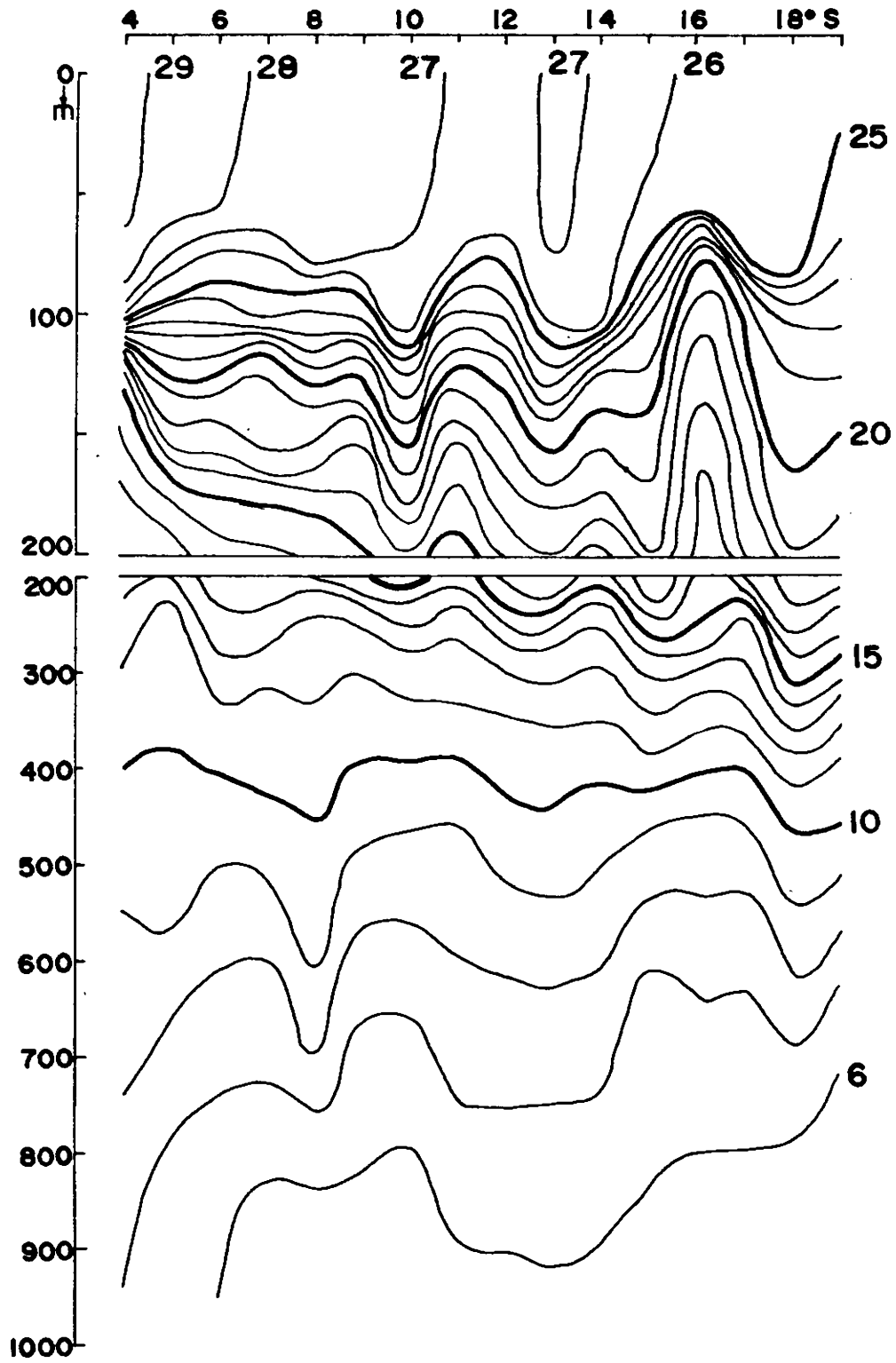
Fig. 2.9 _Vertical section of temperature along 100°E during
July, 1962

sloping towards south. The thickness of the thermocline is 24 m at 4° S increasing to 200 m at 15° S. Pinching is observed at 14° S, with troughing of the thermocline at 10° S, and doming is observed around 16° S. Doming of isotherms, between 11° and 12° S, and also near 16° S, implies rapid changes in flow regimes along this section in the upper layers.

2.10   The sea surface temperature during December along 106° E decreases towards south from 29.2^o C at 7.5^o S to 22.4^o C around 23° S possibly associated with the thermal front (Fig. 2.10). The decrease in the sea surface temperature is rapid south of 17° S. The mixed layer thickness varies between 25 and 66 m and is minimum at 10° S. Eastward flow north of 10° S and westward flow south of it may be inferred from the slope of the isotherms in the surface layers.

Maximum temperature gradient in the thermocline is observed at 7° 30'S (54 m) and a gradual decrease in the gradient is observed towards south upto 17° S. The 21° C isotherm in the mid-thermocline slopes down towards south at 17° S, beyond which it slopes upwards upto 23° S. The isotherm in the lower half of the thermocline , however slopes down uniformly along this transect indicating continuous westward flow at subsurface levels.

2.11   Seven LUSIAD transequatorial sections extending from 5° N to 5° S covered during 1962-'63 used for the

31
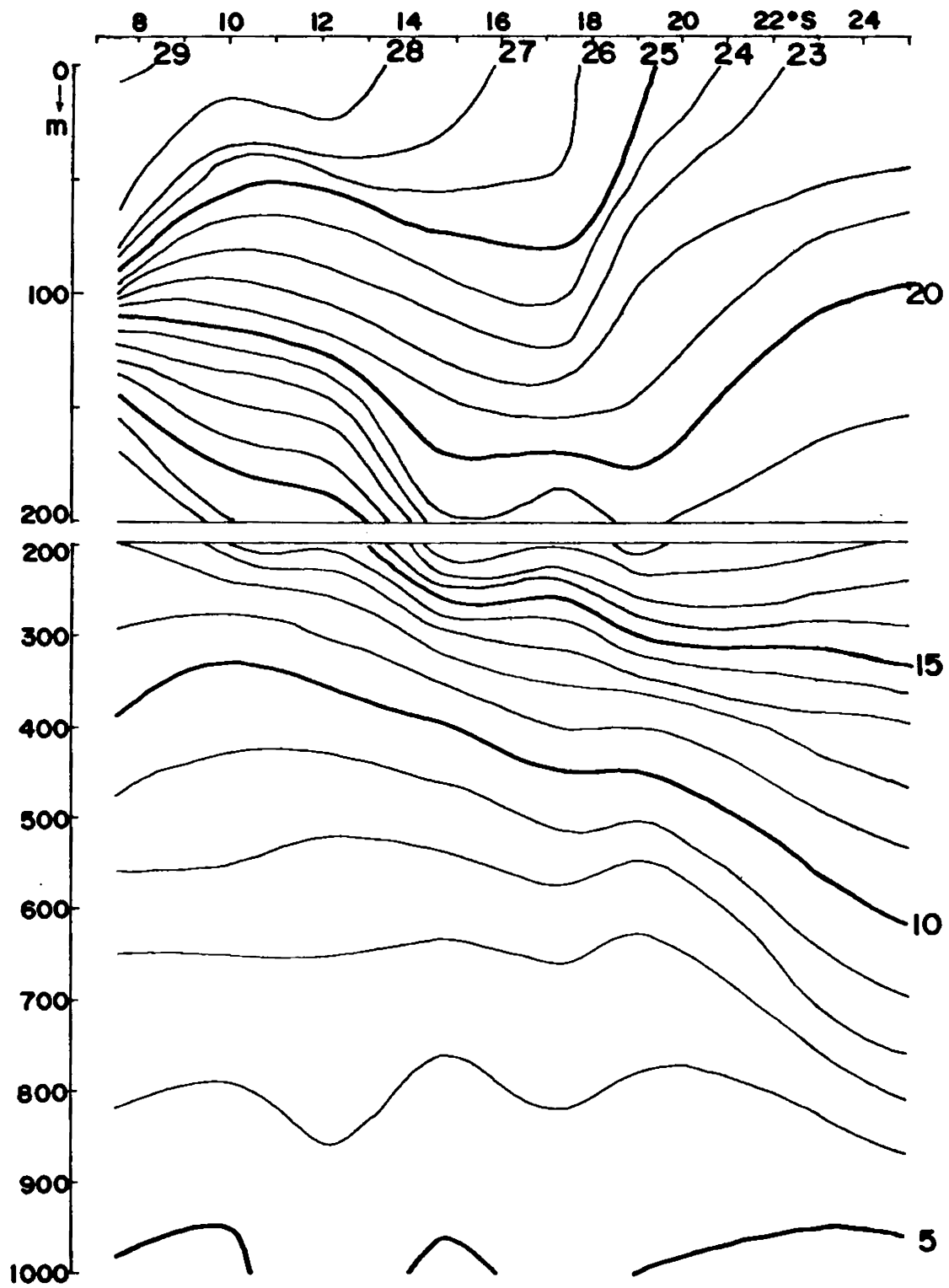
Fig. 2.10 — Vertical section of temperature along 106° E during
December, 1960

computation of zonal fluxes are shown in Fig.1 (Table 1). The distribution of temperature, salinity, and thermosteric anomaly of these sections are not included since they have already been presented by Taft and Knauss (1967), Sharma (1968) and Muraleedharan (1984) in their attempt to study the Equatorial Undercurrent. However, the salient features of the temperature distribution are discussed to get a clear picture of the seasonal and temporal variations.

Due to the lack of latitudinal extent, the LUSIAD temperature sections mainly provide an overview of the thermal structure, which adjusts itself in dynamic response to the changes, near the equator. In the temperature sections, evidence of thermocline spreading at the equator is exhibited at 61° E and 92° E sections, obviously associated with the Equatorial Undercurrent, while pinching of the isotherms in the vicinity of the equator is apparent in the two sections along 53° E, $62^o 20'$ E and along 85° E.

Compared to all the other sections used for this study, maximum spreading of the thermocline in the vicinity of the equator is observed across 61° E during March 1963. Pinching of the isotherms at or near the equator with spreading on either side associated with the Equatorial Jet present during the transition periods between the two monsoons is not very conspicuous at 53° E covered during April-May 1963.

32

But at the same time, the 85°E section worked out during the

northeast monsoon shows this feature with pinching of

isotherms between 2°N and 3°S.

The following features of the current structure could

be deduced from the temperature distribution. Few sections

extend north of 5°N and the most dominant feature observed

north of the equator is troughing of the thermocline around

5°N in the Western Indian Ocean (Fig. 2.1). This trough,

with a steeper front on the northen side, corresponds to an

anticyclonic eddy which is absent during May/June (Fieux and

Levy, 1983) believed to be driven by the south west monsoon

wind stress curl. During the northeast monsoon the isotherms

in the surface layer slope down to the north indicating the

presence of North Equatorial Current (Figs. 2.1 and 2.7).

But the sloping is not as prominent as in the case of the

South Equatorial Current.

The spreading of the thermocline is observed only along

few sections taken during the northeast monsoon (Figs. 2.1

and 2.2). Maximum spreading is observed in the Central

Indian Ocean during March (LUSIAD 61°E section). The

characteristic features in temperature distribution

associated with the Equatorial Undercurrent are well

depicted in the 92°E section in the Eastern Indian Ocean

during April (Taft and Knauss, 1967). The fact that the

typical features are absent in sections taken during the

33

northeast monsoon (Figs. 2.6 and 2.7), points out to the possible interannual variability of the Equatorial Undercurrent. This is related to the strength of the eastward pressure gradient force along the equator which in turn is associated to the strength of easterlies just before the formation of the Equatorial Undercurrent (Taft and Knauss, 1967). Continuous current measurements in the Central Indian Ocean (McPhaden, 1982) prove the absence of the Equatorial Undercurrent in certain years and adds strength to the idea of interannual variations. Cane (1980) suggested that the preceding anomalously strong fall transition winds might have inhibited the formation of an eastward pressure gradient force in the thermocline in the Indian Ocean.

A deep mixed layer and pinching of the thermocline in the vicinity of the equator is well depicted in the 84° E (Fig 2.8) section covered during May, and also in the 70° E section (Fig. 2.5) taken during the fall transition. A similar feature often associated with the Equatorial Jet could be identified in the 85° E LUSIAD section taken in February (Taft and Knauss, 1967).

The South Equatorial Current is present in all sections extending south of 10° S and its northern limit is well demarcated by a ridging of the isotherms around 6° -10° S.

This feature is prominent in the Western and Central Indian Ocean, but not very clear in the eastern most section possibly because of the complex flow pattern existing in this region and also due to the inflow of the Pacific Ocean Water (Sharma et al., 1978). From the temperature sections it is evident that the South Equatorial Current is the most permanent feature of the equatorial current regime in the Indian Ocean, and is broader and penetrates to deeper layers compared to the North Equatorial Current, Equatorial Undercurrent, Equatorial Countercurrent or the Equatorial Jet. Comparing two sections along 65° E (Figs. 2.2 and 2.3) and the section along the same longitude occupied during the southwest monsoon (Sharma, 1976b), it may be safely concluded that the South Equatorial Current shows seasonal variability in its strength and northward extent.

Ridging of the isotherms around 13° S is more conspicuous in sections east of 60° E which has been attributed to the presence of the South Equatorial Countercurrent. From the temperature sections it is obvious that this current does not penetrate to deeper levels and also exhibits seasonal variability. The South Equatorial Countercurrent seems to be present in December and March (Figs. 2.2 and 2.7), but not in February (Fig 2.1) in the Western Indian Ocean. While the South Equatorial

Countercurrent is generally observed north of 10° S (Reid, 1959) in the Pacific, in the Indian Ocean it appears around 13° S. This is not surprising as it can be seen that there is a general southward shift of the entire equatorial current system in the Indian Ocean (Wyrtki, 1973a and Quadfasel and Schott, 1982).

CHAPTER III

TRANSEQUATORIAL SALINITY DISTRIBUTION

In this chapter the salinity distribution along the transequatorial sections in the vertical is presented. Salinity is one of the most important parameters which is conservative in nature and could be used as a natural tracer in identifying the water bodies of particular characteristics. Before presenting the detailed salinity distribution along these sections, a general description of the various watermasses, their origin and spreading in the Indian Ocean is presented. This will facilitate in understanding the salinity structure in this region in relation to the distribution of fluxes with different salinity classes, which are presented in Chapter V.

Compared to the other world oceans, Indian Ocean shows peculiar salinity structure. In addition to the land locked feature in the north, it is connected by the marginal seas in the northwest which inject high saline water into the intermediate layers. In the east it is connected to the Pacific, through Timor and Banda Seas, and in the west with the Atlantic, south of 25$^{\text{o}}$S.

North Indian Ocean is characterised by high evaporation during winter (Venkateswaran, 1956 and Hastenrath and Lamb, 1979). Due to excessive evaporation over precipitation a high salinity water forms near the surface and sinks to depths of 0 - 75 m. After sinking this watermass spreads further south from the area of formation. The spreading of this is seen south of the equator also as a tongue of high saline water. The presence and spreading of this water is influenced by the seasonal reversals in the flow, north of the equator. High salinity water forms in the Southern Ocean between 25° and 30° S due to excessive evaporation. After formation this watermass sinks to about 200 m in the subtropical region and spreads further north. This is termed Subtropical High Salinity Water.

The high salinity water seen in the Arabian Sea, mainly occurring between 140 - 180 cl/t, in the depth range of 200 - 375 m is attributed to the Persian Gulf Water. Persian Gulf is situated in an arid zone, where evaporation exceeds 300 cm/year (Previtte, 1959). Consequently, high saline water forms in the surface layers and sinks during its spreading towards strait of Hormuz. The salinities exceed 40%. at the source region (Dubach, 1964). This high salinity water crosses the sill at Hormuz, between 0 - 75 m, into the Gulf of Oman. Since the waters are of higher

density, they sink to depths of 200 m in the Gulf of Oman and spreads into the Arabian Sea as a tongue of high salinity.

Similar to the Persian Gulf Water, a high salinity water is seen in the intermediate depths in the Indian Ocean, centred around 90 - 100 cl/t, and the depth of occurrence varies from region to region. Evaporation over Red Sea exceeds 400 cm/year (Previtte, 1959), as a consequence of which a high salinity water forms in the surface layer. This water sinks and spreads towards strait of Bab-el Mandeb and spills over the sill and joins the Gulf of Aden (Thompson, 1939 and Patzert, 1972). After crossing over the sill, it sinks to depths of 450 - 500 m in the Gulf of Aden and further spreads towards east and south. The source salinities are slightly less than that of the Persian Gulf Water.

Another important watermass seen in the area of study is the Antarctic Intermediate Water which forms in the zone of Antarctic Convergence. It sinks to depths of 800 - 1000 m and spreads further north as low saline, high oxyty water. This is common in all the three oceans, but its northward extent is limited in the Indian Ocean (Tcherniya et al., 1958). This also occurs at the same density level as that of Red Sea Water in the Southern Indian Ocean.

In the South Indian Ocean, the Pacific Ocean Water is seen as a low salinity tongue embedded in the South Equatorial Current flowing westward. Its presence is evident above 100 cl/t. Its westward extent is reported upto 55°E (Taft, 1963 and Sharma et al., 1978).

Even though Arabian Sea and Bay of Bengal form two arms of the Indian Ocean north of equator in the same latitudinal belt, they show marked differences. Compared to Arabian Sea, Bay of Bengal receives greater run off during the year (Khosla, 1951). Due to this the salinities are lower in Bay of Bengal and the surface salinities reduce to about 18‰. in the shelf regions along the east coast (Rao, 1977). This results in the formation of a low saline surface watermass in the Bay of Bengal. The presence of this watermass is seen in the Arabian Sea along the west coast as a low salinity tongue during. northeast monsoon, when the surface circulation reverses. Part of this water is also carried by the North Equatorial Current flowing westward during the northeast monsoon. The presence of this is seen as low saline layer in the salinity structure.

Seen all along the South Indian Ocean, below the Subtropical High Salinity Water, is a layer of decreasing salinity which is termed as the Subtropical Subsurface Water (Warren et al., 1966).

40

In the equatorial region of the Indian Ocean, below the surface layer, a nearly homogeneous salinity layer extending upto 1000 m is seen. The salinity of this layer does not vary more than 0.2‰.. This is termed as the Equatorial Indian Ocean Water (Sharma, 1976a) or simply the Equatorial Water (Quadfasel and Schott, 1982) and the formation of this is attributed due to the mixing of the various watermasses mentioned above. The thermohaline indices of the various watermasses and their frequency distribution in the Indian Ocean are presented by Pollak (1958), Mamayev (1975) and Sastry et al. (1986).

The presentation and discussion of the salinity distribution in the following pages is confined to the presence/absence of the various watermasses mentioned above. Not many studies have been conducted for understanding the salinity structure south of the equator in the Indian Ocean (Taft, 1963; Sharma, 1972, 1976b and Premchand and Sastry, 1976). Since the salinity structure is not adequately described in the South Indian Ocean, presentation of the salinity distribution is by itself interesting.

3.1 The surface salinity during February in the northern regions does not show much change from 15° to 10° N (Fig. 3.1). A drastic reduction in salinity to 34.8‰. around 1° N is noticed. The salinity is more or less unchanged

41
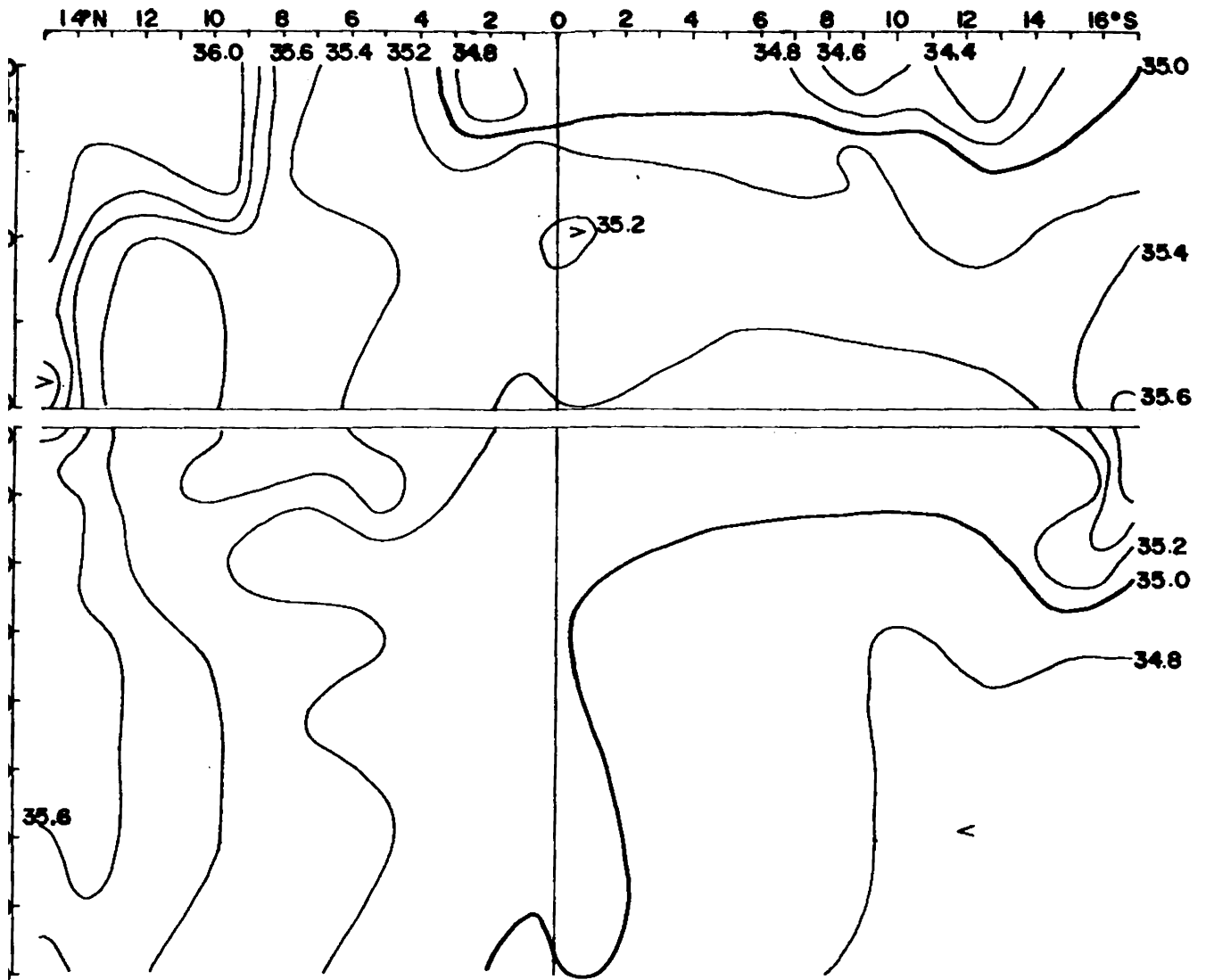
Fig. 3.1 _ Vertical section of salinity along 55°E during February, 1964.

between 1° N and 5° S.   A core of high salinity seen around 50 m at 10° N, sinks to about 300 m near 5° N.   The low saline water   observed   at 2° N may be the result of   the   westward transport of the Bay of Bengal Water by the North Equatorial Current. Between 8°   and 14° S again the salinity   at   the surface is lower (<34.6‰.). The isohalines run more or less parallel between 1° and 13° S in the depth range of 200 - 400 m.   The salinity maximum of subtropical origin is seen around 250 m (17° S) which deepens to 400 m at 14° S.   The salinity maximum that could be attributed to the presence of the Red Sea Water below 550 m noticed, is not very prominent. Salinity is more or less homogeneous between 250 and 900 m north of equator. Feeble salinity maximum is seen around the equator at 100 m.   The salinity north of the equator is always higher at all depths from surface to 1000 m compared to that of the South Indian Ocean.

3.2   The transequatorial salinity distribution along 65° E during March (Fig. 3.2) shows high saline water centred around 1° N between 60 - 175 m depth, the core salinity exceeding 35.4‰. occurring between 100 - 150 m. Compared to the section at 55° E, the core of the salinity maximum is very prominent and is shifted north of the equator (about 1° N).   North of the equator, a high salinity water is seen between 75 - 150 m depth which deepens from north to south. This may be due to sinking and spreading of the Arabian Sea
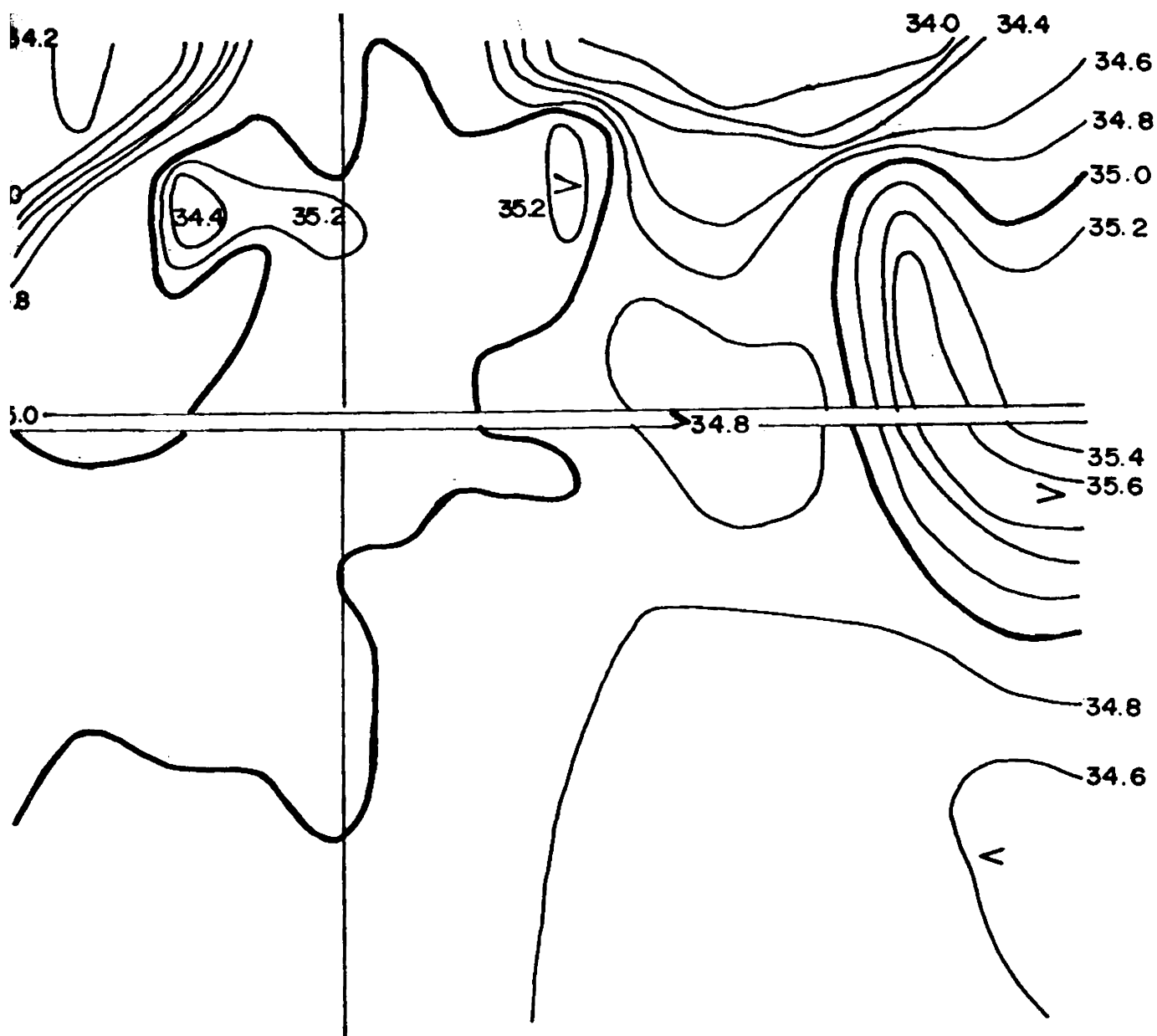
3.2 _ Vertical section of salinity along 65°E during March, 1973

High Salinity Water. Between 2° and 13^oS the salinity in the depth range of 75 - 250 m does not show appreciable change. Lowest surface salinities are seen between 9° and 13^oS possibly due to the presence of the Pacific Ocean Water. South of 13^oS, the isohalines trough upto 200 m. Pockets of high salinity (> 35.4‰.) are seen on either side of this at about 200 m depth. Beyond 13^oS the isohalines tend to deepen from 250 m to 650 m at 20^oS. The surface salinities are higher in the northern hemisphere and decrease towards south. The surface salinity decreases from 35.2‰. to 34.6‰. at the equator, and remains more or less same from 0° to 8^oS. The lowest surface salinity seen between 0° and 3^oS may be due to the presence of the Bay of Bengal Water. The pockets of high salinity around 200 m in the southern hemisphere are the result of the sinking and spreading of the Subtropical High Salinity Water. Around 13^oS the spreading of high salinity from the south abruptly terminates in the subsurface layers.

3.3   Fig. 3.3 shows the salinity distribution during December at the same longitude (65^oE) from equator to 20^oS. Unlike during March, the variations in the surface salinity are small. The variation is from 35.2 to 35.3‰. between 0° and 8^oS. The salinity variation between the layers 200 - 1000 m is only about 0.3‰.. As in March, the high salinity core of the Subtropical High Salinity Water around 200 m at

43
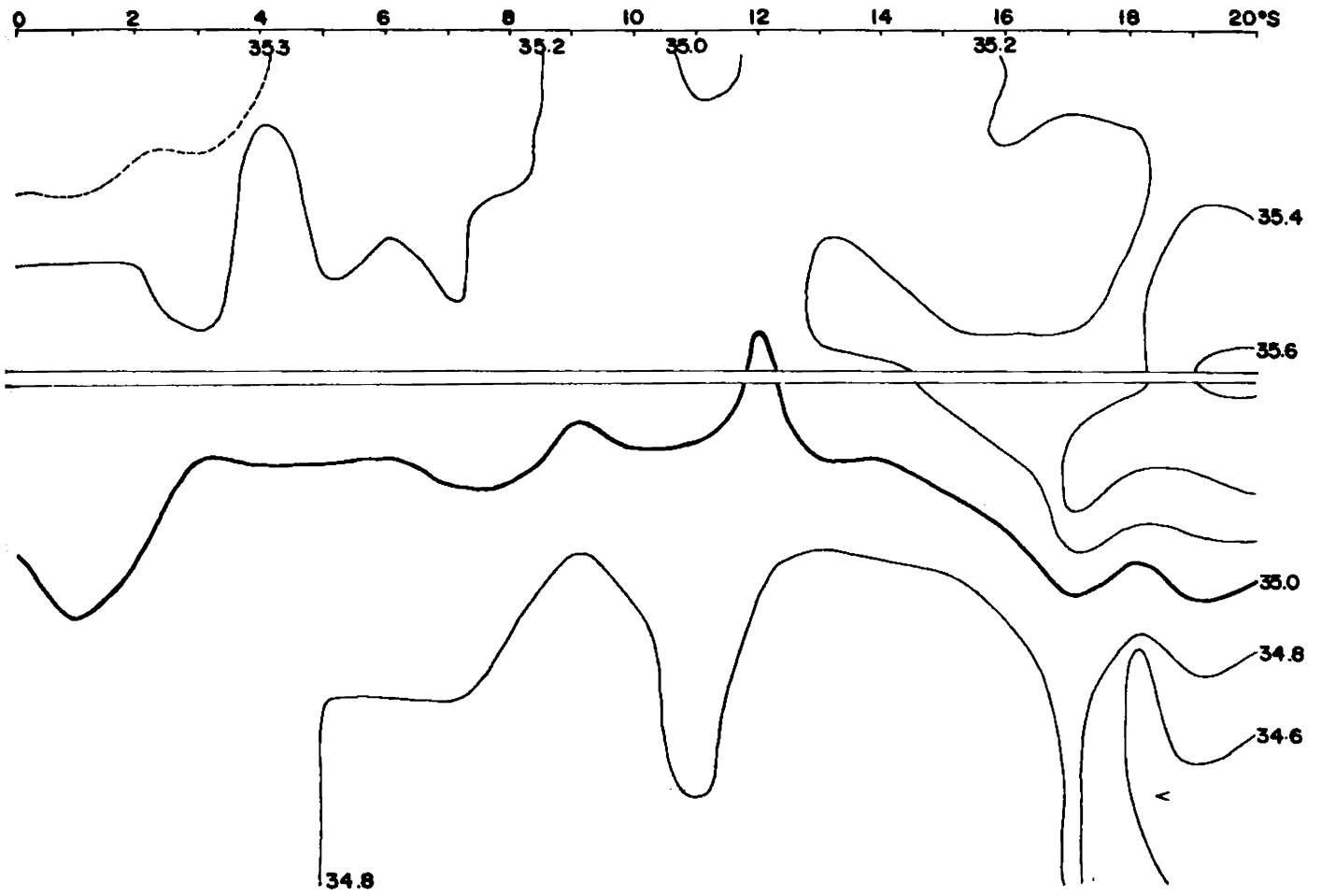
Fig. 3.3 _ Vertical section of salinity along 65°E during December, 1976

20° S is seen at progressively shallower depths from 20° S to 13° S. Further north no such high salinity water is seen. During this month also, low saline water is seen, between 11° and 12° S, though not as significant as seen during March. The presence of the high saline water of the northern hemisphere is not appreciable during this month.

3.4 The salinity distribution during April to May at 67° 30'E is shown in Fig. 3.4. The salinity reduces from 35.6%. in the north to 34.5%. near the equator, is further reduced to about 34%., near 5° S. South of 5° S, the salinity increases to 34.8%. at 20° S. A high salinity core north of equator is seen around 100 m depth which spreads further south upto 3° N. This is attributed to the sinking and spreading of the Arabian Sea High Salinity Water. Another high salinity water is seen around 200 m depth between 13° and 20° S, corresponding to the Subtropical High Salinity Water, below which a low salinity water is seen, extending upto equator with its core appearing at shallower depths. Below 200 m north of equator, isohaline layer is seen between 8° and 1° N upto 900 m depth. No high salinity that could be attributed to Red Sea Water or the Persian Gulf water is seen between 200 - 700 m depths along this section.

3.5 The salinity distribution along 70° E during October-November shows (Fig. 3.5) higher surface salinities in the North Indian Ocean. The salinity reduces to 35.6%.

Fig. 3.4 — Vertical section of salinity along 67° 30' during April_May, 1964
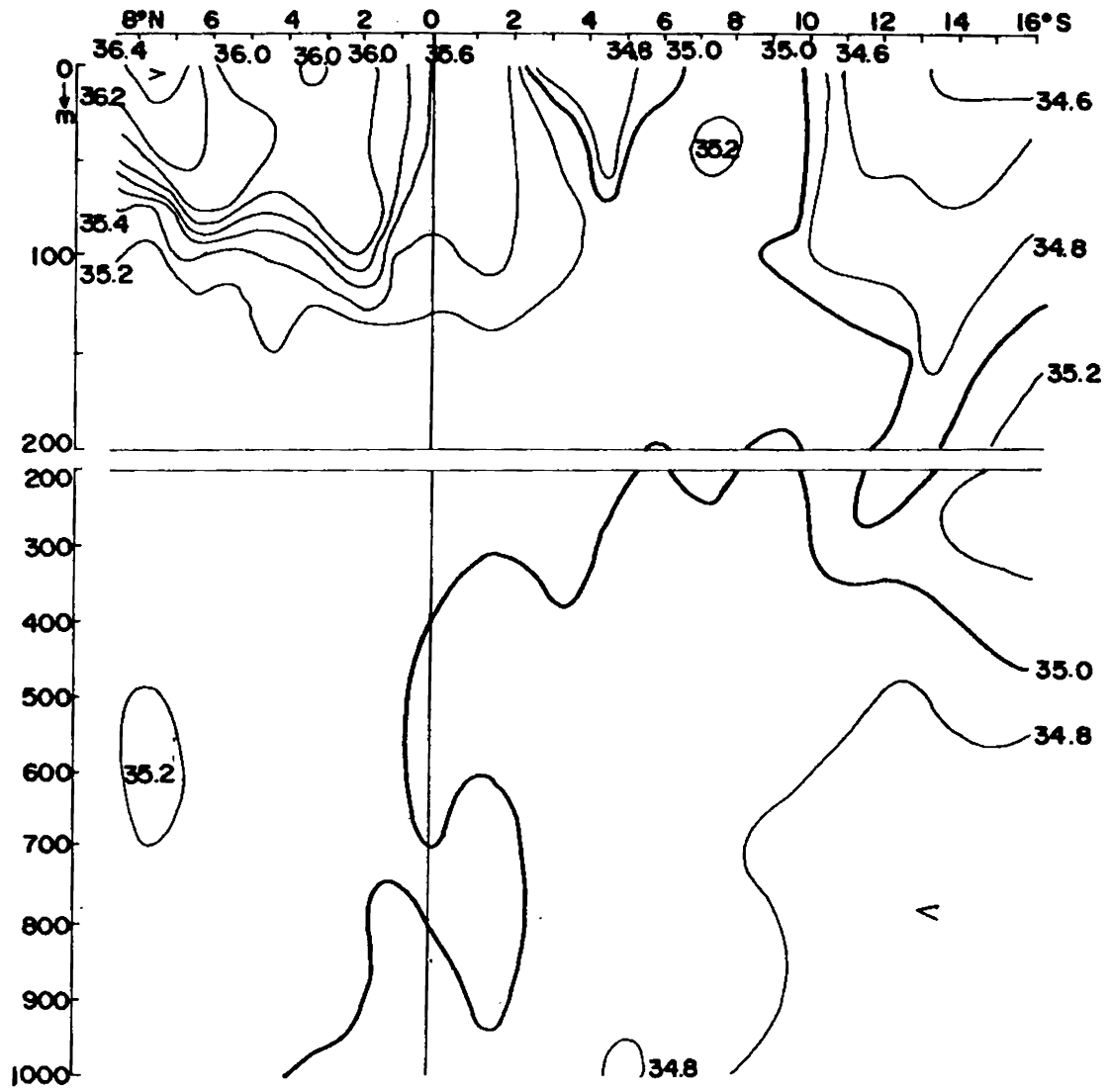
Fig. 3.5 — Vertical section of salinity along 70°E during Oct–Nov, 1970

near the equator. South of equator the surface salinities are lower upto 5° S. Between 6° and 9° S, the salinity does not vary much. Beyond 9° S, the salinity reduces to a minimum of 34.6‰. around 17° S. The high salinity water of North Indian Ocean origin sinks and spreads further south upto 2° N at about 100 m. North of the equator, the salinity in the depth range 150 m to about 700 m, does not vary much. Subtropical High Salinity Water is seen around 200 m depth and the northern limit extends to 11° S only. Low saline water between 500 - 1000 m is seen in the southern region and extends upto equator. A pocket of high salinity is seen north of the equator, which extends further south between 600 - 900 m and this could be attributed to the presence of the Red Sea Water at these depths. The salinity between 900 - 1000 m also shows a decrease from north to south along this section. The low salinity encountered around $3^o - 5^o$ S may be of Bay of Bengal origin. The lower salinity values seen between 10° and 16° S may be due to the westward incursion of the low saline Pacific Waters into the Indian Ocean along the South Equatorial Current.

3.6   The surface salinity along 78° E during December varies from 35.4‰. at 3° N to 33.9‰. at 9° S (Fig. 3.6). Between 6° N and 7° S, the isohalines do not show much variation in depth between 100 - 150 m. Below 150 m depth, a homogeneous salinity water is observed upto 700 m between
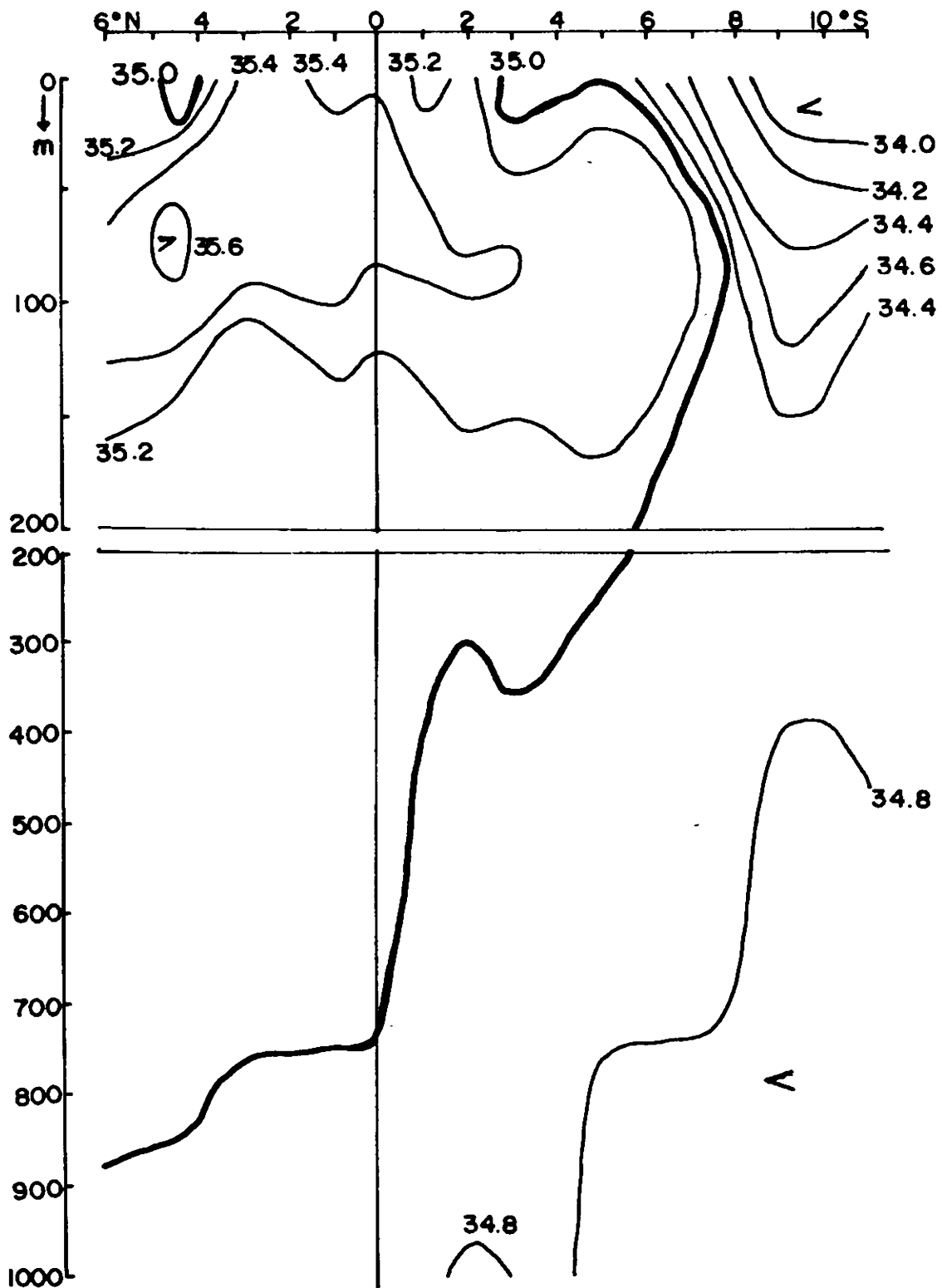
Fig. 3.6 — Vertical section of salinity along 78°E during Dec. 1962

6° N and equator. The salinity in the intermediate layers in the southern region also does not show wide fluctuations. The high salinity core of northern origin extends south upto 7° S. Low salinity water is seen in the upper 100 m, between 8° and 11° S. The low salinities seen in the surface layer, between 3° and 5° N, are due to westward transport of the Bay of Bengal Water through the North Equatorial Current.

3.7   The lowest surface salinities are seen in the Bay of Bengal (Fig. 3.7) as this section extends upto 9° N. Surface salinity increases to about 35%. at 1° S and south of this again lower saline water is seen upto 18° S. The low salinity surface layer extends to about 120 m around 10° S. A salinity maximum centred around 4° N is noticed at 100 m depth, the core extending upto the equator. The layer below 150 m upto 700 m between 2° N and 6° S is more or less homogeneous. A high salinity core is seen around 300 m $(20^{\circ}$ S) which shallows to about 75 m at 14° S. There is an abrupt change in salinity around 13° S at subsurface depths (80 - 400 m). Low saline water is seen between 700 and 1000 m depth in the southern hemisphere. The salinity between equator and 5° S in the depth range 50 - 1000 m is almost uniform (variations are less than 0.1%.). The homogeneous salinity layer is also observed between 250 and 700 m, between 9° N and equator.

46
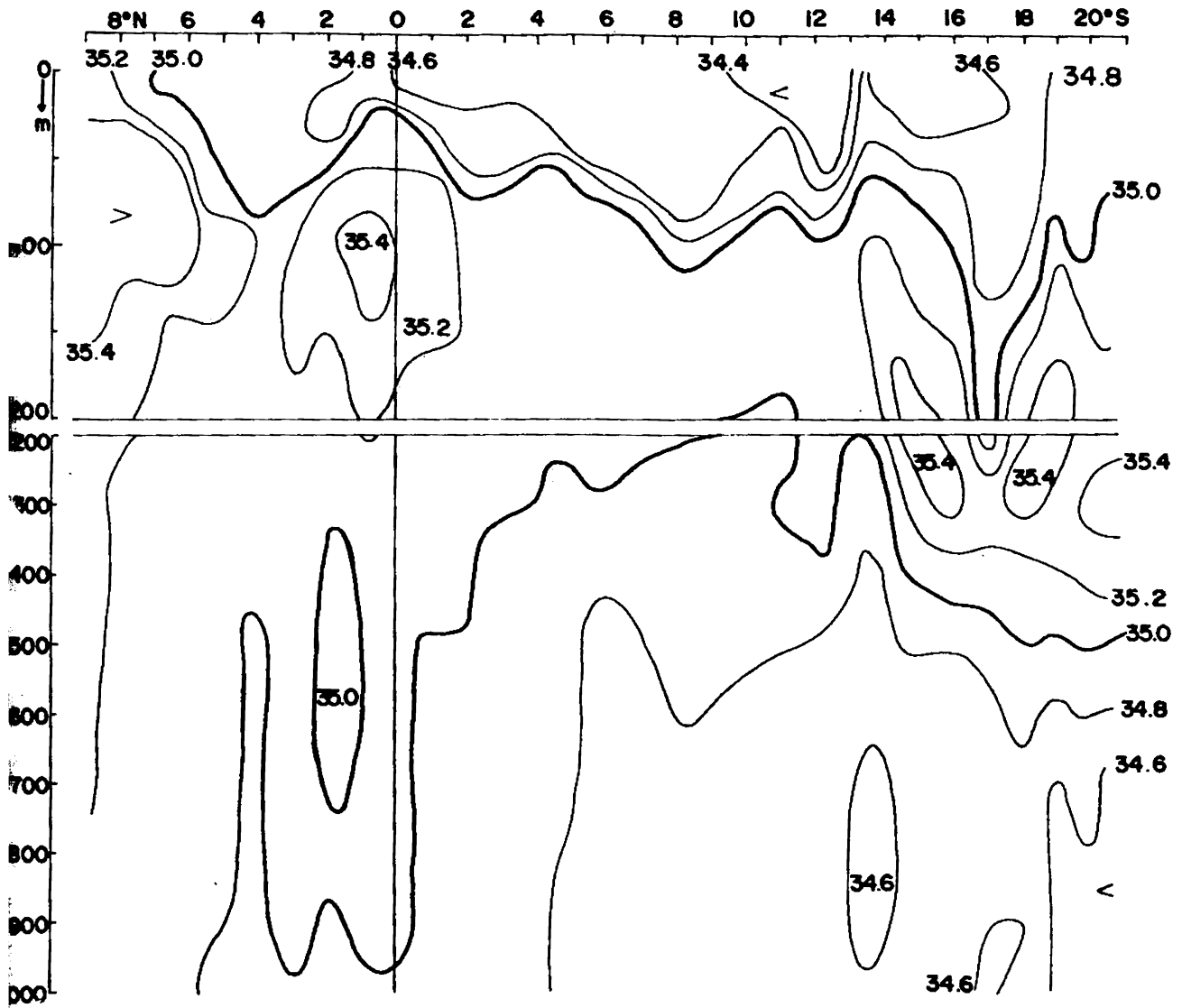
Fig. 3.7 — Vertical section of salinity along 83°E during January, 1961

3.8   Fig. 3.8 shows the salinity distribution along 84° E during May.   Surface salinity varies from 33.8‰.   to   about 34.6‰.   around   2° S.   North of equator a high salinity core seen at 80 m at 5° N,   progressively sinks to about 150 m   at 2° N.   In   the   southern region also a slightly high   saline water   is seen around 100 - 180 m depth.   The water in   the depth   range   180 - 700 m north of   equator   is   homogeneous while   in   the southern hemisphere there is   no   appreciable change in the salinity between 180 and 400 m.   The salinity distribution   is   more   organised than   in   other   sections. Salinities below 400 m in the north are slightly higher than the   southern   region.   Troughing   of isohalines near   the equator   is seen   which could be attributed   the   Equatorial Jet.

3.9   This section extends from 4° S to 19° S (Fig.   3.9). Lowest   surface salinity is   observed at 10° S.   The surface salinities increase further south upto 16° S.   Between   100 and   250 m,   pockets   of low and high salinities   are   seen. Below   200 m a high salinity pocket is noticed at 4° S   which deepens   to   about   400 m at 10° S.   Layers of high   salinity between 100 - 450 m,   and between 20° S and 14° S with salinity exceeding   35.6‰.   are seen.   At 13° S the   salinities   below 200 m   upto   1000 m do not show   any   variation.   Salinity variation   in   the   depth range 200 - 1000 m   is   not   much, between   7 - 13° S.   A pocket of low salinity between   600 -
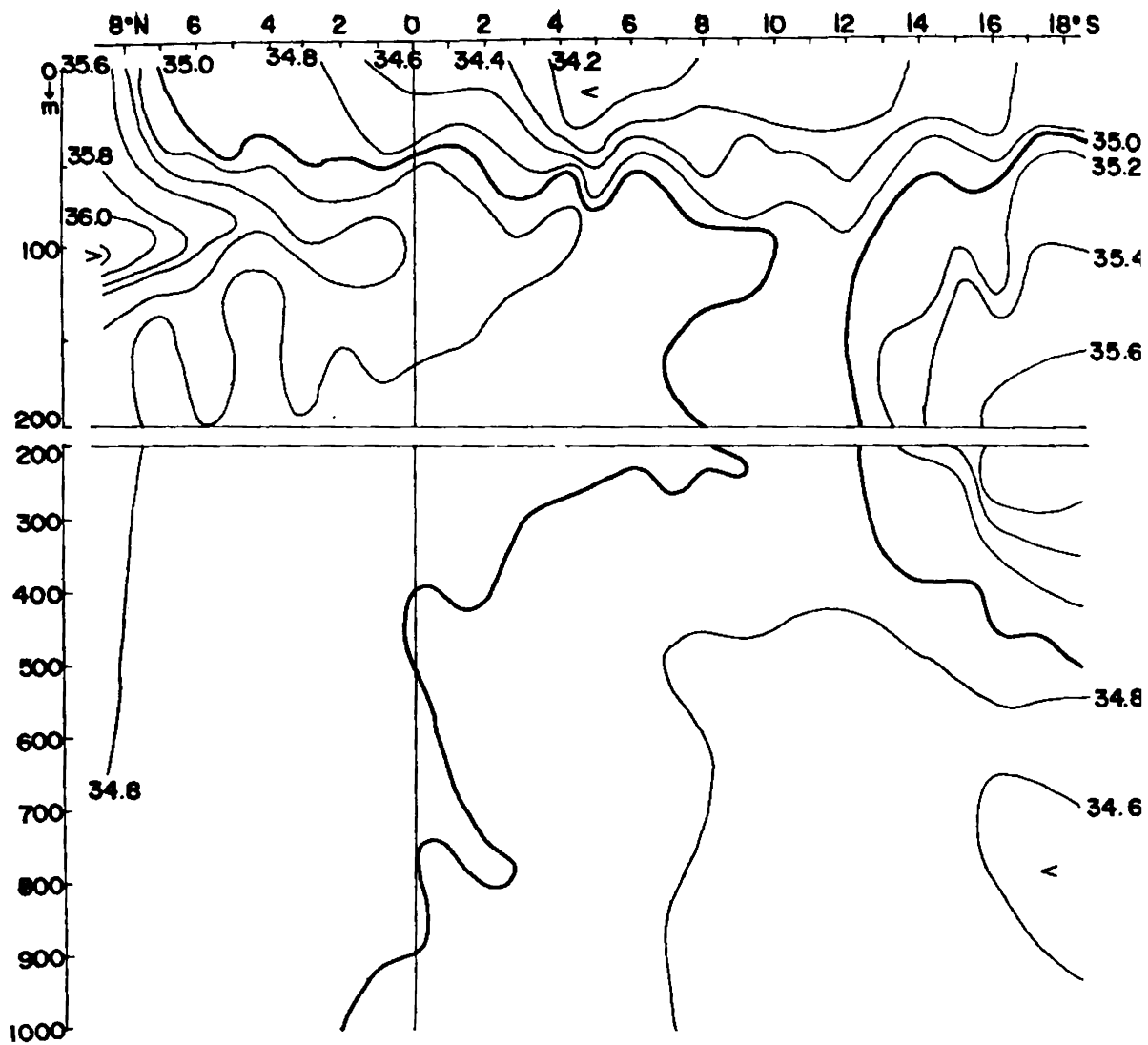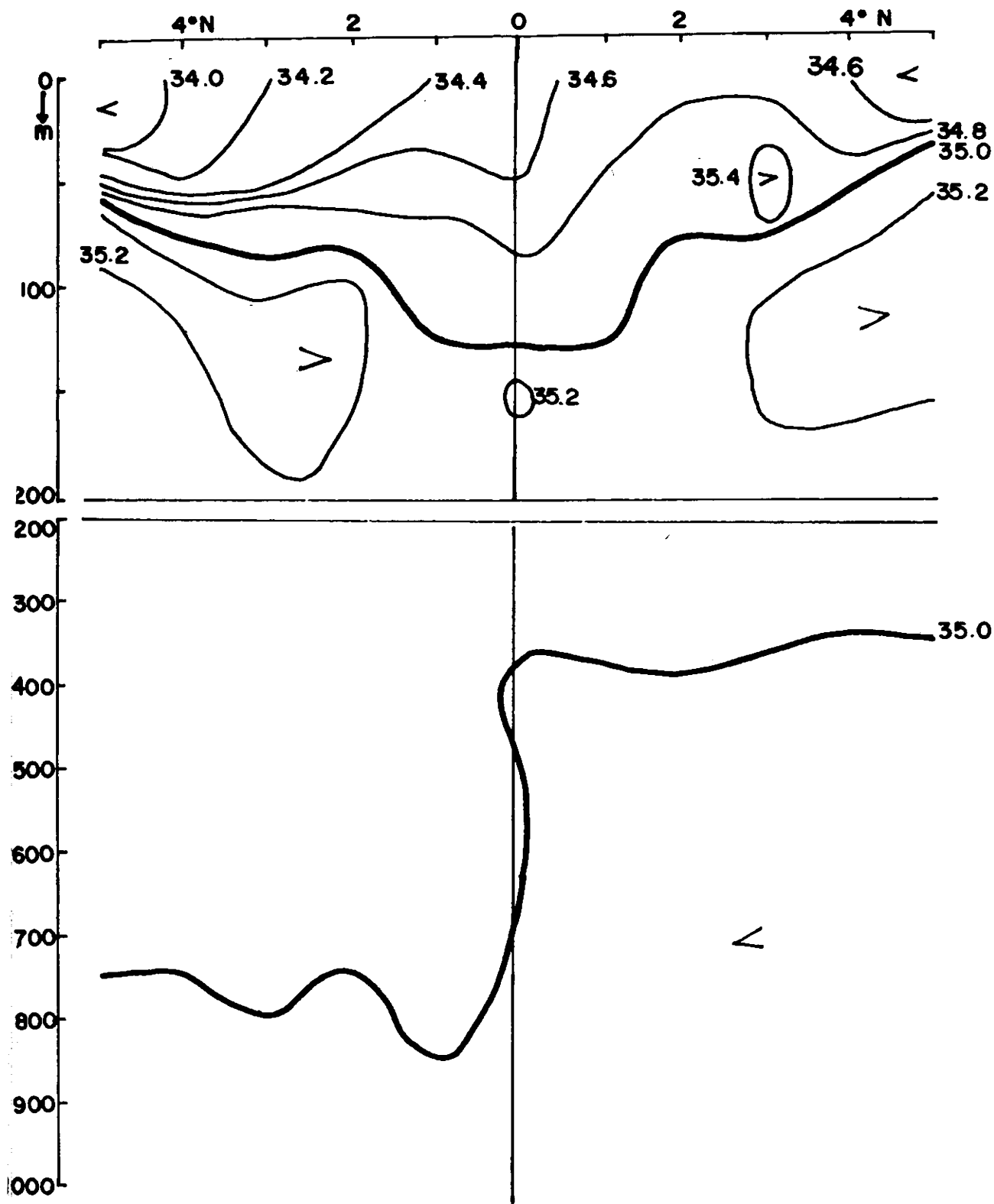
Fig. 3. 8 — Vertical section of salinity along 84°E during May, 1964
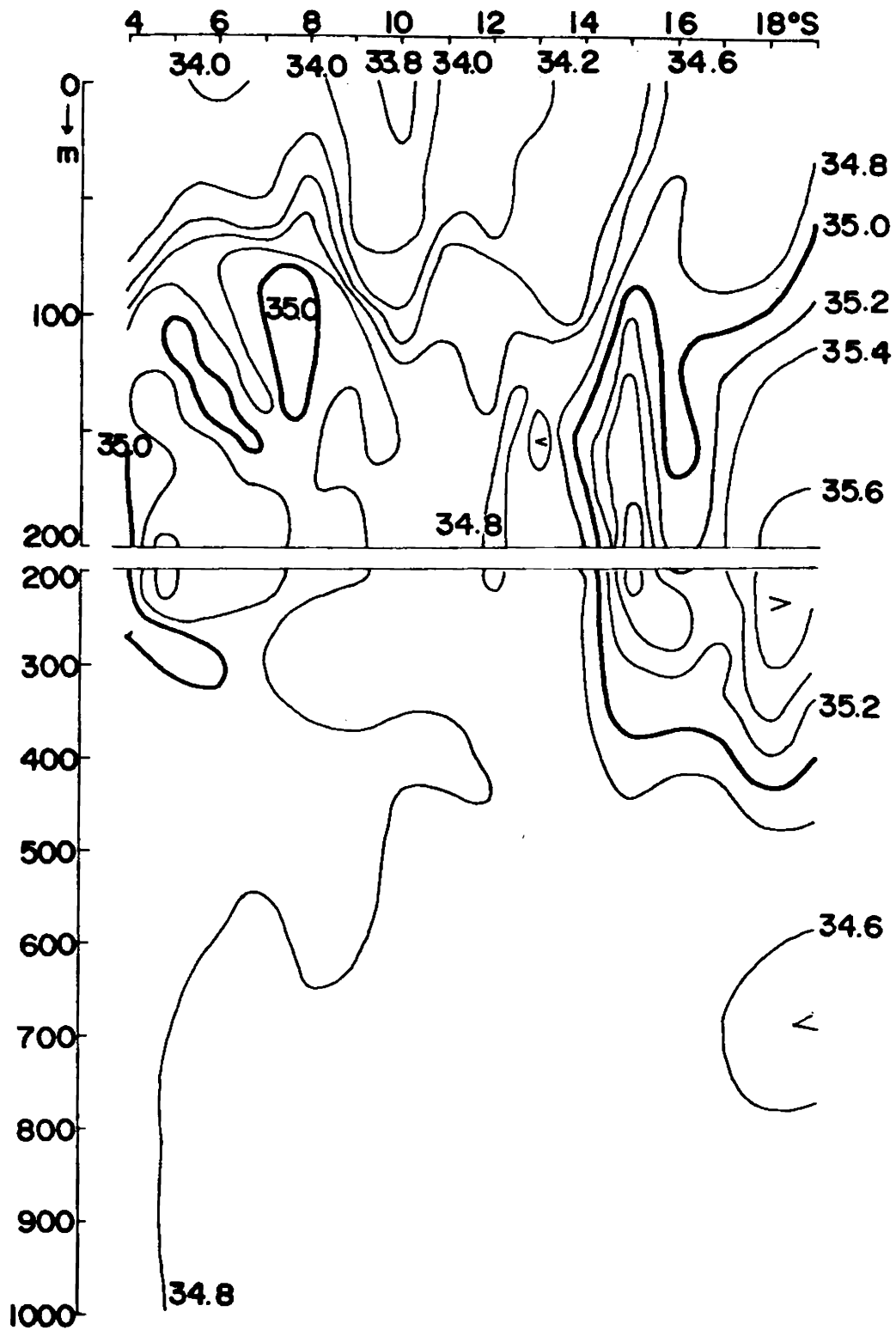
Fig. 3.9 — Vertical section of salinity along 100°E during July, 1962

800 m is observed in the southernmost region of this section.

3.10   This eastern most section extends from 7^oS to 25^oS along 106^oE (Fig. 3.10). Lowest surface salinity is seen around 7^oS (33.6‰.). The surface salinities gradually increase southward to 35.5‰. around 25^oS. The salinity distribution is dominated by numerous pockets of high salinity between 100 and 400 m. Between 17° and 19^oS the salinity is homogeneous in the upper 300 m depth. Another high salinity core (>35.8‰.) is noticed around 150 m which deepens to about 350 m around 18^oS. Below the high saline core the salinity monotonically decreases upto 700 m below which low salinity water is seen. Salinity between 8° and 16^oS is uniform in the depth range 400 - 1000 m. Low salinity water is seen between 200 - 300 m around 10° - 11^oS.

3.11   The salient features of the salinity distribution for the LUSIAD sections (shown in Fig. 1) is presented in the following pages as the detailed vertical salinity distribution for these sections are presented by Taft and Knauss (1967), Sharma (1968) and Muraleedharan (1984). The summary of the salient features of the salinity distribution is presented to facilitate the explanation of the zonal fluxes worked out along these sections which are presented in Chapter V.

48
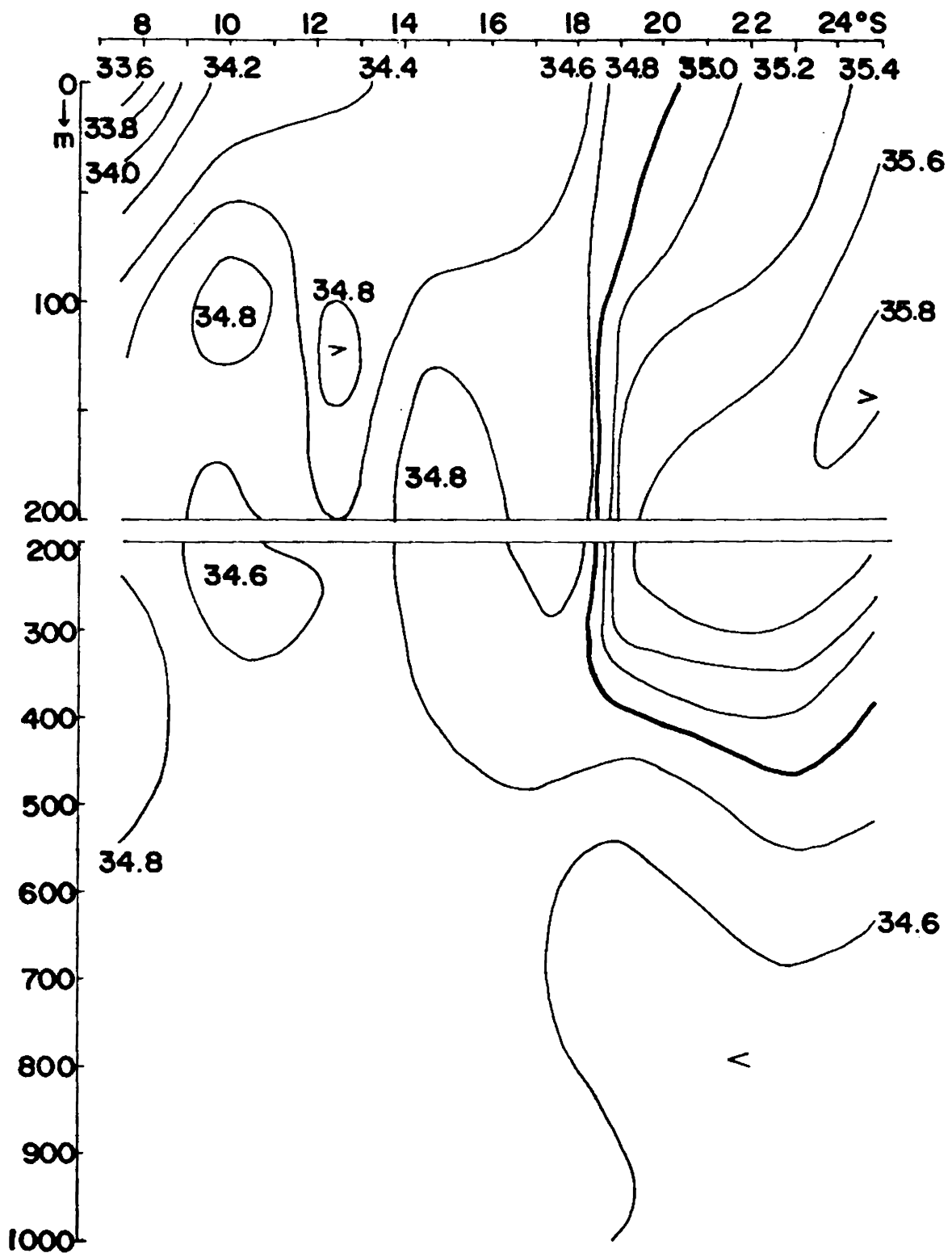
Fig. 3.10 — Vertical section of salinity along 106°E during Dec., 1960

The surface layer salinity decreases from west to east along the equator. Compared to the sections on the eastern side the vertical gradient of salinity is found to be lesser in the Western Indian Ocean. A high salinity core (>35.5‰.) centred around 100 m is seen in the Western Indian Ocean during March-April and the core values decreases eastward. A well defined tongue structure along the equator is seen in salinity distribution between 50 and 200 m depths. During the southwest monsoon period the high salinity core in the depth range of occurrence of Equatorial Undercurrent is not very prominent. The tongue structure noticed upto 85° E during March-April is limited to 79° E and the vertical extent is also limited to 150 m only. The section occupied during July-August along 53° E does not show wide salinity fluctuations in the surface layer. Well defined salinity core centred around 1° N at 100 m is observed. Another high salinity pocket (35.3‰.) is seen around 200 m depth at 4° N, which could be due to the southward spreading of the Arabian Sea Water. Between 100 - 150 m, the salinities are higher than the July-August months.

The salinity distribution along 85° E section in February shows a troughing of the isohalines in the top 100 m in the vicinity of the equator (Fig. 2.8). Surface salinity decreases from north to south with minimum values south of 4° S. South of 2° S, high salinity (>35‰.) water is

49

observed in the depth range of 100 to 150 m. Below 200 m the salinity variation is marginal. In the easternmost LUSIAD section (92° E) the surface sailinty is the lowest with values ranging from 33.8 to 34.2%.. A high salinity core of above 35.3%. is seen around 100 m which is associated with the Equatorial Undercurrent.

The salinity distributions along the various sections presented above shows that the presence of Equatorial Undercurrent is seasonally varying as derived from the presence of high salinity core. The feeble salinity maximum at 100 m during February centred around the equator could be attributed to the Equatorial Undercurrent, as the isotherms also show spreading at these depths. Similar features in salinity could be seen when the Equatorial Undercurrent is established (Swallow, 1964 and Taft and Knauss, 1967). The westward flow from Bay of Bengal could be seen as a low salinity water north of the equator which is brought in through the North Equatorial Current. While interpreting the property distribution on isanosteric surfaces, Taft (1963) and Sharma (1972) concluded that the Pacific Water incursion extends upto these longitudes. Low salinity water is seen, between 8° and 14° S, right from 110° E to 55° E south of the equator. The salinity structure is influenced by the presence of Red Sea Water below 500 m

depth in the Western Indian Ocean (Warren et al., 1966 and Wyrtki, 1971).

In the South Indian Ocean, it appears that the Subtropical High Salinity Water abruptly terminates around 13° -14° S at the boundary of South Equatorial Countercurrent along 65° E. Similar features are seen during December along the same longitude, but the presence of the higher salinity core attributable to Equatorial Undercurrent, is absent. The absence of the high salinity core during December and its presence during March may probably indicate that the Equatorial Undercurrent development takes place after December in the Indian Ocean as this is not seen during May (Fig. 3.4) around the same longitude. The low salinity water of Antarctic Intermediate origin shallows northward and is in line with the presentation of Tchernia et al. (1958) and Premchand and Sastry (1976).

The salinity distribution in the Central Indian Ocean (Fig. 3.5) shows the limited extent of the Subtropical High Salinity Water. The salinity distribution in the eastern side shows a prominent and consistent salinity minimum from surface to 800 m depth. This has been attributed to the presence of Pacific Water in the Indian Ocean (Wyrtki, 1958; Taft, 1963 and Sharma et al., 1978). This is seen in all the sections from 106° E to 53° E. In the Eastern Indian

Ocean the presence of the low salinity water which could be attributed to Antarctic Intermediate Water is seen only in few sections and its northern limit is also restricted to south of equator.

The salient features of the salinity distribution could thus be summarised. The surface salinity variation from north to south is more predominant in the Western Indian Ocean, while salinity gradients are lower compared to the Eastern Indian Ocean. The presence of Arabian Sea High Salinity Water could be seen at deeper levels during its southward spreading. The salinity maxima attributable to the Equatorial Undercurrent could be seen prominently along 65^oE during March and along 92^oE during April. No salinity maxima could be seen in the sections during July - August. Troughing of the isohalines near the equator is observed along 70^oE during November and along 84^oE in May, which can be attributed to the presence of the the Equatorial Jet.

The presence of Red Sea Water is felt only in the Western Indian Ocean and it spreads below the low salinity core of the Antarctic Intermediate Water which progressively is seen at shallower depths in the central region. The presence of low salinity Bay of Bengal Water seen in the Eastern Indian Ocean and also in the central and western regions north of the equator, when the North Equatorial Current is present.

52

Antarctic Intermediate Water, which shallows up during its northward spreading, is more easily identified in the central region. The Subtropical High Salinity Water could be seen around 200 m depth as a high salinity core, south of 14° S. The Subsurface High Salinity Water (a layer of decreasing salinity) is identified in the South Indian Ocean. The thickness of this gets reduced from south to north. The isohaline layer of Indian Ocean Equatorial Water along the equatorial belt is seen over all sections. The presence of the Pacific Water is seen all along the South Equatorial Current from 110° E to 55° E, generally in the latitudinal belt 8° to 14° S.

CHAPTER IV

TRANSEQUATORIAL   THERMOSTERIC ANOMALY DISTRIBUTION

In   the   absence of direct   current   measurements,   the
density   distribution has been invariably used to infer   the
mean flow characteristics in the oceans. Since the effect of
pressure is negligible,   thermosteric anomaly instead of the
commonly   used specific volume anomaly is used to   described
the   density   structure in the upper 1000 m (Montgomery   and
Wooster, 1954).

Using hydrographic station data the temperature against
depth   as   well   as against salinity were   plotted   on   T-S
diagrams with over printed thermosteric anomaly curves.   The
depths   of   the standard isanosteres were read out from   the
diagrams and using this,   vertical sections of   thermosteric
anomaly   were   prepared.   The transequatorial   sections   of
thermosteric anomaly help to identify the significant fluxes
at   different depths and also to delineate the westward   and
eastward   flow based on the slope of the   isanosteres.   The
salient   features   derived   from each vertical   section   of
thermosteric anomaly are presented in the following pages.

4.1   Fig.   4.1 shows the distribution of   thermosteric
anomaly   along 55°E   during February.   High   values   of
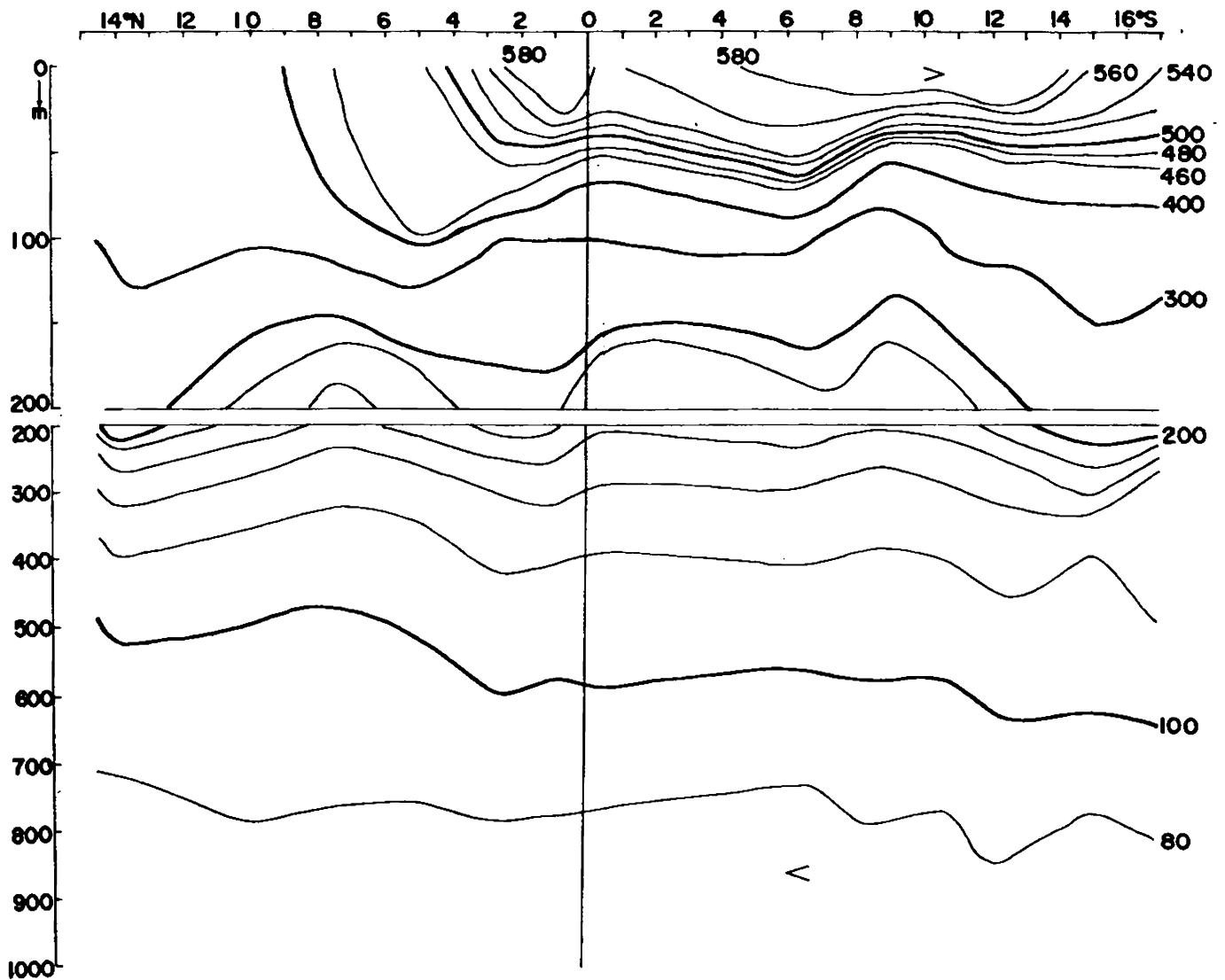
Fig. 4.1 — Vertical section of thermosteric anomaly along 55°E during February, 1964

thermosteric anomaly are seen between 3°N and equator associated with a salinity minimum layer. A similar feature is also observed south of the equator between 7° and 14°S. Spreading of the isanosteres, between 50 and 170 m, around the equator is seen (between 200 and 500 cl/t). Ridging of the isanosteres centred around 9°S which demarcates the northward extent of South Equatorial · Current is also observed along this section. Below 200 m, the isanosteres are found to generally follow the pattern of the isotherms (Fig. 2.1). Troughing of the isohalines, between 3° and 7°N, is seen between surface and 100 m, while an indication of opposing flow is noticed between 200 and 600 m depth (as seen by the ridging of isanosteres).

4.2   Ridging of the isanosteres in the upper 60 m, between 4°N and 3°S, indicates westerly flow (North Equatorial Current) in this region between 70 and 200 m. The spreading of the isanosteres (460 and 180 cl/t) is consistent with the spreading observed in the thermocline. While the isanosteres above 400 cl/t ridge at the equator, the ones below exhibit troughing, which is typical of sections indicating an Equatorial Undercurrent. A high salinity core centred around 1°N at 110 m depth corroborates the inference.
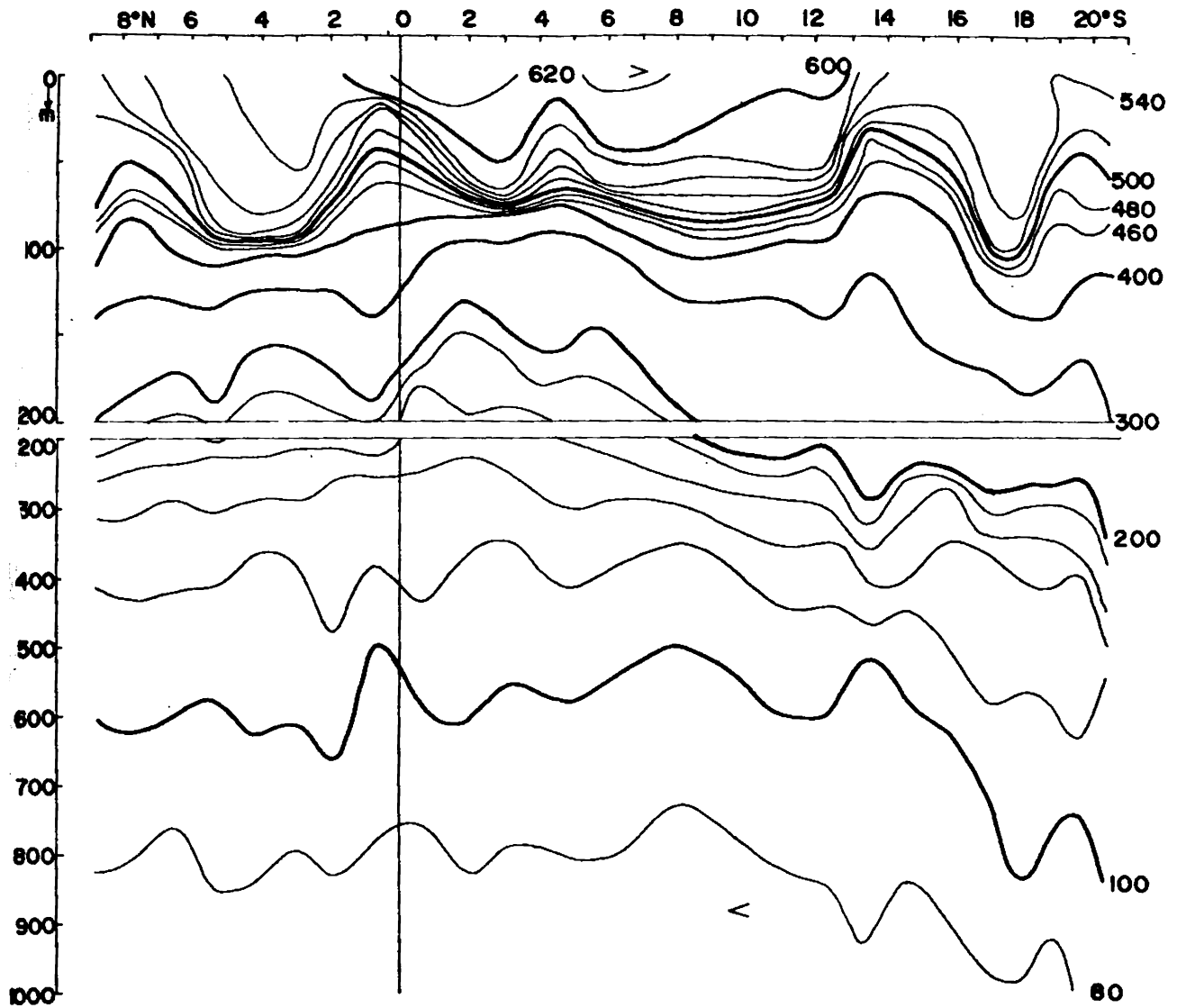
Fig. 4.2 — Vertical section of thermosteric anomaly along 65°E during March, 1973

The isanosteres below 200 cl/t are more or less level in the northern hemisphere, while they slope down to the south in the southern hemisphere. Ridging of the isanosteres above 400 cl/t is observed at 8° N, 4° S and between 13° and 16° S. Thus in the surface layers westward flow could be deduced from 5° N to about 20° S which becomes deeper towards south. Embedded in this westward flow, an easterly flow extending to about 120 m, between 18° and 19° S, probably associated with the Tropical Countercurrent, and a still shallower easterly flow roughly between 12° and 13° S, associated with the South Equatorial Countercurrent are seen in the section.

4.3   The thermosteric anomaly distribution, south of the equator along 65° E is given in Fig. 4.3. Troughing of the isanosteres is observed around 3° S, 6° S, 12° S and 15° S and ridging is observed at 5° S, 10° S and 13° S. Easterly flow, between 3° and 5° S, is possibly due to the northward shift of the Equatorial Countercurrent during this period. The South Equatorial Current is observed south of 5° S, with counter flows around 10° S and 13° S (South Equatorial Countercurrent) in the surface layers. The Tropical Countercurrent, observed south of 18° S during March, appears to have been shifted to 15° to 16° S during December.

4.4   Fig. 4.4 shows the thermosteric anomaly distribution along 67° 30'E, during April-May. Spreading of
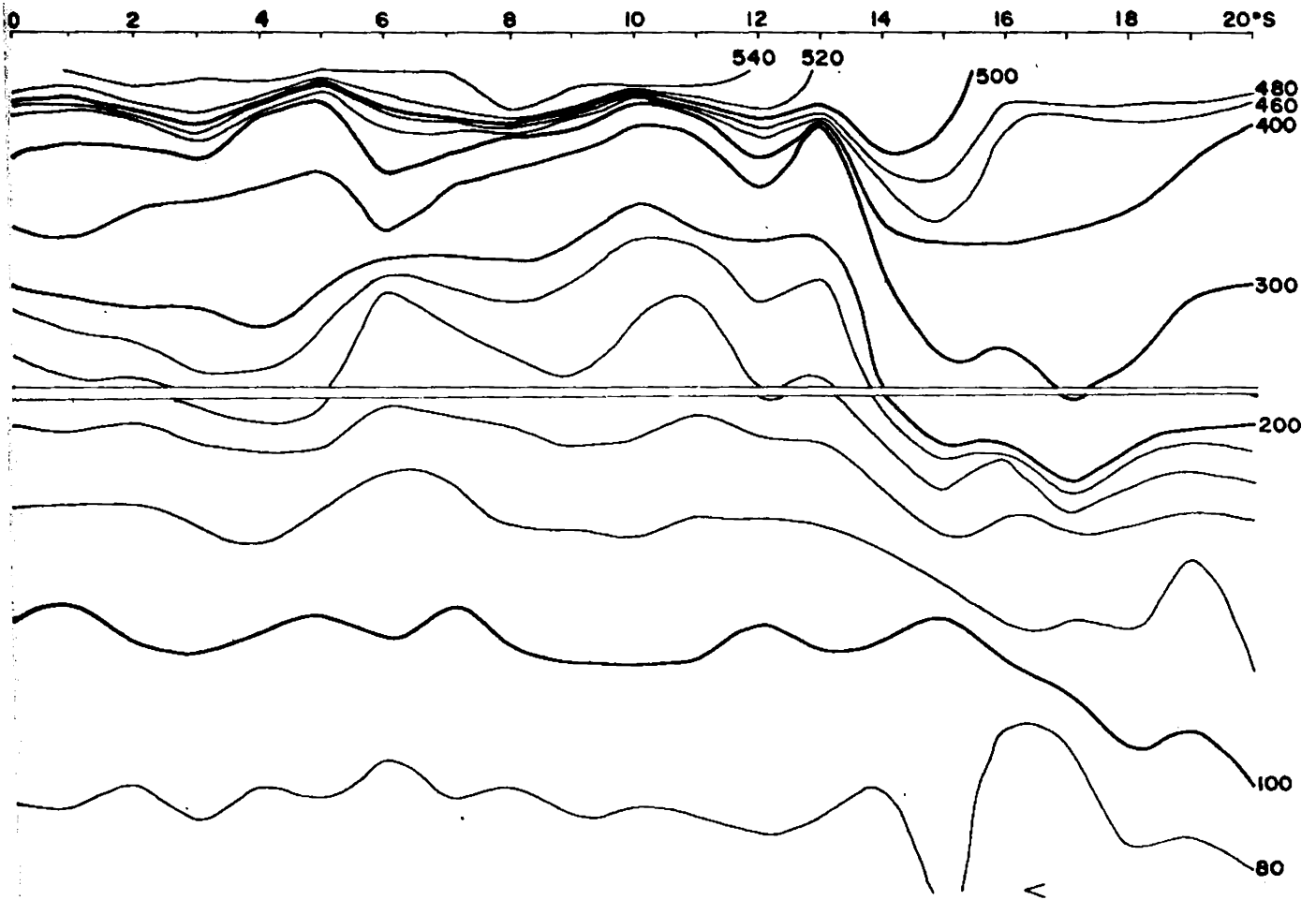
Fig. 4.3 — Vertical section of thermosteric anomaly along 65° E during December, 1976
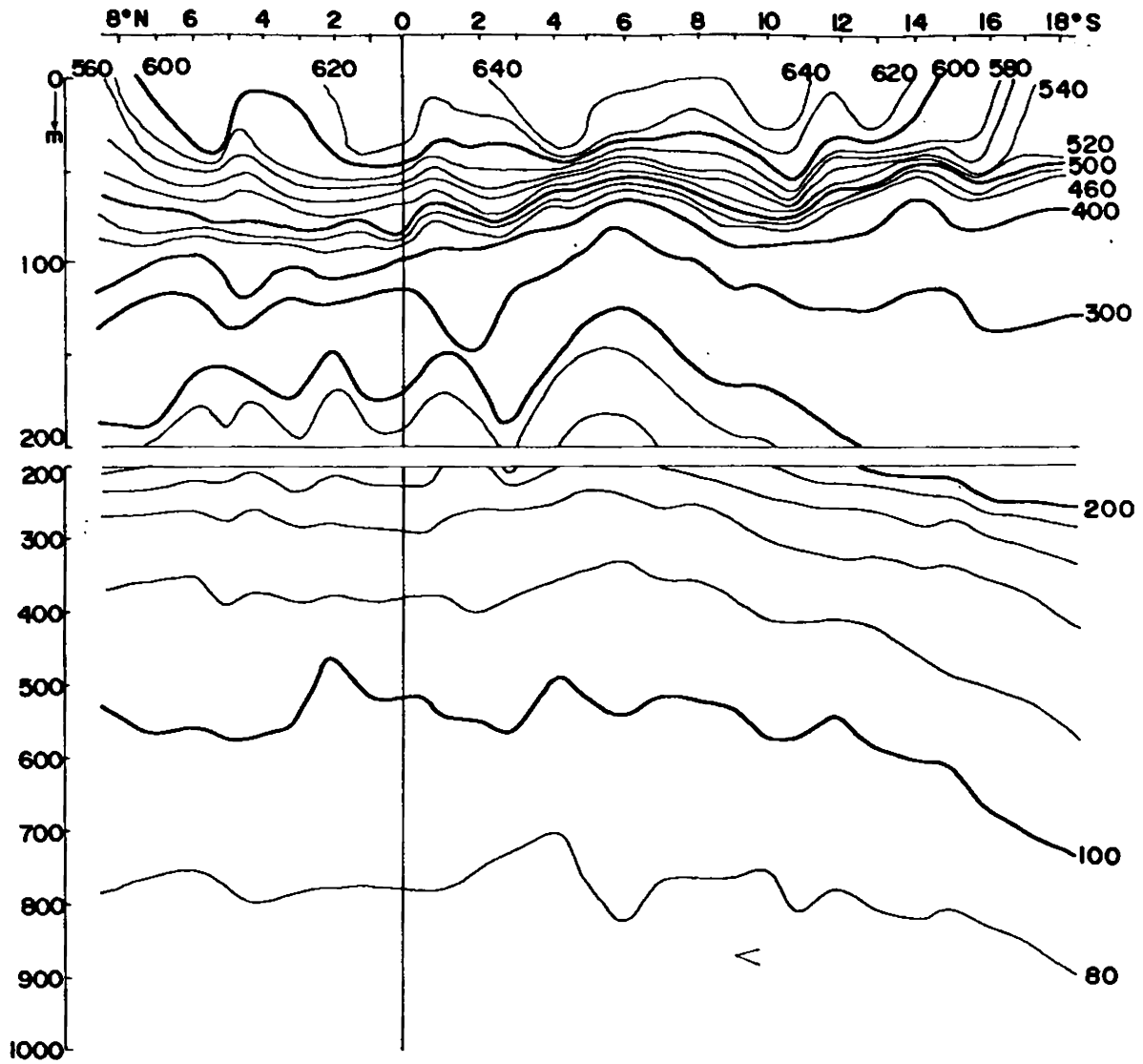
Fig. 4.4 — Vertical section of thermosteric anomaly along 67°30'E during April - May, 1964

the isanosteres is observed around $3°$S, and intense eastward flow may be deduced to occur between $3°$ and $6°$S at depths between 40 and 100 m. Strong easterly flow is seen to occur, between $11°$ and $14°$S, in the surface layers and also between $16°$ and $17°$S possibly due to the presence of the South Equatorial Countercurrent and Tropical Countercurrent respectively across this transect.

The North Equatorial Current seems to be confined between $9°$ and $2°$N, with a strong surface easterly flow centred around $4°$N. Troughing is noticed between $2°$N and $3°$S indicating westward flow. Strong easterly flow centred around $5°$S is also seen. The isanosteres slope down from $6°$ to $11°$S betwen 40 and 80 m, beyond which they trough upto $14°$S. Below 80 m, the isanosteres upto 120 cl/t generally slope down towards south indicating the broad South Equatorial Current. The troughing of the isanosteres between surface and 80 m possibly could be linked to the Tropical Countercurrent which occurs in the same latitudinal belt as in December (Fig. 3.3). In the upper 60 m ridging is observed around $12°$S, which is related to the South Equatorial Countercurrent.

4.5 In the section along $70°$E, covered during the fall transition period (Fig. 4.5), troughing of the isanosteres in the vicinity of the equator is observed in the surface layers, indicating the presence of the Equatorial Jet.
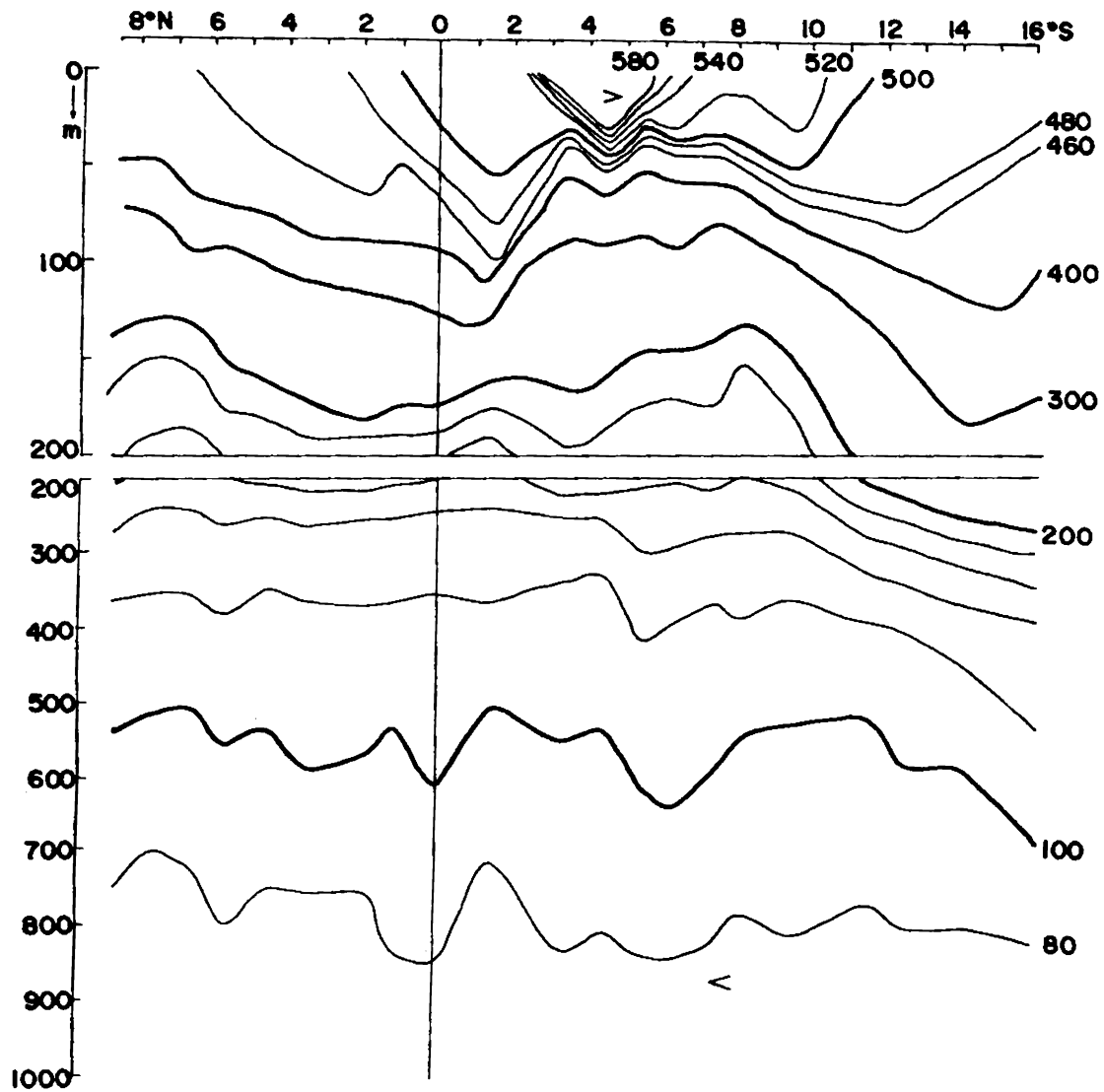
Fig. 4.5 _ Vertical section of thermosteric anomaly along 70°E during Oct _ Nov., 1970

Easterly flow is intense in the surface layers above 100 m depth between 1° and 3° S. No appreciable slope of the isanosteres below 200 cl/t is observed north of the equator. The general flow is westerly in the southern hemisphere which intensifies south of 8° S. The ridging of the isanosteres at 13° S, which is a characteristic feature associated with the South Equatorial Countercurrent, is seen along this section.

4.6   North of 6° S, the thermosteric anomaly at the surface along 78° E covered during December (Fig. 4.6) is comparitively less ($<$560 cl/t), while south of this latitude the surface thermosteric anomaly observed is more than 600 cl/t mainly due to the presence of the low salinity water in the surface layers (Fig. 3.6). Ridging of isanosteres above 200 cl/t around 5° S suggests opposing flows on either side which is consistent with the thermal structure.

4.7   The distribution of thermosteric anomaly along 83° E during December-January is shown in Fig. 4.7. In general, the thermosteric anomaly distribution follows the temperature distribution along this section. South of about 13° S the isanosteres above 200 cl/t slope upto 7° S indicating the Equatorial Countercurrent. South of 7° S, above 100 cl/t the isanosteres slope down towards south indicating a westward flow (South Equatorial Current).
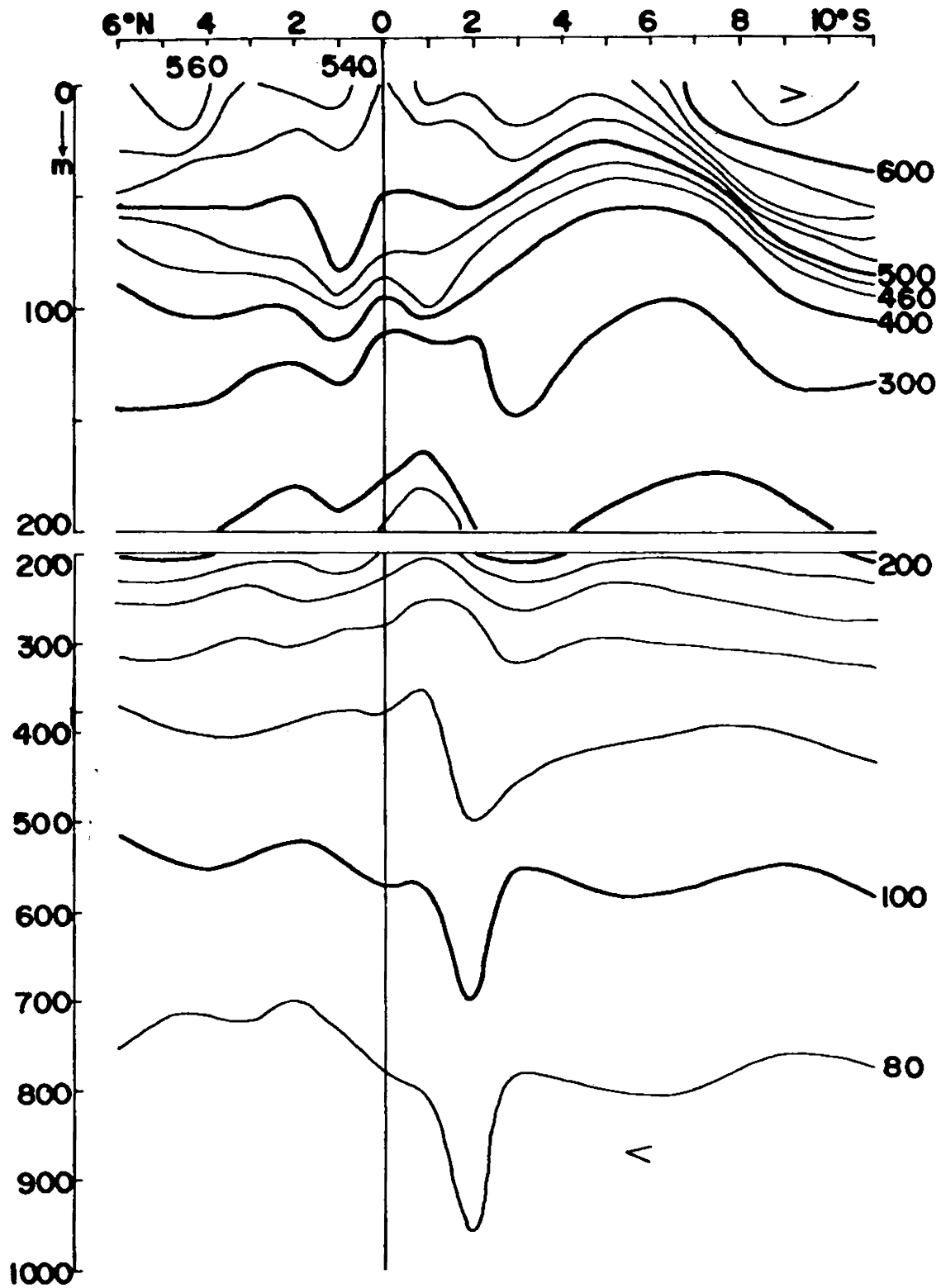
Fig.4.6—Vertical section of thermosteric anomaly along 78°E
during December, 1962
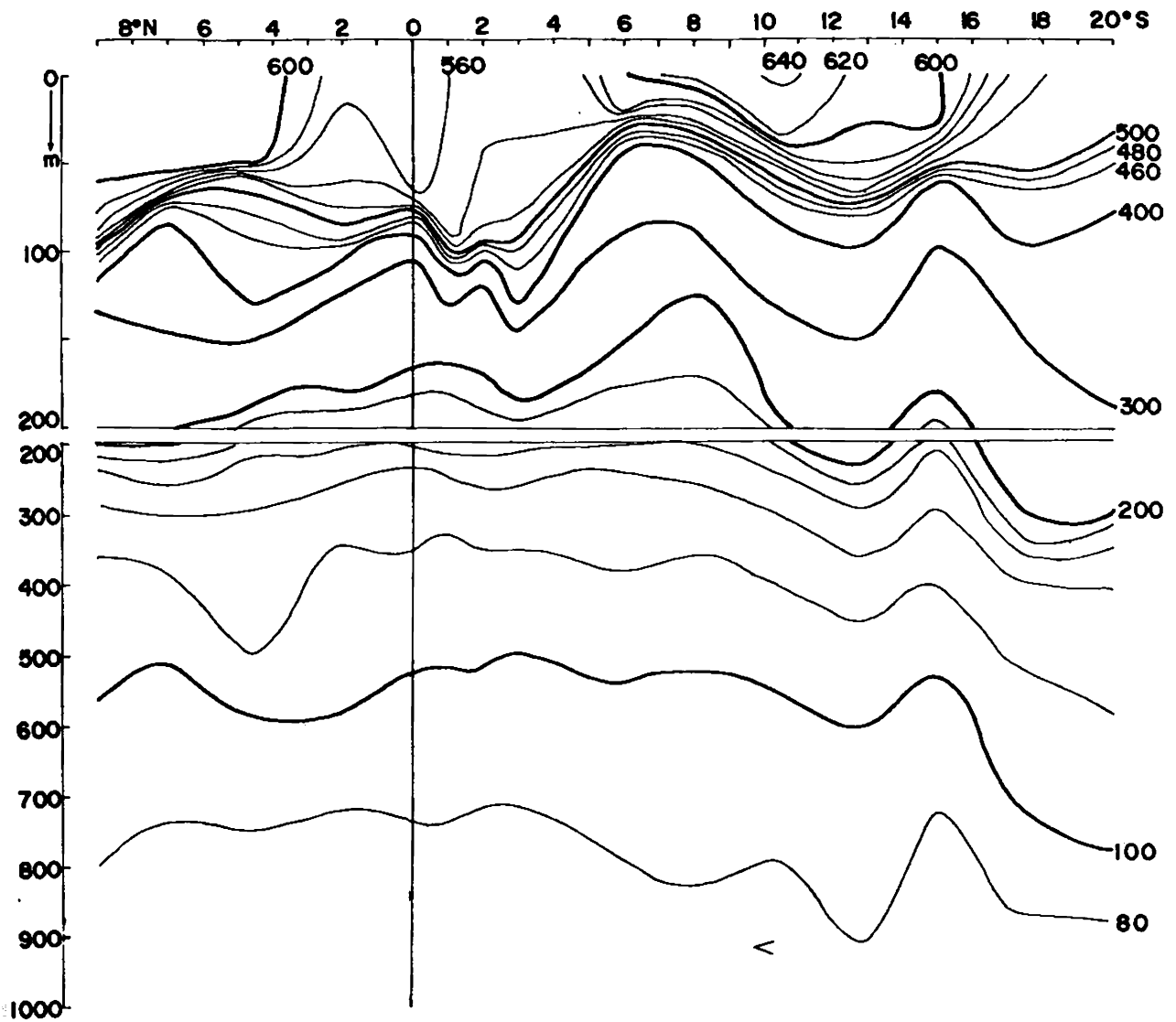
Fig. 4.7 _ Vertical section of thermosteric anomaly along 83°E during January, 1961

Below 500 cl/t the ridging of isanosteres centred around 15°S is possibly associated with the South Equatorial Countercurrent which is found to have been shifted slightly southward compared to the other sections (Figs. 4.2 and 4.3).

4.8   The striking feature observed in the section along 84°E during May (Fig. 4.8) is the troughing of the isanosteres between 600 and 120 cl/t along with pinching in the vicinity of the equator and spreading on either side. This obviously corresponds to strong easterly flow in the surface layers associated with the Equatorial Jet. The isanosteres generally follow the temperature distribution pattern (Fig. 2.8).

4.9   The peculiar feature observed in this section along 100°E during July (Fig. 4.9) in the Eastern Indian Ocean is that the isanosteres trough at around 13°S more conspicuously even in the deeper layers. Ridging of the isanosteres is observed around 6°S, 11°S and 16°S while troughing around 10°S, 13°S and 18°S is noticed. This suggests alternating eastward and westward flows across this section.

4.10   The distribution of thermosteric anomaly along 106°E covered during December is shown in Fig. 4.10. The isanosteres above 300 cl/t dip down sharply to the north
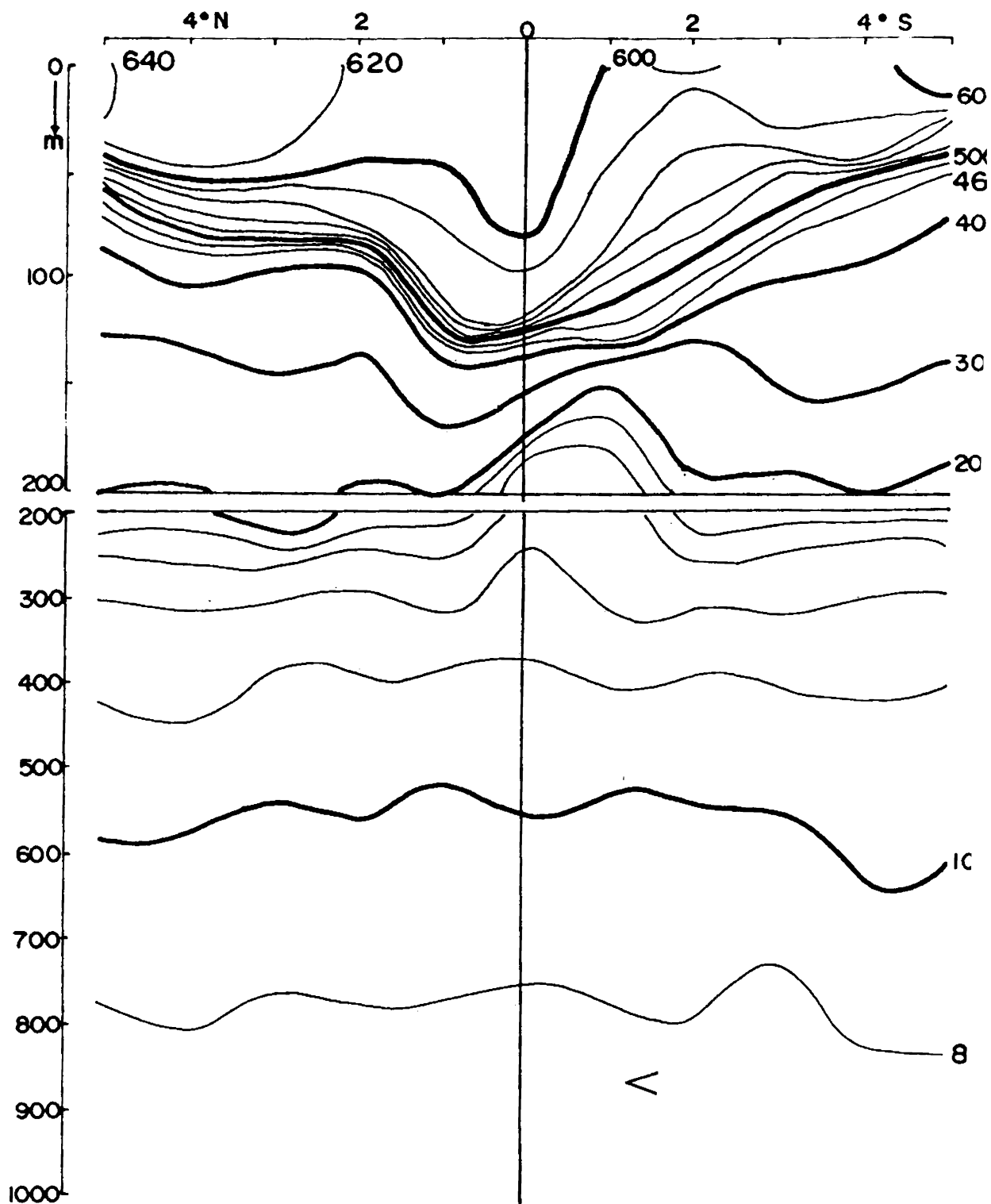
Fig. 4.8 — Vertical section of thermosteric anomaly along 84°E during May, 1964.
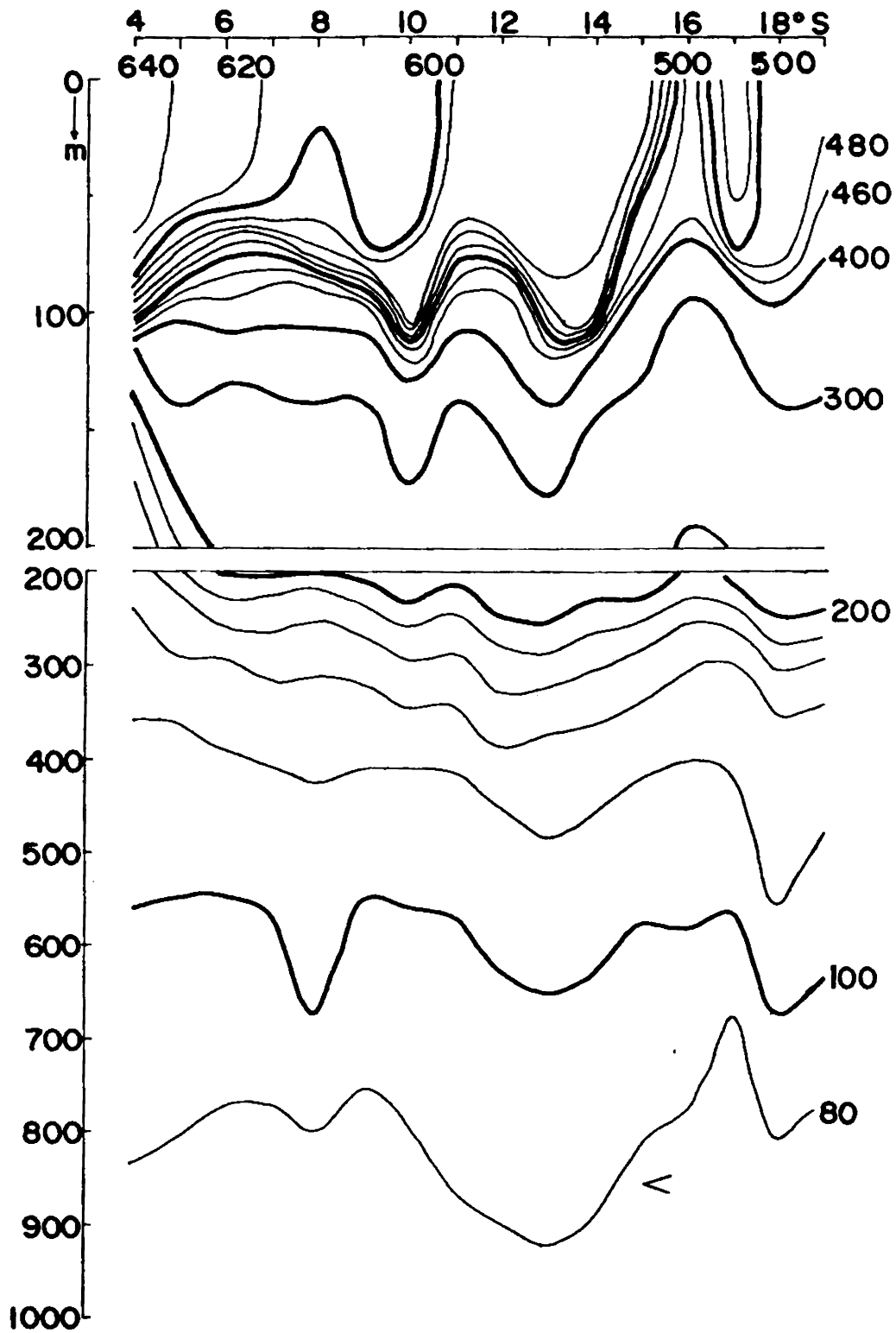
Fig. 4.9 — Vertical section of thermosteric anomaly along
100°E during July, 1962
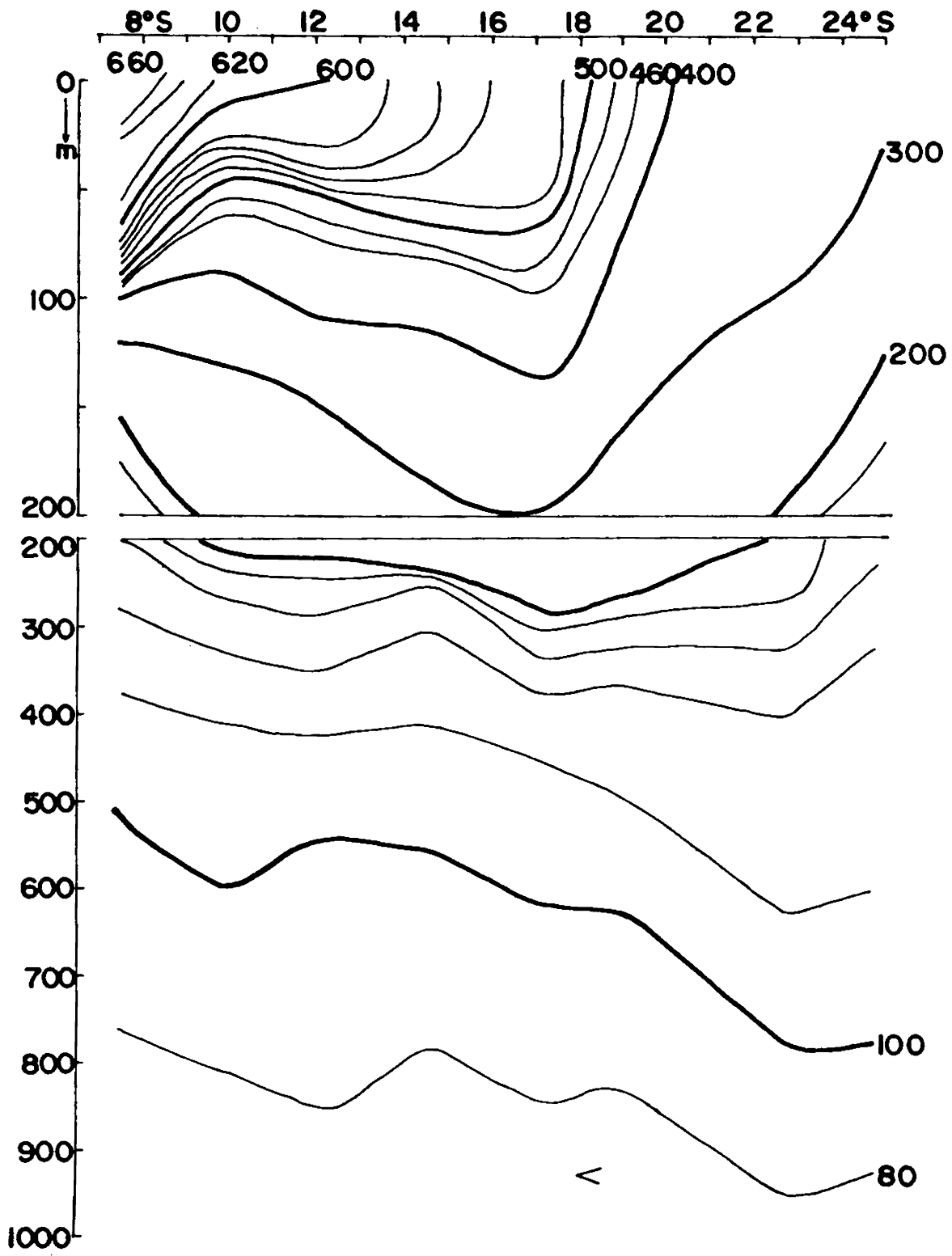
Fig. 4.10 — Vertical section of thermosteric anomaly along 106° E during December, 1960

implying a strong easterly flow extending to about 100 m between 7° and 10° S.

Below this easterly flow at the surface, the isanosteres slope down to the south indicating a general westward flow which is relatively stronger south of 15° S.

4.11   The salient features of the distribution of thermosteric anomaly for the LUSIAD sections are summarised below. In the section covered during July-August along 53° E, an easterly flow above 120 cl/t north of 3° N is seen. The isanosteres in the thermocline exhibit spreading similar to that observed in the temperature sections by which the presence of the Equatorial Undercurrent may be inferred clearly along 61° E and 92° E sections taken during March and April respectively. The features are more prominent in the 92° E section. In the 85° E section easterly flow in the vicinity of the equator is evident from the troughing of the isanosteres. Pinching of the isanosteres with spreading on either side similar to that observed along 84° E is also noticed. This feature, is not as conspicuous as that observed during the transition period when the Equatorial Jet is reportedly present (Wyrtki, 1973b).

The distribution of thermosteric anomaly above 200 cl/t shows both seasonal and spatial variability. In the Western Indian Ocean during northeast monsoon period along 55° E the

spreading of the isanosteres associated with Equatorial Undercurrent is observed. During March along 65° E this feature is more prominently seen (Fig. 4.2). In the Eastern Indian Ocean, very strong features associated with the Equatorial Undercurrent are seen along 92° E. Taft and Knauss (1967) have concluded based on the above feature that the Equatorial Undercurrent generates in the east and propagates towards west contrary to reports from direct current measurement by Swallow (1964) and the inferences drawn from the distribution of physical properties by Sharma (1968), Muraleedharan (1984) and Muraleedharan et al. (1980). Absence of the characteristic features associated with the Equatorial Undercurrent in certain sections taken during the northeast monsoon (Figs. 4.6 and 4.7) points out to its possible interannual variability. The strong eastward Equatorial Jet present during the transition period between 2° N and 2° S (Wyrtki, 1973b and Muraleedharan, 1984) is present along 70° E during October-November and along 84° E during May. Reverdin et al. (1983) reported that the Equatorial Jet is stronger during October-November transition period. A strong 2 cycle/year variation in the zonal winds with maximum in the transition months which drive the zonal jets in the upper ocean was observed by Mc Phaden (1982). The eastward flow seems to be stronger across the 84° E section than along 70° E. This may be due to the fact that compared to the west, the Equatorial Jet is

61

stronger in the east. The Equatorial Countercurrent is present along section 65°E (Fig. 4.3) and along 83°E (Fig. 4.7) between 3° and 7°S. This agrees well with the observations of Narendran Nair (1983).

The South Equatorial Current is the most permanent feature observed in all sections inferred from the sloping down of the isanosteres, south of the equator. The flow seems to extend to deeper layers in the south and shows seasonal variability in its strength and northward extent (Sharma, 1976b). The northern limit of the South Equatorial Current is found between 5° and 10°S. Compared to the 65°E section covered during the southwest monsoon (Sharma, 1976b), the two sections presented here for the northeast monsoon (Figs. 4.2 and 4.3) along this longitude show a southward shift of South Equatorial Current during this season. This observation is in agreement with similar features observed in the Atlantic and Pacific (Tcherniya, 1980).

The South Equatorial Countercurrent along 65°E centred around 13°S in the South Indian Ocean was first reported by Sharma (1976b), which is analogous to the one found by Reid (1959, 1961, 1964a,b and 1965) in the Pacific and in the Atlantic by Wooster (1961) and Tsuchiya (1968). The South Equatorial Countercurrent which is mainly confined to the surface layers could be identified in sections east of 60°E

except along the 70°E transect (Fig. 4.5). The South Equatorial Countercurrent, it appears, is shifted southwards in the Eastern Indian Ocean. The two eastern most sections are quite different in that both exhibit signatures of alternating flow evident from the series of ridging and troughing along these sections.

The Tropical Countercurrent in the Indian Ocean is synonymous to the Subtropical Countercurrent observed in the Pacific by Uda and Hasunuma (1969) and by Voorhis and Hersey (1964) in the Atlantic. The associated thermal feature of this current is a thermal front in the tropics and this could be identified along the easternmost section (Fig. 2.10). Sharma (1976b) has reported the presence of the Tropical Countercurrent round the year between 22° and 26°S, while most of the present sections show the presence of surface eastward flow generally between 18° and 20°S.

Based on the distribution of the water properties, the approximate limits of the different currents in the area of study are made and are presented in Table II. The North Equatorial Current is seen between 9° and 2°N during the northeast monsoon. The North Equatorial Current appears to have been replaced by the Monsoon Current along 67°30¢E and this appears north of the equator upto 5°N. But during southwest monsoon period the Monsoon Current seems to extend further south upto 5°S.

Table II : Major current boundaries delineated across different transequatorial sections.

Section	NEC	Monsoon Current	EUC	Eq. Jet	ECC	SEC	SECC	TCC	Pac.Water incursion
FEB 55E	>300 5N-0	- -	200-500 2N-2S	-	-	>80 S of 9S	- -	- -	>300 9S-15S
MAR 65E	>300 4N-0	-	180-400 3N-2S	-	>300 3S-5S	>80 5S-12S 15S-20S	>300 12S-14S	>300 18S-20S	>300 5S-13S
DEC 65E	-	-	200-400 0-1S	-	>300 3S-5S	>80 5S-8S 10S-12S 14S-20S	>160 12S-13S	>300 14S-20S	>300 10S-13S
MAY 67,30'E	>350 9N-5N	>350 5N-0	-	-	>300 5S-8S	>80 8S-11S 12S-18S	>400 11S-12S	>400 15S-18S	>400 8S-12S
NOV 70E	-	>200 9N-2N	-	>300 1N-2S	>300 2S-6S	>80 6S-14S	-	-	>7S-11S
DEC 78E	>500 6N-2N	-	-	-	>300 0-5S	>80 6S-11S	-	-	>300 6S-11S
DEC-JAN 83E	>200 9N-2N	-	-	-	>300 7S-1S 15S-20S	>80 7S-13S	>300 13S-15S	>400 18S-20S	>300 7S-13S
MAY 84E	-	-	-	>200 2N-2S	-	-	-	-	-
JULY 100E	-	-	-	-	>300 4S-7S	7S-10S 11S-10S 16S-19S	>200 10S-11S 12S-13S	>400 15S-16S	>200 8S-14S
DEC 106E	-	-	-	-	>300 7S-10S	10S-25S	-	>400 17S-25S	>200 8S-16S
AUG 53E	-	>300 5N-4S	-	-	-	-	-	-	-
MAY 53E	-	>300 5N-4S	-	-	-	-	-	-	-
MAR 61E	>120 2N-5N	-	>200-400 2N-2S	-	>300 2S-5S	-	-	-	-
AUG 62,20'E	-	>200 5N-5S	-	-	-	-	-	-	-
AUG-SEP 79	>300 5N-3N	>300 2N-5S	-	-	-	-	-	-	-
FEB 85	400-160 2N-5N	-	-	-	-	-	-	-	-
...	>200	-	200-400	-	>200cl/t	-			-

The Equatorial Undercurrent is found between 3^oN and 2^oS in the present sections between 200 and 400 cl/t. The Equatorial Undercurrent appears to have been confined to the equator and 1^oS along 65^oE during December, while it seems to intensify during March. The Equatorial Jet is noticed between 2^oN and 2^oS across 70^oE during the fall transition and along 84^oE during May. The Equatorial Countercurrent is noticed between 3° and 7^oS during northeast monsoon. The width of the Equatorial Countercurrent increases from west to east and is shifted southward.

The South Equatorial Current seems to be the most consistent feature of the Equatorial Indian Ocean circulation. It is generally found as a broad westward flow south of 10^oS and its northern boundary is found to shift northwards in the Western Indian Ocean. The South Equatorial Countercurrent could be identified across all sections except 70^oE, generally between 12° and 15^oS with seasonal variations in its position. The Tropical Countercurrent is observed in all the sections except at 70^oE south of 15^oS.

With the identification of the different current regions, an attempt to quantify the fluxes is made in the following chapter. An attempt is also made to determine the magnitude of the influx of Pacific Ocean Water into the Indian Ocean by fixing approximate boundaries along different sections.

CHAPTER V

ZONAL FLUX DISTRIBUTION

The zonal fluxes have been calculated across available transequatorial sections extending from 5° N to 20° S covering the Western, Central and Eastern Indian Ocean. Studies on the zonal mass transport in the Indian Ocean are few and confined to particular currents, region or season (Wyrtki, 1973a; Swallow, 1964 and Muraleedharan, 1984). For the first time, an attempt is made to estimate zonal mass transport in the upper 1000 m.

The computed fluxes are displayed on temperature-salinity diagrams. Characteristic classes have been defined by thermosteric anomaly and salinity. The flux through each quadrangle defined by standard isanosteres and whole degrees of latitude is partitioned into classes bounded by each 0.2%. in salinity. The standard (or chosen) isanosteres defining the quadrangles are spaced at intervals of 20 cl/t to 100 cl/t. Therefore, to gain uniform classes of convenient size, the fluxes have been combined or divided, as the case may, be into classes with an interval of 50 cl/t. The east (+ve) and west (-ve) fluxes are separately displayed for each characteristic class. For easy comparison between sections, the fluxes have been summed up for every 5° latitudinal belt and presented on separate

diagrams.   Sums   of   westward   and   eastward   fluxes   by
thermosteric anomaly are shown along the top of each figure,
and   those of salinity on the right hand   side.   The   total
westward and eastward fluxes are shown on the top right hand
corner of the diagram.

The   fewest frequencies that enclose at least 50%   and
75% of the westward flux are demarcated by heavy line and
dashed line boundaries in the figures respectively while for
the eastward flux the symbols (●) and (◊) respectively have
been   used.   The   salinity   and   thermosteric   anomaly
characteristic   of each class is taken as the mean salinity
and thermosteric anomaly of the class.   Besides giving   the
bivariate   distribution   of   the   fluxes   in   salinity   and
thermosteric   anomaly,   these   diagrams   also   give   the
temperature   variation   as   the   isanosteric   surfaces   are
dependant only on temperature and salinity.

As mentioned in Chapter I, the magnitude of the fluxes
in diagrams in the 5 degree latitudinal belt immediately   on
either   side of the equator may be interpreted with caution,
since   in   the vicinity of the equator the method   tends   to
overestimate the fluxes. However, it is possible to compare
the   fluxes obtained in this latitudinal belt for   different
sections and to determine its variability in both space   and
time. The zonal flux distributions across different sections

66

for various latitudinal belts are presented in the following

sections. Keeping in view the boundaries of the various

currents in the region of study, presented in Chapter IV,

the approximate total transports of the various currents

have been estimated and presented along with the flux

distribution.

5.1   The section along 55° E extends from 14° N to 17° S.
North of 10° N the fluxes are characterised by salinities

ranging from 35.2 to 35.8%.. The interesting feature noted

across this belt between 14° and 10° N (Fig. 5.1.1) is that

75% of the total westward flux (4.8 km^3/hr) occurs above 150

cl/t having a mean salinity of 35.3%., whereas, 75% of the

total eastward flux of 16.6 km^3/hr occurs below the 150 cl/t

surface in the salinity range 35.4 to 35.8%.. 50% of the

eastward flux comprising of two frequencies occurs below 100

cl/t with the primary mode accounting for about 47% of the

total eastward flux with a mean salinity of 35.5%..

In contrast to the belt north of 10° N, the westward

flux between 10° and 5° N occur below 200 cl/t (Fig. 5.1.2)

while the eastward flux with a distinct mode at 450 cl/t

comprises of higher saline waters of Arabian Sea origin

ranging from 35.2 to 35.5%.. Above 300 cl/t, westward flux

is absent, while the bulk of the eastward flux (13.7 km^3/hr)

characterised by higher salinity could be due to the

clockwise gyral circulation observed in this area by Bruce

67

Fig. 5.1.1 _ Zonal fluxes across 55° E between 14°N and 10°N during February, 1964

- 4.84
16.61

- 4.55
2.53
- 0.29
10.27
3.613

34 %.

36 %.

36 %.

30°C

25°C

20°C

- 1.65
- 0.11
- 0.18
0.08

- 1.65
- 0.11
0.16
0.07

15°C

- 1.76
0.26

- 1.15
- 0.05
0.47
0.003

- 1.76
0.25

- 0.10
- 0.14
- 0.02
1.54
0.49

10°C

1.39
7.90
3.17

5°C

- 1.20
0.47

- 0.12
3.17
12.46

0 cl/t

550
500
450
400
350
300
250
200
150
100
50
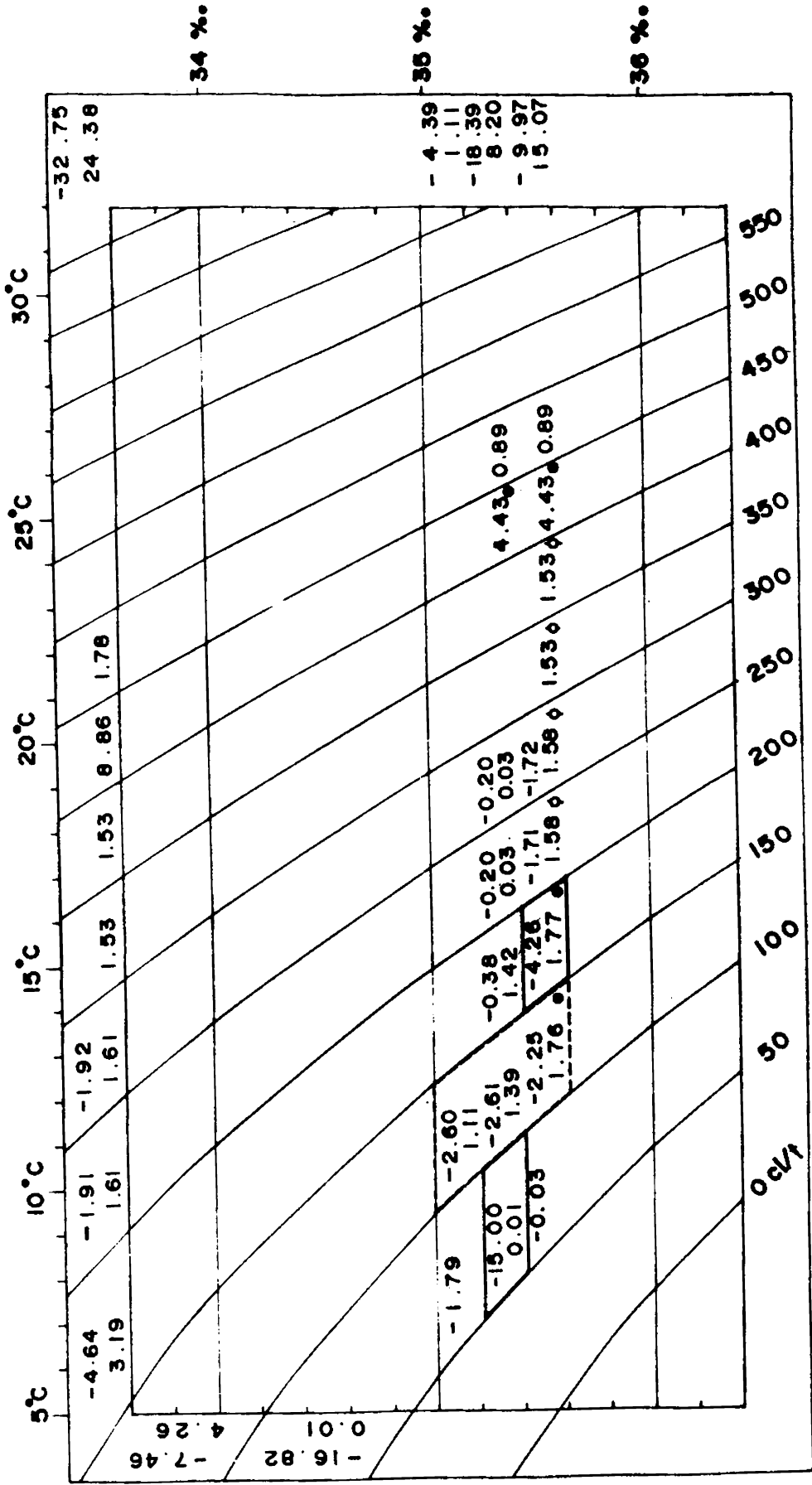
Fig. 5.1.2 – Zonal fluxes across 55° E between 10°N and 5°N during February, 1964

(1979). Compared to the previous belt, the total westward flux is higher (32.7 km^3/hr) and a marginal increase in the total eastward flux (24.4 km^3/hr) is also seen. 50% of the westward flow is confined to 2 frequencies, both below 200 cl/t, while 75% of the westward flux comprises of 5 frequencies all below 200 cl/t. The eastward fluxes exhibit a lot of heterogeneity. Two frequencies at 125 and 175 cl/t with a salinity of 35.5%. along with the mode centered around 450 cl/t constitute 50% of the total eastward flow. 75% of the flux is distributed over 8 frequencies over a wide range in thermosteric anomaly (150 to 450 cl/t).

Compared to the eastward flux, the westward flux is distributed over a wide range of frequencies, between equator and 5°N (Fig. 5.1.3). The westward flow is 203.5 km^3/hr. The primary mode occurs at 175 cl/t with the next four modes occurring between 200 and 300 cl/t having salinity between 35 and 35.4 %.. Above 300 cl/t the total westward transport of 69.3 km^3/hr is obviously due to the presence of the North Equatorial Current in this belt.

Over 50% of the eastward flux is made up of 2 frequencies and 4 frequencies contribute to over 75% of the flux. The primary mode accounts for over 44% of the flux occurring at 75 cl/t with a mean salinity of 35.1%.. The secondary mode occurs at 175 cl/t having a salinity of
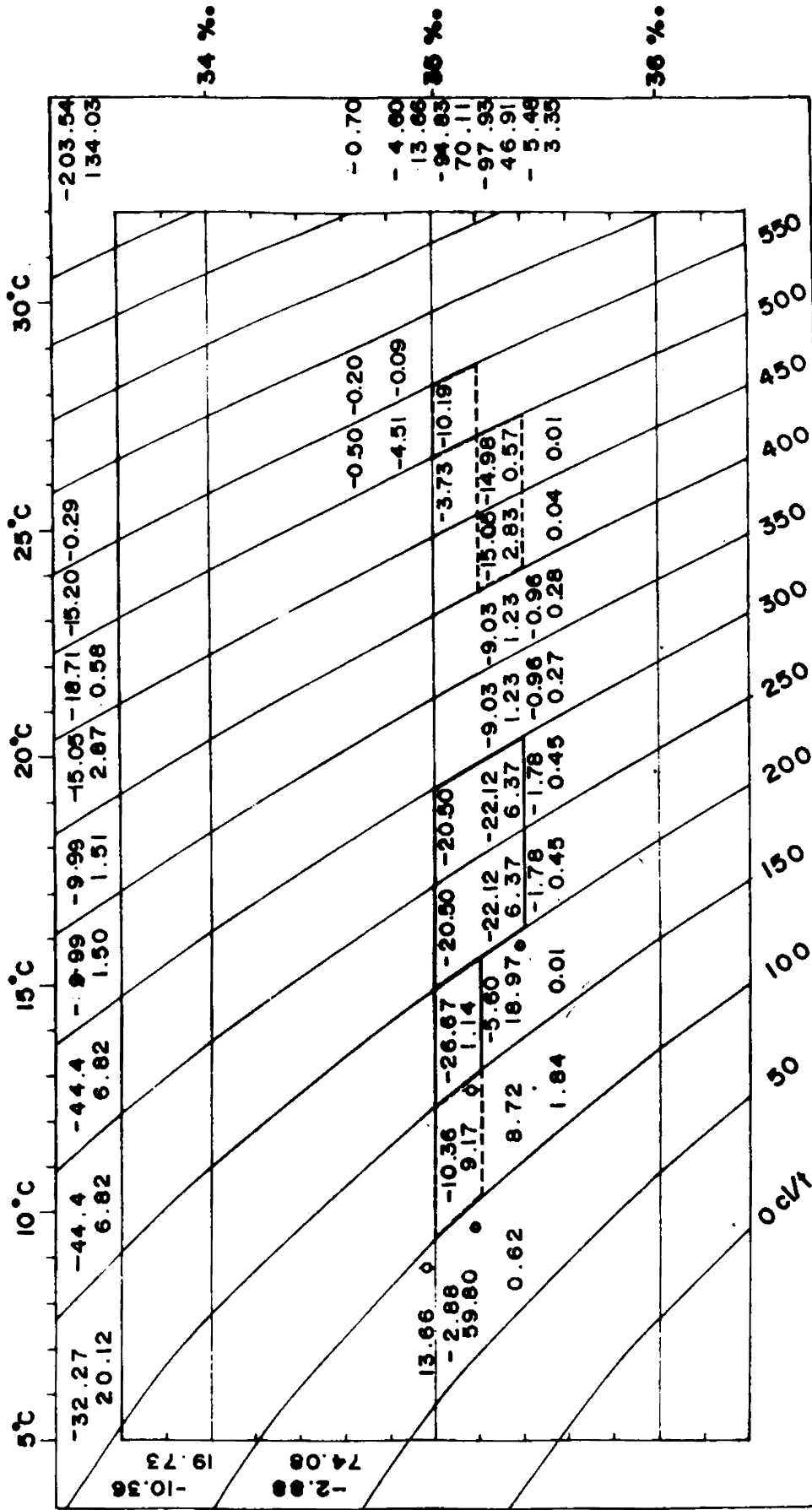
Fig - 5.1.3_Zonal fluxes across 55°E between 5°N and 0° during February, 1964

35.3‰.. 75% of the flux occurs below 200 cl/t. The eastward flux observed between 200 and 500 cl/t across this belt is partly due to the contribution of the Equatorial Undercurrent inferred from the property distributions between 2°N and 2°S.

The total westward flux across 0° to 5°S is 221 km^3/hr (Fig.5.1.4). The primary mode at 75 cl/t with salinity 35.1‰. accounts for over 75% of the flow. The flux distribution is more or less homogeneous with maximum westward flux occurring in waters with salinity greater than 35‰..

The eastward flux amounts to 87 km^3/hr. Three frequencies, all below 150 cl/t contribute to over 50% of the flow. 75% of the flow is distributed over 7 frequencies and the eastward flow is mainly confined to the layers below 450 cl/t. The primary mode contributing over 27% of the flux occurs at 75 cl/t having a mean salinity of 34.9‰.. The frequencies having a mean salinity of 35.3‰. occurring between 200 and 500 cl/t is attributed to the Equatorial Undercurrent. The total transport of the Equatorial Undercurrent estimated across 55°E is 33.9 km^3/hr.

The flux across 5° - 10°S is shown in Fig. 5.1.5. The westward flux is mainly constituted of homogeneous water of mean salinity 34.9‰.. The primary and secondary modes occur
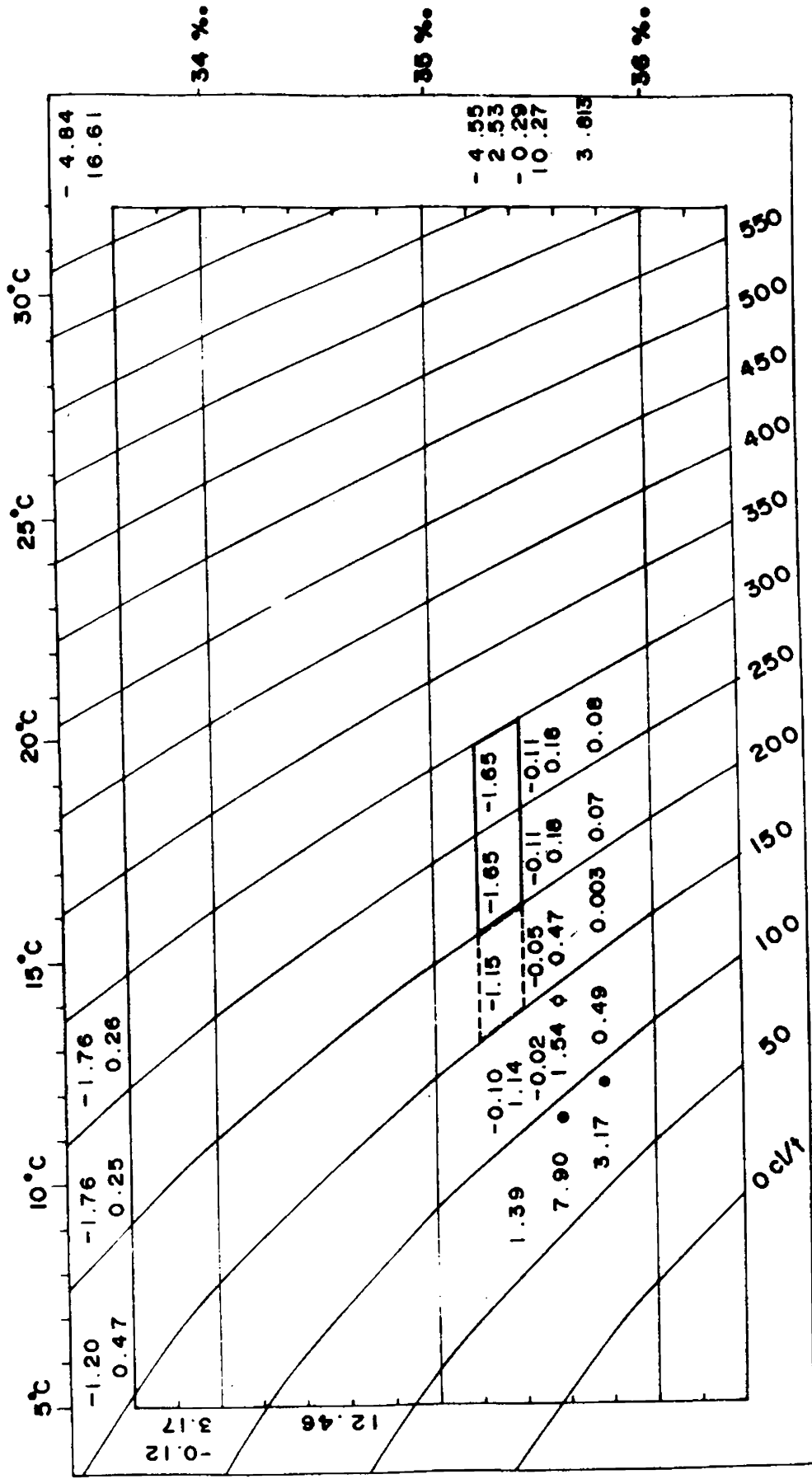
Fig. 5.1.4 - Zonal fluxes across 55°E between 0° and 5°S during February, 1964
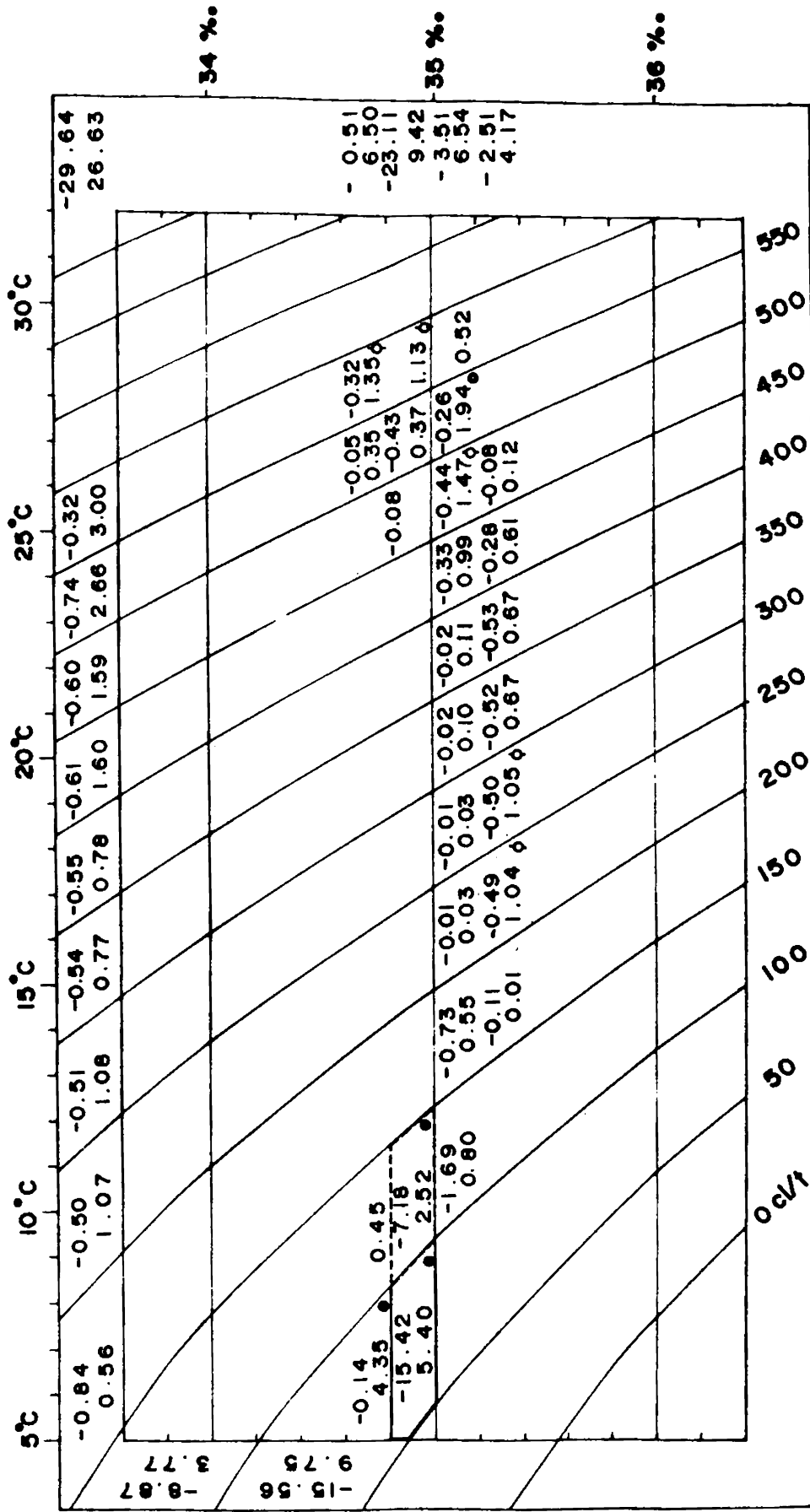
Fig. 5.1.5.- Zonal fluxes across 55°E between 5°S and 10°S during February, 1964

at 75 and 125 cl/t respectively. Nine frequencies contribute to over 75% of the eastward flux with 4 covering over 50% of the flow. The first three modes occur below 150 cl/t with salinities less than 35%.. A fourth mode is seen at 525 cl/t having a salinity of 35.1%..

The westward flux (48 km^3/hr) is about twice that of the eastward flux across 10° - 15° S, and between 150 to 350 cl/t, the fluxes have salinities greater than 35%. (Fig. 5.1.6). 75% of the westward flow is distributed over 9 frequencies, while 5 frequencies contribute to over 50% of the flow. The primary mode occurs at 75 cl/t with salinity 34.7%. and 50% of the flow takes place below 400 cl/t. The westward flux is heterogeneous over thermosteric anomaly, possibly indicating that the South Equatorial Current present, south of 9° S, extends to deeper levels.

Three frequencies, all below 150 cl/t, contribute to over 75% of the eastward flux with salinity ranging from 34.6%. to 35.2%.. The primary mode at 75 cl/t contributes to over 50% of the flux. Between 15° and 17° S, westward flux is 18.6 km^3/hr, mainly confined to layers below 150 cl/t (Fig 5.1.7). The eastward flux is insignificant and mostly confined to the surface layer. The South Equatorial Current transports 69.7 km^3/hr south of 9° S, which is equal in magnitude to that of the North Equatorial Current found north of the equator.
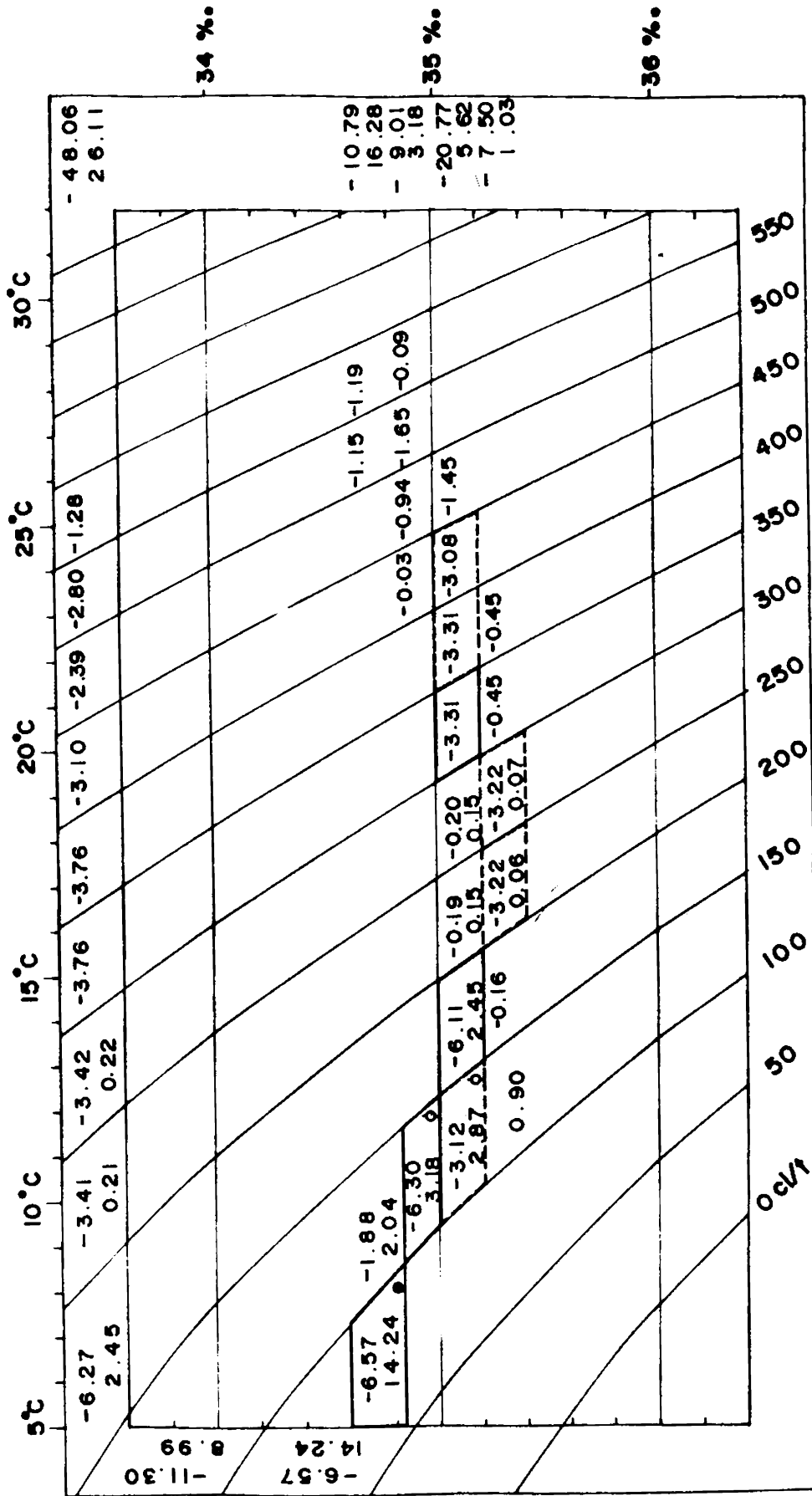
Fig. 5.1.6 - Zonal fluxes across 55°E between 10°S and 15°S during February, 1964
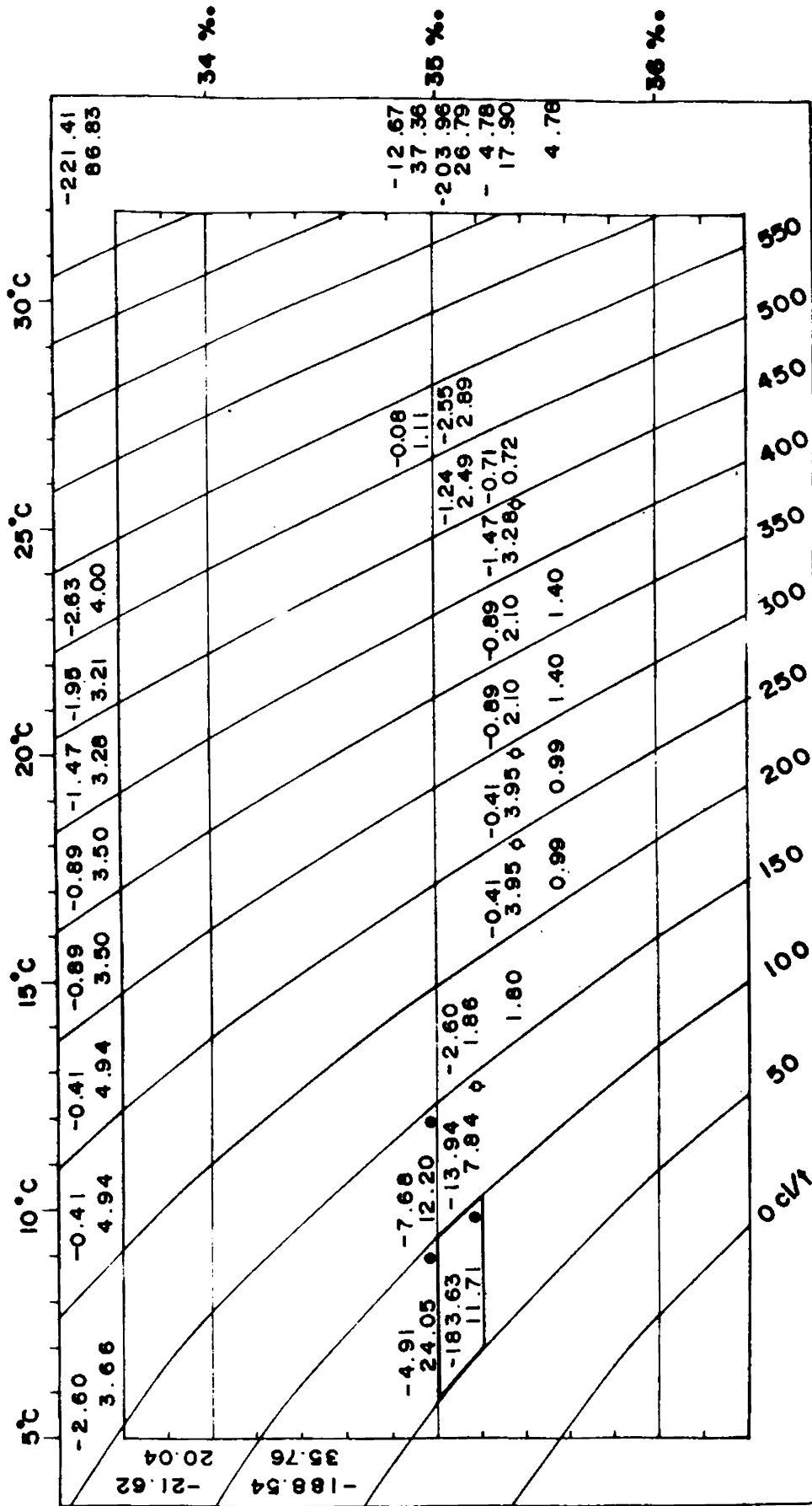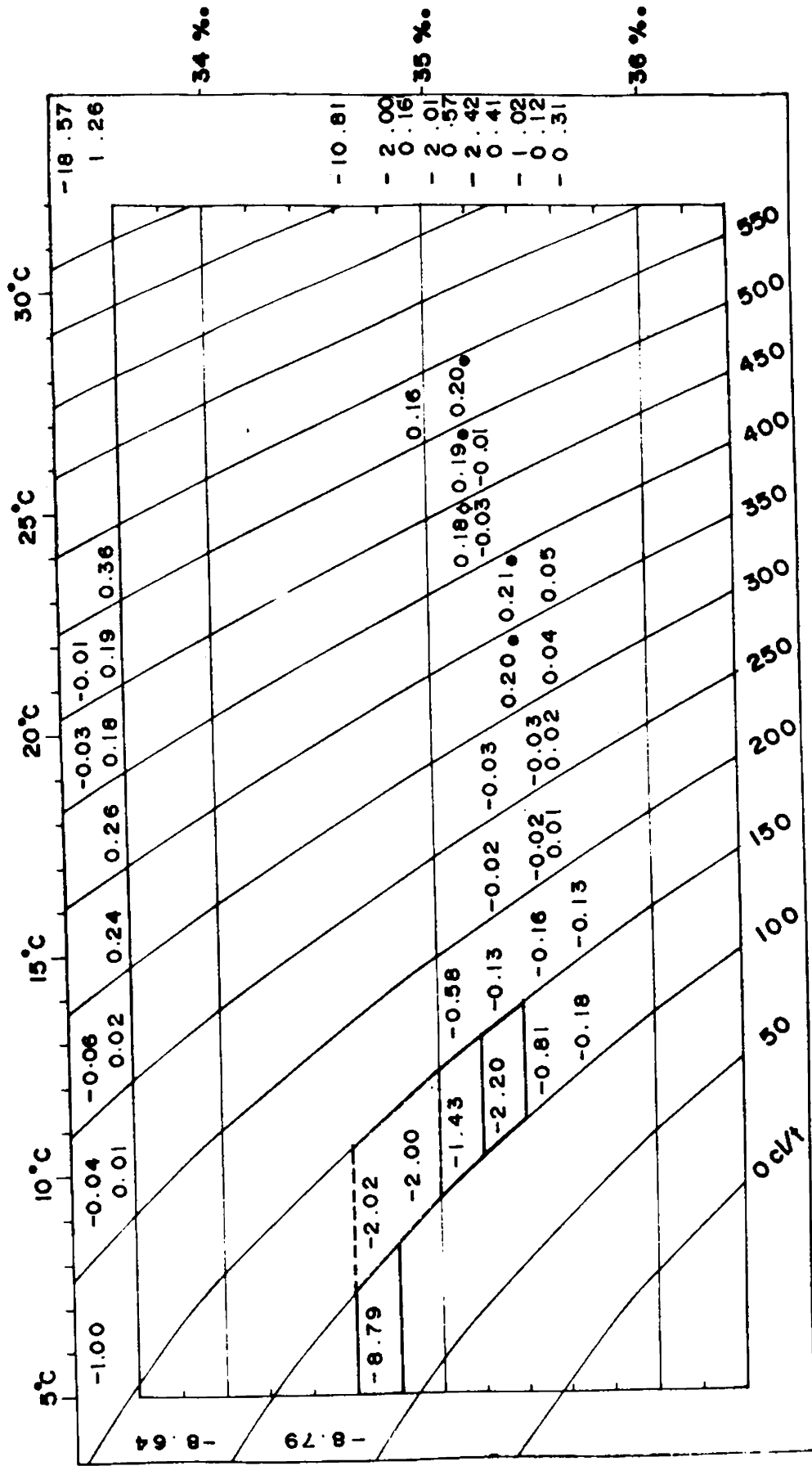
Fig. 5.1.7 - Zonal fluxes across 55°E between 15°S and 17°S during February, 1964

5.2   The zonal flux across 65° E during March is presented in Figs. 5.2.1- 5.2.6. The total westward flux across this belt between 9° and 5° N is 35.9 km^3/hr and 50% of the flux occurs below 150 cl/t with the primary mode (35.1%) occurring at 75 cl/t (Fig. 5.2.1). The eastward flux is 31.8 km^3/hr. Over 50% of the flux occurs again below 150 cl/t. All the eastward and westward fluxes are confined to salinities higher than 35%..

Between 5° N and equator, the flow is mainly westerly and the total flux is 591 km^3/hr (Fig. 5.2.2). Over 50% of the westward flow is confined to layers below 150 cl/t with the primary mode at 75 cl/t and salinity 35.1%.. Westward flux of 31 km^3/hr is observed at 475 cl/t with salinity 35.3%.. In the suface layers (above 300 cl/t) the westward flux attributable to the North Equatorial Current is 99.8 km^3/hr across 65° E during March. The total eastward flux is only 62.6 km^3/hr. A strong primary mode centred at 125 cl/t having salinity 35.1%. contributes to over 50% of the flux. Part of the eastward flux, above 200 cl/t, with salinity higher than 35.2%., could be attributed to the Equatorial Undercurrent.

The total westward flux between equator and 5° S is 277 km^3/hr (Fig. 5.2.3). The primary mode is at 125 cl/t with a secondary mode at 75 cl/t but with lower salinity (34.9%.).

Fig. 5.2.1.—Zonal fluxes across 65°E between 9°N and 5°N during March, 1973

Fig. 5.2.2_Zonal fluxes across 65°E between 5°N and 0° during March, 1973

34 ‰•

35 ‰•

36 ‰•

-277.31
180.81

-1.12

- 9.63
4.49
-116.85
55.26
-147.22
53.80
- 2.49
67.26

30°C

-0.01 -1.11 -3.00

-1.28 -1.00
4.49 3.59
-0.10 -0.69 -0.07
1.46 15.99 1.00

-4.11

-2.36 9.08

25°C

0.08
-0.92 -0.07
7.20 15.76

-0.63 0.62
11.16 15.76

-0.79 17.45

-0.92 23.04

-1.53 0.56
11.92 11.92

20°C

-0.63 11.78

-1.53 12.48

-5.16 1.46
11.92 8.17

15°C

-1.53 12.48

-5.16 1.46
8.17 8.17

-18.99 7.77

-2.49 0.16

-5.16 9.63

-0.68

-37.58 20.01
-99.79 14.96

10°C

-5.16 9.63

-77.49 30.12
-12.75 2.22

-5.35

-22.16 7.93

5°C

0 cV/t

550 500 450 400 350 300 250 200 150 100 50

-137.37
34.97
-95.59
32.34

Fig. 5.2.3.-Zonal fluxes across 65°E between 0° and 5°S during March, 1973

The primary mode of the eastward flux occurs around 75 cl/t. The distribution of the eastward flux is more heterogeneous as 75% of the flux is distributed over 9 frequencies. The high salinity classes that appear in the distribution of the eastward flux, between 180 and 400 cl/t, is that of the Equatorial Undercurrent. The total transport of the Equatorial Undercurrent ($61.5 \text{ km}^3/\text{hr}$) across 65° E during March is twice that of the transport across 55° E during February which shows the strengthening of the Equatorial Undercurrent in the Western Indian Ocean by March.

The total westward flux is $55.8 \text{ km}^3/\text{hr}$ between 5° and 10° S (Fig. 5.2.4), which is comparatively weaker to that between equator and 5° S. While 6 frequencies make up 75% of the westward flux, 3 frequencies contribute towards 50% of the flow. The primary and secondary modes of the flux occur below 150 cl/t. The primary mode alone contributes to about 30% of the flux with a mean salinity of 34.7%. and thermosteric anomaly of 75 cl/t. The secondary mode at 125 cl/t has a salinity of 34.9%.. The distribution exhibits a tertiary mode of $5.7 \text{ km}^3/\text{hr}$, with salinity 34.5%., around 575 cl/t.

The eastward flux is homogeneous with little variation in its salinity characteristics. 75% of the flow is contributed by 3 frequencies, all occurring below 200 cl/t. The primary mode contributes to more than 47% of the
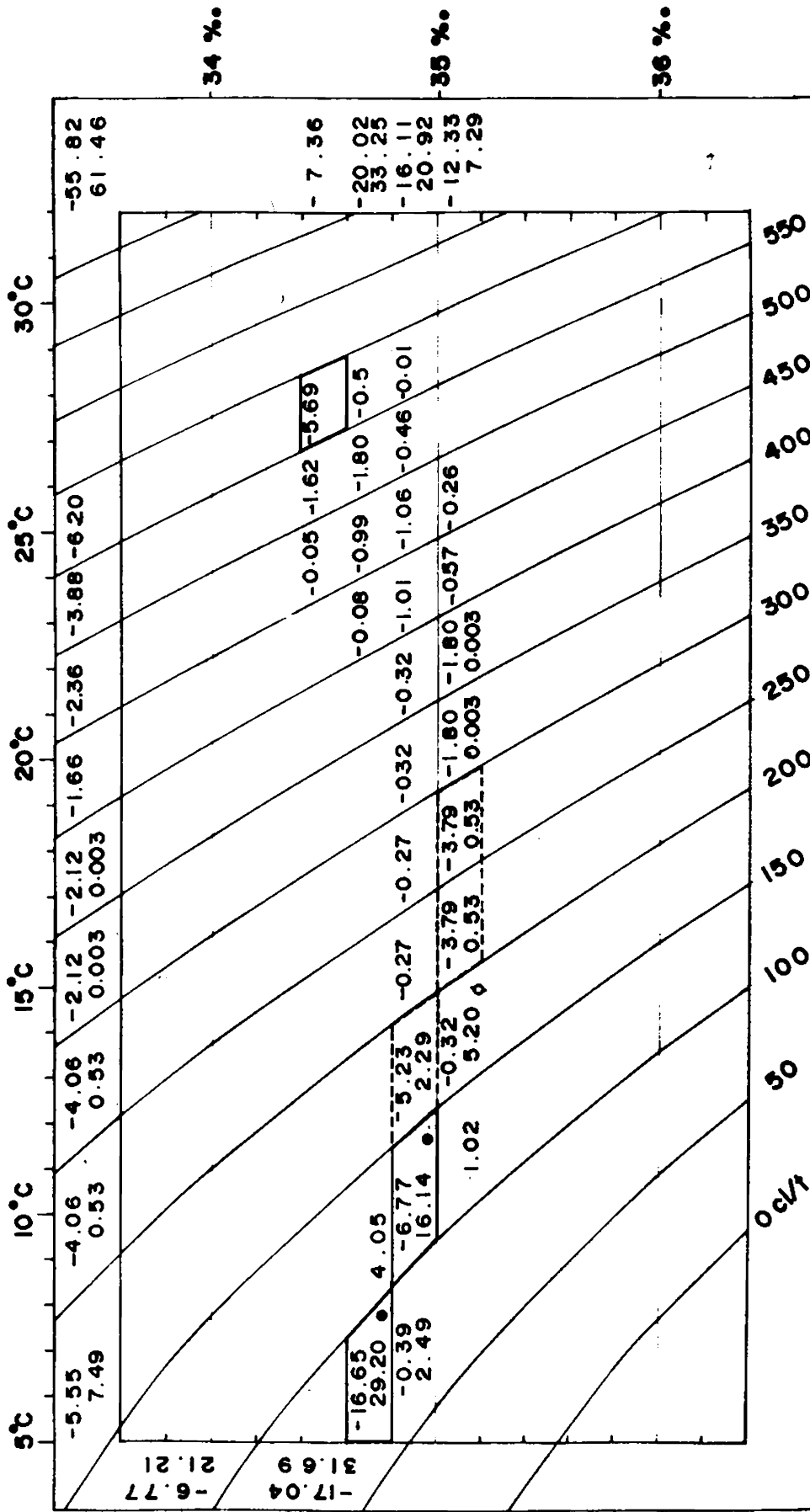
Fig. 5.2.4.—Zonal fluxes across 65°E between 5°S and 10°S during March, 1973

eastward flux, having the same water characteristics as the primary mode of the westward flux across this belt. The secondary and tertiary modes appearing at 125 and 175 cl/t respectively show an increase in the salinity towards upper levels. Along this section, the total eastward flux is greater than the westward flux. Above 200 cl/t the eastward flux is insignificant, showing the absence of any counter current and also the persistence of the westward flow of the South Equatorial Current in this belt.

75% of the westward flux is distributed over 8 frequencies, between 10° and 15° S (Fig. 5.2.5) showing heterogeneous character. The contribution of the primary mode at 75 cl/t is about 25%, and it has a mean salinity of 34.7%.. 75% of the flow takes place below 250 cl/t with a major portion having a salinity less than 35%..

The total eastward flux is 2.5 km^3/hr which is insignificant compared to the westward flux. Nonetheless, the distribution is homogeneous, with more than 50% of the flow occurring below 150 cl/t. The two frequencies above 300 cl/t, with salinity 35.1%., could be attributed to the South Equatorial Countercurrent, even though the total transport of the countercurrent is less (about 1 km^3/hr).

Eight frequencies contribute to 50% of the total westward flux (101.2 km^3/hr) between 15° and 20° S (Fig.
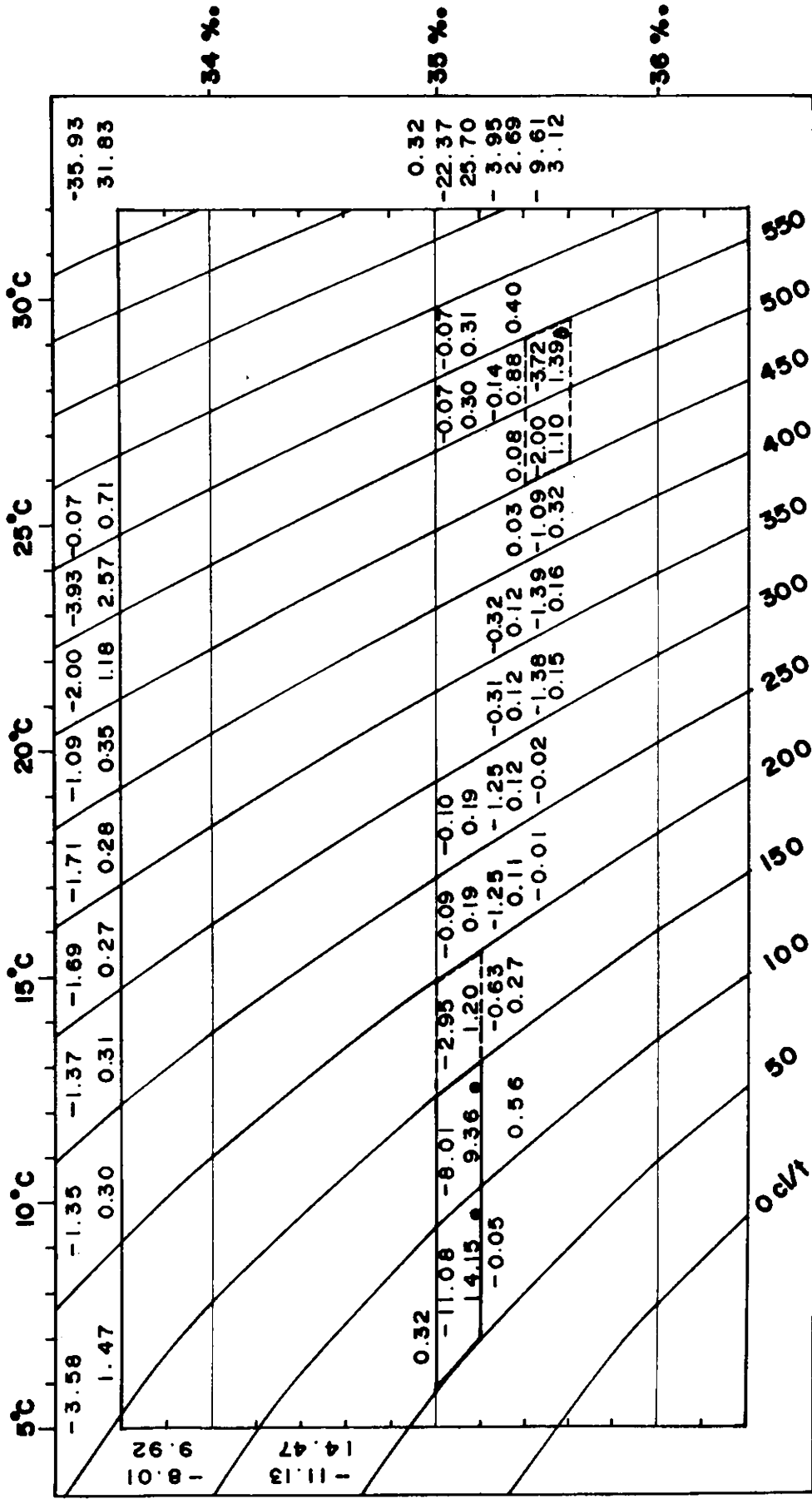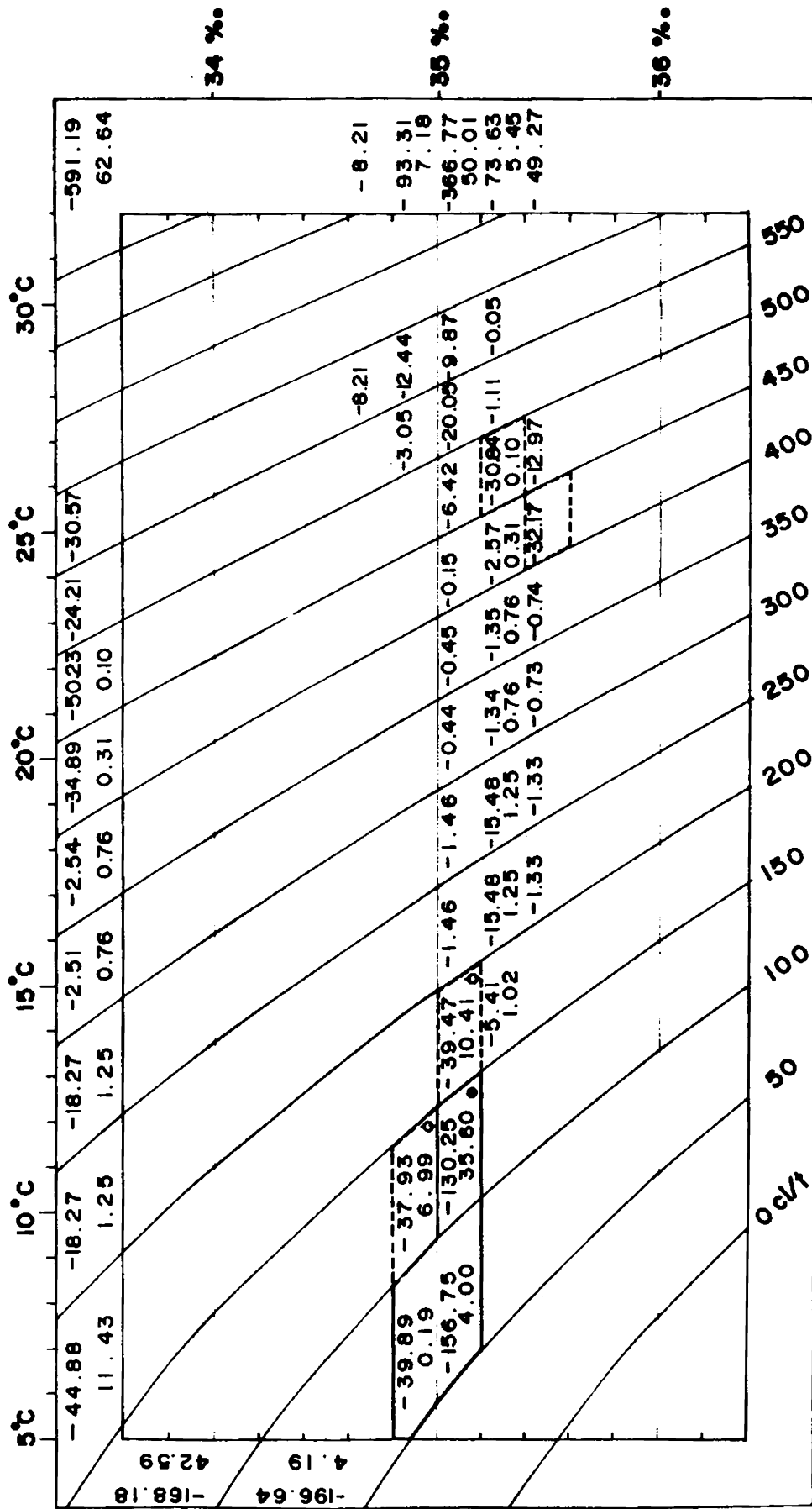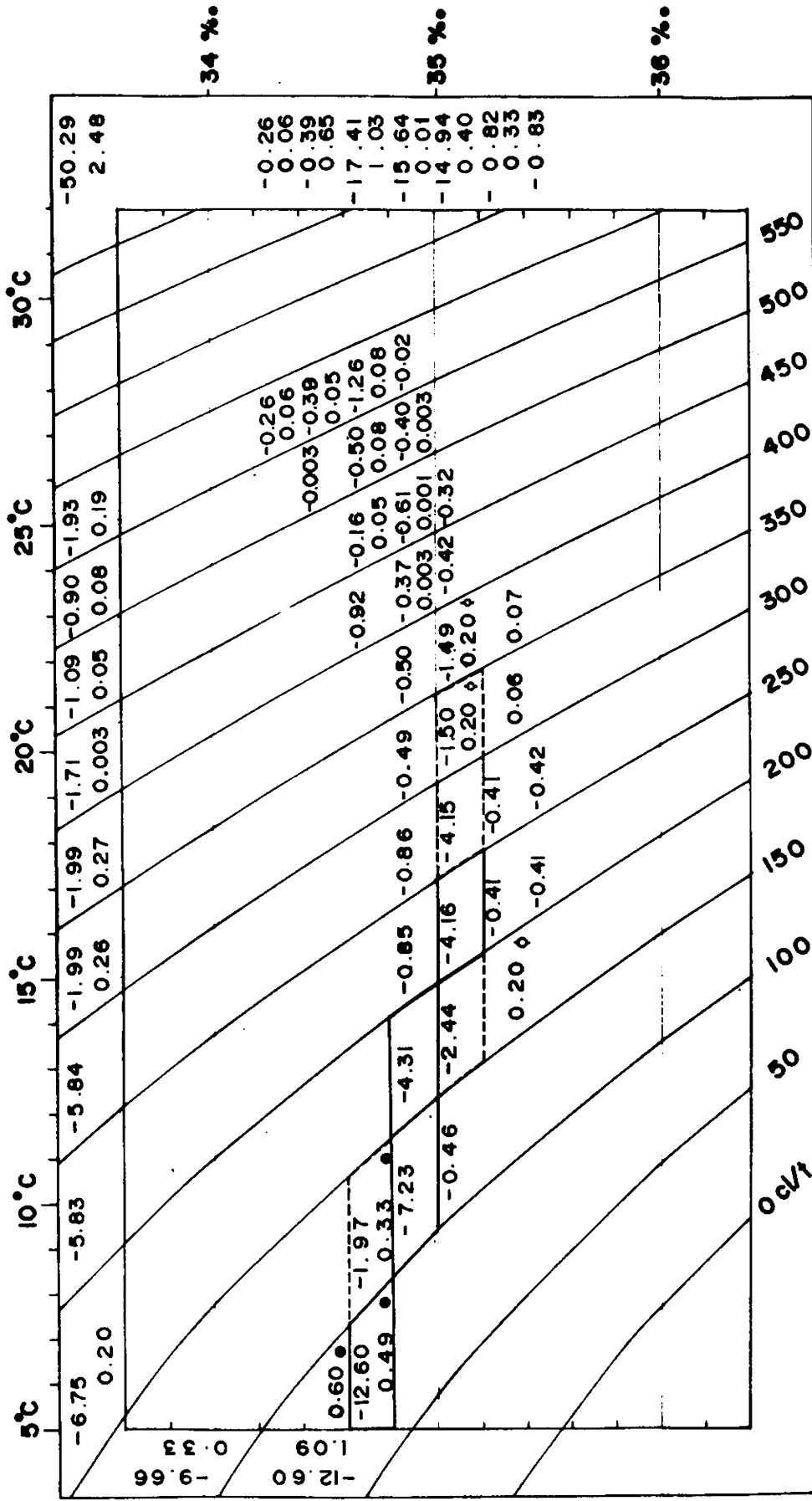
Fig. 5.2.5_Zonal fluxes across 65°E between 10°S and 15°S during March, 1973

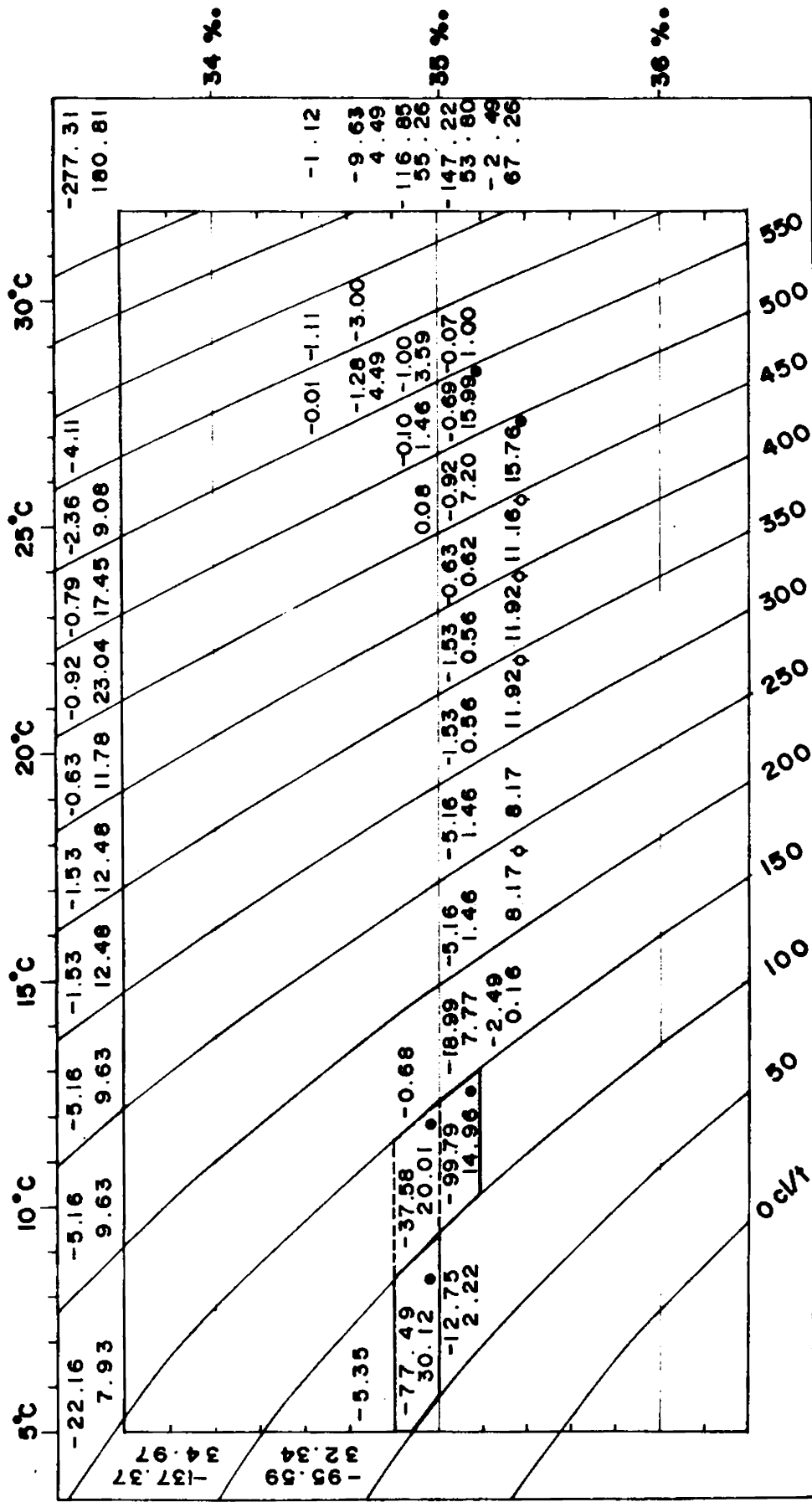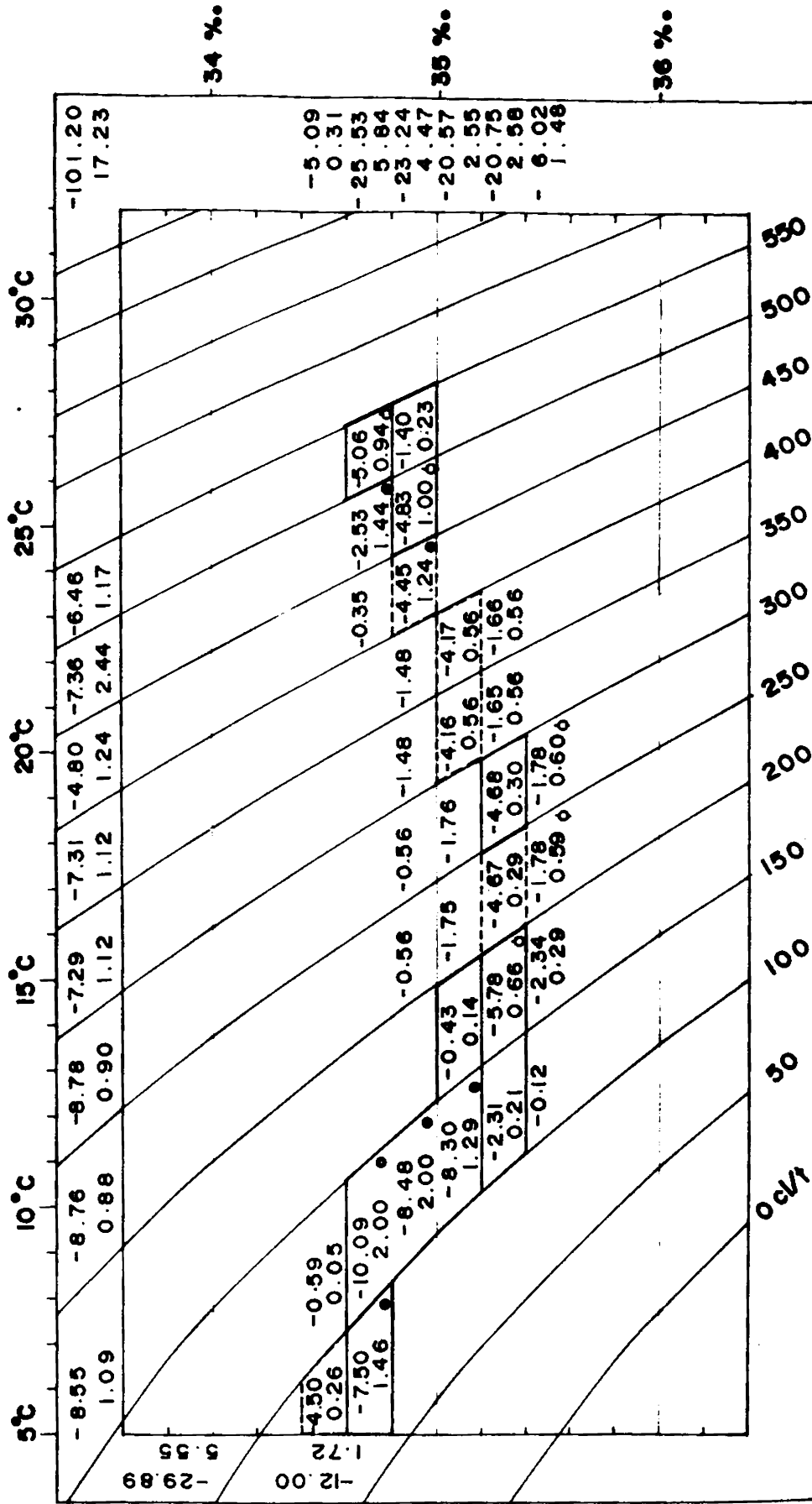Fig. 5.2.6_Zonal fluxes across 65°E between 15°S and 20°S during March, 1973

5.2.6) and 75% of the flow is contributed by 13 frequencies, indicating the heterogeneous nature of the flow. The first 3 modes occur at 125 cl/t and together contribute to over 25% of the flow with the primary mode having a mean salinity of 34.7‰.. The South Equatorial Current is found to extend south of 5^oS and the total westward flux of the South Equatorial Current is 165.5 km^3/hr, between 5° and 20^oS.

The total eastward flux is 17.2 km^3/hr. While 11 frequencies make up 75% of the flow, 50% of the flux is distributed among 6 frequencies. The flux distribution is heterogeneous with the primary mode of 50% at 475 cl/t and salinity 34.7‰.. In the southern hemisphere, heterogeneity is found to be more, with classes of higher salinity, compared to that in the northern hemisphere. This may be due to the presence of the Subtropical High Salinity Water at these depths. The Tropical Countercurrent observed above 300 cl/t between $18^o - 20^o$S, accounts for 7.1 km^3/hr.

5.3   The total westward flow between equator and 5^oS across 65^oE is 166.9 km^3/hr (Fig. 5.3.1). The flux distribution appears to be more or less homogeneous with salinities ranging from 34.8‰. to 35.2‰.. Six frequencies contribute to over 75% of the westward flux. The primary mode occurring at 75 cl/t has a mean salinity of 34.9‰..
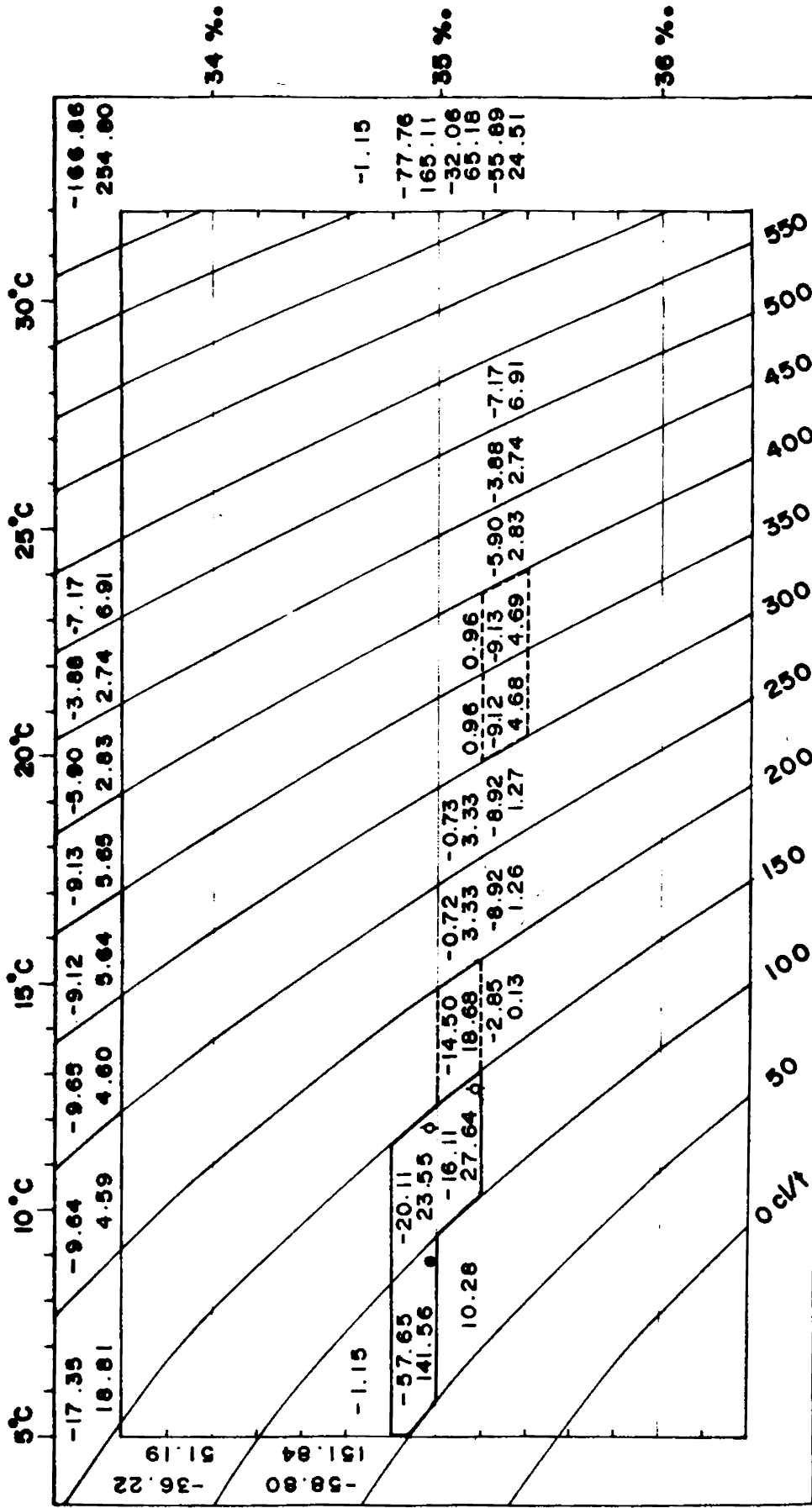
Fig. 5.3.1._Zonal fluxes across 65°E between 0° and 5°S during December, 1976

The primary mode of the eastward flow also shows the same bivariate characteristics as that of the westward flow and accounts for over 50% of the total eastward flow of 254.8 km^3/hr. The secondary mode occurs at 125 cl/t with a higher mean salinity of 35.1%.. The Equatorial Undercurrent, between 0° and 1° S, and Equatorial Countercurrent, between 3° and 5° S, account for the eastward flux of 20.5 km^3/hr and 23.8 km^3/hr respectively. Since this section is limited to south of the equator, it does not cover the Equatorial Undercurrent completely. In the salinity range 35.2 to 35.4%., the westward flux is twice that of the eastward flux across this latitudinal belt.

The flux across 5° to 10° S (Fig. 5.3.2) is considerably reduced, compared to the one north of it, and shows similar distribution characteristics, except that the primary modes of both the eastward and westward flux appear at a lower salinity of 34.7%.. Five frequencies constitute 75% of the westward flow of 63 km^3/hr, while 50% of the flux is distributed over 3 frequencies all below 150 cl/t. Above 150 cl/t the fluxes have salinities more than 35%..

The primary mode of the eastward flow is seen at 75 cl/t and 4 frequencies occurring below 200 cl/t contribute to 50% of the total eastward flow of 54.6 km^3/hr. The secondary mode occurs at 175 cl/t and has a salinity of 35.1%.. Seven frequencies constitute 75% of the eastward
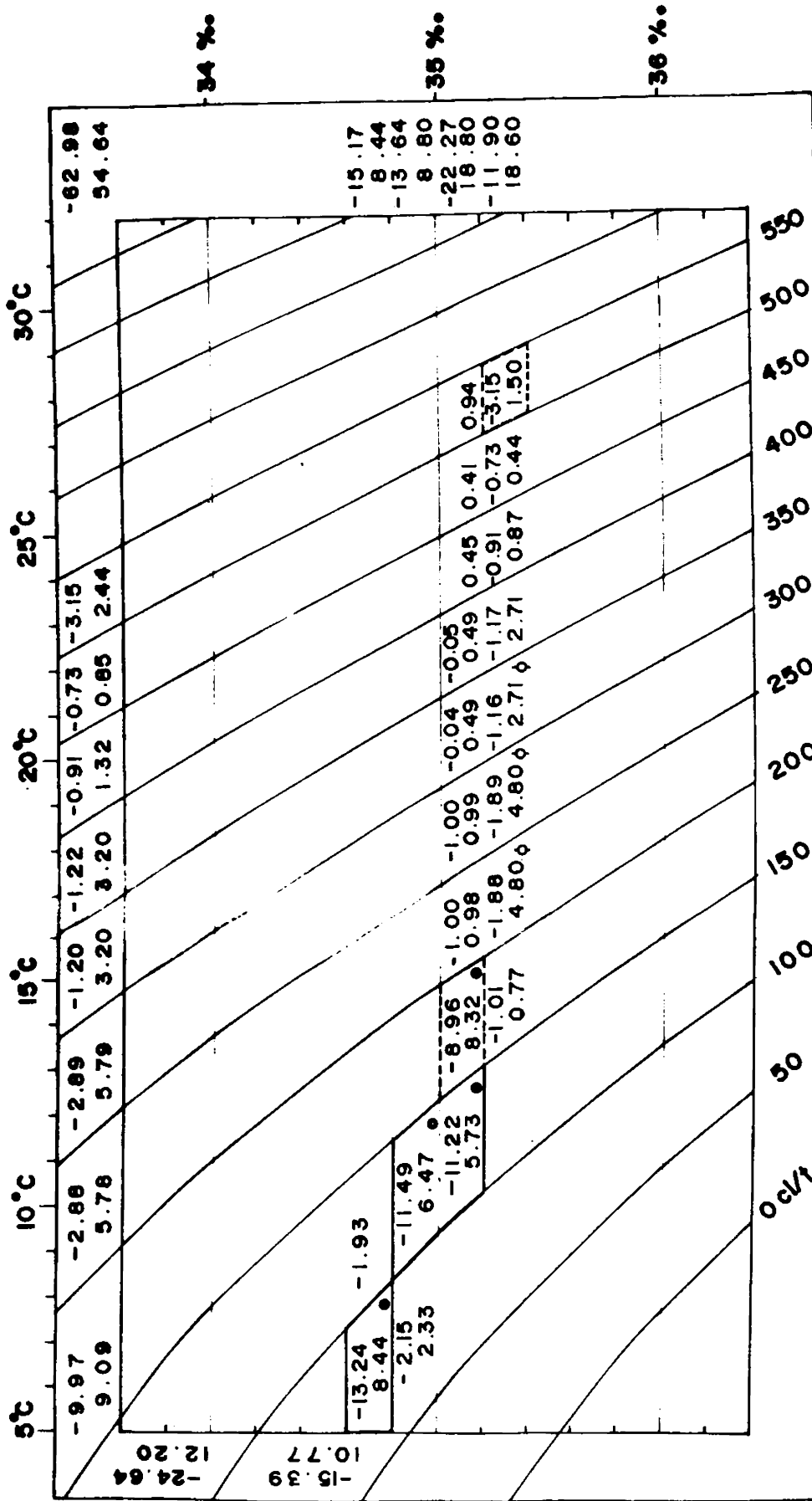
Fig. 5.3.2_Zonal fluxes across 65° E between 5° S and 10° S during December, 1976

flux, the last three, which contribute to 25% of the total, occur between 200 and 350 cl/t with a mean salinity of 35.3‰..

The westward flow, between 10° and 15^oS (Fig. 5.3.3), is stronger than in the preceeding belt,with a total of 135.5 km^3/hr. The primary mode occurs at 125 cl/t having salinity 34.9‰., while the secondary mode with salinity of 34.7‰. is seen at 75 cl/t. 50% of the flow is distributed over 5 frequencies and 8 frequencies add upto 75% of the flow. Strong westward flow is observed between 400 cl/t and 500 cl/t with mean salinity of 35.1‰., the tertiary mode (16 km^3/hr) appearing at 475 cl/t.

The total eastward flux is only 13.5 km^3/hr, a part of which (3.7 km^3/hr) is accounted by South Equatorial Countercurrent. The primary mode occurs at 75 cl/t with a salinity of 34.7‰., while the secondary mode is found at 175 cl/t having a salinity of 35.1‰.. Together they contribute to over 50% of the eastward flow.

The heterogeneity in the bivariate distribution, between 15° and 20^oS (Fig. 5.3.4), is evident with salinity varying from 34.4‰. to 35.8‰.. The primary mode of the total westward flux of 87.2 km^3/hr is observed at 125 cl/t having a salinity of 34.9‰.. The total transport of the
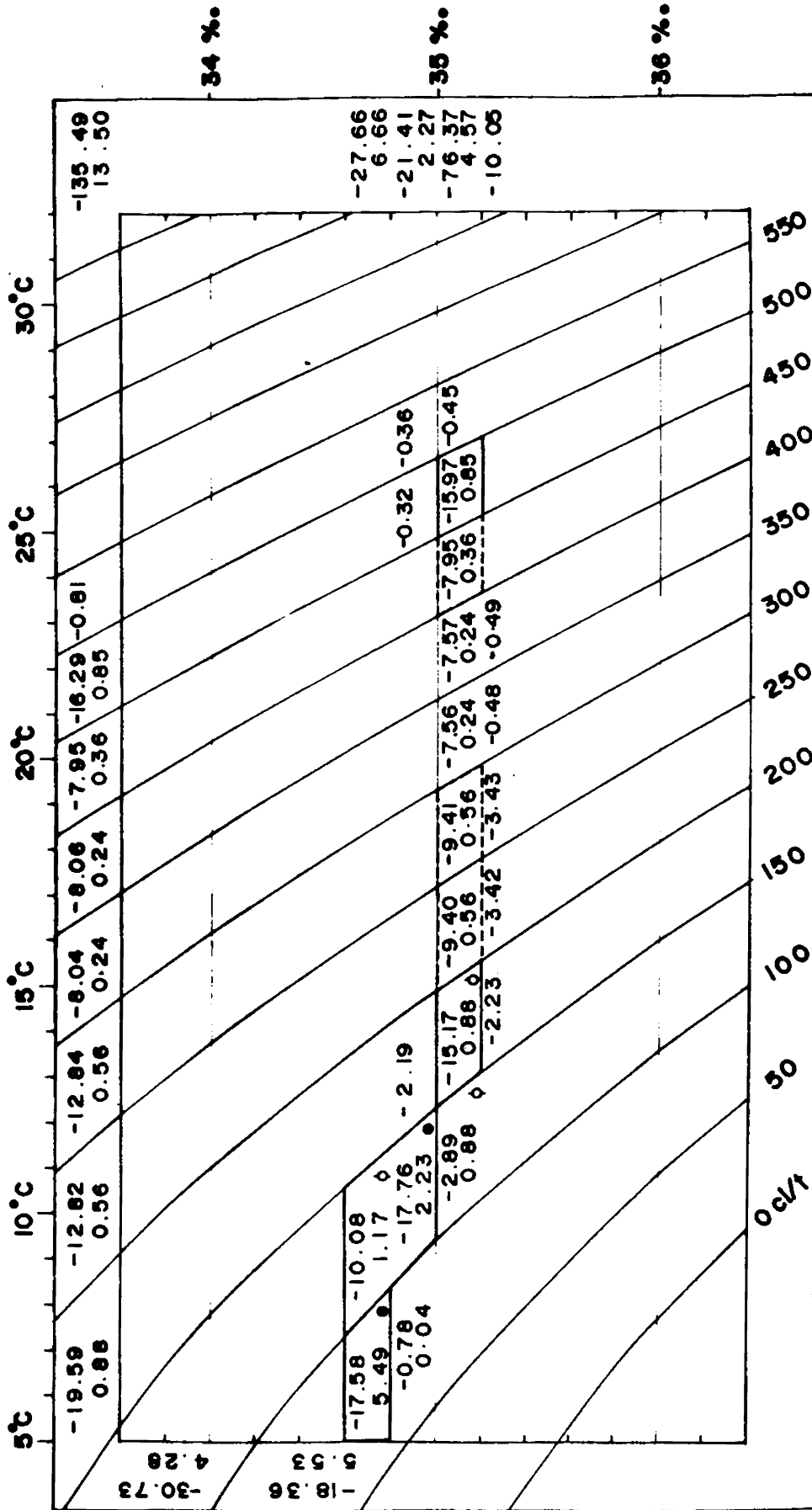
Fig. 5.3.3.–Zonal fluxes across 65° E between 10°S and 15°S during December, 1976
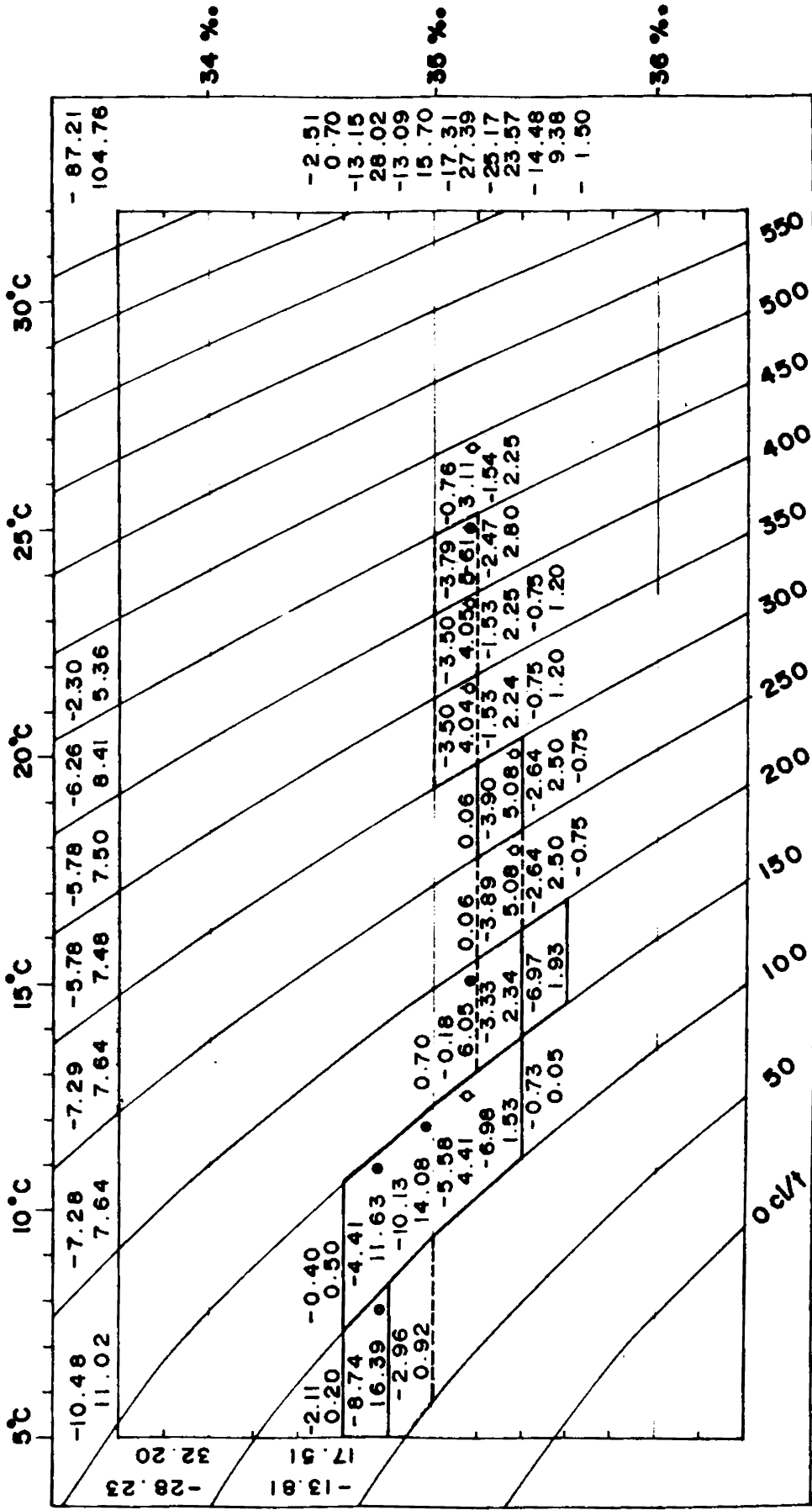
Fig. 5.3.4. Zonal fluxes across 65°E between 15°S and 20°S during December, 1976

South Equatorial Current north of 20°S during December across 65°E is 138 km^3/hr.

The total eastward flux observed is 104.8 km3/hr. The primary mode occurs at 75 cl/t with salinity 34.7%., which is lower than the primary mode of the westward flow. The total transport of the Tropical Countercurrent is estimated to be 28.7 km^3/hr, occurring above 300 cl/t with a mean salinity of 35.1%..

5.4   The zonal flux distribution, across 67°30'E, during April-May, is presented in Figs. 5.4.1 to 5.4.6. Both the eastward and westward fluxes, between 9° and 5°N, are of the same magnitude (Fig. 5.4.1). Six salinity classes comprise of 50% of the westward flux, 3 of them occurring below 200 cl/t with a mean salinity of 35%., whereas, the other three classes occur above 450 cl/t in the surface layers with different salinities. 75% of the westward flux comprises of 11 frequencies occurring at different isanosteric levels indicating lot of heterogeneity. The higher salinity classes occurring above 300 cl/t, even upto 4°S across this longitude, are due to the southward spreading of the high salinity water of Arabian Sea origin.

Two frequencies account for 50% of the total eastward flux occurring between 125 and 175 cl/t. 75% of the flux is distributed over 4 frequencies occurring below 200 cl/t.
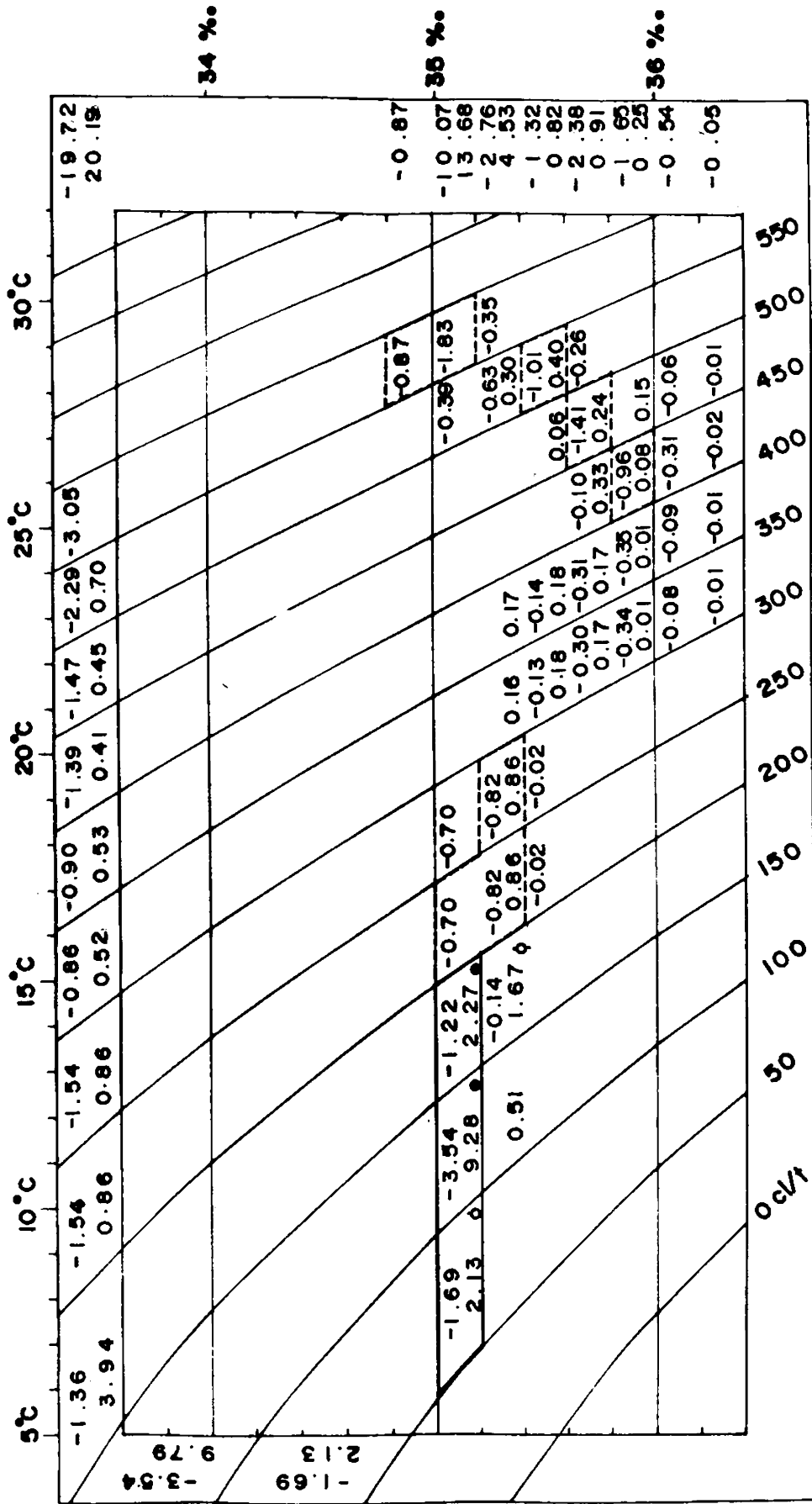
Fig- 5.4.1 - Zonal fluxes across 67°30'E between 9°N and 5°N during April-May, 1964

Between 300 and 500 cl/t, frequencies with salinity higher than 36‰. are seen.

Seven frequencies contribute to 75% of the total westward flux (141.2 km^3/hr) and 3 frequencies to over 50% of the flux which have a mean salinity of 35.1‰. between 5^oN and the equator (Fig. 5.4.2) occurring below 200 cl/t. The primary mode occurs at 125 cl/t which contributes 23% of the total flow.

Over 36% of the eastward flux occurs at 75 cl/t. The primary mode has a salinity of 35.1‰.. The secondary mode, having the same salinity as the primary, together contribute to over 50% of the flux of near homogeneous characteristics. However, 75% of the total flux is distributed over a wider range in thermosteric anomaly, in the salinity range 34.8 to 35.3‰.. Between 9° and 5^oN, the total transport of the North Equatorial Current is 9.1 km^3/hr above 350 cl/t, while the eastward flux, between equator and 5^oN (45.1 km^3/hr), is attributed to the formation of the Monsoon Current by May itself.

50% of the westward flux is distributed over 3 frequencies all below 200 cl/t, while 75% of the flow is made up of 7 frequencies in the latitudinal belt $0^o - 5^o$S (Fig. 5.4.3) showing heterogeneity. Over 25% of the flux is
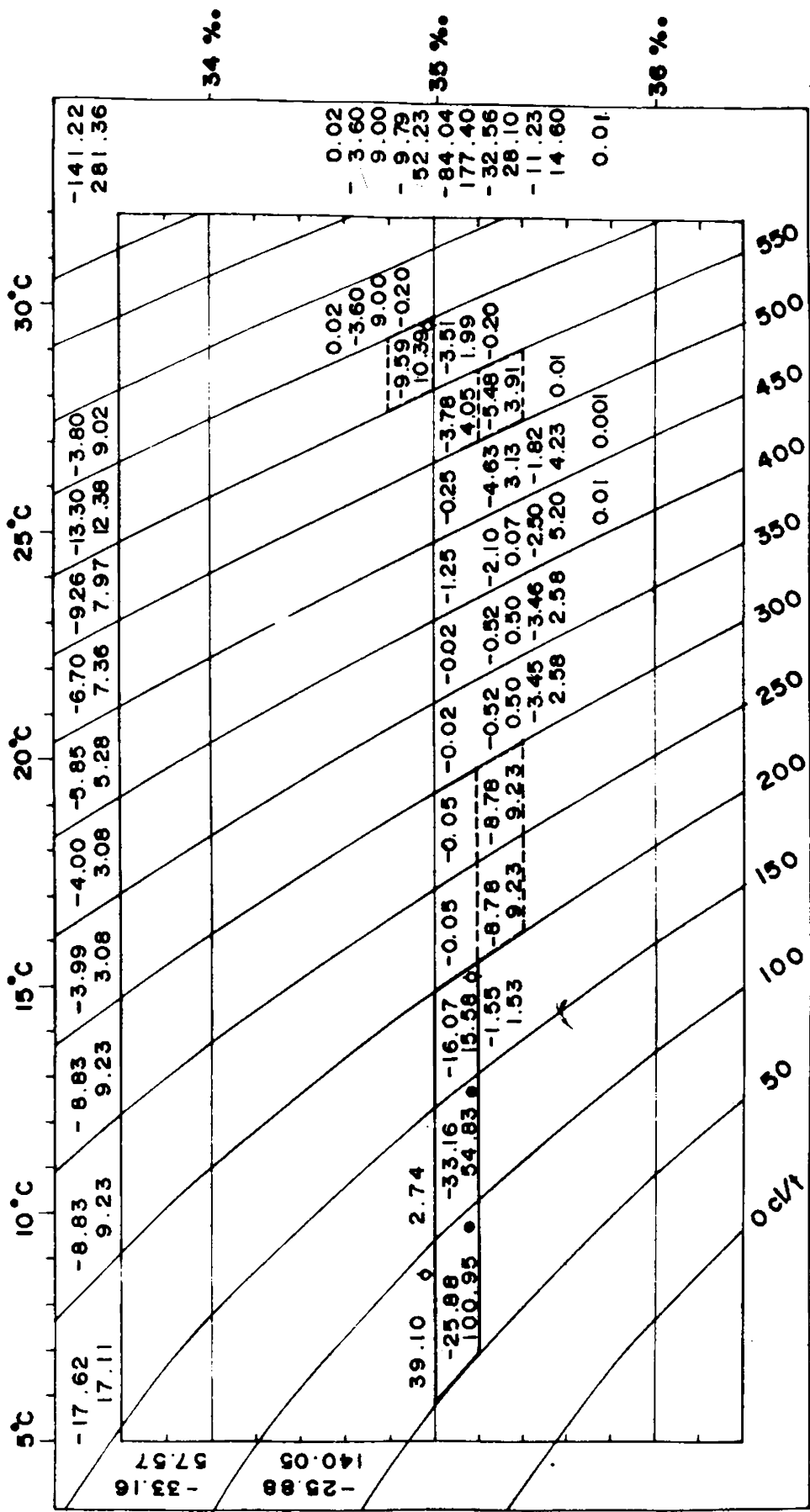
Fig. 5.4.2._ Zonal fluxes across 67°30'E between 5°N and 0° during April–May, 1964

Fig. 5.4.3 _ Zonal fluxes across 67° 30' E between 0° and 5° S during April–May, 1964

contributed by the primary mode at 75 cl/t having salinity 34.9‰..

The total eastward flux is 276.4 km^3/hr. 75% of the flux is distributed over 12 frequencies and 6 frequencies account for over 50% of the flux. The distribution is heterogeneous in nature and exhibit 3 modes. The primary mode occurs at 75 cl/t with a mean salinity of 34.9‰.. A secondary mode of 35.7 km^3/hr occurs at 525 cl/t at a salinity of 35.3‰. A low saline (34.7‰.) tertiary mode of 29 km^3/hr is seen very near the surface at 625 cl/t.

The total westward flow is 72 km^3/hr, between 5° and 10° S (Fig. 5.4.4). Four frequencies contribute to over 50% of the flux and 75% of the flux is distributed among 10 frequencies. The distribution is heterogeneous with the low salinity classes contributing to 50% of the flux above 550 cl/t. The lower salinities noticed in the surface layer above 400 cl/t, around 10° S, could be attributed to the incursion of the Pacific Ocean Water. The primary mode occurs at 125 cl/t with a mean salinity of 34.9‰.. The secondary mode, having the same salinity characteristics, occurs at 75 cl/t. A tertiary mode occurs at 625 cl/t with a salinity of 34.3‰..

Three frequencies contribute to over 75% of the eastward flux, while over 50% is accounted for by only 2
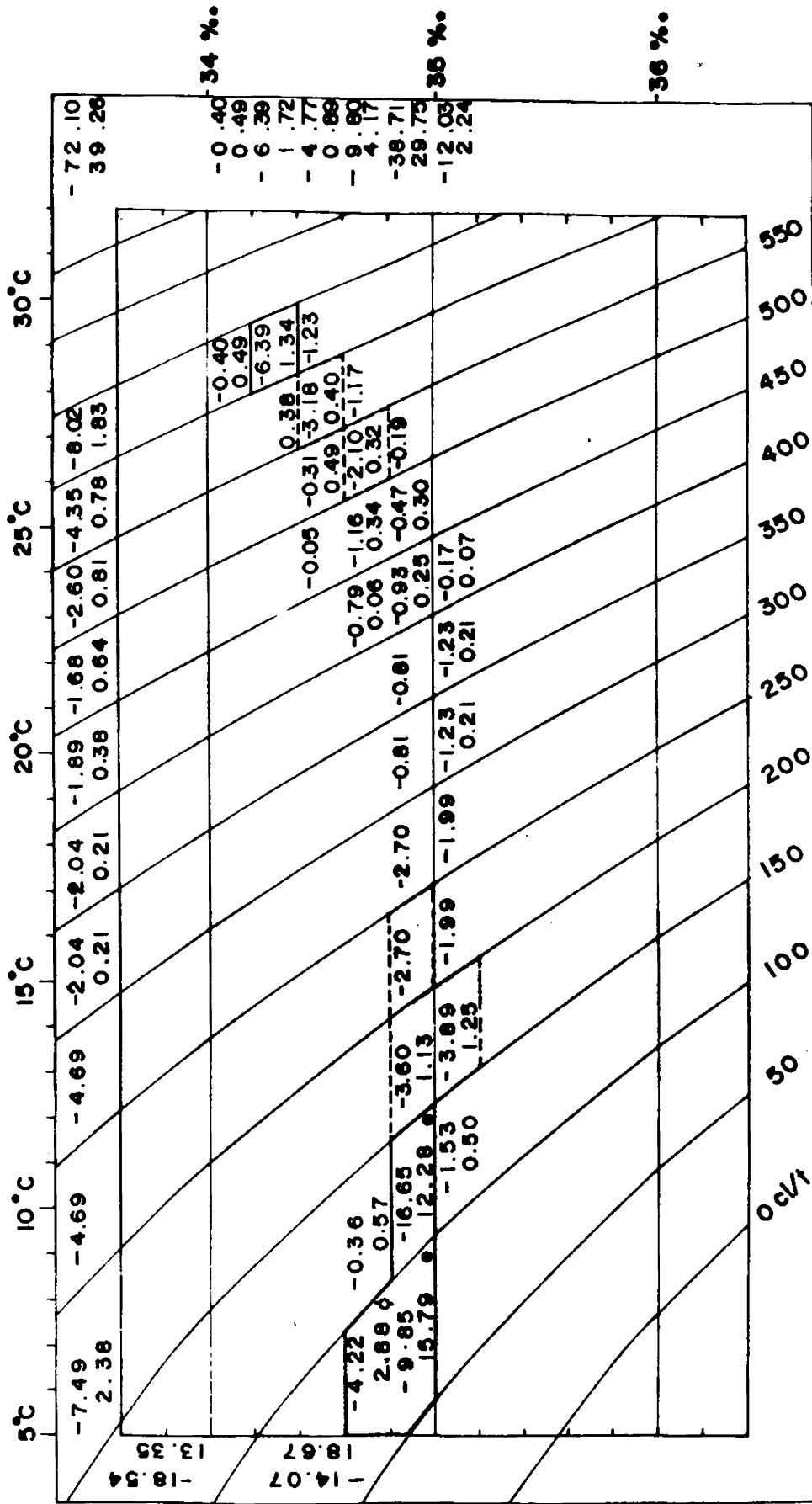
Fig. 5.4.4 _ Zonal fluxes across 67°30'E between 5°S and 10°S during April–May, 1964

frequencies. The primary mode occurs at 75 cl/t. Along this belt the salinities never exceed 35.2‰.. The eastward flow, though insignificant compared to the westward flow in this belt, is due to the Equatorial Countercurrent noticed between 5° and 8^oS which appears to have been shifted southward compared to the previous sections.

The westward flux between, 10° and 15^oS (Fig. 5.4.5), is about 46 km^3/hr. The distribution is heterogeneous, with salinities ranging from 34.2 to 35.6‰.. 75% of the westward flux is distributed over 8 frequencies, while 3 frequencies contribute to over 50% of the flux.

Four frequencies contribute to over 75% of the eastward flux. 50% of the flux contained by 2 frequencies occurs below 150 cl/t. The primary mode occurs at 75 cl/t having salinity 34.7‰.. The secondary mode occurs at 125 cl/t with a salinity 34.9‰.. The tertiary mode also occurs at this surface, but with a salinity of 34.7‰.. The South Equatorial Countercurrent, observed between 11° and 12^oS, above 400cl/t, accounts for an eastward flux of 2 km^3/hr.

The flow is mainly westerly (46.7 km^3/hr) and the distribution is heterogeneous in nature between 15° and 19^oS (Fig 5.4.6). 75% of the flow is distributed over 14 frequencies, with 8 of them contributing to 50% of the flux. Major contribution to 50% of the flux is made by 4

Fig. 5.4.5 – Zonal fluxes across 67°30'E between 10°S and 15°S during April–May, 1964
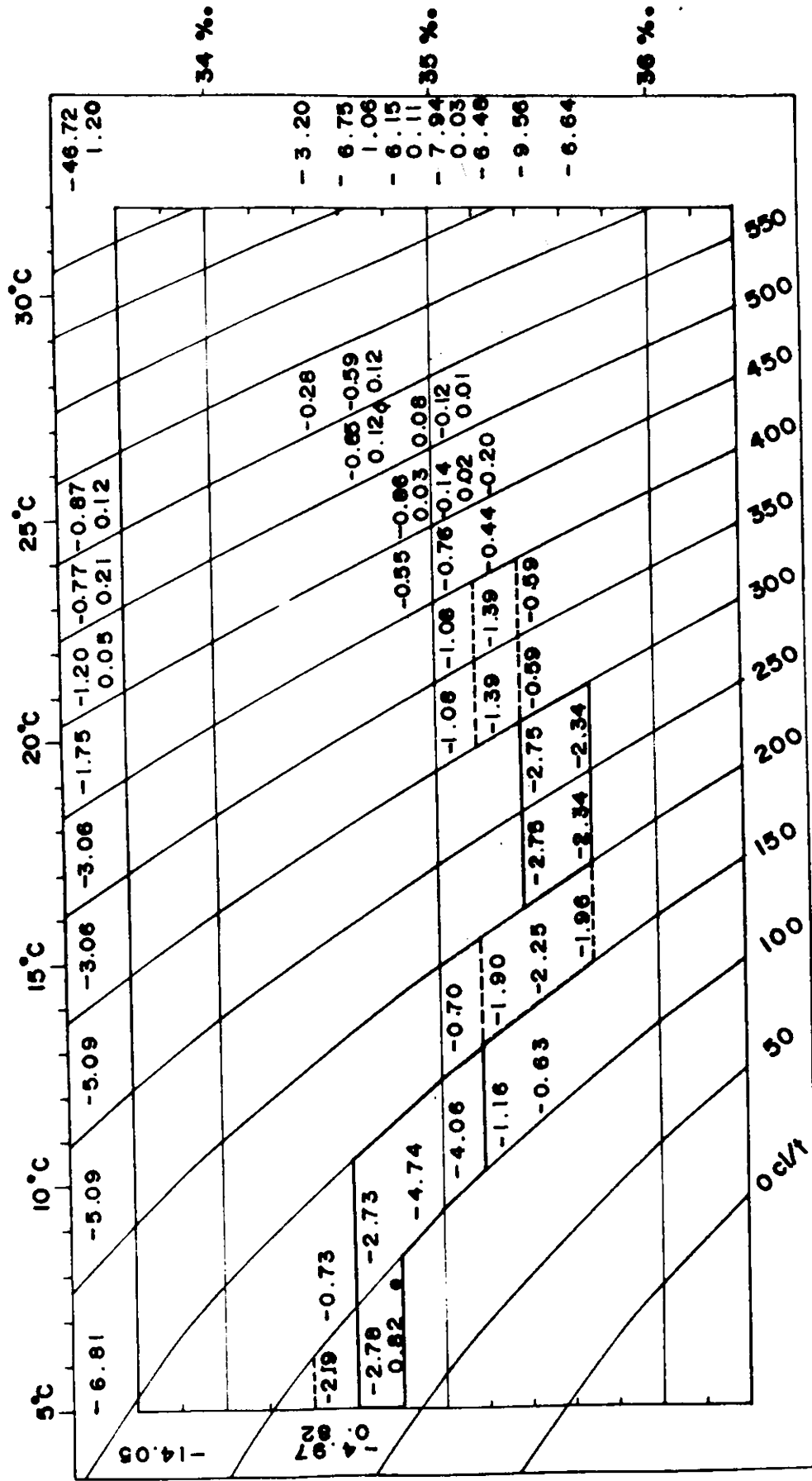
Fig. 5.4.6.— Zonal fluxes across 67°30'E between 15°S and 19°S during April-May, 1964

frequencies having salinity greater than 35.4%. between 200 cl/t and 300 cl/t. In this region, the flux between 150 and 400cl/t, contains several frequencies with salinities exceeding 35.0%., while the deeper layers (below 100 cl/t) and near surface layers (above 450 cl/t) constitute waters of lower salinity (< 34.8%). The Tropical Countercurrent, observed between 15° and 18° S, is limited to surface layers (above 400 cl/t) and accounts for 0.4 km^3/hr only. The total transport of the South Equatorial Current across this section is 101.3 km^3/hr.

5.5   The total eastward and westward fluxes across 70° E, between 9° and 5° N (Fig. 5.5.1), are of same magnitude. 50% of the total westward flux (44.2 km^3/hr) is limited to below 150 cl/t, comprising of 2 frequencies having same salinity characteristics (35.1%.). Four frequencies, all below 200 cl/t, add upto 75% of the westward flux.

The eastward flux (48.3 km^3/hr) is also mainly confined to layers below 150 cl/t. Two frequencies make up to 50% of the flow and 75% of the flux is made up of 3 frequencies having same salinity (35.1%.). The flux distribution has salinity higher than 35%..

The total westward flux is only 5.8 km^3/hr, insignificant compared to the eastward flux of 37.8km^3/hr (Fig. 5.5.2). Over 50% of the westward flux occur at 125

Fig - 5.5.1 - Zonal fluxes across 70°E between 9°N and 5°N during Oct - Nov, 1970
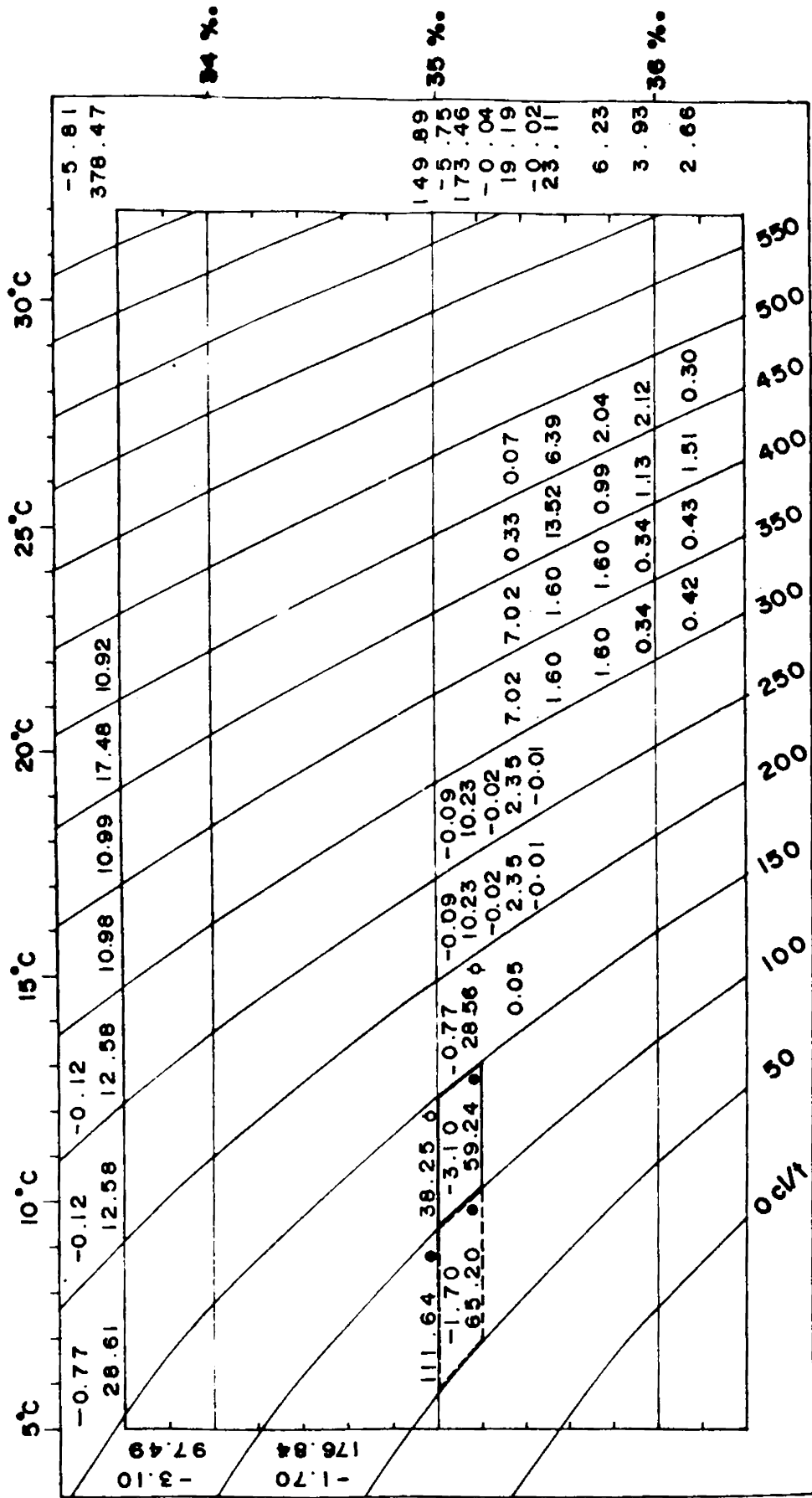
Fig - 5.5.2 - Zonal fluxes across 70°E between 5°N and 0° during Oct–Nov, 1970

cl/t with salinity 35.1%., which is the primary mode.
Together with the secondary mode having same salinity
characteristics but occurring at 75 cl/t, it constitutes 75%
of the flux.

Five frequencies, all below 200 cl/t, contribute to 75%
of the flow in the region between 5 N and equator (Fig.
5.5.2). The flux distribution is homogeneous in character
with the salinities varying between 34.8 and 35.2%.. The
primary mode alone contributes to about 30% of the flux
which is at 75 cl/t having a mean salinity of 34.9%..

The total westward flux is less than 1/6th of the
eastward flux (665.7 km^3/hr) between equator and 5 S (Fig.
5.5.3). The primary and secondary modes, occurring at 75
cl/t and 125 cl/t respectively and having a salinity of
34.9%., account for 50% of the flow. 75% of the flow is
distributed among 4 frequencies, all occurring below 200
cl/t. The 3rd and 4th modes of the distribution have a mean
salinity of 35.1%.. Five frequencies contribute to 75% of
the eastward flow occurring below 200 cl/t. The flux is
homogeneous in character with 3 frequencies contributing to
over 50% of the flow. Over 25% of the flux is contributed
by the primary mode at 125 cl/t and salinity 34.9%.. Above
300 cl/t, the eastward flow is due to the presence of the
Equatorial Jet during this month, as reported by Wyrtki
(1973b) and Cresswell et al. (1977). The total flux of the
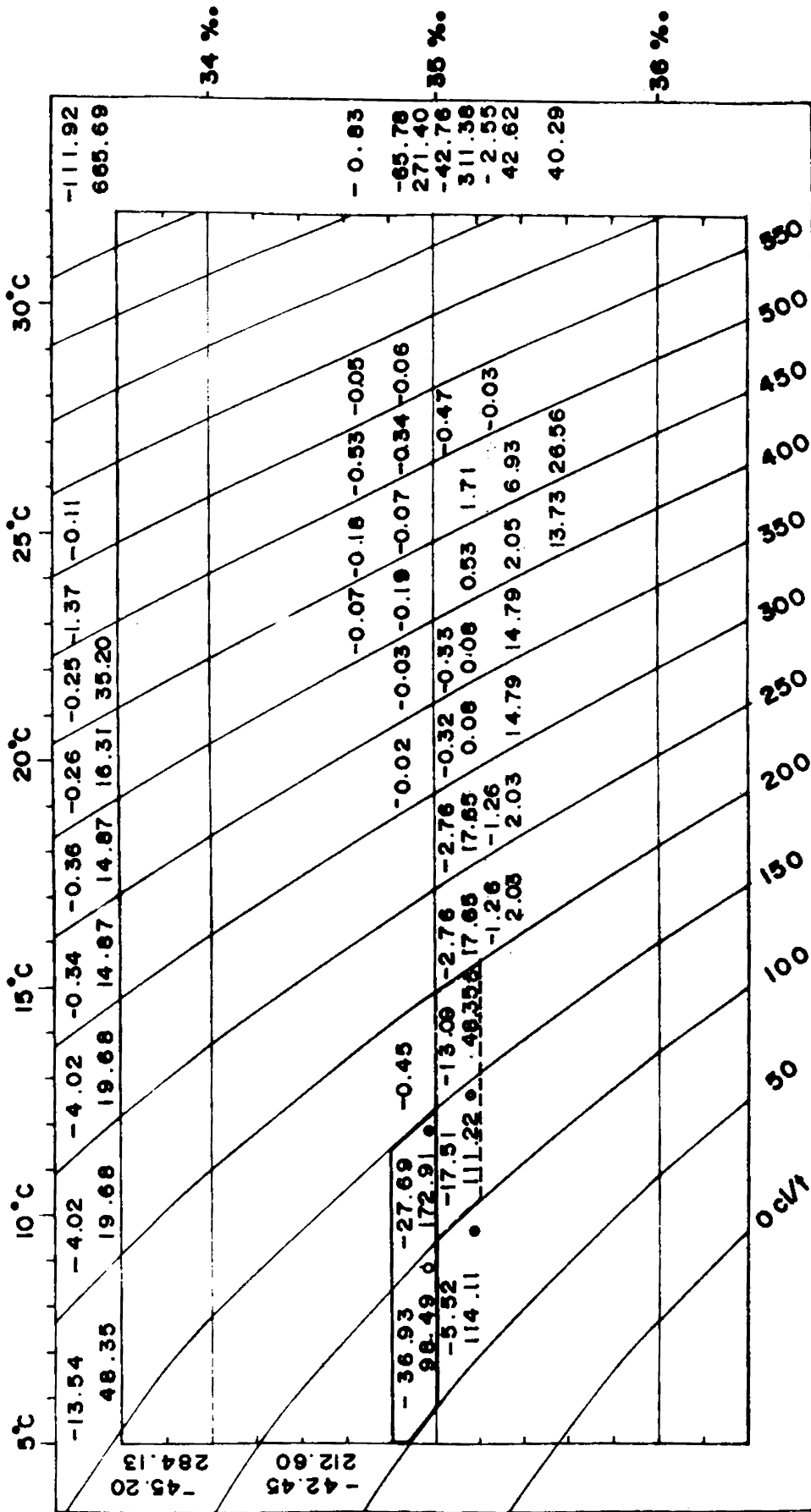
Fig. 5.5.3.- Zonal fluxes across 70°E between 0° and 5° S during Oct-Nov, 1970

Equatorial Jet which is seen between 1° N and 2° S is estimated to be 129.2 km^3/hr.

The total westward flux (40 km^3/hr) is almost equal to the eastward flux in the region 5° -10° S (Fig. 5.5.4). 75% of the flux is distributed among 6 frequencies of which 3 frequencies contribute to over 50% of the flow. The distribution is homogeneous, with the primary mode centred at 125 cl/t with a mean salinity of 34.9%.. The secondary mode also has the same salinity characteristics as the primary but occurs at 75 cl/t. The tertiary mode has a higher salinity 35.1%., occurring at 175 cl/t.

The distribution of the eastward flux is homogeneous in nature and has similar characteristics of the westward flux across this belt. Two frequencies make up 50% of the eastward flux and 75% of the flux is distributed among 5 frequencies. The first three modes of the eastward flux appear in the same frequencies as in the case of the westward flux. The Equatorial Countercurrent could be identified between 2° S and 6° S above 300 cl/t. This has a transport of 12.8 km^3/hr.

The flow, between 10° and 16° S (Fig. 5.5.5), is mainly westward (86.7 km^3/hr). The distribution of the flux is heterogeneous in nature with the westward flux between 150 cl/t and 300 cl/t having a salinity more than 35%.. While 13
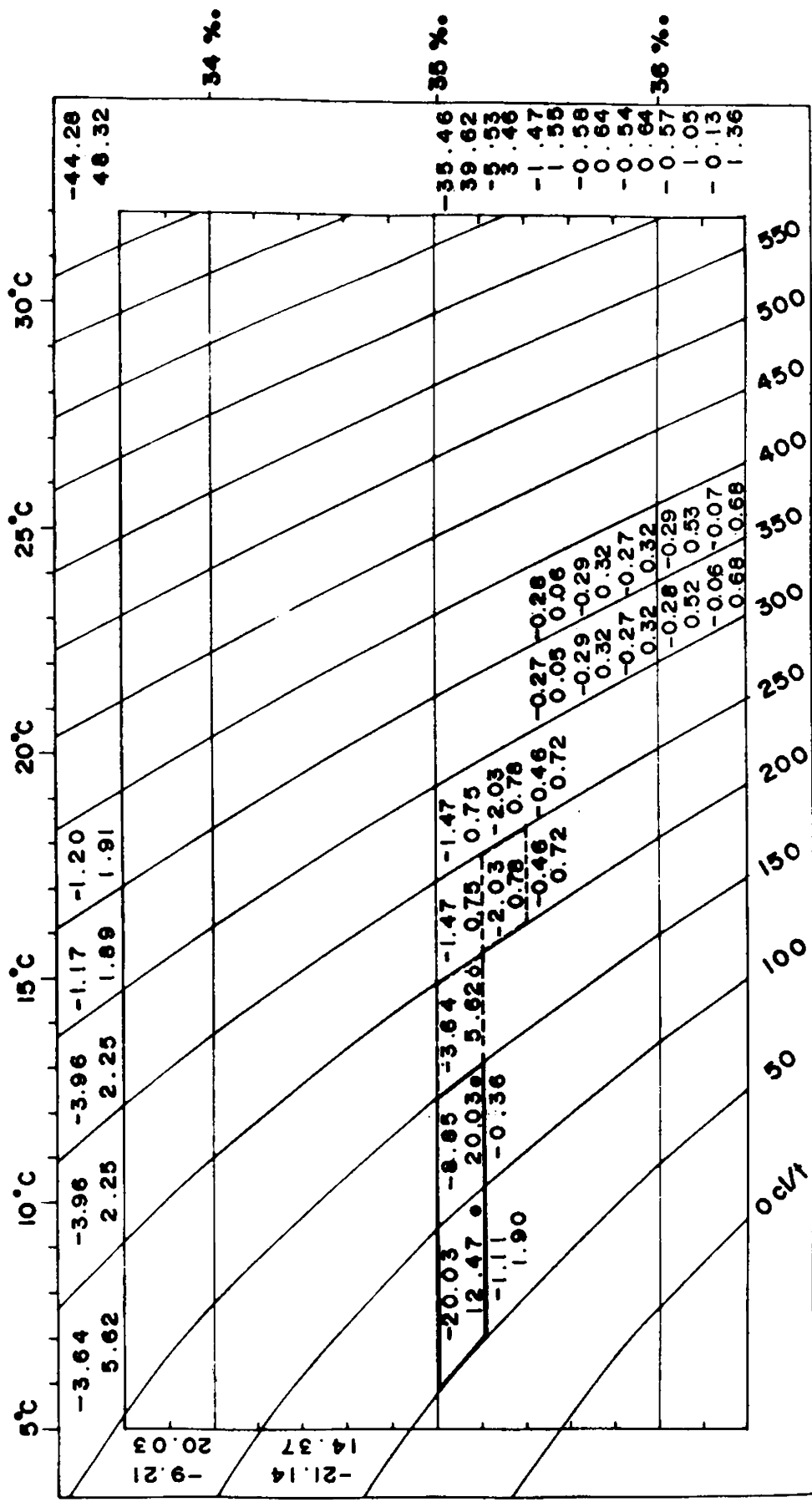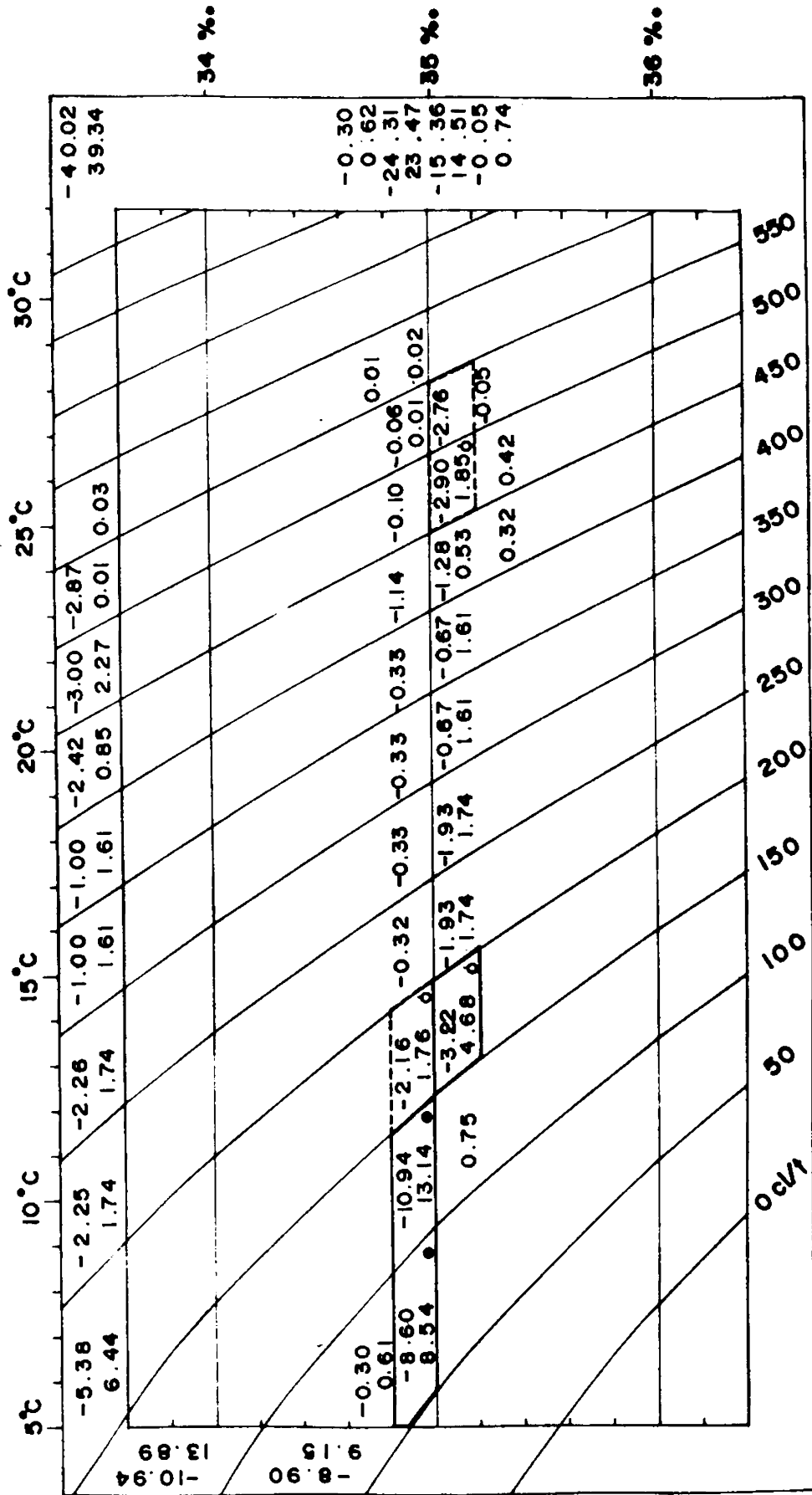
Fig— 5.5.4.— Zonal fluxes across 70°E between 5°S and 10°S during Oct—Nov, 1970
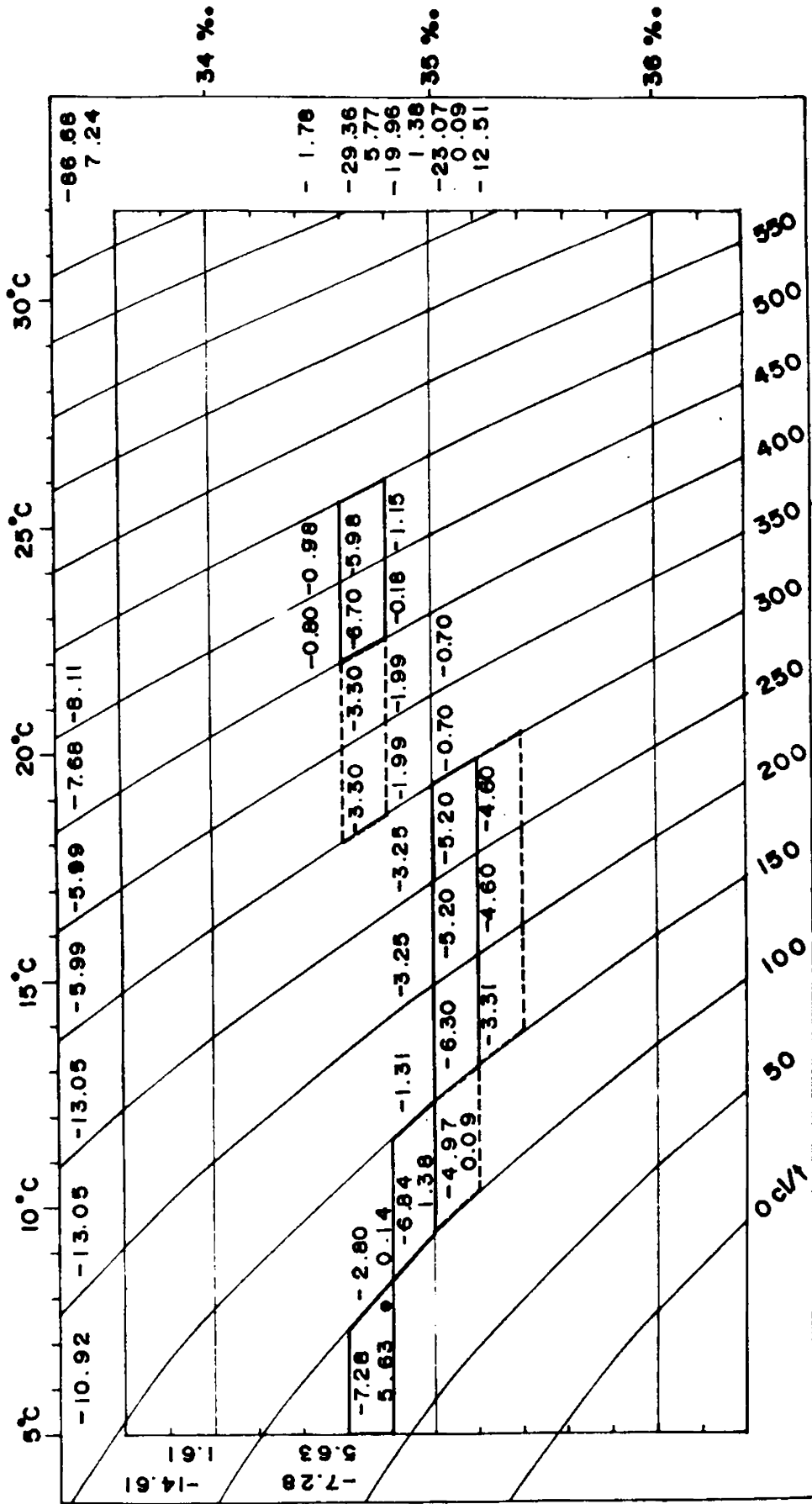
Fig. 5.5.5 – Zonal fluxes across 70°E between 10°S and 16°S during Oct–Nov., 1970

frequencies make up 75% of the flow, 50% of the flux is distributed over 7 frequencies. The primary mode occurs at 75 cl/t and salinity 34.7%.. A secondary mode is seen at 125 cl/t with a mean salinity of 34.9%.. A tertiary mode occurs at 425 cl/t with salinity 34.7%.. The South Equatorial Current appears south of 6^oS and the transport of the current between 6° and 16^oS is 110.5 km^3/hr. The distribution of westward flux over many frequencies indicates that it extends to deeper levels towards south.

5.6   The zonal flux distribution, between 6^oN and 11^oS, are shown in Figs. 5.6.1 to 5.6.3. The total westward flux ($167km^3$/hr) between 6^oN and equator along 78^oE is comparatively lower than that of the eastward flux (Fig. 5.6.1). 50% of the westward flux is contributed by 3 frequencies, two of them occurring below 100 cl/t with the primary mode at 475 cl/t and salinity of 35.5%.. Six frequencies contribute to over 75% of the westward flux. The westward flux above 500 cl/t is only 6.1 km^3/hr. However, the primary mode of 43.9 km^3/hr of the westward flux occurring at 475 cl/t with a mean salinity of 35.5%. could also be attributed to the North Equatorial Current.

The total eastward flux is around $429km^3$/hr, 75% of which is accounted by 3 frequencies, all below 150 cl/t, with salinity 34.8 to 35.2%.. The salinities are always
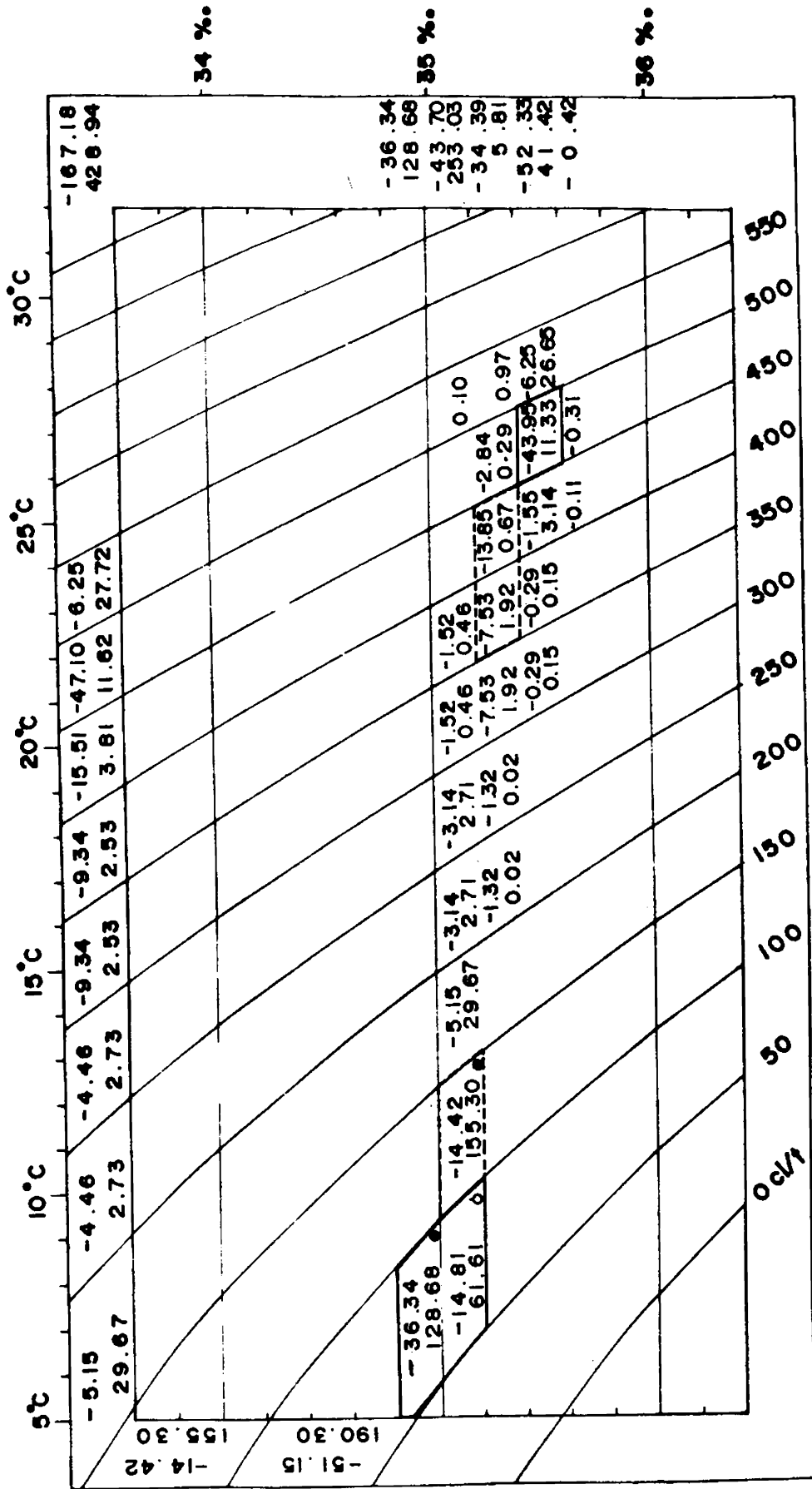
Fig. 5.6.1.- Zonal fluxes across 78°E between 6°N and 0° during December, 1962

higher than 35‰. except for the class below 100 cl/t with a salinity of 34.9‰..

The westward flux (731.1 km^3/hr) is more than twice that of the eastward flux (Fig. 5.6.2). The bulk of both the eastward and westward fluxes occurs below 300 cl/t within the salinity range 34.8 and 35.2‰., except that of a strong westward flux occurring in the surface around 525 cl/t with a salinity of 35.5‰.. An interesting feature observed in the flux distribution is that above 200 cl/t the salinity is more than 35‰., with 50.5 km^3/hr of the westward flux having a mean salinity of 35.5‰ (above 300 cl/t). 75% of the westward flux is contributed by 5 frequencies, all below 200 cl/t except one at 525 cl/t and 6 frequencies constitute 75% of the eastward flux. The Equatorial Countercurrent is seen between 0° and 5° S, above 300 cl/t, having a transport of 60.2 km^3/hr. Compared to all the other sections the westward extent of the Equatorial Countercurrent seems to have been shifted northward upto the equator.

More than half of the total westward flow (55.9 km^3/hr) has a mean salinity of 34.7‰.(Fig. 5.6.3). The first two modes occur at this salinity having mean thermosteric anomaly of 75 and 125 cl/t respectively. Out of the 9 classes that account for 75% of the flow, six of them are found below 300 cl/t and the rest occur above 500 cl/t with salinity varying between 34 and 34.4‰..
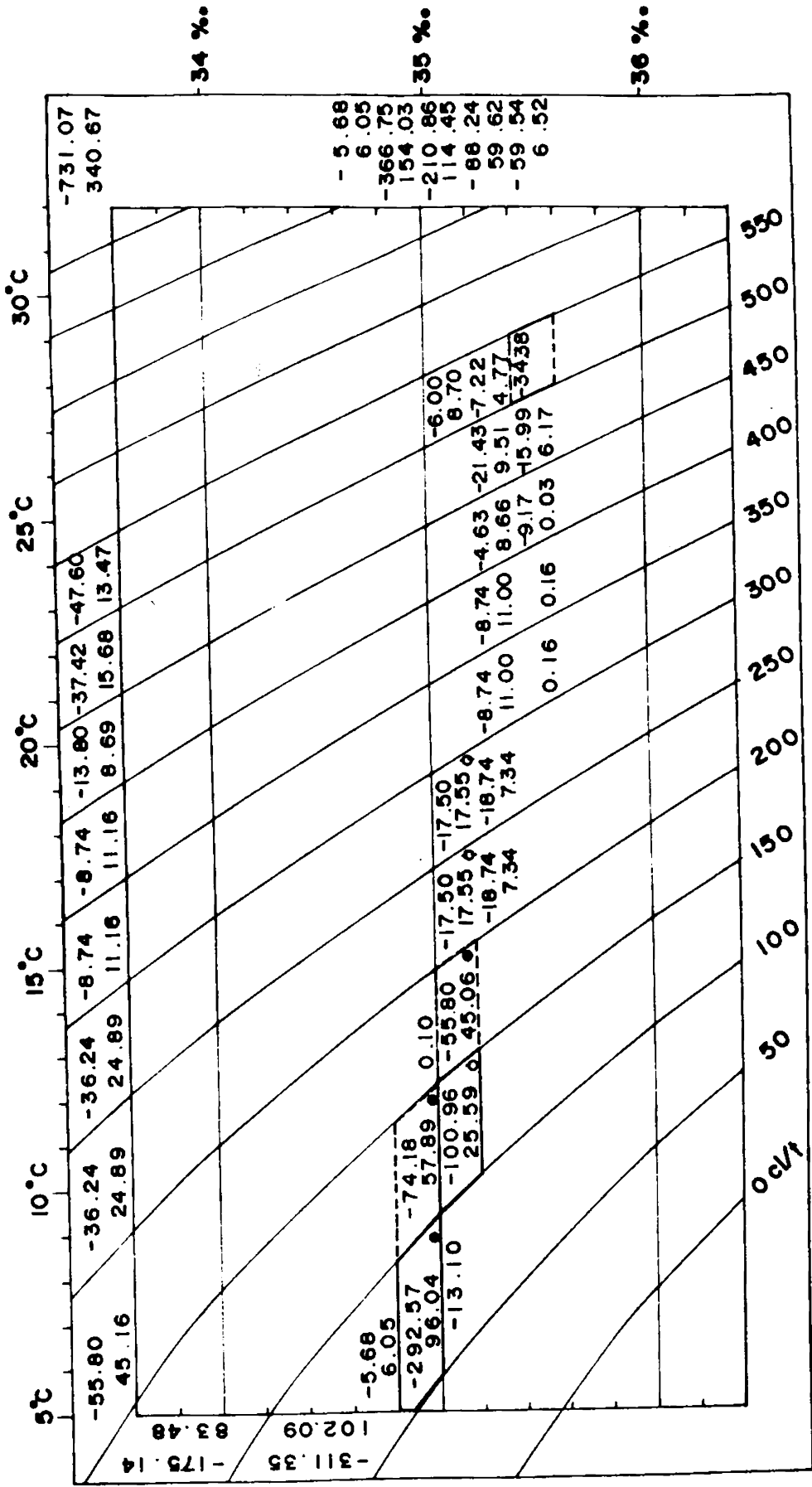
Fig. 5.6.2 – Zonal fluxes across 78° E between 0° and 5° S during December, 1962
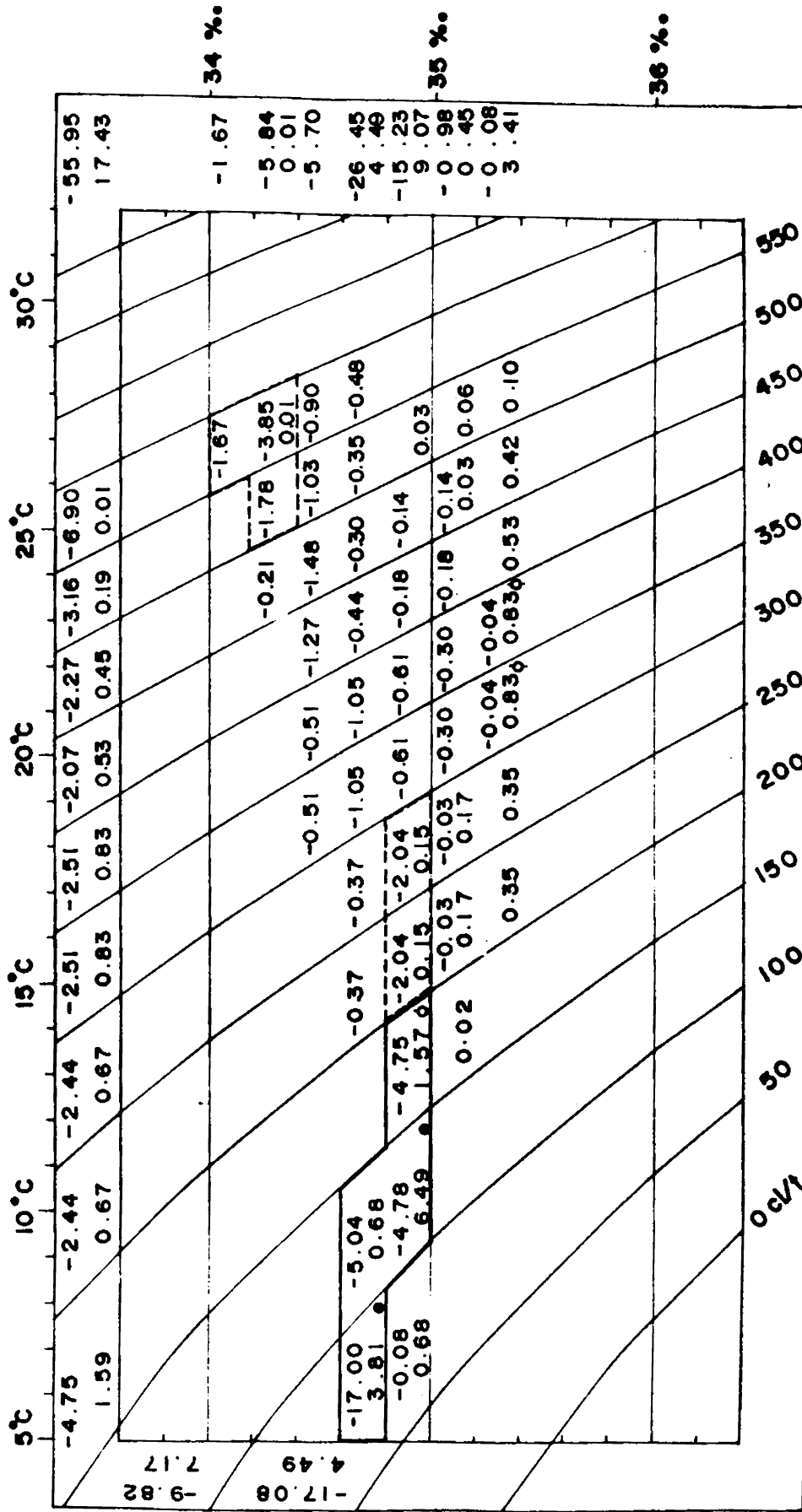
Fig. 5.6.3 – Zonal fluxes across 78°E between 5°S and 11°S during December, 1962

5°C   10°C   15°C   20°C   25°C   30°C

34 %•

35 %•

36 %•

-55.95   17.43   -1.67   -5.84   0.01   -5.70   -26.45   4.49   -15.23   9.07   -0.98   0.45   -0.08   3.41

-4.75   -2.44   -2.44   -2.51   -2.51   -2.07   -2.27   -3.16   -6.90   0.01
1.59   0.67   0.67   0.83   0.83   0.53   0.45   0.19

-17.00   -5.04   -4.75   -0.37   -0.37   -0.51   -0.51   -1.27   -1.78   -3.85
3.81   0.68   1.57   -2.04   -1.05   -1.05   -1.48   -1.03   0.01

-0.08   -4.78   1.57   -0.03   -0.61   -0.61   -0.44   -0.30   -0.90
0.68   6.49   0.15   0.15   -0.18   -0.35

0.02   -0.03   -0.30   -0.30   -0.18   0.03   -0.48
0.17   0.17   -0.04   -0.04   -0.14   0.06

0.35   0.35   0.83   0.83   0.53   0.42   0.10
0.63   0.03   0.03

0 cl/t   50   100   150   200   250   300   350   400   450   500   550

-9.82   -17.08   7.17   4.49

The total eastward flux across this latitudinal belt
is 17.4 km^3/hr and, compared to the westward flux, they have
relatively higher salinity characteristics. 12.5 km^3/hr of
the eastward flux occur in the salinity range 34.8 to
35.4‰.. The primary mode occurs at 125 cl/t, which along
with the secondary mode at 75 cl/t and salinity 34.7‰.,
accounts for over 50% of the total flow.

The South Equatorial Current is seen south of 6°S and
the total westward flux between 6°S and 11°S is 39 km^3/hr.
Along this section the westward flux is maximum between
equator and 5°S and it is least on the southern side,
whereas, the eastward flux is maximum in the latitudinal
belt between 6°N and equator and progressively reduces
towards south.

5.7 The zonal fluxes across 83°E, during January, are
presented in Figs. 5.7.1 to 5.7.6. Both the eastward and
westward fluxes, between 9° and 5°N (Fig. 5.7.1), have same
magnitude. 75% is distributed over 4 frequencies, one
occurring at 575 cl/t (with a low salinity of <34.8‰.). This
is due to the westward transport of the Bay of Bengal Water
through the North Equatorial Current.

Eight frequencies constitute 75% of the flow, 3 of
which are confined to a salinity of 34.9‰. over a wide range
in thermosteric anomaly. Another significant feature seen in
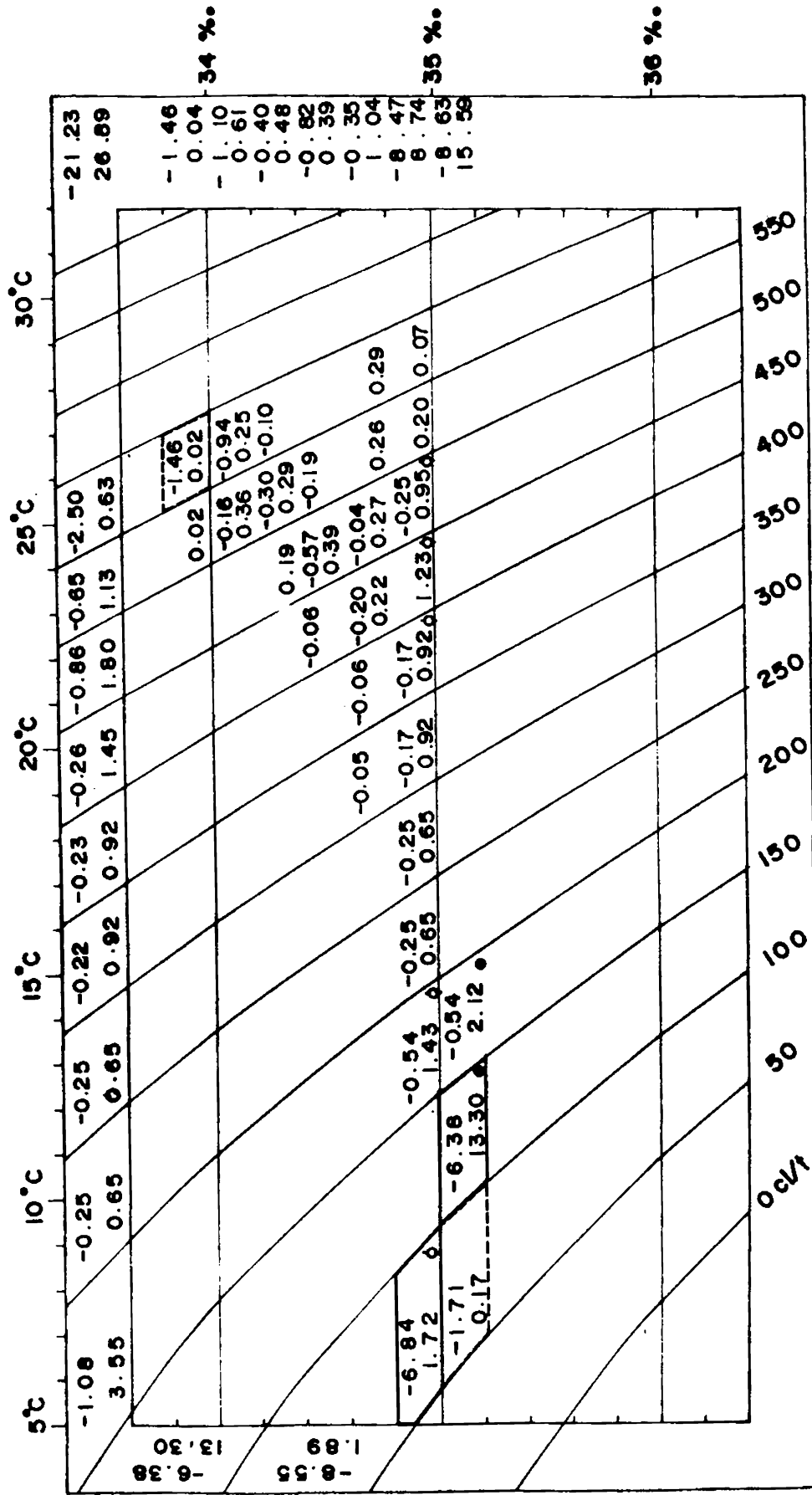
Fig. 5.7.1 - Zonal fluxes across 83°E between 9°N and 5°N during January, 1961

this belt is that the salinities above 200 cl/t are always less than 35‰., while below this the salinities are higher.

The total westward flow is 232 km^3/hr between 0° and 5°N (Fig. 5.7.2). 75% of the flux is distributed over 10 frequencies, indicating heterogeneity in its bivariate distribution. The primary mode occurs at 125 cl/t, which contribute 25% of the flux. The secondary mode at 75 cl/t, with salinity 34.9‰., accounts for nearly 10% of the flow. A tertiary mode is observed at 525 cl/t, having the same salinity as the primary mode (35.1‰.). The North Equatorial Current, between 9° and 2°N, has a total transport of 50.4 km^3/hr, occurring above 200 cl/t. Low salinity frequencies that appear in the surface layer are due to the presence of the Bay of Bengal Water.

The flux distribution, between 0° and 5°S (Fig. 5.7.3), is more or less homogeneous in its salinity characteristics, especially above 100 cl/t. The total westward flux is 170.3 km^3/hr and the primary mode is seen at 75 cl/t, which contribute to about 36% of the flow. A secondary mode occurs at 525 cl/t with salinity 35.1‰. and a tertiary mode having the same salinity is seen at 125 cl/t. The first two modes contribute to over 50% of the flow, while 75% of the westward flux is distributed over 6 frequencies, 4 of them occurring below 200 cl/t.

Fig. 5.7.2 — Zonal fluxes across 83°E between 5°N and 0° during January, 1961
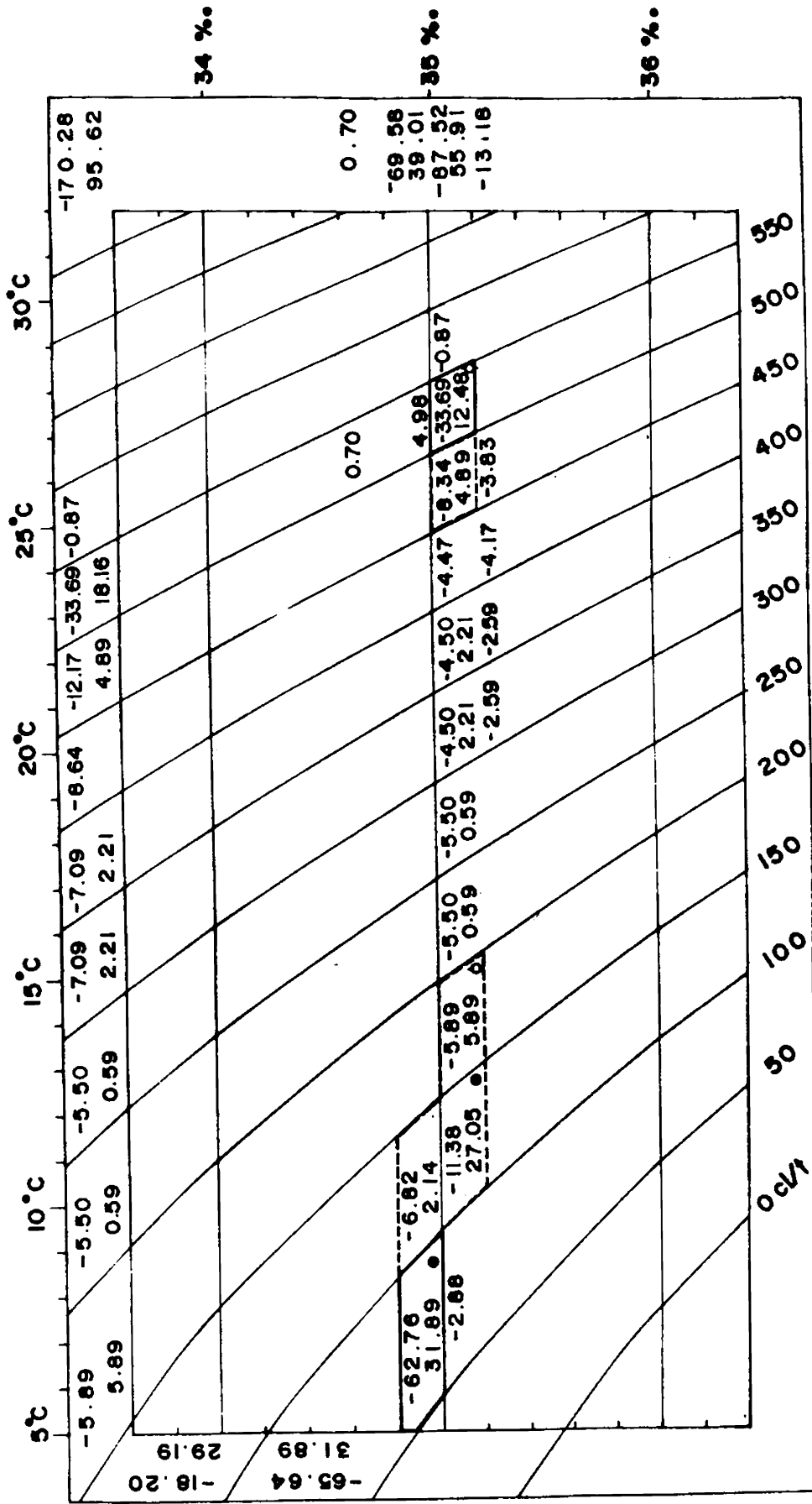
Fig. 5.7.3 — Zonal fluxes across 83°E between 0° and 5°S during January, 1961

The total eastward flux is 95.6 km^3/hr. Four frequencies contribute to over 75% of the flow. The primary mode, with salinity 34.9‰, occurs at 75 cl/t, while the secondary mode, with slightly higher salinity of 35.1‰, is seen at 125 cl/t. A tertiary mode with salinity 35.1‰ is observed at 525 cl/t. The salinity classes above 150 cl/t are always higher than 35‰, except very near the surface, centered around 575 cl/t, where 2 frequencies having low salinity are observed.

The flux distribution, between 5° and 10°S, is heterogeneous, especially in the upper layers, with westward flow having low salinities and eastward flow having higher salinities (Fig. 5.7.4). The total westward flow is 50.2 km^3/hr. Eleven frequencies contribute to over 75% of the flux all below 200 cl/t.

Eight frequencies constitute over 75% of the total eastward flux of 14.6 km^3/hr, mainly confined to salinities between 34.8 and 35.2‰. Four frequencies, all above 400 cl/t, make up 50% of the eastward flux. The primary mode occurs at 475 cl/t with salinity 34.7‰. The second and third modes have a salinity of 35.1‰, occurring between 400 and 500 cl/t. The westward flux, mainly constituted of lower salinity, is possibly due to the incursion of Pacific Ocean Water. The surface eastward fluxes have higher salinities
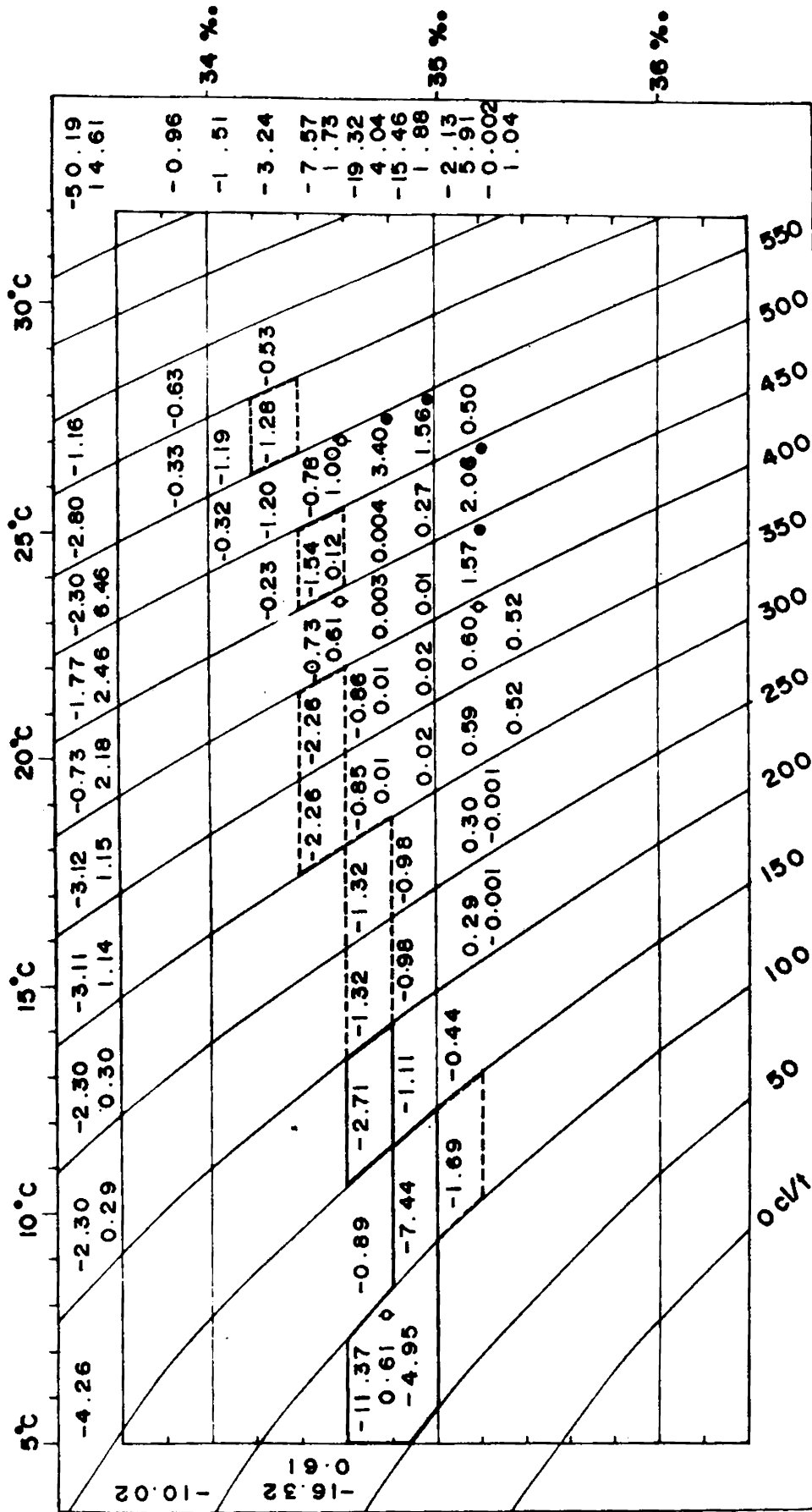
Fig. 5.7.4 - Zonal fluxes across 83°E between 5°S and 10°S during January, 1961

showing the transport of the high salinity waters from the Western Indian Ocean. The Equatorial Countercurrent seen between 1° and 7° S above 300 cl/t has a total transport of 31.6 km^3/hr. Compared to the section at 78° E, the transport is only half along 83° E, though the width of the Equatorial Countercurrent is more.

Between 10° and 15° S (Fig. 5.7.5), 11 frequencies contribute to over 75% of the total westward flow (54.8 km^3/hr). 26% of the total eastward flux (63 km^3/hr) is contributed by the primary mode at 75 cl/t (34.7%.). The second and third modes are found at 125 cl/t, the former having a salinity of 34.9%.. A fourth mode is observed at 575 cl/t having salinity 34.3%.. Thirteen frequencies, showing extreme heterogeneity, constitute 75% of the eastward flux. The transport of the South Equatorial Countercurrent found between 13° and 15° S along this section above 300 cl/t is 19.1 km^3/hr.

The eastward flux, between 15° and 20° S, is insignificant compared to the westward flux (Fig. 5.7.6).The flux distribution is heterogeneous, with higher salinities occurring at intermediate layers. Sixteen frequencies contribute to 75% of the westward flux across this belt (99 km^3/hr). The primary mode occurs at 125 cl/t, with salinity 34.9%.. The eastward flux mode at 475 cl/t has a mean salinity of 34.5%.. The South Equatorial Current is observed
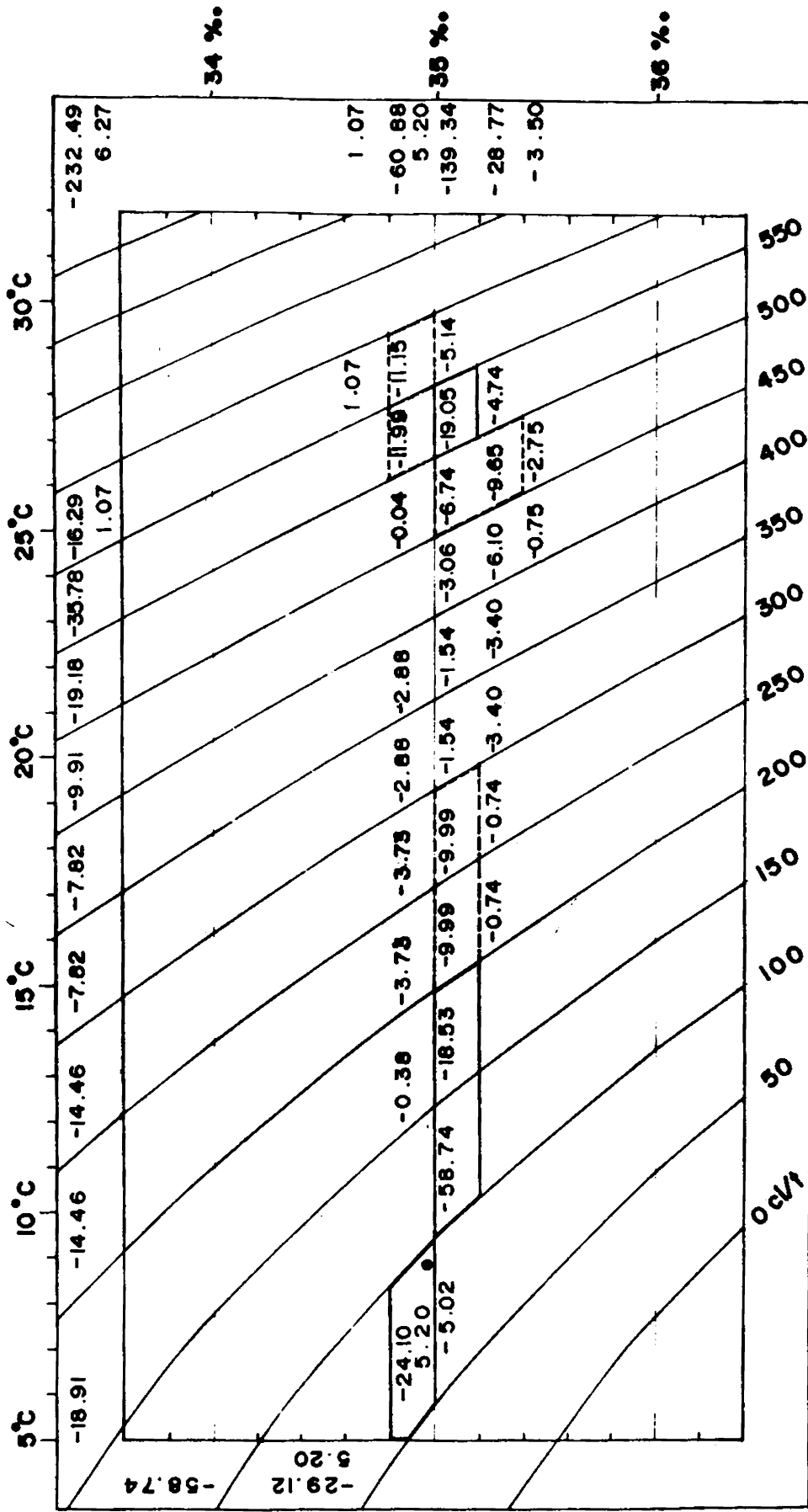
Fig. 5.7.5 – Zonal fluxes across 83°E between 10°S and 15°S during January, 1961
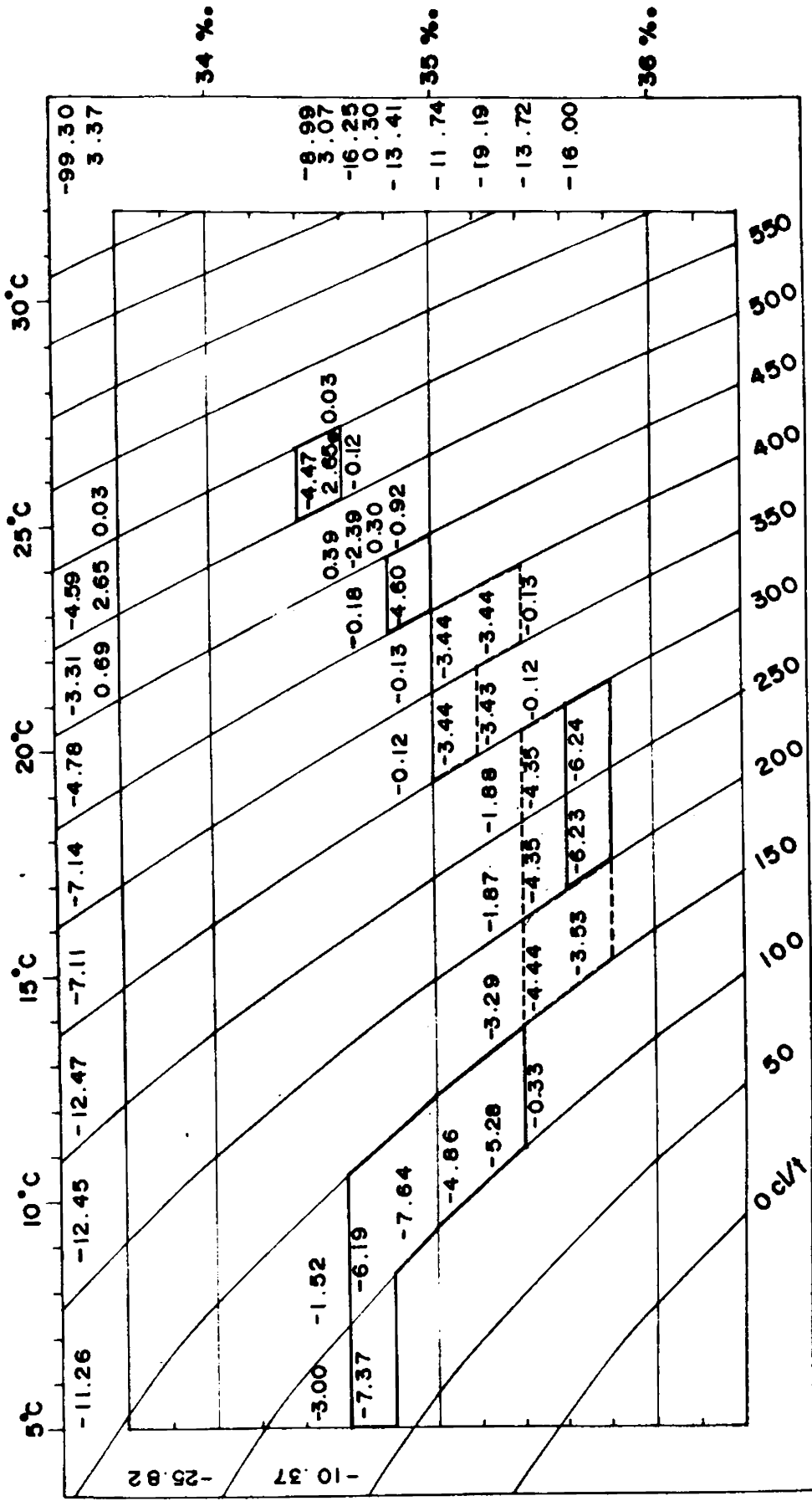
Fig. 5.7.6 — Zonal fluxes across 83°E between 15°S and 20°S during January, 1961

between 7° and 13° S and between 15° and 20° S and the total transport of the current is 83.9 km^3/hr. The Tropical Countercurrent, seen between 18° and 20° S, confined to surface layers, accounts for 3.4 km^3/hr of the eastward transport.

5.8   The zonal flux across 84° E, between 5° N and equator, during May, is given in Fig. 5.8.1. The westward flux (251 km^3/hr) is more than twice that of the eastward flux (109.7 km^3/hr). The flux distribution shows heterogeneity in its bivariate distribution with salinity ranging from 34 to 35.4%.. Maximum westward flow occurs mainly due to waters with salinity higher than 35%., while the eastward flux in the surface layers has a salinity less than 35%.. The westward flux mainly takes place below 200 cl/t with primary and secondary modes at 125 and 175 cl/t respectively. A tertiary mode occurs at 575 cl/t with a salinity of 34.9%.. The first four modes constitute more than 50% of the westward flux while, 75% of the westward flux is distributed over 7 frequencies in the salinity range 34.8 to 35.2%., all occurring below 400 cl/t except the tertiary mode.

The primary and secondary modes of the eastward flux, which contribute to over 50% of the flow, is centred at 575 cl/t with salinity 34.6 to 35%.. Except in the surface
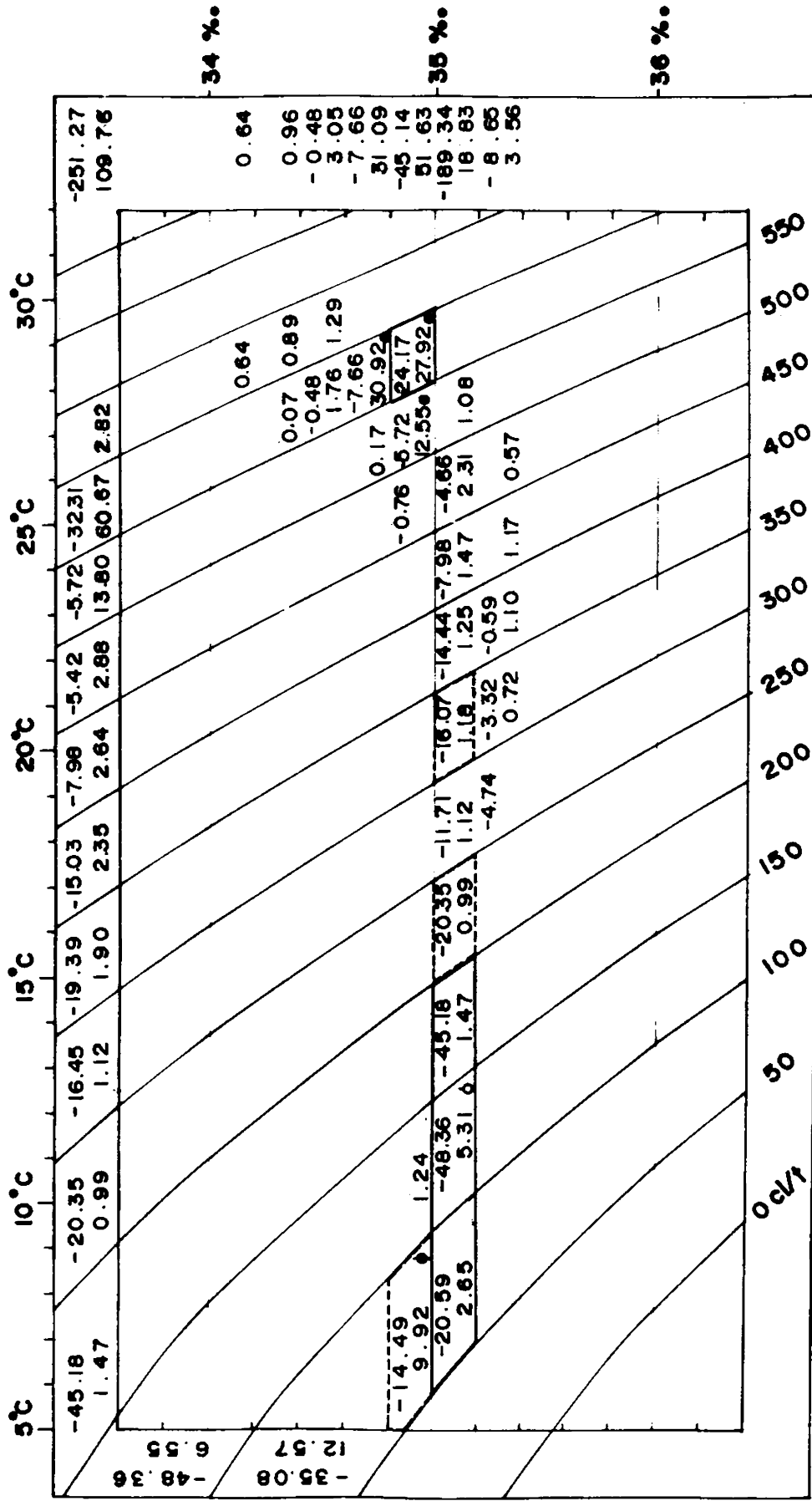
Fig. 5.8.1 _ Zonal fluxes across 84°E between 5°N and 0° during May, 1964

layers and the layers below 150 cl/t the eastward transport is not appreciable in the intermediate layers.

The zonal flux, between 0° and 5° S (Fig. 5.8.2), is similar to that north of the equator, but comparatively less heterogeneous in its distribution, and fewer frequencies (3), all below 200 cl/t, comprise 50% of the total westward flux (241 km^3/hr). Though the primary mode of eastward flux appears at 75 cl/t with salinity 34.9%., the secondary and tertiary modes occur at 525 cl/t and 575 cl/t respectively with the same salinity of 34.9%.. These three modes constitute 50% of the eastward flux. The dominant eastward flow seems to be confined to the surface layers with low salinities. The Equatorial Jet observed across this section, between 2° N and 2° S, similar to the one along 70° E, has a total eastward flux of 156.5 km^3/hr.

5.9   Across 100° E, the westward flux of 91 km^3/hr is about twice as that of the eastward flow (45 km^3/hr), between 5° and 10° S (Fig. 5.9.1). The highest 3 frequencies that comprise more than 50% of the total westward flux occur below 150 cl/t. Even the eastward flux shows a similar distribution pattern. It is thus obvious that the major flow is in the intermediate depths, although the velocity in the surface layer is supposed to be comparatively higher than at intermediate depths. It is interesting to note that in the surface layers there is a lot of heterogeneity. The salinity

91
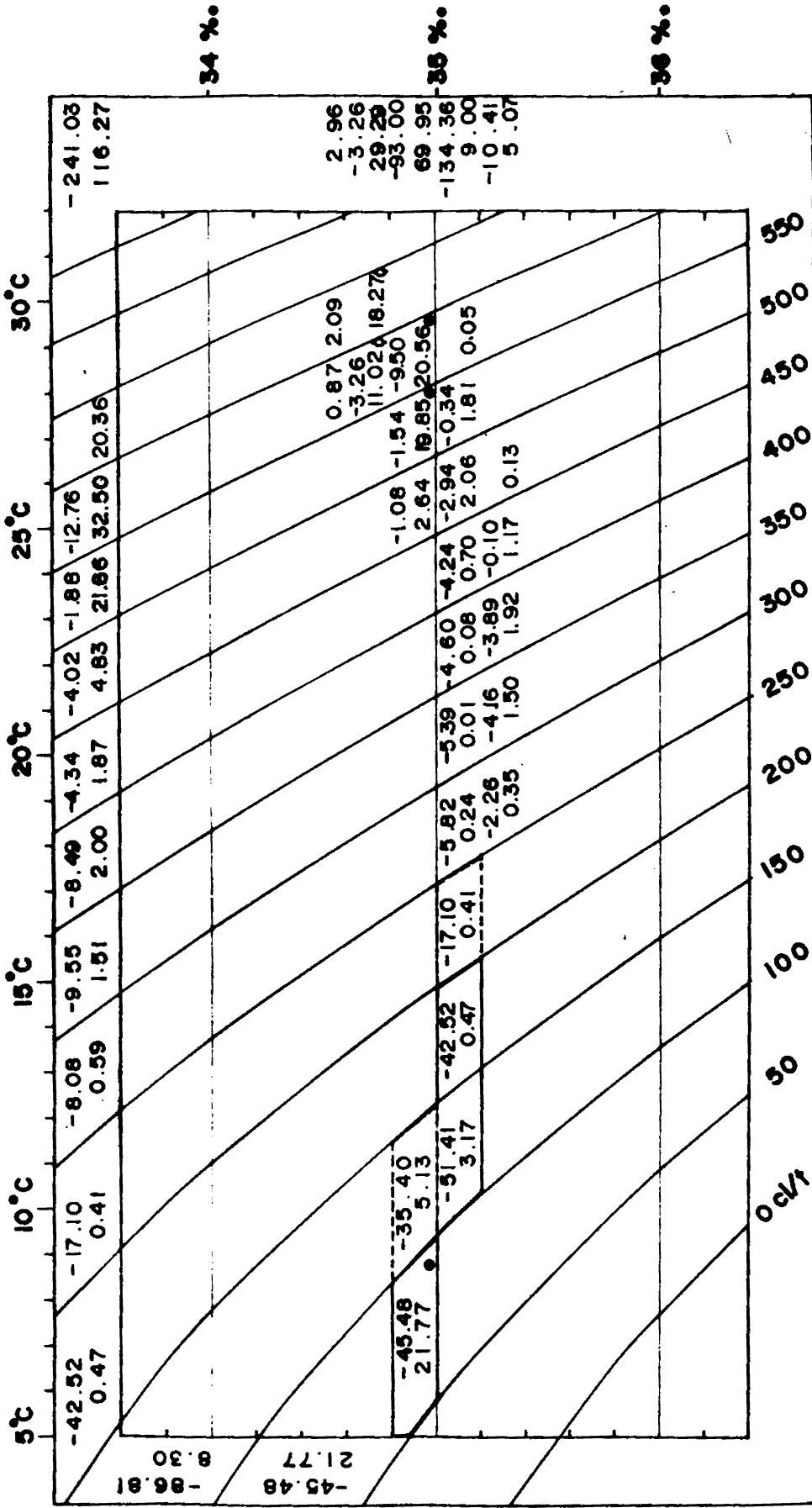
Fig. 5.8.2.—Zonal fluxes across 84°E between 0° and 5°S during May, 1964
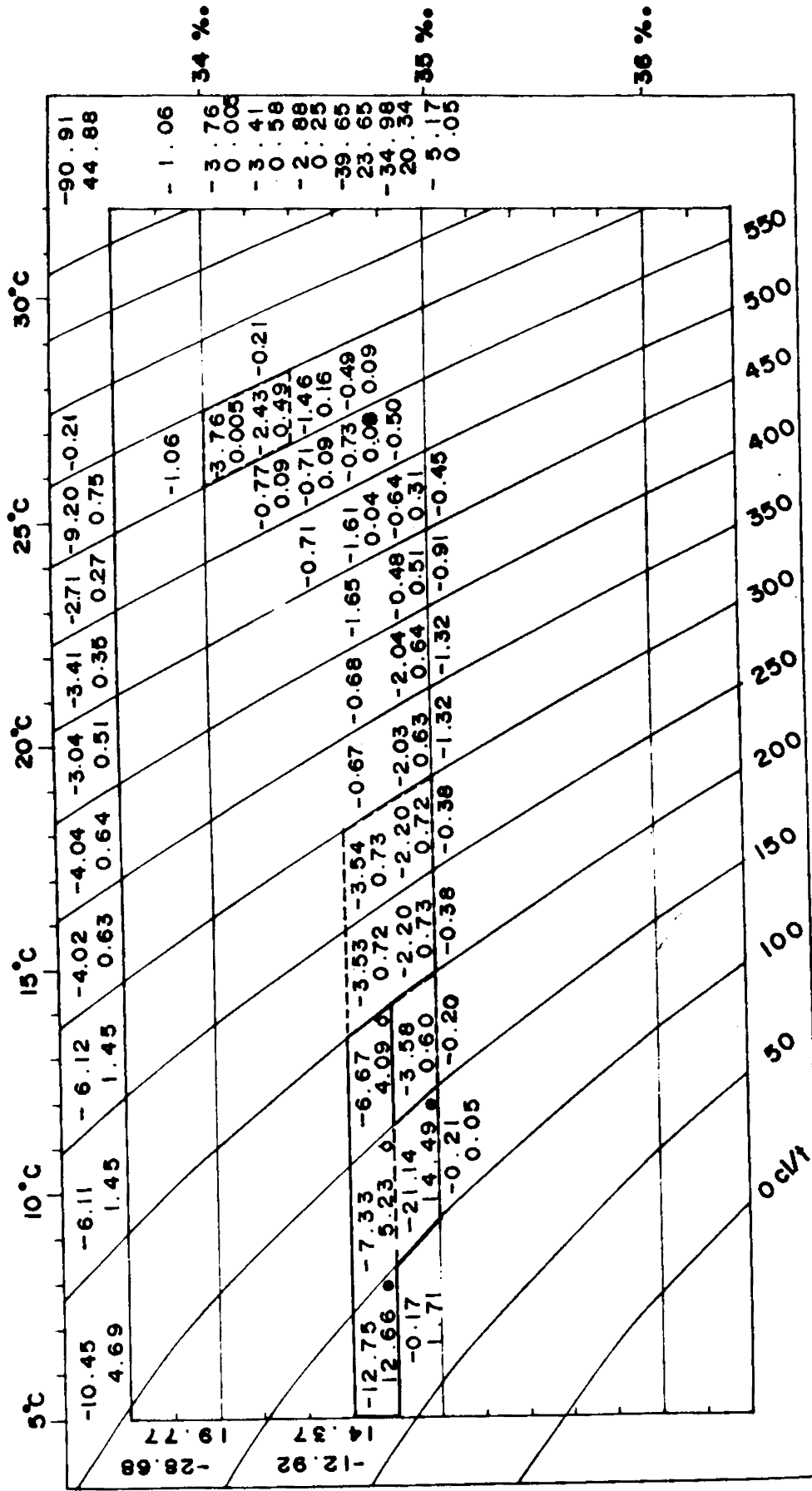
Fig. 5.9.1.- Zonal fluxes across 100°E between 5°S and 10°S during July, 1962

variation of the maximum flux in both directions is confined between 34.6 and 35%. (below 300 cl/t). The Equatorial Countercurrent above 300 cl/t between 4° and 7° S accounts for 3.1 km^3/hr.

The westward flux, between 10° and 15° S, is 64.7 km^3/hr (Fig. 5.9.2), and is almost equal to the eastward flow unlike in the belt between 5° S and 10° S. The primary mode in the westward flux occurs below 200 cl/t in the salinity range of 34.6-34.8%.. The first and second modes of the eastward flow are found below 150 cl/t and in the same salinity range as that of the westward flow, but there is a prominent mode of 16.7 units in eastward flow in the upper layers, within the salinity range of 34.4 and 34.6%.. From the distribution of the frequencies, it is clear that much heterogeneity in the salinity distribution is seen with lower values in the surface and higher values in the subsurface layers. Narrow bands of eastward flow above 200 cl/t, between 10° and 11° S and also between 14° and 15° S, could be due to the South Equatorial Countercurrent having a total 27.3 km^3/hr. It seems that the South Equatorial Countercurrent extends to deeper levels across this section.

Between 15° and 19° S (Fig 5.9.3), in general, there is a reduction in the total flux in both directions compared to the above which implies that the strength of the currents is
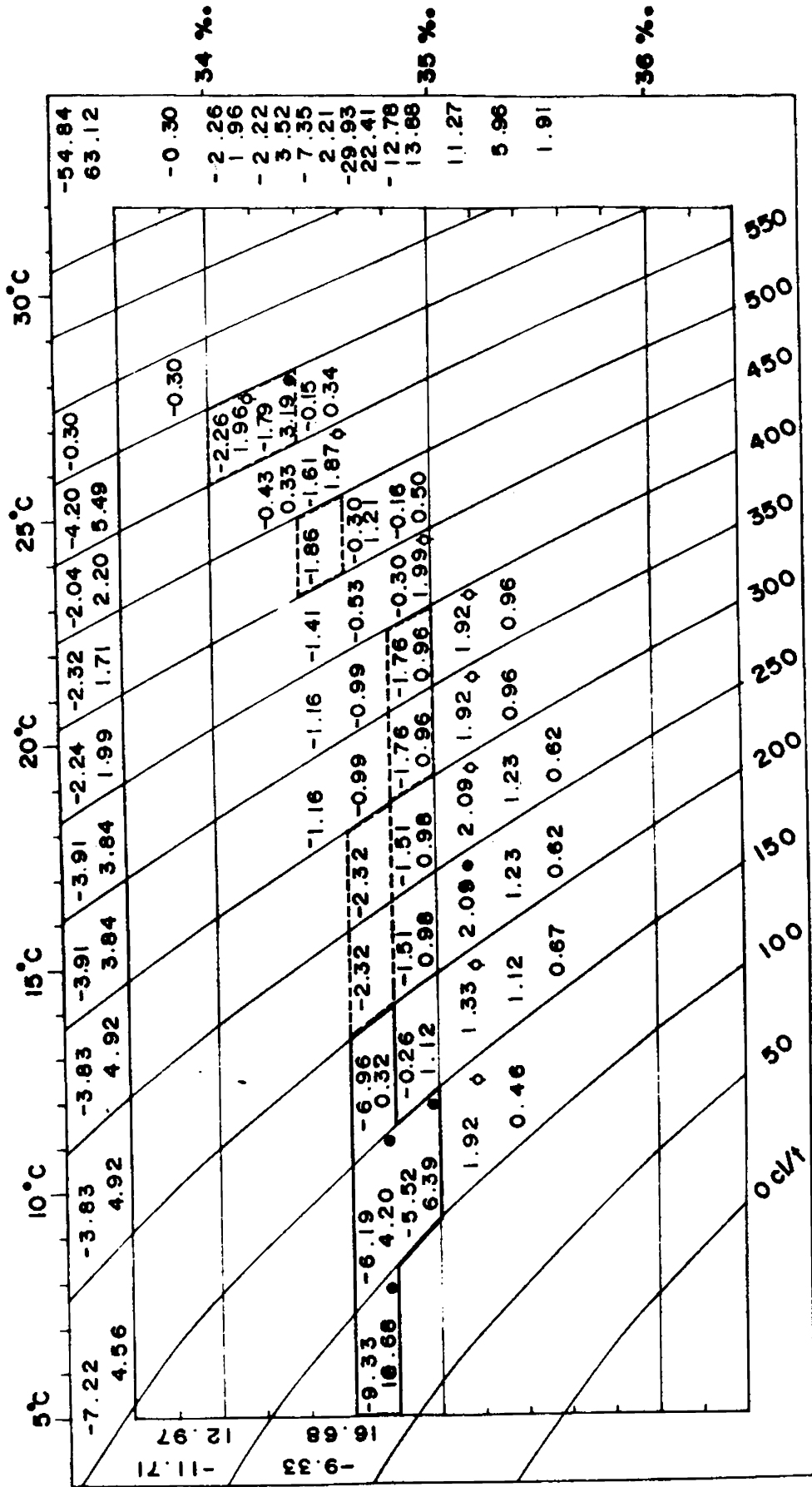
Fig. 5.9.2 - Zonal fluxes across 100° E between 10° S and 15° S during July, 1962
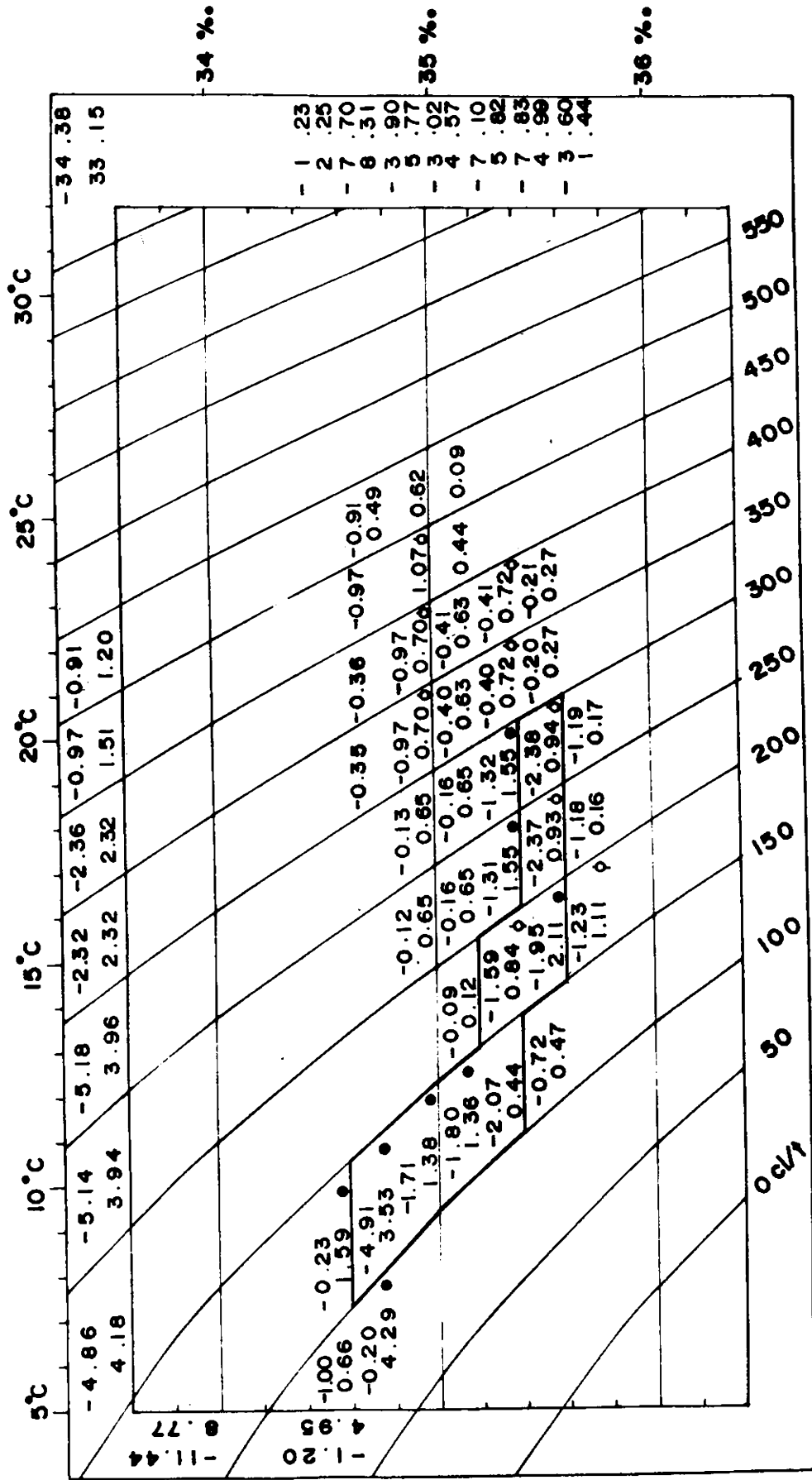
Fig. 5.9.3 — Zonal fluxes across 100°E between 15°S and 19°S during July, 1962

weakened. From the distribution of the frequencies over the bivariate properties, it is clear that the 50% of the eastward as well as westward flux vary from 300 to 50 cl/t and 34.6 to 35.6‰. in salinity. It is normally expected that the higher salinities are associated with eastward flow and low salinities with westward flow. But in the present section it appears that the opposite is prevailing. It may be due to the subtropical gyral circulation in this region. The South Equatorial Current, across this section, is found south of 7° S and its total transport is 163 km^3/hr, which is broken up into three bands with eastward flow attributed to the South Equatorial Countercurrent and Tropical Countercurrent embedded in it. The total transport of the Tropical Countercurrent is 3.2 km^3/hr.

5.10   The flux distribution, across 106° E, is presented in Figs. 5.10.1 to 5.10.4 for the different latitudinal belts. Between 7° and 10° S (Fig. 5.10.1),the westward flux of 53.3 km^3/hr comprises of water with salinities less than 35‰.. No eastward flux is observed. Seven frequencies contribute to over 75% of the westward flux while 50% of the flux is distributed over 3 frequencies. The primary mode occurs at 75 cl/t with salinity 34.7‰.. The secondary and tertiary modes also have the same salinity and is found at 125 and 175 cl/t surfaces respectively.
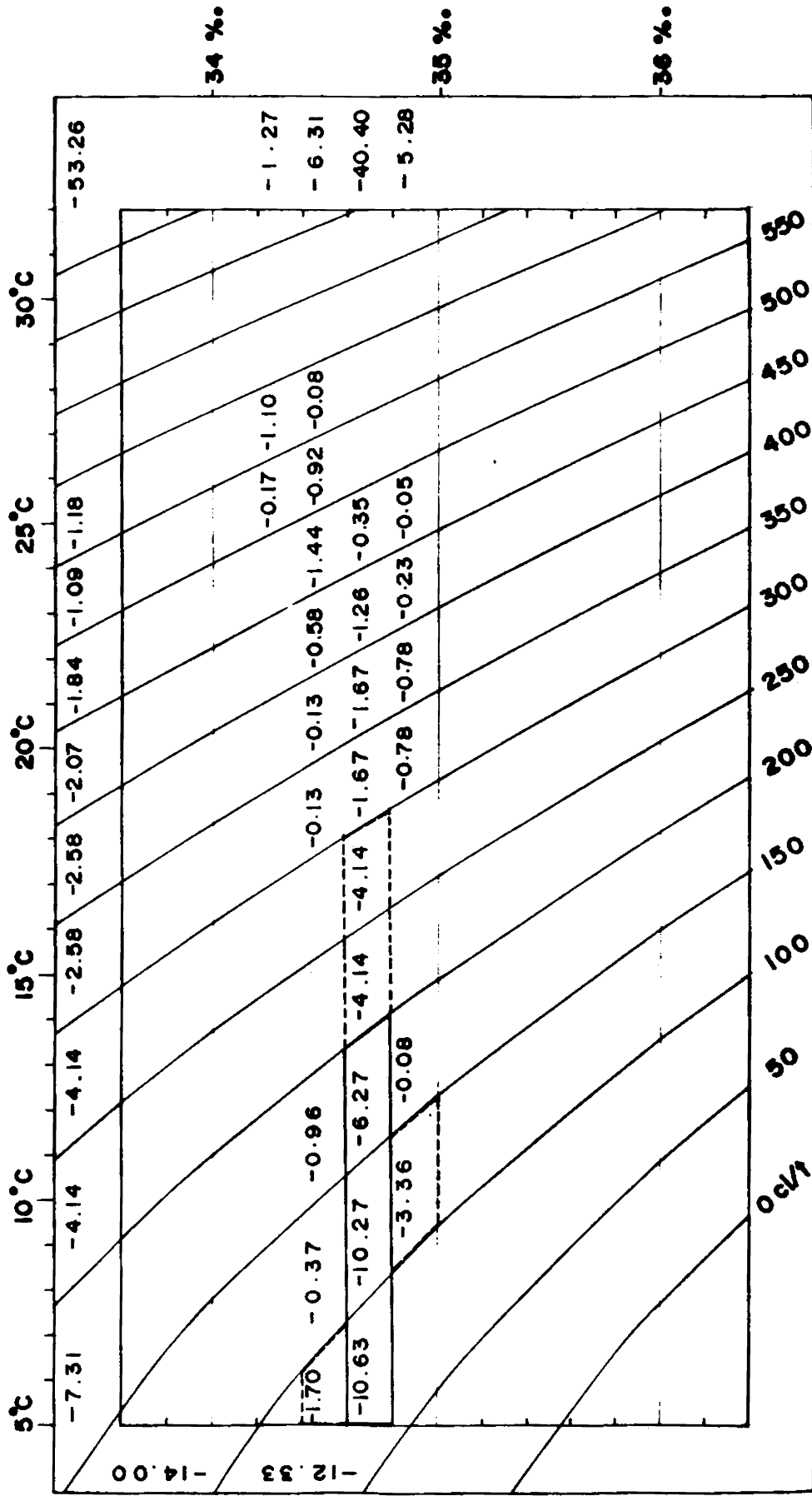
Fig. 5.10.1. Zonal flux across 106°E between 7°S and 10°S during December, 1960

Frequencies with higher salinities occur at intermediate depths, between 100 and 200 cl/t isanosteric surfaces, in the latitudinal belt 10° to 15^oS (Fig. 5.10.2). Eleven frequencies contribute to over 75% of the westward flow (13.9 km^3/hr). The primary mode is found at 575 cl/t with a salinity of 34.3%.. The secondary mode is seen at 75 cl/t with a salinity 34.7%.. A tertiary mode occurs at 475 cl/t also with salinity 34.3%..

The eastward flow of 8 km^3/hr is mainly confined to layers below 200 cl/t having a mean salinity of 34.7%. with the primary mode occurring at 125 cl/t. These three modes contribute to over 75% of the flux with 50% of the flux taking place below 150 cl/t. Above 200 cl/t, the flux distribution is confined to salinities less than 35%.. Between 7° and 15^oS, all the significant frequencies of the westward flow occur in salinity less than 34.8%. implying the westward incursion of the low salinity Pacific Ocean Water.

The flux distribution is heterogeneous and the flow is mainly westward (47.8 km^3/hr) between 15° and 20^oS (Fig. 5.10.3). Twelve frequencies contribute to 75% of the flow. 50% of the flux is distributed over 4 frequencies. The first three modes occur below 150 cl/t with salinity ranging between 34.6 and 35%.. A fourth mode occurs at 425 cl/t
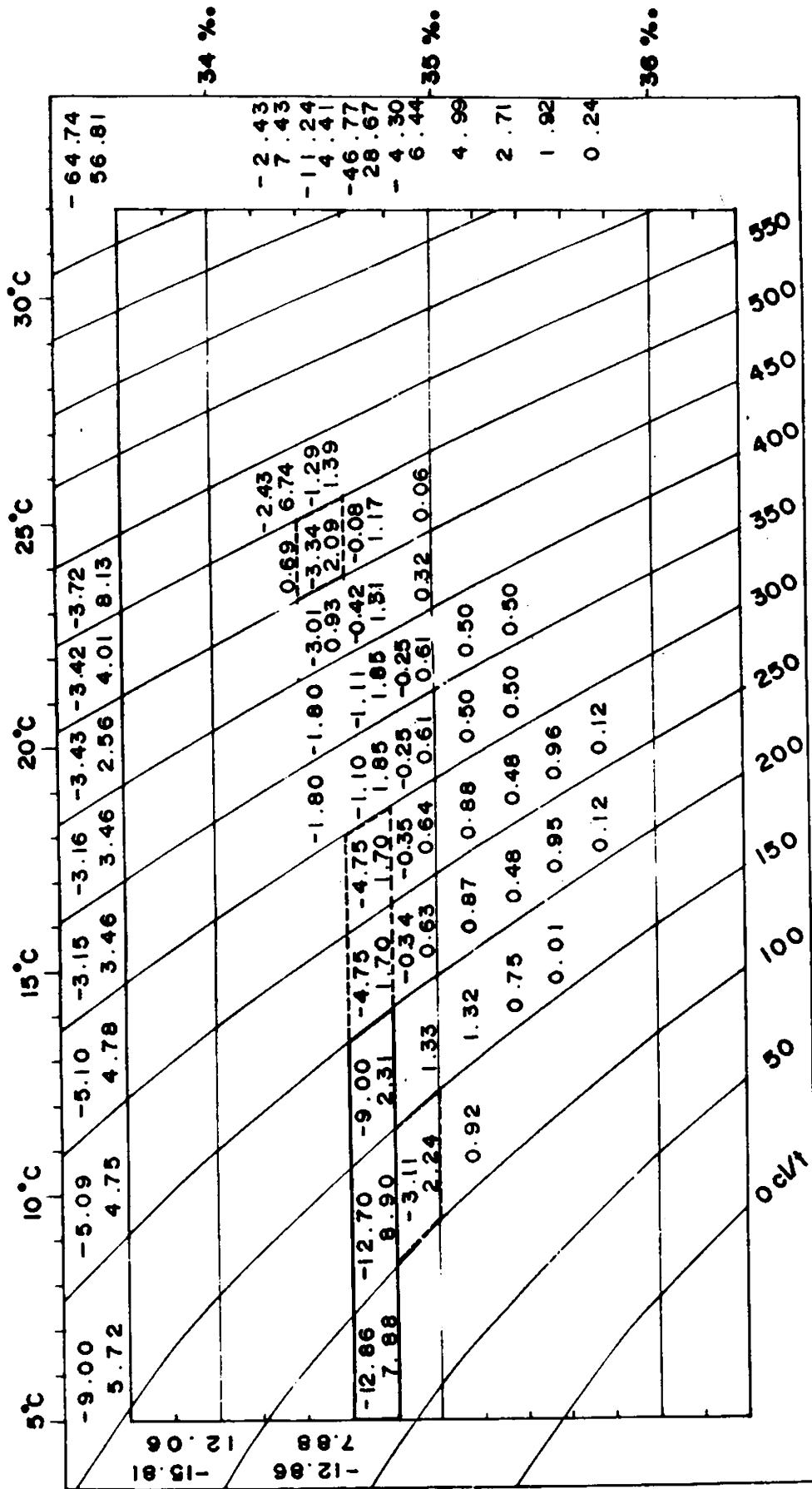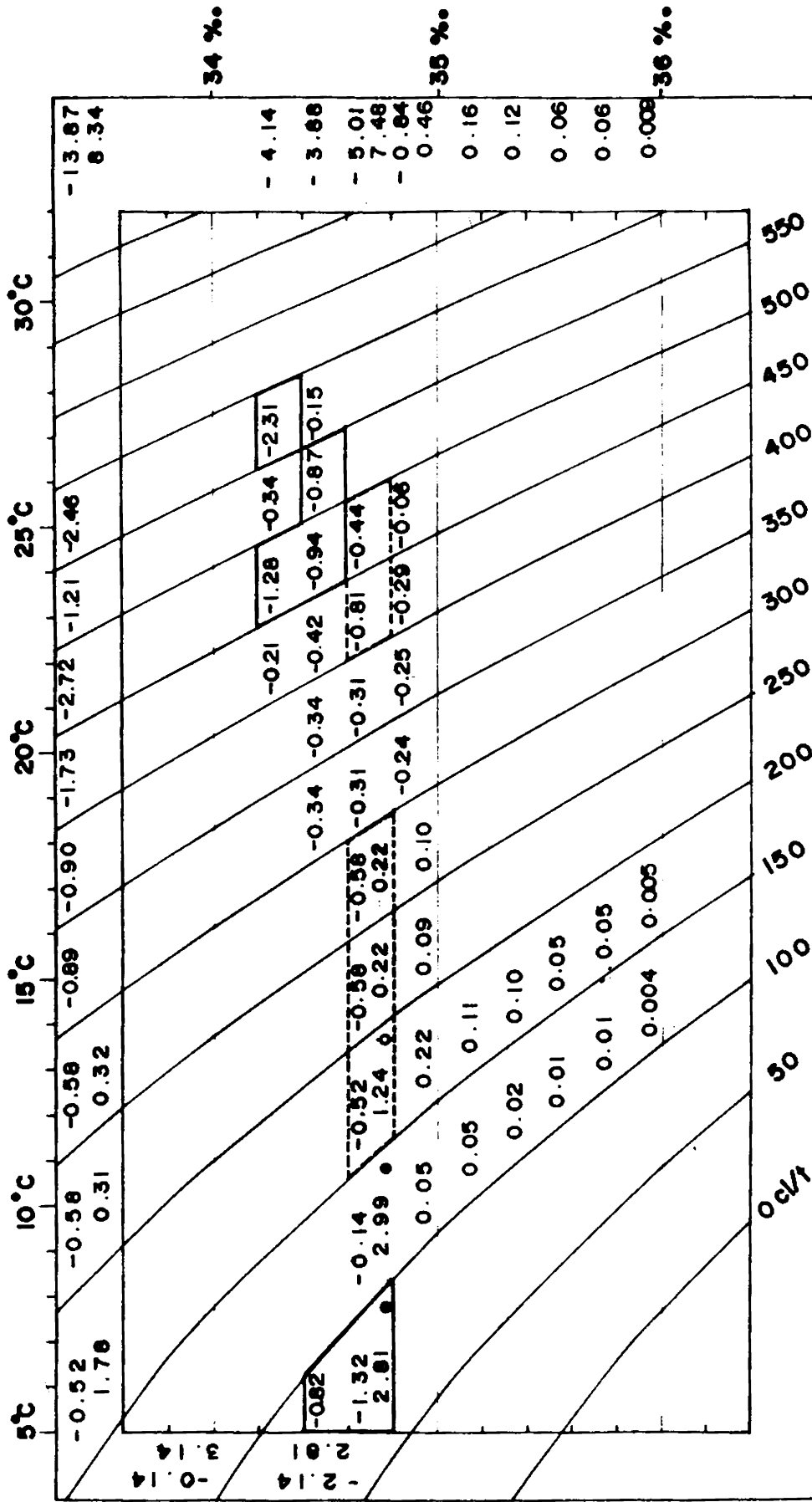
Fig. 5.10.2_Zonal fluxes across 106°E between 10°S and 15°S during December, 1960
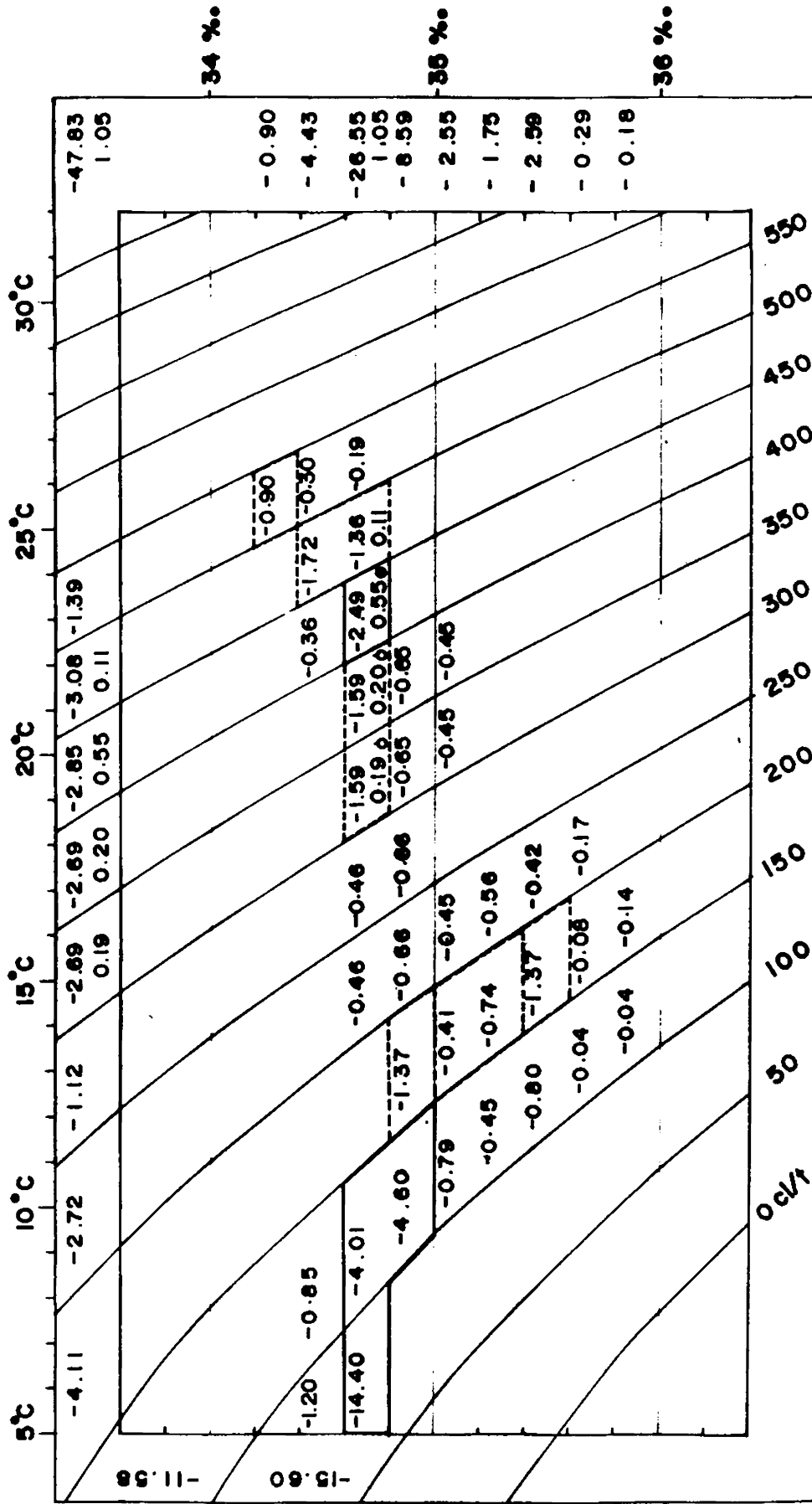
Fig. 5.10.3. Zonal fluxes across 106° E between 15° S and 20° S during December, 1960

having salinity 34.7%.. The westward flow with salinity characteristics greater than 35.2 is found between 100 and 200 cl/t. The eastward flux is negligible (1 km^3/hr).

The flux between 20° and 25° S (Fig. 5.10.4) is distributed over a wide range in salinity, varying from 34.4 to 36%.. Above 150 cl/t frequencies with salinities lower than 35%. are absent. The fluxes in the higher salinity range in the surface layers are predominantly easterly.

The total westward flux observed is 22 km^3/hr with the highest 4 frequencies adding upto over 50%. Except for the tertiary mode, which occurs at 175 cl/t having a mean salinity of 35.7%., the bulk of the flow occurs below 150 cl/t with salinities lower than 34.8%..

The total eastward flux (16.7 km^3/hr) is comparable in magnitude with that of the westward flux. The distribution is also more heterogeneous with 10 frequencies constituting 75% of the flow. Except for the secondary mode of the eastward flux occurring at 75 cl/t (34.5%.) the flow mainly occurs between 150 and 300 cl/t in the salinity range 35.6%. to 36%.. The South Equatorial Current, between 10° and 25° S, with an eastward Tropical Countercurrent confined to the surface layers between 17° and 25° S, accounts for 103.6 km^3/hr. The Tropical Countercurrent has a transport of 11.1 km^3/hr. Eventhough the width of the South Equatorial Current

Fig. 5.10.4_Zonal fluxes across 106°E between 20°S and 25°S during December,1960

is broader compared to the section along 100°E in July, the transport is much less, which may probably indicate the strengthening of the South Equatorial Current during the southwest monsoon.

5.11   The zonal flux across 53°E, between 5°N and equator, in August, is shown in Fig. 5.11.1. While the total westward flow is 347 km^3/hr, eastward flow is only 153.5 km^3/hr. Distribution of the flux is mainly confined to salinities higher than 35‰.. The primary and secondary modes for both the eastward and westward flow have the same characteristics in salinity and thermosteric anomaly. While 3 frequencies below 200 cl/t with mean salinity 35.1‰. account for 50% of the westward flux, 75% of the westward flux comprises of 5 frequencies, the additional frequencies having a mean salinity of 35.5‰. and occurring above 400 cl/t, is obviously of Arabian Sea origin. 50% of the eastward flux is confined to thermosteric anomaly less than 200 cl/t comprising of 3 frequencies. The primary mode accounts to 25% of the flux.

In the 5-degree-latitudinal belt south of the equator (Fig. 5.11.2), the bivariate distribution shows more heterogeneity than to its north. The bulk of the total westward flux of 453 km^3/hr takes place below 150 cl/t, having a mean salinity of 34.9‰., while the major portion of the eastward flux occurs above 150 cl/t, mainly having
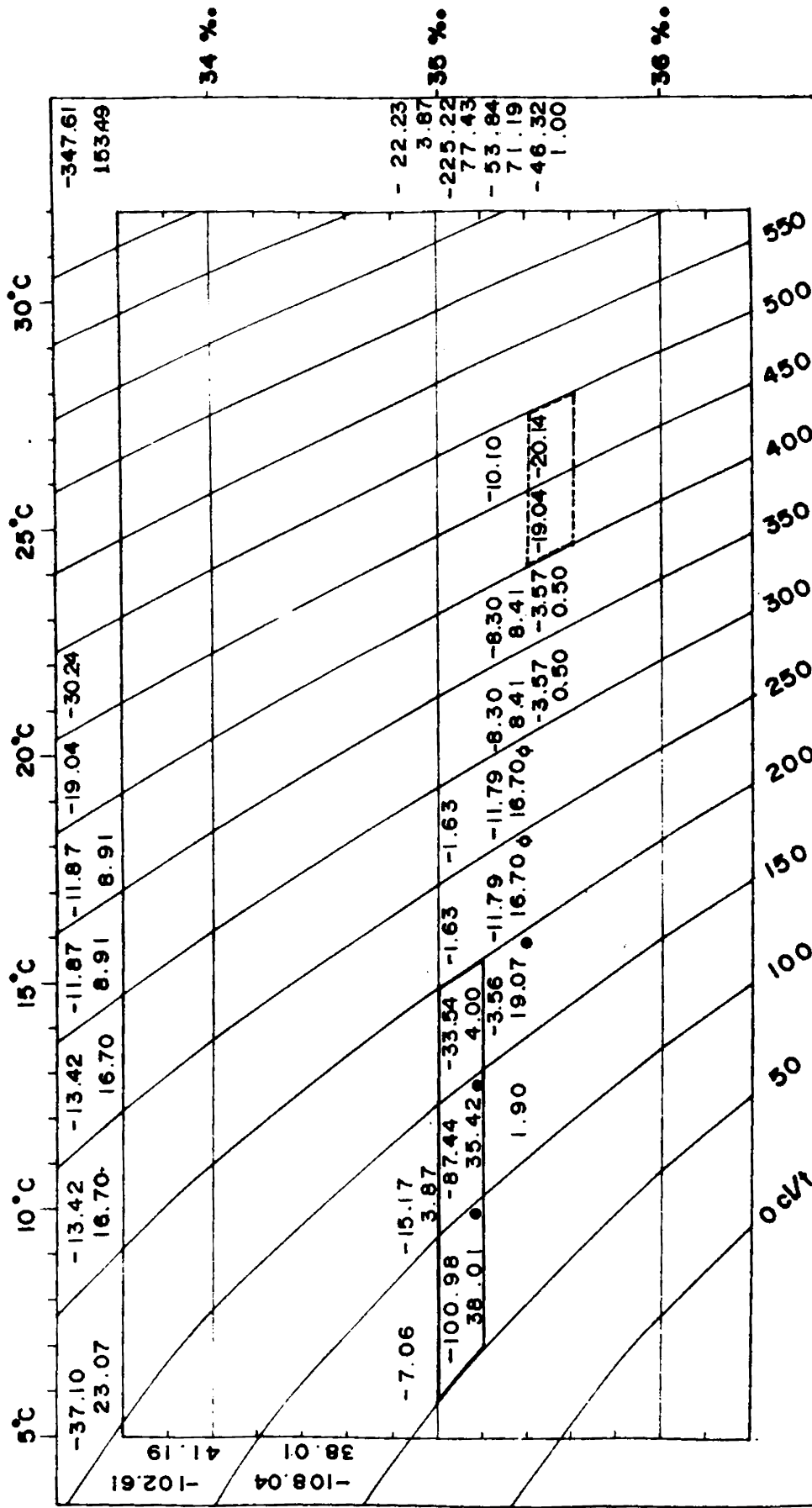
Fig. 5.11.1 _ Zonal fluxes across 53°E between 5°N and 0° during Jul._Aug., 1962

Fig. 5.11.2.— Zonal fluxes across 53°E between 0° and 5°S during Jul.—Aug., 1962

salinities greater than 35.2‰..   While 3 frequencies in the salinity range 34.8‰. and 35.2‰. make up 75% of the westward flux, the eastward flow is distributed over 9 frequencies. The total westward flux increases south of the equator, whereas, the eastward transport appears to be consistent. The Monsoon Current appears between 5° N and 4° S in the Western Indian Ocean, above 300 cl/t, with a total transport of 104.4 km^3/hr.

5.12   The flux distribution across 53° E north and south of the equator (May 1963) is presented in Figs. 5.12.1. and 5.12.2. respectively.   The distribution shows more heterogeneity in its bivariate characteristics, compared to the section covered during July-August of the previous year.   The bulk of the total eastward flux (129.8 km^3/hr) occurs below 200 cl/t in the salinity range 34.8 to 35.2‰..   The distribution shows a strong westward flow in the surface layers. The eastward flux during this period north of the equator is similar in magnitude during July-August.

South of the equator (Fig. 5.12.2), more than half of both the eastward and westward flux occurs below 200 cl/t in the salinity range 34.8 to 35.2‰..   The primary and secondary modes of the total eastward flux (243.3 km^3/hr) have a mean salinity of 34.9‰.. The first two modes of the
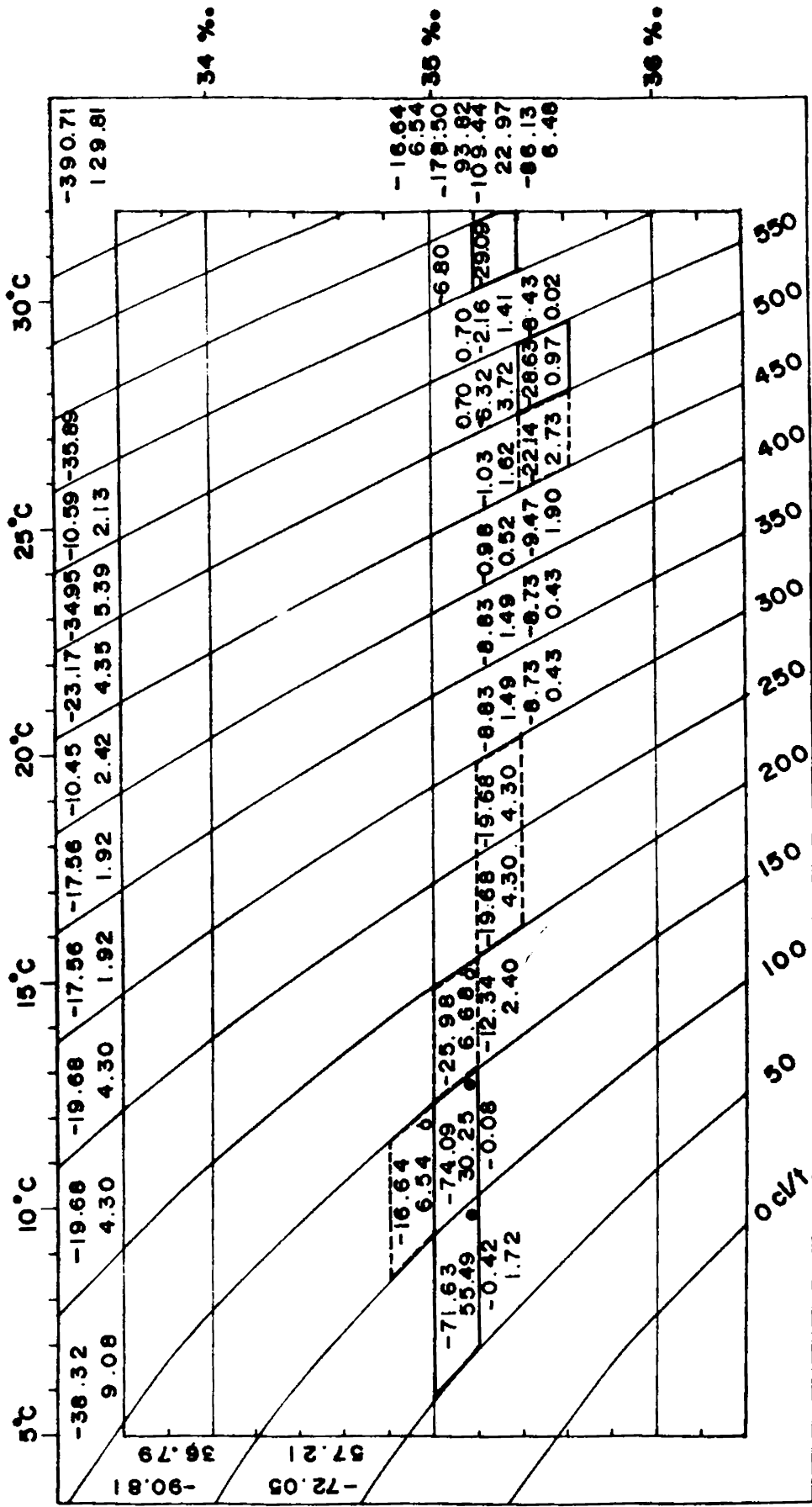
Fig. 5.12.1—Zonal fluxes across 53°E between 5°N and 0° during May, 1963
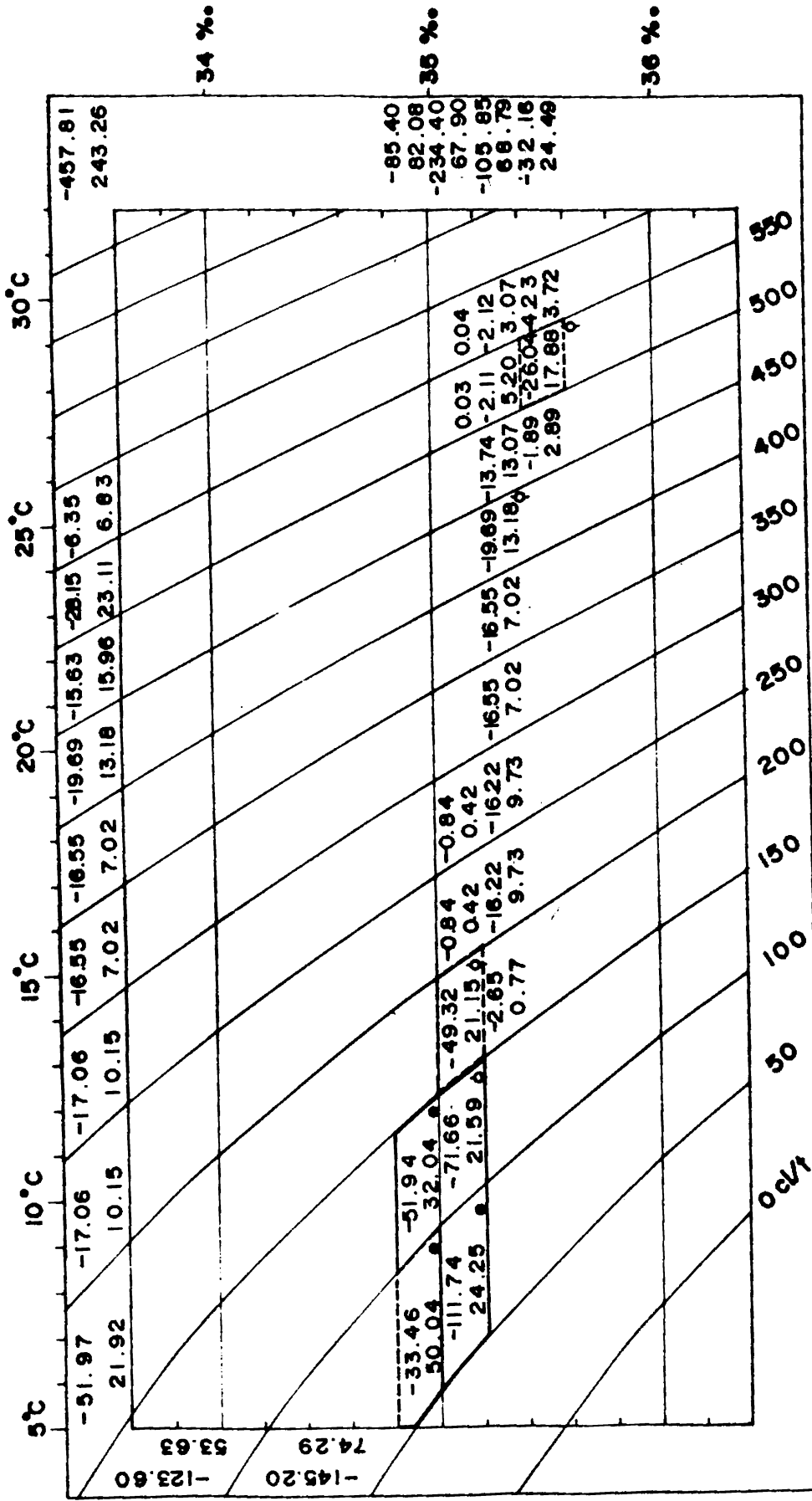
Fig. 5.12.2 _Zonal fluxes across 53°E between 0° and 4°S during May, 1963

total westward flux (457.8 km^3/hr) have a higher mean salinity. The eastward flux between 0° and 5°S during July-August is half of that observed between 0° and 4°S in May. The Monsoon Current observed during August seems to have generated by May itself and it has an eastward transport of 91.2 km^3/hr.

5.13 The zonal fluxes across 61°E in the 5 degree belt north of the equator is shown in Fig.5.13.1. The distribution of the fluxes is again mainly confined to salinities higher than 35‰.. The westward flow is mainly confined to the surface layers with 5 of the 6 frequencies that contribute to 50% of the flow occurring above 300 cl/t. 75% of the westward flow is distributed over ten frequencies. In contrast, the bulk of the total eastward flow (110 km^3/hr) is seen below 250 cl/t, with the two frequencies that contribute over 50% of the east flux having a mean salinity of 35.1‰..

The total westward flow (486 km^3/hr) is more than twice of the eastward flow (Fig. 5.13.2). 75% of the eastward flux occur below 200 cl/t having a mean salinity of 34.9‰.. 50% of the westward flux also has the same salinity while the 2 additional classes that together make up 75% of the flow occur at a salinity of 35.1‰., below 150 cl/t. The westward flux is confined to layers below 200 cl/t, south of the equator, compared to the southern half. The total westward
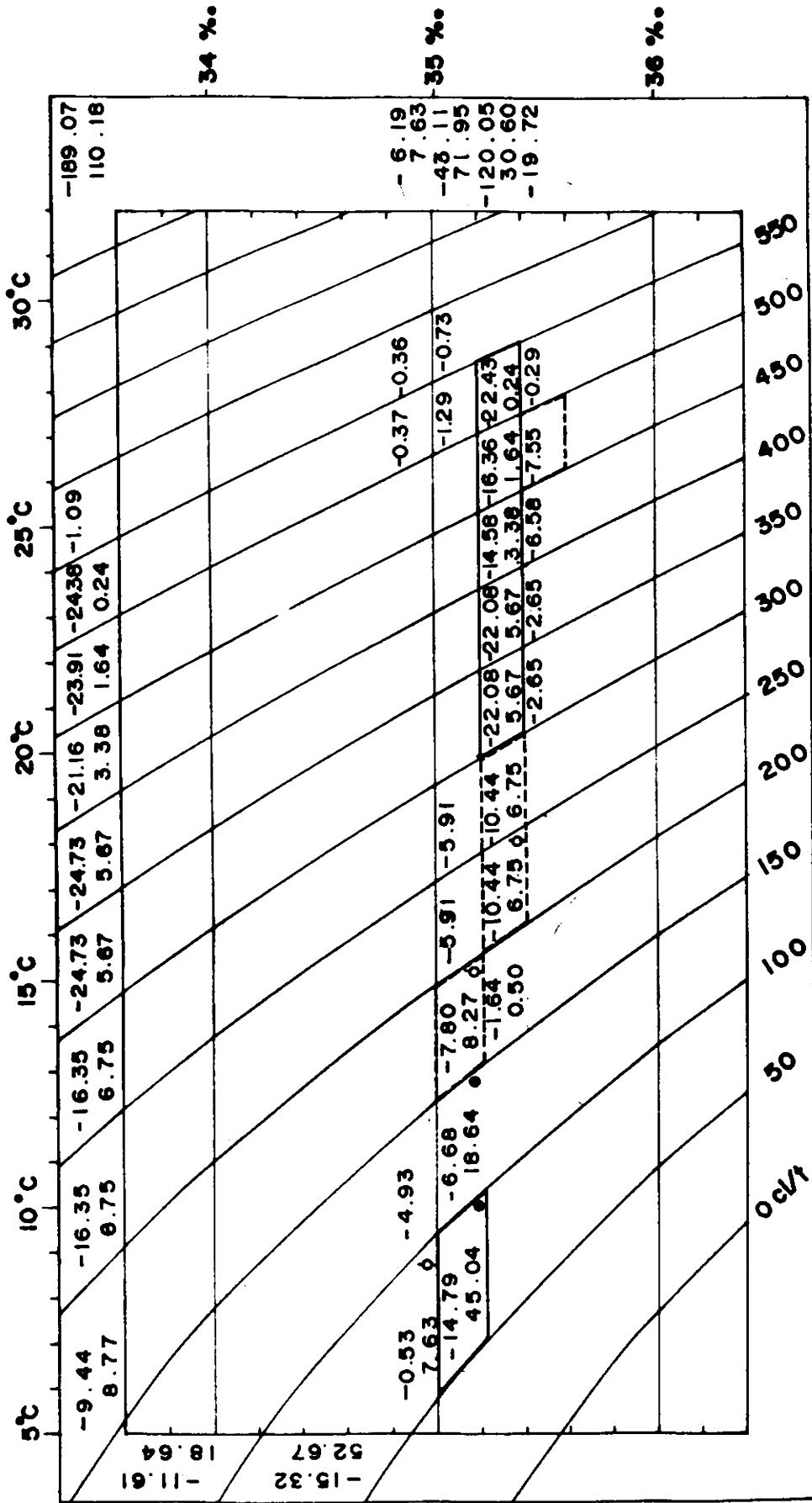
Fig. 5.13.1.—Zonal fluxes across 61°E between 5° N and 0° during March, 1963
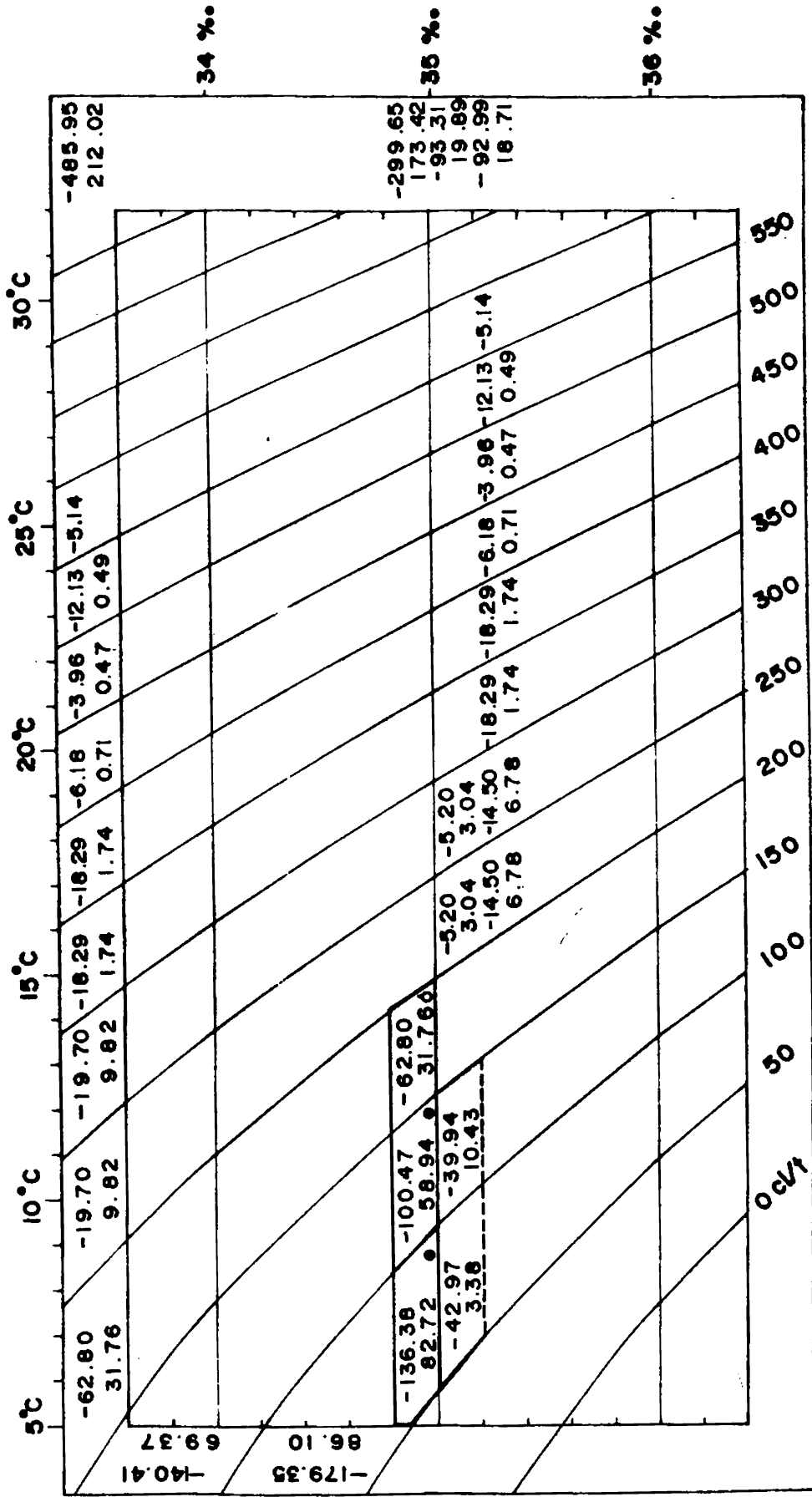
Fig- 5.13.2_Zonal fluxes across 61°E between 0° and 5°S during March, 1963

flux, south of the equator, is very high compared to north of the equator. The North Equatorial Current is found beteen 5° and 2° N above 120 cl/t with a transport of 66.9 km^3/hr. Across this section the Equatorial Undercurrent is noticed between 2° N and 2° S (between 200 and 400 cl/t) with a transport of 33.5 km^3/hr with waters having higher salinities.

5.14   The bivariate distribution exhibits more heterogeneity north of the equator than to its south (Figs. 5.14.1. and 5.14.2.) along 62° 20'E. In the northern half, the flow is mainly confined to salinities higher than 35.0%.. 50% of the total westward flux of 121.9 km^3/hr is distributed over 5 frequencies, while that of the eastward flow (96.7 km^3/hr) is confined to below 150 cl/t with a mean salinity of 35.1%.. About 30 km^3/hr of the westward flux occurs above 450 cl/t having a mean salinity of 35.5%.. The Monsoon Current is seen between 5° N and 5° S above 300 cl/t and it has a transport of 29.6 km^3/hr.

The bulk of both the eastward and westward flow (Fig. 5.14.2) takes place below 250 cl/t in the salinity range 34.8%. to 35.4%.. The total westward flow is 252 km^3/hr and the eastward flux is 134.5 km^3/hr. Westward flow of 38 km^3/hr occur in the surface layers. The total westward flux

Fig. 5.14.1 — Zonal fluxes across 62°20'E between 5°N and 0° during August, 1962
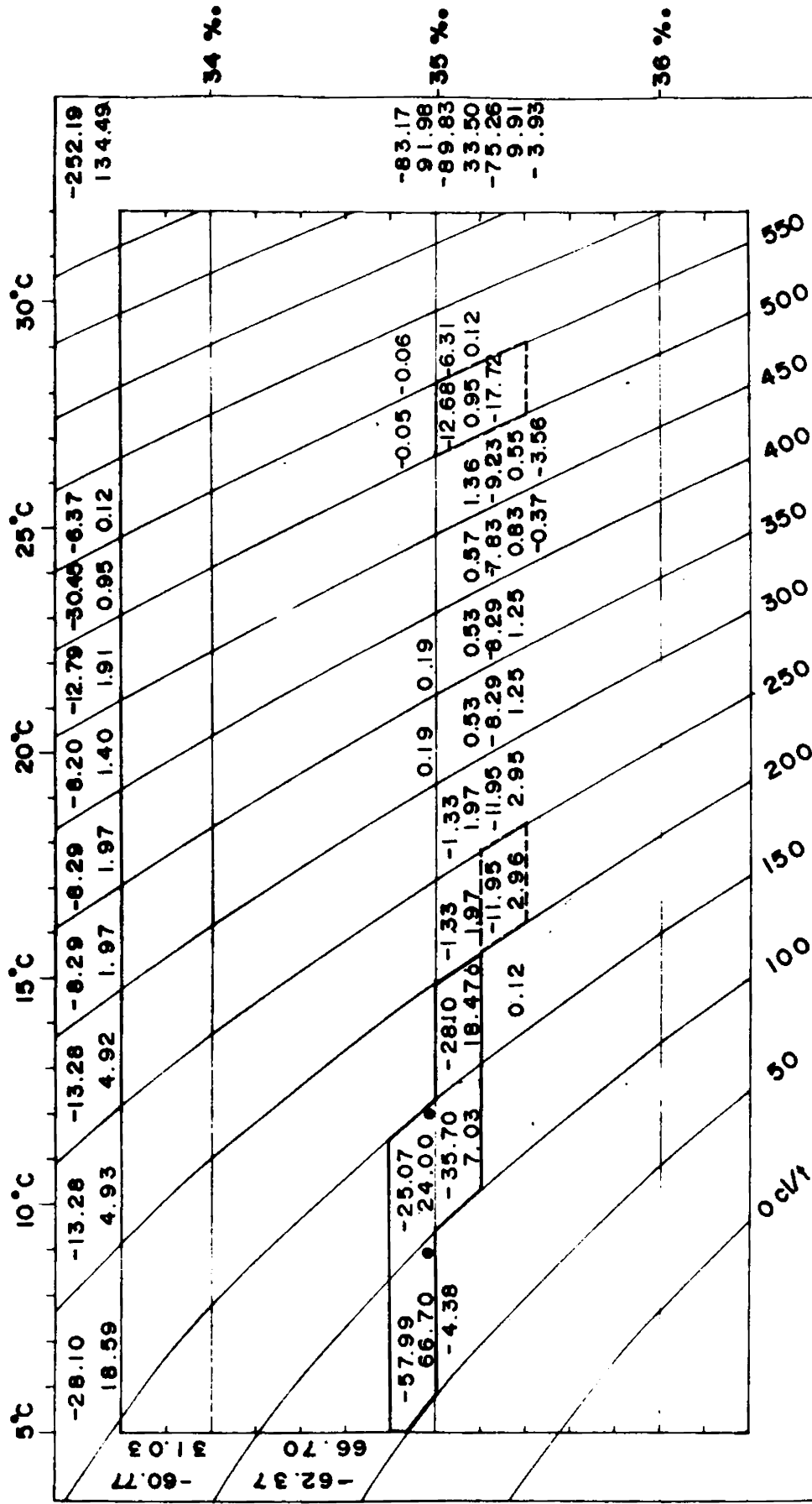
Fig. 5.14.2 _ Zonal fluxes across 62° 20'E between 0° and 5°S during August, 1962

south of the equator is more than twice to that north of the equator.

5.15   Compared to the sections in the western part (Figs. 5.11.1, 5.11.2, 5.12.1, 5.12.2, 5.13.1, 5.13.2, 5.14.1 and 5.14.2), this section along 79^oE (Fig 5.15.1) is peculiar in that low salinity classes appear in the bivariate distribution in the surface layers. Eastward flux with 538 km^3/hr dominates the westward flow (78 km^3/hr) north of the equator. The distribution is more heterogeneous in both salinity and thermosteric anomaly with salinity ranging from 34.2‰. to 35.6‰.. The primary modes of both eastward and westward flow occur at 125 cl/t and salinity 35.1‰.. 50% of the westward flow occurs below 200 cl/t (35.1‰.) and 75% of flux is distributed over 7 frequencies, while the bulk of the eastward flux occurs below 150 cl/t. Westward flux of 7 km^3/hr between 400 and 500 cl/t is observed with a mean salinity of 34.9‰.. The total westward flux above 300 cl/t between 5° and 3^oN may be attributed to the North Equatorial Current, which has a transport of 19.9 km^3/hr.

The total eastward flux (567.8 km^3/hr) is considerably more than the total westward flux (Fig. 5.15.2). 75% of the eastward flow occurs in 3 frequencies below 150 cl/t, with 50% having a mean salinity of 34.9‰.. 50% of the westward flux is distributed over 5 frequencies, all occurring below

Fig. 5.15.1. Zonal fluxes across 79°E between 5°N and 0° during Aug.—Sep., 1962
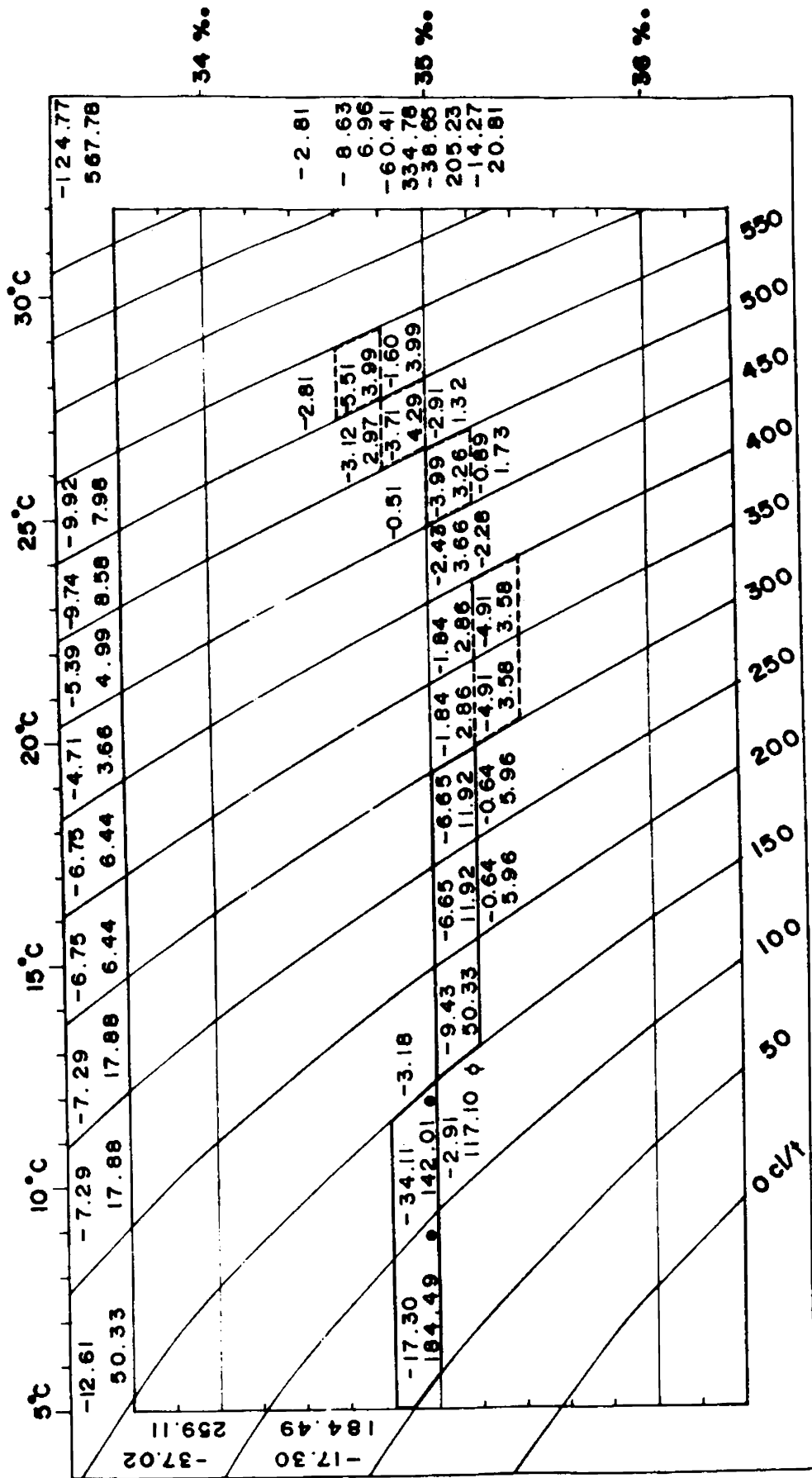
Fig. 5.15.2 — Zonal fluxes across 79°E between 0° and 5°S during Aug—Sep., 1962

300 cl/t in the salinity range 34.8 to 35.2‰.. Compared to the section along 62° 20'E the eastward fluxes are dominant along 79° E. The westward flux north of the equator do not vary much across these two sections whereas south of the equator the westward flux along 62° 20'E is double that at 79° E. The Monsoon Current appears between 2° N and 5° S, with a transport of 63.4 km^3/hr.

5.16 The flux distribution across 85° E are shown in Figs. 5.16..1. and 5.16.2. respectively. In this section covered during February, westward flow (331.2 km^3/hr) seems to be stronger, north of the equator. 75% of the westward flux is distributed over 7 frequencies. The total eastward flow across this belt is 149.3 km^3/hr, with the first four frequencies that constitute 75% of the flux, occurring in the salinity range 34.8% to 35.2‰.. 50% of the flow occurs below 150 cl/t, while the tertiary mode is seen at 475 cl/t.

South of the equator (Fig 5.16.2), the flux distribution is heterogeneous with salinity varying between 34.2‰. and 35.4‰.. Below 200 cl/t, the flow is mainly westerly, and 4 of the first 5 frequencies that contribute to 75% of the westward flow, occur in the salinity range 34.8‰. to 35.2‰.. The fifth occurs at 525 cl/t with mean salinity 35.1‰.. The total eastward flow is more or less equal to that of the total westward flux (240 km^3/hr) and

101
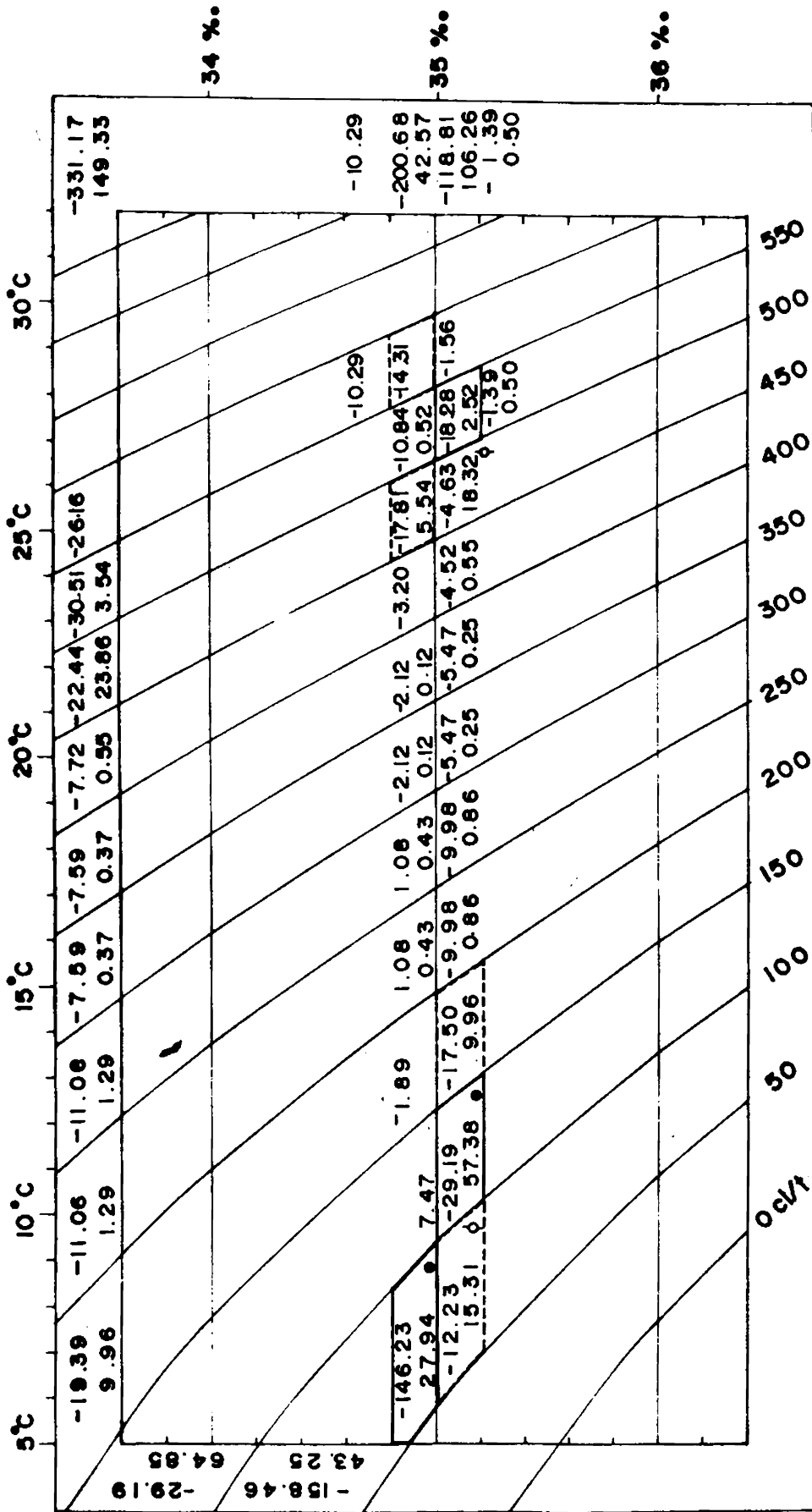
Fig. 5.16.1 – Zonal fluxes across 85°E between 5°N and 0° during February, 1963

Fig. 5.16.2. Zonal fluxes across 85°E between 0° and 5° S during February, 1963

75% of it is distributed over 9 frequencies. 47 km^3/hr of the eastward flow in the surface layer has a salinity less than 34.8%..

5.17 The zonal fluxes, across 92° E, are presented in Figs. 5.17.1. and 5.17.2. The heterogeneity is more, compared to the western and central regions, and more so south of the equator. The total westward flow, north of the equator, is 127 km^3/hr and 61% of the flow occurs below 150 cl/t. The 3 additional frequencies that together contribute to 75% of the westward flux are found above 600 cl/t in the surface layers in the salinity ranging from 34 to 34.4%.. The bulk of the eastward flux is confined to the layer below 300 cl/t with 7 frequencies constituting 75% of the total eastward flow of 138 km^3/hr.

The total westward flow, south of equator (Fig. 5.17.2), is more than twice of the eastward flow (126.4 km^3/hr). 75% of the westward flux is distributed over 9 frequencies. The primary mode of the eastward flux occurs at 125 cl/t and 4 frequencies, all below 200 cl/t in the salinity range 34.8 to 35.2%., make up to over 50% of the flow. 75% of the eastward flux is distributed over 11 frequencies obviously pointing out to the heterogeneity of the distribution.
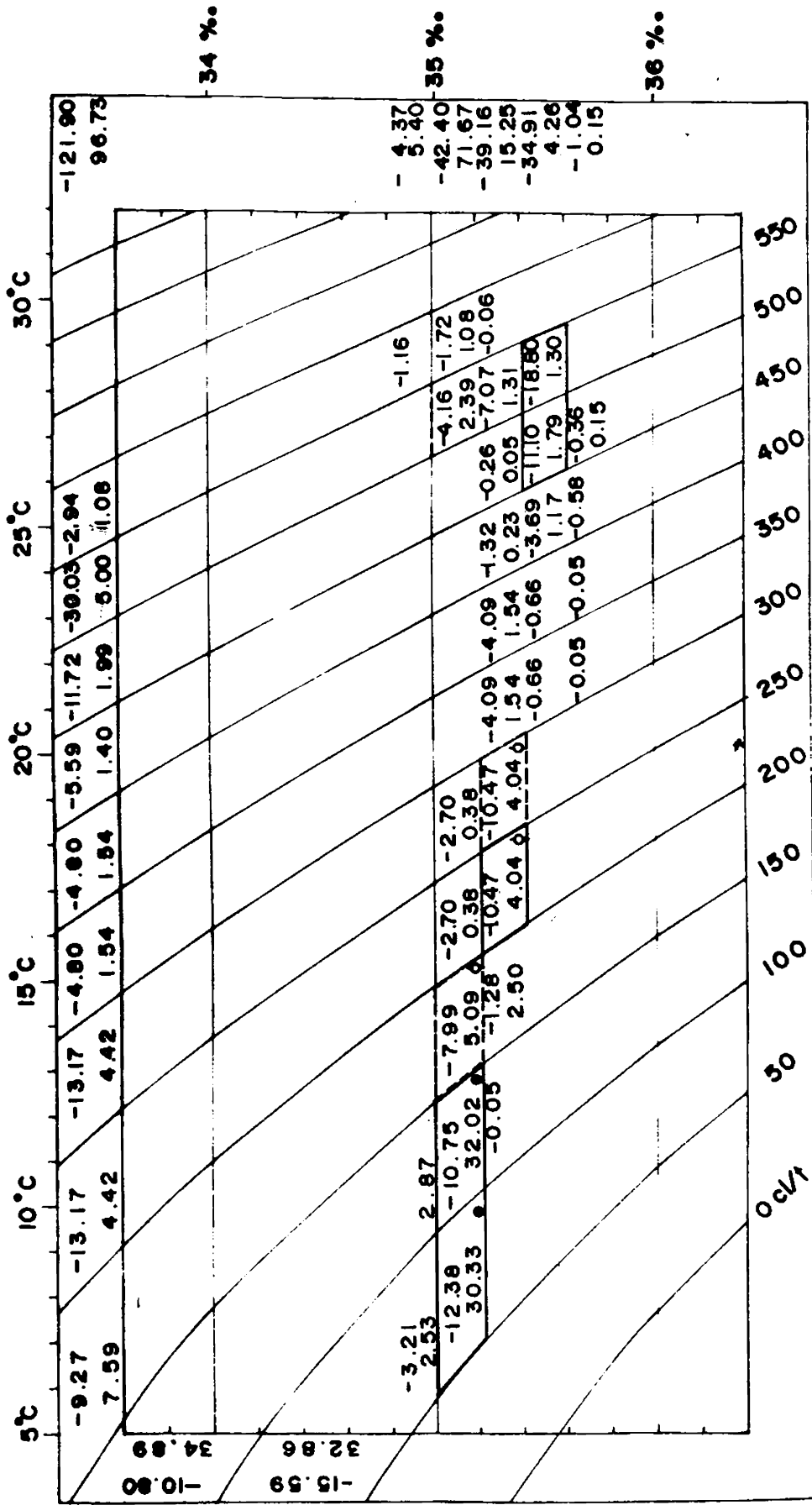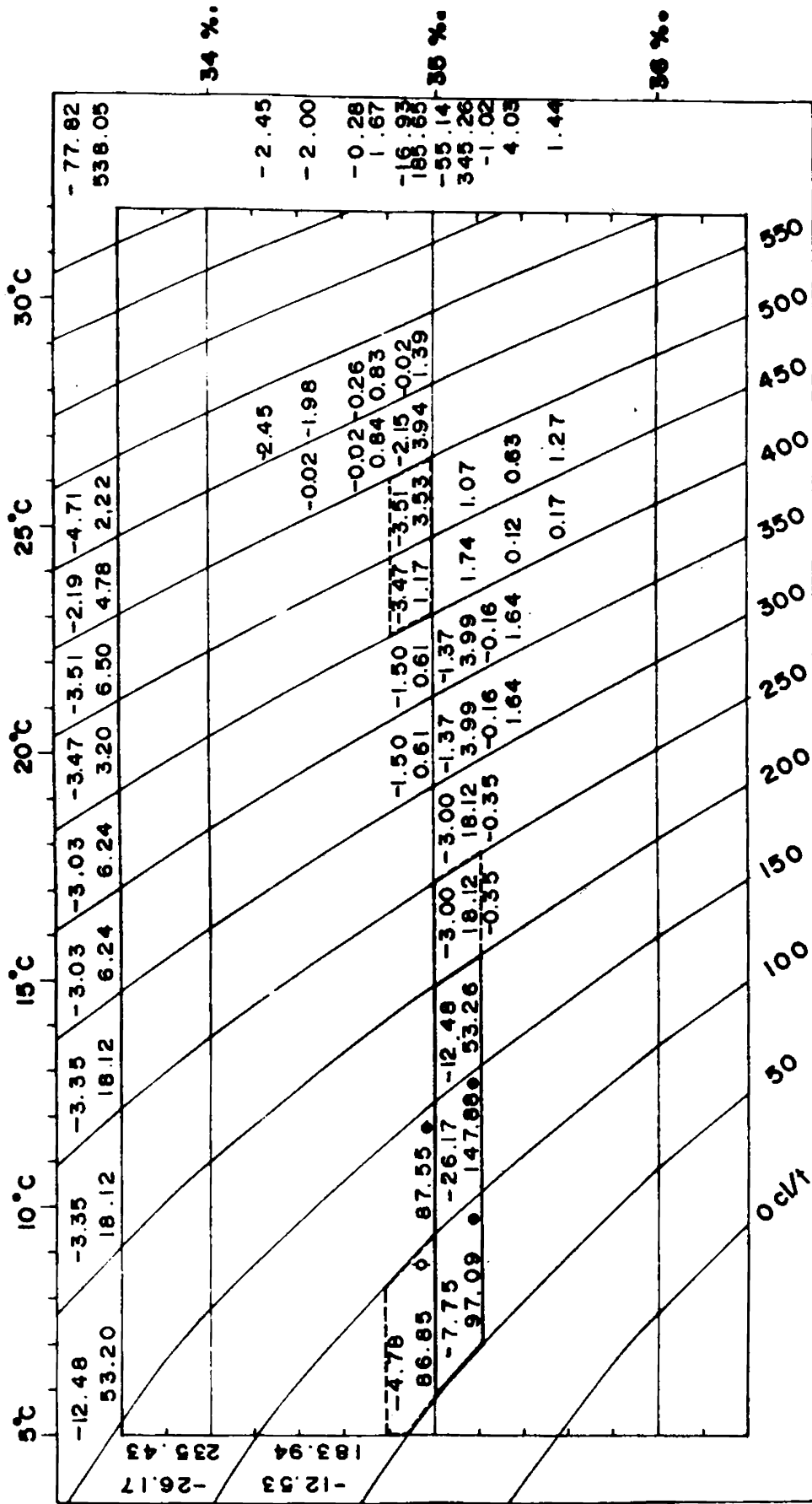
Fig. 5.17.1 Zonal fluxes across 92° E between 5°N and O° during April, 1963
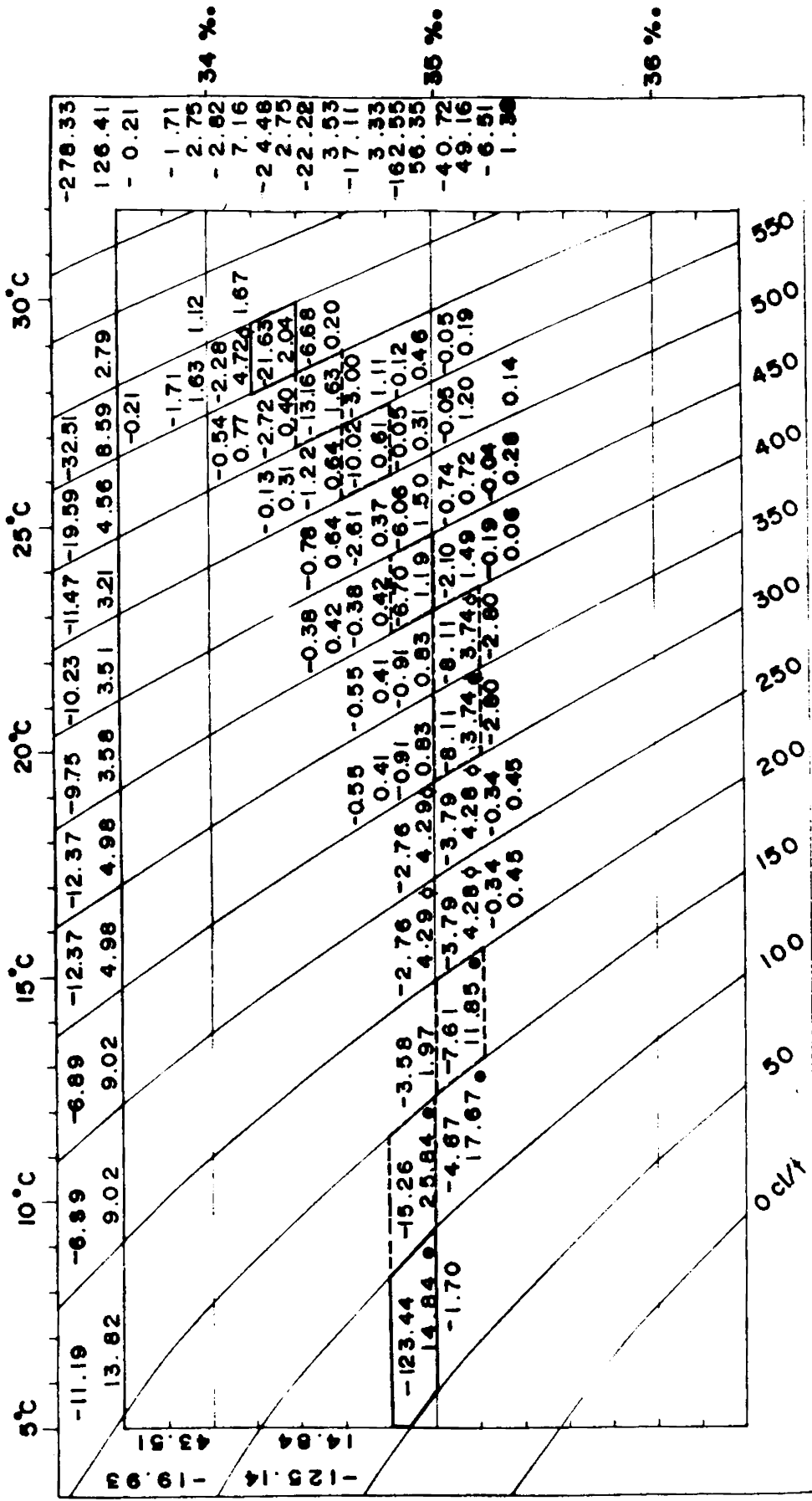
Fig. 5.17.2 _ Zonal fluxes across 92°E between 0° and 5°S during April, 1963

Considerable variation is noticed in the bivariate distribution characteristics of the eastward and westward fluxes in the 5° belts north and south of the equator. However, it can be seen that the primary modes of the eastward and westward fluxes are generally encountered at 75 and 125 cl/t in the salinity range 34.8 to 35.2%.. This is because, though the computed velocities in the deeper levels are low, in the deeper layers, the thickness bounded by the chosen isanosteres is large, compared to the surface layers. Both westward and eastward fluxes show nearly homogeneous characteristics during the southwest monsoon, with higher salinities observed in the primary modes north of the equator. Similar distribution characteristics are evident across 70°E during the fall transition period. During December to May, the bivariate distribution shows more heterogeneity, especially south of the equator, which tends to increase to the east.

The total transports for the different currents which are identified based on property distributions are presented in Table III. An attempt has been made to quantify the incursion of the Pacific Ocean Water in to the Indian Ocean. The westward flux of 48.5 km^3/hr, seen across 106°E, between 8° and 16°S, is due to the incursion of the low saline Pacific Ocean Water, which decreases progressively towards west upto 70°E, where it is only 14.8 km^3/hr. The decrease

TABLE III. Zonal transports of different currents across various sections.

Section	NEC	Monsoon Current	EUC	Eq. Jet	ECC	SEC	SECC	TCC	Pac.Water incursion
FEB 55E	68.5	-	33.9	-	-	69.7	-	-	20.0
MAR 65E	99.8	-	61.5	-	34.0	165.5	1.0	7.1	27.0
DEC 65E	-	-	20.5	-	23.8	138.0	3.7	28.7	41.1
MAY 67.30'E	9.1	45.1	-	-	4.9	101.3	2.0	0.4	19.9
NOV 70E	-	26.7	-	129.2	12.8	110.5	-	-	14.8
DEC 78E	6.1	-	-	-	60.2	39.0	-	-	19.5
DEC-JAN 83E	50.4	-	-	-	31.6	83.9	19.1	3.4	36.2
MAY 84E	-	-	-	156.5	-	-	-	-	-
JULY 100E	-	-	-	-	3.1	163.1	27.3	3.2	44.6
DEC 106E	-	-	-	-	-	103.6	-	11.1	48.5
AUG 53E	-	104.4	-	-	-	-	-	-	-
MAY 53E	-	91.2	-	-	-	-	-	-	-
MAR 61E	66.9	-	33.5	-	-	-	-	-	-
AUG 62.20'E	-	29.6	-	-	-	-	-	-	-
AUG-SEP 79	19.9	63.4	-	-	-	-	-	-	-
FEB 85E	30.4	-	-	-	-	-	-	-	-
APR 92E	36.1	-	51.6	-	31.5	-	-	-	-

in transport may be due to the mixing of low salinity water with waters of higher salinity in the western region. The extent of intrusion agrees well with earlier observations of Taft (1963), Sharma (1972) and Sharma et al. (1978). Model transport values for the Pacific Water throughflow in the Indian Ocean reported by Kindle et al. (1986) shows wide seasonal as well as interannual variability with flows ranging from 7.2 to 43 km^3/hr.

The North Equatorial Current, which is a permanent feature in the Pacific and Atlantic (Tsuchiya, 1961; Masuzawa, 1964 and Reid, 1964a) is seasonal in the Indian Ocean (Wyrtki, 1973a). The Monsoon Current replaces the North Equatorial Current during the southwest monsoon, even though the North Equatorial Current could be seen even after the onset of the southwest monsoon (Sharma, 1976b). The estimated transport of the North Equatorial Current shows wide variation. During February, the transports are higher in the western region, compared to the Central Indian Ocean.

The Monsoon Current seems to set in by the beginning of May and the eastward transport of the current is 45.1 km^3/hr across $67^o30'E$. The transport is very much higher during August, which shows the strengthening of the Monsoon Current with the advance of the southwest monsoon, when it also merges with the Equatorial Countercurrent. The Equatorial

Countercurrent found mostly south of the equator also shows considerable variability in its extent and magnitude.

The transport of the Equatorial Undercurrent in the Western Indian Ocean is 61.5 km^3/hr in March, while it is 33.9 km^3/hr in February, indicating the strengthening of the Equatorial Undercurrent during the northeast monsoon. Similar conclusions are drawn by Sharma (1968) and Muraleedharan (1984). However, across 61°E, the computed transport in March is only 33.5 km^3/hr which shows possible interannual variability. The transport of the Equatorial Undercurrent across 92°E in April, estimated from direct current measurements by Taft and Knauss (1967) is $11x10^6$ m^3/s, while it is found to be 51.6 km^3/hr ($14.3x10^6$ m^3/s) which shows good agreement.

The Equatorial Jet, present in the Indian Ocean during the transition periods between the two monsoons, is seen across 70°E during October-November and 84°E during May. The eastward transport of the Equatorial Jet (159 km^3/hr) is much higher than the estimates of Wyrtki (1973b), but is comparable to the estimates made by Muraleedharan (1984), which is 173 km^3/hr.

The South Equatorial Current is the most permanent feature of the equatorial current system in the Indian Ocean, similar to its counterparts found in the Pacific and

Atlantic. The westward transport due to the South Equatorial Current across different sections generally varies between 69 and 165 km^3/hr. Variation in strength and northward extent of the South Equatorial Current, in tune with the strength and persistence of the southeast trade winds, is noticed. The South Equatorial Current has a mean transport of 100 km^3/hr which agrees well with that of Wyrtki (1973a).

The South Equatorial Countercurrent and Tropical Countercurrent seems to be present round the year. The South Equatorial Countercurrent is stronger in the Eastern Indian Ocean. Though it is a consistent feature observed between 13° and 15°S (Sharma, 1976b and Sharma et al., 1982), the transport seems to be marginal in the western and central parts. The Tropical Countercurrent noticed, south of 18°S, shows wide fluctuations in magnitude. This may be partly due to the limited extent of the sections.

The total eastward and westward transports estimated across various sections for 5° latitudinal belts for different seasons are presented in table IV . The mean westward and eastward transports for each belt is computed and the net transport is also given. It is interesting to note that, during the northeast monsoon, the net transport is westward, while it is eastward during the southwest monsoon. During the transition period too, the net transport is eastward north of 5°S, while it is westward south of 5°S.

106

TABLE IV. Net zonal transport for different seasons

(a) Northeast monsoon

	55E FEB	61E MAR	65E MAR	65E DEC	78E DEC	83E JAN	85E FEB	106E DEC	Mean	Net
10N	-32.8 24.4	-	-35.9 31.8	-	-	-21.2 26.9	-	-	-30.0 27.7	-2.3
5N	-203.5 134.0	-189.1 110.2	-591.2 62.6	-	-167.2 428.9	-232.5 6.3	-331.2 149.3	-	-285.8 148.6	-137.2
0	-221.4 86.8	-486.0 212.0	-277.3 180.8	-166.9 254.8	-731.1 340.7	-170.3 95.6	-240.0 252.4	-	-327.6 203.3	-125.9
5S	-29.6 26.6	-	-55.8 61.5	-63.0 54.6	-55.9 17.4	-50.2 14.6	-	-53.3 -	-51.3 29.1	-22.2
10S	-48.1 26.1	-	-50.3 2.5	-135.5 13.5	-	54.8 63.1	-	-13.9 8.3	-60.5 22.7	-37.8
15S	-18.6 1.3	-	-101.2 17.2	-87.2 104.8	-	-99.3 3.4	-	-47.8 1.1	-70.8 25.5	-45.3
20S										

(b) transition period.

	53E MAY	67,30'E MAY	70E OCT	84E MAY	92E APR	Mean	Net
10N	-	-19.6 20.2	-44.3 48.3	-	-	-32.0 34.3	2.3
5N	-390.7 129.8	-141.2 281.4	-5.8 378.5	-251.3 109.8	-127.1 138.0	-183.2 207.5	24.3
0	-457.8 243.3	-140.8 276.4	-111.9 665.7	-241.0 116.3	-278.3 126.4	-245.9 285.6	39.7
5S	-	-72.1 39.3	-40.0 39.3	-	-	-56.1 39.3	-16.8
10S	-	-46.0 11.0	-87.7 7.2	-	-	-66.3 9.1	-57.2
15S							

(c) Southwest monsoon

	53E AUG	62,20'E AUG	79E SEP	Mean	Net
5N	-347.6 153.5	-121.9 96.7	-77.8 538.5	-182.4 262.8	80.3
0	-453.2 142.5	-252.2 134.5	-124.8 567.8	-276.7 281.6	4.9

CHAPTER VI

SUMMARY AND CONCLUSIONS

In the equatorial oceans, the meridional currents are far less energetic than their zonal counterparts. The response of the Equatorial Indian Ocean to the seasonal reversals in the zonal wind field, is quite interesting and unique. A modest attempt, considering the shortcomings in the hydrographic data availability and distribution, is made to evaluate the variability in the zonal transport of mass, in both space and time. The peculiarities in its hydrological regime imposed upon by the seasonally varying winds is best appreciated when compared with the quasi-permanent circulation characteristics of the Pacific and Atlantic. The major features of the equatorial mass transport is outlined in the introductory chapter of this thesis for the Pacific and Atlantic. Mass transport studies in the Indian Ocean, as can be seen from the earlier studies, is the least known and understood, though could have captured the attention of both the experimentalist and the theoretician alike, owing to its complexity. Since in the Indian Ocean, the studies on the zonal mass transport are limited and are confined to the equator only, an attempt has been made to compute the mass transport extending from 5°N to 20°S.

The method of Montgomery and Stroup (1962) is adopted to compute the zonal mass transport using transequatorial hydrographic sections in the upper 1000 m in order to estimate the eastward and westward fluxes through five degree latitudinal belts. The fluxes are displayed on temperature-salinity diagrams, through bivariate distribution over salinity and thermosteric anomaly. Vertical sections of temperature, salinity and thermosteric anomaly are also presented and discussed which augment in delineating the different flow regimes and characteristics associated with certain current structures.

The thermal structure along the equator in the Indian Ocean differs from that of the Atlantic and the Pacific. Sea surface temperature in the Indian Ocean generally increases from the west to east. The upper portion of the thermocline slopes down to the east in the central and eastern parts of the ocean.

Transequatorial temperature structure shows considerable seasonal and latitudinal variations. In the Western Indian Ocean, the most dominant feature is a trough in the thermocline, corresponding to an anticyclonic gyral circulation. While, in the two eastern most sections, the distribution is quite different from the western sections possibly due to the different meteorological regime and also because of the influence of the intrusion of the Pacific

Ocean Water into the Indian Ocean.

Vertical separation of the isotherms within the thermocline in the vicinity of the equator is quite interesting because of its association with the Equatorial Jet and the Equatorial Undercurrent (Taft and Knauss, 1967; Bruce, 1973 and Eriksen, 1979). Spreading of the thermocline in the vicinity of the equator is evident on all sections west of 65° E during December to March, and across 92° E in April. The thickness of the thermocline along 65° E at the equator is 107 m and 118 m during December and March respectively, while it is reported to have a thickness 63 m (Sharma, 1976b), which clearly shows the presence of the Equatorial Undercurrent during the northeast monsoon.

During the transition period between the two monsoons, the thermocline is very sharp between 2° N and 2° S at 84° E and 70° E, with spreading observed on either side, a feature often associated with the Equatorial Jet. Pinching of isotherms is more prominent along 84° E during May compared to the section covered during October-November along 70° E.

Along the equator, the salinity at the surface decreases from west to east, with little vertical gradient in the surface layers on the western side compared to the east. In the Central Indian Ocean, the three water masses generally encountered are the Arabian High Salinity Water,

109

the homogeneous Equatorial Indian Ocean Water and the Subtropical High Salinity Water. A high salinity core associated with the Equatorial Undercurrent could be found on few sections covered during the northeast monsoon season. Low salinity water found at the equator across $67^\circ 30'E$ may be of Bay of Bengal origin. The incursion of the Pacific Ocean Water with salinity less than 34.6‰. (Tsuchiya , 1968) could be traced around $11^\circ S$ extending upto $55^\circ E$. This low salinity tongue is found more displaced to the south in the eastern part of the ocean. The sharp salinity gradient occurring south of the low salinity tongue coincides with the northern boundary of the South Equatorial Countercurrent.

Vertical sections of thermosteric anomaly generally follow the temperature distribution pattern since the density in the tropical oceans is primarily determined by temperature. The most conspicuous feature observed in these sections is the ridging of the isanosteres around $10^\circ S$ which demarcates the northern boundary of the South Equatorial Current. However, the northern limit of the South Equatorial Current varies from section to section and can be safely concluded that at $65^\circ E$ the South Equatorial Current is found nearer to the equator during the southwest monsoon. The South Equatorial Countercurrent associated with a ridging of the isanosteres in the surface layers seems to be

well established in the eastern sections. The pinching of the isanosteres in the vicinity of the equator along 84° E and along 70° E is attributed to the presence of the Equatorial Jet. Pinching at the equator and spreading of thermocline on either side indicates that the Equatorial Jet is in geostrophic balance. Recent model studies (O'Brien and Hurlburt, 1974 and Cane, 1980) confirm this. The eastern most sections are peculiar in that south of 5° S, there are a series of ridging and troughing indicative of alternating current regimes.

Based on the property distributions along different transequatorial sections the approximate boundaries of the various currents in the Equatorial Indian Ocean are made. The North Equatorial Current is generally found between 9° and 2° N during the northeast monsoon and the sloping of the isanosteres are less prominent compared to the South Equatorial Current. By May, the North Equatorial Current appears to have been replaced by the Monsoon Current along 67° 30'E which appears north of equator extending further south (upto 5° S) with the advance of the southwest monsoon. The Equatorial Countercurrent is observed between 3° S and 7° S during northeast monsoon and its width increases from west to east and is found shifted southward.

Between 200 and 400 cl/t, the Equatorial Undercurrent is identified between 3° N and 2° S across 55° E and 65° E,

while it is absent in the sections along 78° E and 83° E during northeast monsoon. The Equatorial Undercurrent is not present during southwest monsoon across 53° E and along 79° E. Across 65° E it is confined to the equator during December and is found to intensify during March. The transient Equatorial Jet present in the Indian Ocean during the two transition periods between the monsoons could be identified along 70° E during October-November and along 84° E in May. However, it is not clear during April-May along 67° 30'E.

The South Equatorial Current is the most permanent feature south of equator, generally found south of 10° S. In the Eastern Indian Ocean, the South Equatorial Current is noticed to have been shifted more to the south. It narrows down and shifts northward in the Western Indian Ocean. Its northward extent varies with season and is found upto 5° S during southwest monsoon.

The South Equatorial Countercurrent and Tropical Countercurrent, similar to that found in the Atlantic and Pacific could be identified in most of the sections. The South Equatorial Countercurrent is observed between 12° and 15° S except along 70° E. Its position varies from season to season and is more prominent in the Eastern Indian Ocean. The Tropical Countercurrent is generally observed south of 18° S above 300 cl/t, except along 70° E. It is found to have been shifted southwards in the eastern parts.

112

Perhaps the most interesting feature of the current regime is its interannual variability, since certain distribution characteristics associated with a particular current regime sometimes appear out of place and out of time. This is further substantiated by the flux distribution characteristics. A word of caution may be mentioned here firstly regarding the magnitude of the flux in the vicinity of the equator because of overestimation due to extremely low value of the Coriolis Parameter,and secondly the choice of a common reference level for the entire width of the ocean.

The bivariate distribution of westward and eastward fluxes show considerable variation in their characteristics in the five degree belts north and south of the equator. Nevertheless, the following general conclusions can be drawn. Primary modes of both east and west fluxes are generally encountered at 75 and 125 cl/t in the salinity range 34.8‰. to 35.2‰.. This is so because, though the computed velocities in the deeper levels are low, the thickness of the layers are large compared to the surface layers. Both westward and eastward fluxes show near homogeneous characteristics during the southwest monsoon with higher salinities observed in the primary modes north of the equator. Similar distribution characteristics are evident at 70°E during the October-November transition

period.

During December to May, the bivariate distribution shows more heterogeneity, especially south of the equator and tends to increase to the east. High salinity modes that occur in the western sections in the surface layers are due to the presence of the Arabian Sea High Salinity Water.

In the Western Indian Ocean, (west of 60° E) during February the westward flux is 203.5 km^3/hr while it is 390 km^3/hr during May, which shows an increase in the flux in the 5° belt north of the equator. The total eastward flux seems to be constant. South of the equator, the westward flow between 0° and 4° S during May (458 km^3/hr) is twice that of the transport during February. This may possibly be due to the northward shift of the South Equatorial Current as it approaches the Malagasy Island in the south and the African coast in the west. The total eastward flux during May also shows a marked increase (243 km^3/hr), which may be due to the setting up of the Monsoon Current by May itself as deduced from the distribution of thermosteric anomaly.

During the southwest monsoon, the westward flux is of the same magnitude (390 km^3/hr) as that of the transport during May, north of the equator. South of the equator, there is a slight increase in the eastward flow from May to August indicating the strengthening of the eastward flowing

Monsoon Current. Between $10°$ and $15°$S, the westward flux across $55°$E is 48 km^3/hr and is found to increase upto $65°$E in the Western Indian Ocean.

In the Central Indian Ocean (between $60°$ and $80°$E), the westward flow shows maximum transport between equator and $5°$N during March (591 km^3/hr), compared to the beginning of the northeast monsoon across $78°$E (167 km^3/hr). The opposite is true for the eastward transport which is about 62.6 km^3/hr during March, whereas, it is 428.9 km^3/hr across $78°$E which shows an increase from west to east in the eastward transport. South of equator, the westward flow is maximum (731 km^3/hr) across $78°$E during December, while it is considerably reduced across $61°$E during March (485.9 km^3/hr), exhibiting both seasonal and spatial variability in the Central Indian Ocean. The eastward flux is also maximum during December across $78°$E (340.6 km^3/hr) and does not show wide variability in its magnitude.

During northeast monsoon the westward flux between $5°$ and $10°$S is steady between $65°$ and $78°$E (around 56 km^3/hr), while the eastward flux is found to decrease from west to east (61.4 to 17.4 km^3/hr). Eastward flow seems to increase between $15°$ and $20°$S across $65°$E during March compared to the belt between $10°$ and $15°$S which may be due to the presence of the Tropical Countercurrent.

The total eastward flow across 79°E is 538 km^{3}/hr whereas it is 96.7 km^{3}/hr across 62°20'E during August which indicates an increase in the eastward transport towards east. This could be due to the strengthening of the Monsoon Current which merges with the Equatorial Countercurrent during this period. South of the equator also the eastward flux is higher during August-September across 79°E possibly due to the extension of the Equatorial Countercurrent south of equator. During the transition periods between the two monsoons, fluxes are found to be variable across the different latitudinal belts in the Central Indian Ocean, north of 5°S.

Across the easternmost section (106°E), only westward flux of 53.2 km^{3}/hr is seen between 7° and 10°S, whereas the westward flux between 10° and 15°S is about 13.9 km^{3}/hr with a slight eastward transport (8.3 km^{3}/hr), during the northeast monsoon. It is in this region that the incursion of the Pacific Ocean Water is observed. Similar features are observed during the southwest monsoon season across 100°E with a substantial increase in both eastward and westward transports north of 15°S. This could be related to the broadening of the South Equatorial Current towards west and the presence of the South Equatorial Countercurrent in this latitudinal belt.

Individual flux values do not merit further elucidation

116

owing to its considerable variability. However, as shown in Table IV (Chapter V), net fluxes tend to show marked seasonal variability. While the average of the net flux is westward during the north-east monsoon, it is eastward during the southwest monsoon and the transition periods between the two monsoons.

The fluxes for different current regions demarcated (Table III) based upon the distribution of properties discussed in chapters II, III, and IV are summarised below. The North Equatorial Current is stronger in the western and central regions during March across 65° E (99.8 km^3/hr), while it is considerably reduced in the eastern parts during the northeast monsoon. The transport of Monsoon Current is 91.2 km^3/hr during May and in August (104.4 km^3/hr) along 53° E, east of which it exhibits considerable variability as well as reduction in magnitude.

The transport of the Equatorial Undercurrent is maximum (61.5 km^3/hr) in March across 65° E, and a gradual strengthening of the Equatorial Undercurrent from December to March is observed in the Western Indian Ocean. The Equatorial Jet shows higher transport of 156.5 km^3/hr in May across 84° E compared to 129 km^3/hr observed during October-November across 70° E. The Equatorial Countercurrent shows considerable variability in its latitudinal extent and its transport varies from 4.9 km^3/hr to 34 km^3/hr.

The transport of South Equatorial Current is maximum (165.5 km^3/hr) during March across $65°E$ and is about the same magnitude as observed during July in the Eastern Indian Ocean. However, the transport is of the order of (100 km^3/hr) for the other sections which extend upto $20°S$.

The estimates for both South Equatorial Countercurrent and Tropical Countercurrent show considerable variability. The South Equatorial Countercurrent which seems to be present both in the northeast and southwest monsoon, is seen to be stronger in the eastern parts. A maximum eastward flux of 27.3 km^3/hr is observed during July while it is 19.1 km^3/hr during December-January. The Tropical Countercurrent has an eastward transport of 11 km^3/hr in December across the eastern most section while the estimated value of 28.7 km^3/hr is observed across $65°E$ during the same period. The estimates for these two currents which are confined to the surface layers may be viewed with caution because of the possible masking of the transports due to deeper reference surface chosen for this study.

Incursion of the Pacific Ocean Water into the Indian Ocean is seen along all sections with transports of the order of 45 km^3/hr in the Eastern Indian Ocean. A decrease to about half is observed in the central and western regions possibly due to mixing with waters of higher salinity.

Continuous current measurements by McPhaden (1982) in the Central Indian Ocean seems to substantiate the strong interannual variability which is closely linked to the vagaries in the overlying atmospheric circulation. Such a conclusion has also been arrived at by Fieux and Levy (1983) from their studies in the Western Indian Ocean. As the observations made in different years during the same season show considerable variability, a careful study of the correlation between the wind stress variations has to be made to further understand and evaluate the variability in the mass transport in the Equatorial Indian Ocean. Furthermore, to substantiate the conclusions drawn in this thesis more concerted efforts are required to carry out observational net work at closer intervals of space and time domains. The direct current measurements are indeed meagre to make any comparison of the estimated fluxes from hydrographic data. Hence, a suggestion is made that the hydrographic observations of temperature and salinity should be made simultaneously along with the current observations. Continuous measurements by moored buoy systems may be a better approach for a detailed further investigation on the seasonal variability of currents in the Equatorial Indian Ocean.

REFERENCES

Air Ministry, London, 1939. South Pacific Ocean currents. M.O. 435, Mar. Met. Office, 11 figs, 8 pl.

Austin,T.S., 1958. Variations with depth of oceanographic properties along the equator in the Pacific. Trans. Amer. Geophys. Union., 39: 1055-1063.

Austin, T.S. and M.O.Rinkel, 1958. Variations in upwelling in the equatorial Pacific. Proc. Pacific Science Congress, 9th, Bankok, 16: 67-71.

Arthur,R.S., 1960. A review of the calculation of ocean currents at the equator. Deep-Sea Res., 6: 287-297.

Basil Mathew, R.N.Nair, and G.S.Sharma, 1982. The Tropical Countercurrent in the Indian Ocean. Ind. J. Mar. Sci., 11: 208-211.

British Admirality, 1949. General surface current circulation. The world Adm. chart No. 5310 (Great Britain).

Bruce, J.G., 1973. Equatorial Undercurrent in the Western Indian Ocean during southwest monsoon. J. Geophys. Res., 74: 6386-6394.

Bruce, J.G., 1979. Eddies off the Somali coast during southwest monsoon. J. Geophys. Res., 84: 7742-7748.

*Buchanan, J.Y., 1886. On similarities in the physical geography of the great oceans. Proc. Roy. Geogr. Soc. 8: 753-770.

Cane, M.A., 1979. The response of an equatorial ocean to simple wind stress pattern - II: Numerical results. J. Mar. Res., 37: 253-299.

Cane, M.A., 1980. On the dynamics of equatorial currents with application to the Indian Ocean. Deep-Sea Res., 27A: 525-544.

Charney, J.G., 1960. Nonlinear theory of a wind-driven homogenous layer near the equator. Deep-Sea Res., 6: 303-310.

Christensen, N., 1971. Observations of the Cromwell Current near Galapagos Islands. Deep-Sea Res., 18: 27-34.

Cochrane, J.D., 1965. Equatorial currents of the Western Atlantic. Dept. of Oceanogr., Prog. Rep. Ref. 65-T, Texas A&M Univ.: 6-19pp and 27.

Cochrane, J.D., 1968a. The equatorial thermostad in the Western Atlantic Ocean. Trans. Amer. Geophys. Union, 49: 199-200.

Cochrane, J.D., 1968b. The currents and waters in the Western Tropical Atlantic Ocean. Dept. of Oceanogr. Prog. Rep. Ref. 68-8T, Texas A&M Univ.: 21-25.

Cochrane, J.D., F.J.Kelly, Jr., and C.R.Olling, 1979. Subthermocline Countercurrents in the Western Equatorial Atlantic Ocean. J. Phys. Oceanogr., 9(4): 724-738.

Colborn, J.G., 1975. The thermal structure of the Indian Ocean. IIOE Oceanogr. Monographs, 2, Univ. Press Hawaii, Honolulu: 173.

Cornus, H.P., and J. Meincke, 1979. Observation of near surface layer changes related to the Atlantic Equatorial Undercurrent. Deep-Sea Res., 26A: 1291-1299.

Cox, M.D., 1979. A numerical study of Somali Current eddies. J. Phys. Oceanogr., 9: 311-326.

Cresswell, G., M. Fieux and J. Gonella, 1981. The Wyrtki Equatorial Jet, May/June 1980. Tropical Ocean-Atmosphere Newsletter - January, 1981. Unpublished manuscript.

Cromwell, T., R.B.Montgomery and E.D.Stroup, 1954. Equatorial Undercurrents in the Pacific Ocean revealed by new methods. Sci., 119: 648-649.

*Defant, A., 1935. Der Aquatoriale Gegenstrom. Sitz. Ber. Preuss. Akad. Win., Phys-Math. Kl.: 28.

*Defant, A., 1941. Die absolute Topographie des physilalischen Meeresniveans und der Druckflachen, sowie die Wasserbewegungen im Atlantischen Ozean. Meteor-Werk, 6(2): 191-260.

Defant, A., 1961. Physical Oceanography. Pergamon Press: 728.

Dubach, H.W., 1964. Summary of temperature-salinity characteristics of the Persian Gulf. N.O.D.C. Gen. Ser. Pub., G-4:223.

Dubravin, V.F., 1970. Results of observations made on currents in the Gulf of Guinea during the months of August-October, 1965. Tr. Atlant. NIRO, (27): 150-172.

Duing, W., 1970. The monsoon regime of the currents in the Indian Ocean. IIOE Monograph, 1, Hawaii Inst. Geophys., Contribution No. 330, East-West Centre Press, Honolulu.

Eriksen, C.C., 1979. An equatorial transect of the Indian Ocean. J. Mar. Res., 37: 215-232.

Eriksen, C.C., 1981. Deep currents and their interpretation as equatorial waves in the Pacific Ocean. J. Phys. Oceanogr., 11: 48-70.

Eriksen, C.C., 1982. Geostrophic equatorial deep jets. J. Mar. Res., 40(Suppl.): 143-147.

Fieux, M. and C. Levy, 1983. Seasonal observations in the Western Indian Ocean. in Hydrodynamics of the Equatorial Ocean, J.C.J Nihoul (Ed.), Elsevier Oceanogr. Ser., 36: 17-29.

Firing, E., C.Fenander and J.Miller, 1981. Profiling current meter measurements from the NORPAX Hawaii to Tahiti Shuttle Experiment, Hawaii Inst. Geophys. Rep., HIG-81-2.

Fofonoff, N.P., 1960. Transport computations for the North Pacific Ocean, 1955-1958. Fish. Res. Bd. Canada, M.S. Rep., Oceanogr. and Limnol. Ser.,85: 181.

Fuglister, F.C., 1960. Atlantic Ocean atlas, temperature profiles and data from the Int. Geophys. Year of 1957-1958, Woodshole Oceanogr. Inst., Atlas Ser., 1: 209.

*Gonella, J., M.Fieux and S.G.H.Philander, 1981. Mise en evidence d'ondes de Rossby equatoriales dans l'ocean Indien a partir de bonees derivantes. C.R.Acad. Sci., Paris, T.292: 1397-1399.

Hastenrath, S. and P.J.Lamb, 1979. Climatic atlas of the Indian Ocean, Part II. Univ. Wisconsin Press: 93.

*Holland-Hansen, B., 1916. Nogen Hydrografiske metoder. Forh. Skand. Naturforsster Mote, 16: 357-359.

*Hisard, P., 1973. Variations saisonnieres a l'equateur dans le Golfe de Guinea. Cah. OSTROM, Ser. Oceanogr., 11(3): 349-358.

*Hisard, P., J.Citeau and A.Morliere, 1976. Le system des Contrecourants equatoriaux subsuperficiels, permanence et extension de la branche sud dans l'ocean Atlantique. Cah. ORSTOM, Ser. Oceanogr., 14: 209-220.

Hisard, P., Y.Magnier and B.Wauthy, 1969. Comparison of hydrographic structure of equatorial waters north of New Guinea and at 170 E. J. Mar. Res., 27(2): 191-205.

*Hisard, P. and A.Morliere, 1973. La terminaison du contrecourant equatorial subsuperficiel Atlantique (courant de Lomonosov) dans le Golfe de Guinea. Cah. ORSTOM Ser. Oceanogr., 11(4): 455-464.

Katz, E.J., R.L.Molinari, D.E.Cartwright, P.Hisard, H.U.Lass, A. De Mesquita, 1981. The seasonal transport of the Equatorial Undercurrent in the Western Atlantic. Oceanologica Acta, 4: 445-450.

Khanaichenko, N.K., 1970. Confirmation of the existence of the south branch of the Equatorial Countercurrent in the Atlantic Ocean. Dokl. USSR Acad. Sci. Earth Sci. Soc., 187: 235-236.

Khanaichenko, N.K., 1974. The system of equatorial countercurrents in the ocean (translated from Russian). A.D.Dobrovlskii (Ed.) Oxonian Press, New Delhi: 158.

Khanaichenko, N.K. and N.Z.Khlystov, 1966. The south branch of the Equatorial Countercurrent in the Atlantic Ocean. Dokl. USSR Acad. Sci., 166: 205-207.

Khosla, A.N., 1951. Appraisal of water resources: Analysis and utilisation of data. Proc. U.N. Sci. Conf. Conser. Util. Resources (4).

Kindle, J.C., G.W.Heburn and R.C.Rhodes, 1986. An estimate of the Pacific to Indian Ocean throughflow from a global numerical model (unpublished manuscript)

King,J.E., T.S.Austin. and M.S.Doty, 1957. Preliminary report on Expedition Eastropic. U.S.Fish. Wildlife Surv. Spec. Sci. Rep., Fisheries Ser., 201: 155.

Knauss,J.A., 1960. Measurements of the Cromwell Current. Deep-Sea Res., 6: 265-286.

Knauss,J.A.,1961. The structure of the Pacific Equatorial Countercurrent. J. Geophys. Res., 66(1): 143-155.

Knauss,J.A., 1962. Recent measurements of the Cromwell Current. J. Geophys. Res., 67: 3571-3572.

Knauss,J.A., 1966. Further measurements and observations on the Cromwell Current. J. Mar. Res., 24: 205-240.

Koninklijk Netherlands Meteorologisch Institut, 1952. 'Indische Ocean', Oceanografische en Meteorologische gegevens, Publication No. 135, 2nd Ed., 2 Vols, 24 sheets.

Knox, R.A., 1976. On a long series of measurements of Indian Ocean equatorial currents near Addu Attol. Deep-Sea Res., 23: 211-221.

Leetmaa, A. and H.Stommel, 1980. Equatorial current observations in the Western Indian Ocean in 1975 and 1976. J. Phys. Oceanogr., 10: 258-269.

Love, C.M., ed., 1972. EASTROPAC Atlas, Vol. 1, Physical Oceanographic and Meteorological Data from Principal Participating Ships, First Survey Cruise, Feb-March, 1967. NOAA, Nat. Mar. Fish. Service Circular, 330, 12+ xii pp., 255 fig. ⟨83,188⟩.

Luyten, J.R., M.Fieux and J.Gonella, 1980. Equatorial currents in the Western Indian Ocean. Science, 209: 600-603.

Luyten, J.R., and D.H.Roemmich, 1982. Equatorial currents at semi-annual period in the Indian Ocean. J. Phys. Oceanogr., 12: 406-413.

Mamayev, O.I., 1975. Temperature-salinity analysis of world ocean waters. Elsevier Oceanogr. Ser., Amsterdam, 11: 374.

Masuzawa, J., 1964. Flux and water characteristics of the Pacific North Equatorial Current. Stud. on Oceanogr.: 121-128.

Mazieka, P.A., 1968. Eastward flow within the South Equatorial Current in the eastern south Atlantic. J. Geophys. Res., 73: 5819-5828.

McCreary, J., 1981. A linear stratified ocean model of the Equatorial Undercurrent. Phil. Trans. Roy. Soc. London, A 298: 603-635.

McPhaden, M.J., 1982. Variability in the central equatorial Indian Ocean, Part I: Ocean Dynamics. J. Mar. Res., 40: 157-176.

Metcalf, W.G., A.D.Voorhis and M.C.Stalcup, 1962. The Atlantic Equatorial Undercurrent. J. Geophys. Res., 67(6): 2499-2508.

Montgomery, R.B., 1937. A suggested method for representing gradient flow in isentropic analysis. Bull. Amer. Met. Soc., 18: 210-212.

Montgomery, R.B., 1938. Circulation in the upper layers of the southern North Atlantic deduced with the use of isentropic analysis. Pap. Phys. Oceanogr. Met., 6: 55.

Montgomery, R.B., 1962. Equatorial Undercurrent observations in review. J. Oceanogr. Soc. Japan, 20th Ann. vol.: 487-498.

Montgomery, R.B., and E.Palmen, 1940. Contribution to the question of the Equatorial Countercurrent. J. Mar. Res., 3: 112.

Montgomery, R.B., and A.F.Spilhaus, 1941. Examples and outline of certain modifications in the upper air analysis. J. Aero. Sci., 8: 276-283.

Montgomery, R.B. and E.D.Stroup, 1962. Equatorial waters and currents at 150 W in July-August 1952. Johns Hopkins Oceanogr. stud., 1: 68.

Montgomery, R.B. and W.S.Wooster, 1954. Thermosteric anomaly and the analysis of serial oceanographic data. Deep-Sea Res., 2: 63-70.

Moore, D.W. and S.G.H.Philander, 1977. Modelling of tropical oceanic circulation. in The Sea, 6, John Wiley, New York: 319-361.

Munk, W.H., 1950. On the wind-driven ocean circulation. J. Met., 1(2): 79-93.

Muraleedharan, P.M., 1984. Studies on Equatorial Undercurrent in the Indian Ocean. Ph.D. thesis, Univ. Cochin: 160.

Muraleedharan, P.M., Basil Mathew and R.N.Nair, 1980. Some studies on the Undercurrent and Equatorial Jet in the Indian Ocean from the hydrographic characteristics. Bull. Dept. Mar. Sci., Univ. Cochin, 11:113-126.

Muromtsev, A.M., 1958. The principal hydrological features of the Pacific Ocean, Atlas of vertical sections and charts of temperature, salinity, density and oxygen content. Appendix II (translated from Russian): Jerusalem, Israel Prog. Sci. Translations: 296.

Narendran Nair, R., 1983. Circulation in the Indian Ocean in relation to the monsoon circulation of the atmosphere. Ph.D. thesis, Univ. of Cochin, Cochin: 149

*Neumann, G., 1947. Uber die Entstchung des aquatorialen Genenstromes. Forschungen u. Fortschritte (Berlin), 16-18: 177-179.

Neumann, G., 1960. Evidence for an equatorial undercurrent in the Atlantic Ocean. Deep-Sea Res., 6: 328-334.

Neumann, G. and R.Williams, 1965. Observations of the Equatorial Undercurrent in the Atlantic Ocean at 15 W during Equalant I. J. Geophys. Res., 70(2): 297-304.

O'Brien, J.J. and H.E.Hurlburt, 1974. Equatorial Jet in the Indian Ocean: theory. Science, 184: 1075-1077.

Panfilova, S.G., 1972. Seasonal variability of temperatures of ocean surface water. Okeanologia, 12(3): 394-406.

Parr, A.E., 1938. Analysis of current profiles by a study of pycnomeric distortion and identifying properties. J. Mar. Res., 1(2): 119-132.

Patzert, W.C., 1972. Seasonal variation in structure and circulation in the Red Sea. Tech. Rep., HIG-72-13: 58.

Philander, S.G.H., 1979. Nonlinear coastal and equatorial jets. J. Phys. Oceanogr., 9: 739-747.

Philander, S.G.H. and R.C.Pacanowski, 1980. The generation of equatorial currents. J. Geophys. Res., 85: 1123-1136.

Pollak, M.J., 1958. Frequency distribution of potential temperatures and salinities in the Indian Ocean. Deep-Sea Res., 5: 128-133.

Premchand, K. and J.S.Sastry, 1976. Hydrological characteristics and transequatorial transport in the West Indian Ocean. Ind. J. Mar. Sci., 5: 169-178.

126

Previtte, D.W., 1959. Monthly charts of evaporation from the North Indian Ocean including the Red Sea and Persian Gulf. Quart. J. Roy. Met. Soc., 85(366): 424-428.

*Puls, C., 1895. Oberflachentemperaturen und Stromungs-verhaltnisse des Aquatorialgurtels des Stillen Ozeans. Archiv. d. Deutschen Seewarte, 8(1).

Quadfasel, D.R., 1982. Low frequency variability of the 20 ^{o}C isotherm topography in the Western Indian Ocean. J. Geophys. Res., 87, C3: 1990-1996.

Quadfasel, D.R. and F.Schott, 1982. Water mass distributions at intermediate layers off the Somali coast during the onset of the southwest monsoon, 1979. J. Phys. Oceanogr., 12:1343-1357.

Rao, D.P., 1977. A comparitive study of some physical processes governing the potential productivity of the Bay of Bengal and Arabian Sea. Ph.D. thesis, Andhra University: 135.

Reid, J.L., 1959. Evidence of a South Equatorial Countercurrent in the Pacific Ocean. Nature, 184, Suppl. 4: 209-210.

Reid, J.L., 1961. On the geostrophic flow at the surface of the Pacific Ocean with respect to the 1000-decibar surface. Tellus, 13: 489-502

Reid, J.L., 1964a. A transequatorial Atlantic oceanographic section in July 1963 compared with other Atlantic and Pacific sections. J. Geophys. Res., 69: 5205-5216.

Reid, J.L., 1964b. Evidence of a South Equatorial Countercurrent in the Atlantic Ocean in July 1963, Nature, 203: 182.

Reid, J.L., 1965. Intermediate waters of the Pacific Ocean. Johns Hopkins Oceanogr. Stud., 2: 85.

Reid, J.L. and R.J.Lynn, 1971. On the influence of Norwegian -Greenland and Weddell Seas upon the bottom waters of the Indian and Pacific oceans. Deep-Sea Res., 18: 1063-1088.

Reid, R.O., 1948. A model of the vertical structure of mass in the equatorial wind driven currents of a baroclinic ocean. J. Mar. Res., 7(3): 304-312.

Reverdin, G., M.Fieux, J.Gonella and J.R.Luyten, 1983. Free
drifting buoy measurements in the Indian Ocean
Equatorial Jet. in Hydrodynamics of the Equatorial
Ocean, J.C.J.Nihoul (Ed.), Elsevier Oceanogr. Ser., 36:
99-120.

Rinkel, M.O., P.Sund and G.Neumann, 1966. The location of
the termination area of the equatorial undercurrent in
the Gulf of Guinea based on observations during
Equalant III. J. Geophys. Res., 71(16): 3893-3901.

Ripa, P. and S.P.Hayes, 1981. Evidence for equatorial
trapped waves at the Galapagos Islands. J. Geophys.
Res., 86: 6509-6516.

Sakai, C., 1972. Time variations$_o$in the distribution of
physical properties along 145 W in the region of the
Pacific Equatorial Undercurrent. M.S. thesis, Univ.
Hawaii: 111.

*Sandstrom, J.W and B. Helland-Hansen, 1903. Uber die
Berechung von Meeresstromungen. Rep. on Norwegian Fish-
ery and Marine Investigations. Bd., 2(4): 43.

Sarkisyan, A.S. and V.P.Keonjiyan, 1975. Review of numerical
ocean circulation models using observed density field.
in Numerical Models of Ocean Circulation. Symp. Proc.
Durham, New Hampshire, 1972. Nat. Acad. Sci.,
Washington D.C.: 76-93.

Sastry, J.S., K.Premchand and C.S.Murthy, 1986. Water mass
structure in the Western Indian Ocean. Part I - Water
masses and their thermohaline indices. Mausam, 37(1):
107-110.

*Schott, G., 1898. Weltkarte zur Ubersicht der
Meeresstromungen und Schiffswege. Ann. d. Hydr. Marit.
Met., 26: 409.

*Schott, G., 1942. Grundlagen einer Weltkarte der
Meeresstromungen. Ann. d. Hydr. u. Marit. Met., 70:
329.

*Schumacher, A., 1940. Monatskarten der Obgrflachen-
stromungen im Nordatlantischen Ozean (5 N - 5 S). Ann.
d. Hydr. u. Marit. Met., 68: 109.

*Schumacher, A., 1943. Monatskarten der Oberflachen-
stromungen im aquatorialen und sudlichen Atlantischen
Ozean. Ann. d. Hydr. u. Marit. Met., 71: 209.

Sharma, G.S., 1968. Some inferences on the Equatorial Undercurrent in the Indian Ocean based on the physical properties of the waters. J. Mar. Biol. Ass. India, 10(2): 224-236.

Sharma, G.S., 1971. Studies on the divergence of the surface waters in the North Indian Ocean. Ph.D. thesis, Andhra Univ., Waltair: 102.

Sharma, G.S., 1972. Water characteristics at 200 cl/t in the Intertropical Indian Ocean during the southwest monsoon. J. Mar. Res., 30(1): 102-111.

Sharma, G.S., 1976a. Transequatorial movement of water masses in the Indian Ocean. J. Mar. Res., 34(2): 143-154.

Sharma, G.S., 1976b. Water characteristics and current structure at 65°E during the southwest monsoon. J. Oceanogr. Soc. Japan, 32(6): 284-296.

Sharma, G.S. and Basil Mathew, 1985. Hydrography and circulation off the Antarctica in the Indian Ocean region. Proc. Ind. Acad. Sci.(E&P Sciences), 94(1): 13-27.

Sharma, G.S., A.D.Gouveia and Shubha Satyendranath, 1978. Incursion of the Pacific Ocean Water into the Indian Ocean. Proc. Ind. Acad. Sci., 87A(3) (E&P Sciences): 29-45.

Sharma, G.S., R.Narendran Nair and Basil Mathew, 1982. Current structure in the intertropical Indian Ocean during northeast monsoon. Ind. J. Mar. Sci., 11: 7-14.

Stommel, H., 1948. The westward intensification of wind-driven ocean currents. Trans. Amer. Geophys. Union, 29(2): 202-206.

Stommel, H., 1960. Wind-drift near the equator. Deep-Sea Res., 6: 298-302.

*Sverdrup, H.U., 1932. Arbeider i luft-og havsforskning. Chr. Mich. Inst. for Videnskap og Andsfrihet, Beretninger (Bergen) 2(5).

Sverdrup, H.U., 1947. Wind driven currents in a baroclinic ocean. Proc. Nat. Acad. Sci., 33: 318-326.

Sverdrup, H.U., M.W.Johnson and R.H.Fleming, 1942. The Oceans, their physics, chemistry and general biology. Prentice-Hall, New York: 1087.

Swallow, J.C., 1964. Equatorial Undercurrent in the Western Indian Ocean. Nature, 204(4957): 436-437.

Taft, B.A., 1963. Distribution of salinity and dissolved oxygen on surfaces of uniform potential specific volume in the South Atlantic, South Pacific and Indian Ocean. J. Mar. Res., 21(2): 129-146.

Taft, B.A., B.M.Hickey, C.Wunsch and D.J.Baker, Jr., 1974. Equatorial Undercurrent and deeper flows in the Central Pacific. Deep-Sea Res., 21: 403-430.

Taft, B.A. and J.H.Jones, 1973. Measurements of the Equatorial Undercurrent in the eastern Pacific. in Prog. in Oceanogr., B.A.Warren (Ed.), Pergamon Press, New York, 6: 47-110.

Taft, B.A. and J.A.Knauss, 1967. Equatorial Undercurrent of the Indian Ocean as observed by the LUSIAD Expedition. Bull. Scripps Inst. Oceanogr., 9: 163.

Tait, J.B., 1955. Long-term trends and changes in the hydrography of the Faroe-Shetland Channel region. Deep-Sea Res., 3(Suppl.): 482-498.

Tchernia, P., 1980. Descriptive Regional Oceanography. Pergamon Press, Mar. Ser., 3: 253.

Tchernia, P., H.Lacombe and P.Guibout, 1958. Some new hydrological observations relative to the equatorial region of the Indian Ocean. Comite. Central d'Oceanogr. et d'Etude des Cotes, Bull. d'Information, 10(3):115-143.

Thompson, E.F., 1939. Chemical and physical investigations, the exchange of water between Red Sea and the Gulf of Aden over the 'sill'. John Murray Exped., 1933-34., Scientific Rep., 2(4): 105-119.

*Thorade, H., 1941. Der aquatoriale Gegenstrom im Atlantischen Ozean und seine Entstehung. Ann. d. Hydr. u. Marit. Met., 69: 201-209.

*Timofeev, V.T., 1956. The annual water balance of the Arctic Ocean (in Russian). Priroda, 7: 89-91.

Tsuchiya, M., 1968. Upper waters of the Intertropical Pacific Ocean. Johns Hopkins Oceanogr. Stud., 4: 55.

Tsuchiya, M., 1975. Subsurface countercurrents in the Eastern Equatorial Pacific Ocean. J. Mar. Res., 33(Suppl.): 145-175.

Uda, M. and K.Hasunuma, (1969). The eastward Subtropical Countercurrent in the Western North Pacific Ocean. J. Oceanogr. Soc. Japan, 25: 201-210.

United States Hydrographic Office, 1944. Atlas of surface currents. Indian Ocean. H.O. No. 566.

Varadachari, V.V.R. and G.S.Sharma, 1967. Circulation of the surface waters in the North Indian Ocean. J. Ind. Geophys. Union, IV(2): 61-73.

Venkateswaran, S.V., 1956. On evaporation from the Indian Ocean. Ind. J. Met. Geophys., 7(3): 265-284

*Voigt, K., 1961. Aquatoriale Unterstromung auch im Atlantik. Beitr. Meeresk., 1: 56-60.

Voorhis, A.D. and J.B.Hersey, 1964. Oceanic thermal fronts in the Sargasso Sea. J. Geophys. Res., 69: 3809-3814.

Warren, B.A., H.Stommel and J.C.Swallow, 1966. Water mass and patterns of flow in the Somali Basin during southwest monsoon of 1964. Deep-Sea Res., 13: 825-860.

Weisberg, R.H., A.Horigan and C.Colin, 1979. Equatorially trapped Rossby-gravity wave propagation in the Gulf of Guinea. J. Mar. Res., 37: 67-86.

Wooster, W.S., 1961. Further evidence of a Pacific South Equatorial Countercurrent. Deep-Sea Res., 8: 294-297.

Wooster, W.S. and M.Gilmartin, 1961. The Peru-Chile Undercurrent. J. Mar. Res., 19(3): 97-122.

Wunsch, C. and A.E.Gill, 1976. Observations of equatorially trapped waves in Pacific sea level variations. Deep-Sea Res., 23: 371-390.

Wyrtki, K., 1958. The water exchange between the Pacific and the Indian Ocean in relation to upwelling processes. Proc. 9 Pacific Science Congress, Bangkok, 1957, 16: 61-66.

Wyrtki, K., 1963. The horizontal and vertical field of motion in the Peru current. Bull. Scripps Inst. Oceanogr., 8(4): 313-346.

Wyrtki, K., 1967. Circulation and watermass in the Eastern Equatorial Pacific Ocean. Int. J. Oceanogr. Limno., 1(2): 117-147.

Wyrtki, K., 1971. Oceanographic atlas of the International Indian Ocean Expedition. Washington D.C., Nat. Sci. Foundation: 531.

Wyrtki, K., 1973a. Physical oceanography of the Indian Ocean. in Ecological Studies, Analysis and Synthesis, 3, B.Zeitzchel (Ed.), Springer-Verlag, Berlin:19-36.

Wyrtki, K., 1973b. An equatorial jet in the Indian Ocean. Science, 181: 262-264.

Wyrtki, K. and G.Meyers, 1975. The trade wind field over the Pacific Ocean Part I, the mean field and the mean annual variation. Hawaii Inst. Geophys. Rep., HIG-75-1, Univ. Hawaii, Honolulu: 26.

Wyrtki,K., G.Meyers, D.McLain and W.Patzert, 1977. Variability of the thermal structure in the central equatorial Pacific Ocean. Hawaii Inst. Geophys. Rep., HIG-77-1: 75.

Yoshida, K., 1959. A theory of the Cromwell Current (the Equatorial Undercurrent) and of the equatorial upwelling - an interpretation in a similarity to a coastal circulation. J. Oceanogr. Soc. Japan, 15: 159-170.

Zuta, S., T.Rivera and A.Bustamente, 1978. Hydrologic aspects of the main upwelling areas off Peru. in Upwelling Ecosystems, R.Boje and M.Tomczak (Eds.), Springer-Verlag: 303.

---

* Original not referred.